

DEVELOPMENT OF A COMPOSITE CAD PACKAGE TO PREDICT AND REDUCE EM RADIATION FROM A PCB

A thesis for the degree of Ph.D.
presented to
DUBLIN CITY UNIVERSITY

by

PRAN KANAI SAHA, B.Sc. Engg., M.E.

SCHOOL OF ELECTRONIC ENGINEERING
DUBLIN CITY UNIVERSITY

RESEARCH SUPERVISOR
MR. JIM DOWLING
and
DR. THOMAS CURRAN

February 1995

DECLARATION

I hereby certify that this material, which I now submit for assessment on the programme of study leading to the award of Ph.D. is entirely my own work and has not been taken from the work of others save and to the extent that such work has been cited and acknowledged within the text of my work.

Signed

: P. Kanai Saha

Pran kanai Saha

Date: 7th February, 1995.

Student number: 90700911

ACKNOWLEDGEMENTS

I am greatly indebted to my supervisor, Jim Dowling, a man of good reasoning and forbearance for his guidance and tuition in the course of this work. I found his constant help, support and encouragement enormously fulfilling throughout the long road to this dissertation. Indeed, without his enthusiasm at every step and brilliant touch at every paragraph of this dissertation, it would have been impossible for me to organize this thesis in the present form.

To, Dr. Thomas Curran, a special word of appreciation and sincerest gratitude for his enthusiasm and for affording me the opportunity to pursue this work.

I am grateful to my wife Shilpi, for all her love, encouragement, patience and understanding especially over the last three years, I remain in her debt. I must acknowledge my dearest son Parnab and daughter Purnita for their patience.

My colleague, Dr. Hafizur Rahman, was a co-worker in this EMC laboratory and the useful discussions which I had with him played a vital role towards the technical fulfilment of this work. I would therefore, like to thank him for all his co-operation. I must also acknowledge Dr. Ziaul Karim from school of electronic engineering and Mr. Imtiaz Ahmed Choudhury and Mr. Mohiuddin Ahmed from school of Mechanical and Manufacturing Engineering for their continuous supports from the very beginning of this work. All other Bangladeshi friends, here in DCU, helped me a lot on different occasions regarding this research work and I also thank them all.

This project has been funded by FORBAIRT and TELTEC, Ireland and I am thankful to those organisations for their support. Especially I thank Mr. John McAuly for his kind help and suggestions during performing the experiments in the EMC laboratory of FORBAIRT. I am also grateful to Power Electronic Ireland, University of Limerick for allowing me to use their anechoic chamber and instruments.

I would like to thank Dr. Jeevakumar Kanagrathnam from the Speech laboratory and Mr. Declan Friel from Telecommunication laboratory for their help and valuable suggestion during developing the computer programme and preparing this thesis.

I am grateful to Prof. Charles McCorkell, Dr. David Cameron and Dr. Ronan Scaife of this school and Prof. M.S.J. Hashmi of the school of Mechanical and Manufacturing Engineering for inspirational discussions and timely assistance towards fulfilling this work. I would like to thank John Whelan, David Condell, Liam Meany, Conor Maguire, Paul Wogan, Peter McGorman and Stephen Neville of Electronic Engineering department for their help and co-operation throughout this work.

Finally I would like to acknowledge all of my relatives and friends, at home and abroad, who gave me mental supports and encouragement during my disastrous time when I lost my parents forever during this research.

Dedicated
To my Mum and Dad.

DEVELOPMENT OF A COMPOSITE CAD PACKAGE TO PREDICT AND REDUCE EM RADIATION FROM A PCB

Pran Kanai Saha

ABSTRACT

A composite CAD package to predict and reduce radiation from a printed circuit board (PCB) is presented in this thesis. The composite CAD package is implemented using an electromagnetic (EM) computation tool linked with other circuit design packages (CDPs) such as ORCAD (a schematic design package), PSPICE (a circuit simulation package) and Boardmaker (a board layout tool). Software is developed to link all the packages so that one can incorporate EMC verification in the design process of an electronic product.

The well-known Numerical Electromagnetic Code (NEC) version 2 is used as an EM computation tool. In using NEC-2 to predict PCB radiation, the PCB is simulated as a loaded thin wire structure just above (but not contacting) the surface of an imperfect ground. An algorithm is developed and implemented to automate the geometrical modelling of a wire structure for NEC-2.

The data required by NEC-2 (geometrical, load and electrical) for prediction of PCB radiation can be obtained from various CDPs. The development and implementation of data extraction algorithms are presented in this thesis. Single and double sided PCBs can be accommodated and the work can be extended to handle multilayer PCBs.

The use of NEC-2 for this type of application has been validated experimentally and theoretically (by comparing NEC-2 predicted radiation with that obtained where the EM radiation from a pair of parallel PCB tracks running between two components/devices is computed using transmission line modelling-TLM). Both methods of evaluation are described in detail in this thesis and results showing good agreement are presented.

TLM is employed by considering, (i) the effective dielectric constant of the medium (air and substrate) surrounding the PCB tracks and (ii) the displacement current between the two PCB tracks. The effect of displacement current in near field radiation is highlighted. The use of TLM for prediction of PCB radiation is verified experimentally. Measured radiation is in good agreement with prediction.

In the developed composite CAD package, one can compare the predicted radiation with the mandatory EMC requirement laid down by the regulating bodies and "close the loop" to modify the design where these requirements have not been met. Various techniques to reduce radiation can also be employed. Reduction of radiation by providing shielding in some section of the circuit is proposed. An algorithm is developed and implemented to find the section of the circuit where shielding is necessary.

The optimum layout (track separation to width ratio) that can minimise radiation is found theoretically. An optimum layout is also determined experimentally and compared with the theoretical value. A good agreement is found in this comparison. Thus a guideline to choose optimum layout for minimum radiation is provided.

CONTENTS

	PAGE
ACKNOWLEDGEMENTS	<i>ii</i>
ABSTRACT	<i>iv</i>
LIST OF SYMBOLS	<i>xvi</i>
LIST OF ACRONYMS	<i>xvii</i>
CHAPTER 1: EQUIPMENT AND PCB EMC	
1.1 INTRODUCTION	<i>1</i>
1.2 EMC: AN OVERVIEW	<i>2</i>
1.2.1 ASPECTS OF EMC	<i>2</i>
1.2.2 EMC REQUIREMENTS	<i>4</i>
1.3 EQUIPMENT EMC	<i>5</i>
1.3.1 CABLES	<i>5</i>
1.3.2 PCB	<i>6</i>
1.3.2.1 Grounding	<i>6</i>
1.3.2.2 Crosstalk	<i>6</i>
1.3.2.3 Susceptibility	<i>6</i>
1.3.2.4 Radiated emission	<i>7</i>
1.3.3 CONNECTORS	<i>7</i>
1.3.4 COMPONENTS	<i>7</i>
1.3.5 POWER SUPPLIES	<i>8</i>
1.3.6 ENCLOSURE	<i>8</i>
1.3.7 RELAYS, SWITCHES AND MOTORS	<i>9</i>
1.4 WAYS TO ACHIEVE EMC REQUIREMENTS	<i>9</i>
1.5 PCB DESIGN WITH EMC	<i>10</i>
1.6 PROBLEM STATEMENT AND PROPOSED SOLUTION	<i>12</i>
1.7 BENEFITS	<i>13</i>

1.8	AIM AND OBJECTIVES OF THIS RESEARCH	14
1.9	CONTRIBUTION FROM THIS RESEARCH	14
1.10	ORGANISATION OF THIS THESIS	15

CHAPTER 2: PCB RADIATION:

PREDICTION TECHNIQUES & MEASUREMENT

2.1	INTRODUCTION	18
2.2	FIELD REGION	18
2.3	EM COMPUTATION SOFTWARE TOOLS	20
2.3.1	GEMACS	20
2.3.2	SEMCAP AND IEMCAP	20
2.3.3	NEC PROGRAMME	21
2.3.3	MININEC	22
2.3.4	WIRE PROGRAMME	22
2.4	METHODS TO PREDICT PCB RADIATION	22
2.4.1	ANALYTICAL MODELS	22
2.4.1.1	Simplified Method	23
2.4.1.2	Circuit concept approach	24
2.4.1.3	Transmission line modelling (TLM)	25
2.4.2	NUMERICAL MODELS	28
2.4.2.1	Finite element method (FEM)	28
2.4.2.2	Finite difference time domain (FDTD) method	28
2.4.2.3	Method of moments (MoM)	29
2.5	CIRCUIT DESIGN PROCESS	31
2.6	PROPOSED TECHNIQUE AND THEORETICAL VALIDATION	32
2.7	EMISSION MEASUREMENT	33
2.7.1	INSTRUMENTATION	33

2.7.2	MEASUREMENT METHODS	34
2.7.2.1	Open area test site (OATS)	35
2.7.2.2	Shielded room	36
2.7.2.3	Hooded antenna technique	37
2.7.2.4	TEM cell	38
2.7.2.5	Reverberating chamber	39
2.7.2.6	Anechoic chamber	40
2.8	SUMMARY	40
CHAPTER 3: USE OF NEC-2 FOR THE PREDICTION OF PCB RADIATION		
3.1	INTRODUCTION	41
3.2	THEORETICAL BACKGROUND OF THE NEC PROGRAMME	41
3.2.1	THE EFIE	41
3.2.2	NUMERICAL TECHNIQUE FOR SOLVING EFIE	43
3.2.3	GROUND EFFECT	45
3.2.4	EVALUATION OF RADIATED FIELD	46
3.3	MODELLING GUIDELINES	47
3.3.1	SEGMENT LENGTH	47
3.3.2	WIRE RADIUS	47
3.3.3	SEGMENT CONNECTION	48
3.3.4	WIRE SEGMENTATION	48
3.4	SIMULATION OF A PCB	48
3.5	MODIFICATION OF NEC-2 PROGRAMME	50
3.5.1	AUTOMATION OF SEGMENTATION SCHEME	53
3.6	ANALYSIS OF SEGMENTATION SCHEME	54
3.6.1	SHORT CIRCUITED TRACK CONFIGURATION	54

3.6.2	A CENTRE FED DIPOLE	57
3.7	EFFECT OF h	58
3.8	EFFECT OF DIELECTRIC SUBSTRATE AT FAR FIELD REGION	59
3.9	CONCLUDING REMARKS	61
CHAPTER 4: THEORETICAL VALIDATION		
4.1	INTRODUCTION	62
4.2	TLM	62
4.2.1	EFFECTIVE DIELECTRIC CONSTANT	63
4.2.2	PUL PARAMETERS	65
4.2.3	CHARACTERISTIC IMPEDANCE	66
4.2.4	COMPUTATION OF CURRENT AND VOLTAGE	67
4.2.5	DISPLACEMENT CURRENT	69
4.2.6	RADIATED FIELD DUE TO FUNCTIONAL CURRENTS	70
4.2.6.1	Vector and Scalar potential	71
4.2.6.2	Radiated electric field	73
4.2.6.3	Radiated magnetic field	74
4.2.7	RADIATED FIELD DUE TO DISPLACEMENT CURRENT	75
4.2.8	TOTAL RADIATED FIELDS	76
4.3	NUMERICAL METHOD AND SOFTWARE	77
4.4	RESULTS AND COMPARISON	78
4.4.1	AT DIFFERENT OBSERVATION POINT	78
4.4.2	AT DIFFERENT FREQUENCIES	80
4.4.3	DIFFERENT LOAD IMPEDANCES	83
4.5	EFFECT OF DISPLACEMENT CURRENT	83
4.6	CONCLUDING REMARKS	85

CHAPTER 5: COMPOSITE CAD PACKAGE

5.1	INTRODUCTION	87
5.2	DEVELOPMENT OF COMBINED CAD PACKAGE	87
5.3	CIRCUIT DESIGN PACKAGES	89
5.3.1	SCHEMATIC DESIGN TOOL (ORCAD™)	89
5.3.2	CIRCUIT SIMULATION TOOL (PSPICE™)	90
5.3.2.1	Preparation of input file for PSPICE	91
5.3.3	PCB LAYOUT DESIGN TOOL (Boardmaker™)	94
5.4	DATA EXTRACTION ALGORITHMS	95
5.4.1	EXTRACTION OF GEOMETRICAL AND LOAD DATA	95
5.4.1.1	Layout Data Extraction Routine (LDER)	96
5.4.1.2	Subroutine TDSP	99
5.4.1.3	Subroutine COMV	102
5.4.1.4	Subroutine STC	104
5.4.1.5	Subroutine TEWG	107
5.4.1.6	Subroutine RSG	109
5.4.1.7	Subroutines TEWG1 and RSG1	112
5.4.1.8	Subroutine PESG	112
5.4.2	EXTRACTION OF ELECTRICAL DATA	114
5.5	INCORPORATING THE RADIATION REDUCING TECHNIQUES WITH COMPOSITE CAD PACKAGE	117
5.5.1	REDUCING PCB RADIATION BY MODIFYING DESIGN	118
5.5.2	REDUCING PCB RADIATION BY PROVIDING SHIELDING	120
5.6	OPTIMUM LAYOUT FOR MINIMISING PCB RADIATION	122
5.7	CONCLUDING REMARKS	123

CHAPTER 6: COMPOSITE CAD PREDICTED RADIATION

6.1	INTRODUCTION	124
6.2	PREDICTION OF RADIATED EM FIELDS FROM PCB USING COMPOSITE CAD PACKAGE	124
6.2.1	CIRCUIT #1	124
6.2.2	CIRCUIT #2	126
6.2.3	CIRCUIT #3	132
6.3	EFFECT OF SHIELDING	135
6.4	DETERMINATION OF OPTIMUM LAYOUT	136
6.5	CONCLUDING REMARKS	137

CHAPTER 7: EXPERIMENTAL VALIDATION

7.1	INTRODUCTION	138
7.2	INSTRUMENTS AND ACCESSORIES	138
7.2.1	NEAR FIELD PROBES	139
7.2.2	BROADBAND ANTENNAS	140
7.2.3	EMI RECEIVER/SPECTRUM ANALYSER	140
7.2.4	SIGNAL GENERATOR	141
7.2.5	PRE-AMPLIFIER	141
7.3	NEAR FIELD MEASUREMENT	141
7.3.1	TEST SET-UP	142
7.3.2	MEASUREMENT PROCEDURE	142
7.3.3	TEST RESULTS AND COMPARISON	143
7.3.3.1	Circuit #1	145
7.3.3.2	Circuit #2	152
7.3.3.3	Circuit #3	154

7.3.3.4	Comparison between the extended TLM predicted and measured electric field	157
7.3.3.5	Determination of s/w ratio	159
7.3.3.6	Verification of shielding effect	160
7.4	EMISSION MEASUREMENT IN A SHIELDED ROOM	162
7.4.1	DETERMINATION OF POSITION OF FIELD MAXIMA	164
7.4.2	MEASUREMENT OF RADIATED ELECTRIC FIELD IN LOADED ROOM	168
7.4.2.1	Room loaded with electric field absorber	168
7.4.2.2	Room loaded with ferrite tile	172
7.4.2.3	Comparison between the measured and predicted field	174
7.5	EMISSION MEASUREMENT IN AN ANECHOIC CHAMBER	177
7.5.1	MEASUREMENT SET-UP AND PROCEDURE	179
7.5.2	TEST RESULTS AND COMPARISON	180
7.6	CONCLUDING REMARKS	185
CHAPTER 8: CONCLUSIONS AND REMARKS		
8.1	CONCLUSIONS	186
8.1.1	EM COMPUTATION TOOL (NEC-2)	186
8.1.2	THEORETICAL VALIDATION	187
8.1.3	THE EXTENDED TLM	187
8.1.4	COMPOSITE CAD PACKAGE	188
8.1.5	DATA EXTRACTION	188
8.1.6	REDUCING EM RADIATION	189
8.1.7	APPLICATION AND EXPERIMENTAL VALIDATION OF COMPOSITE CAD PACKAGE	189
8.1.7.1	Reliability of the composite CAD predicted results	190

8.2	DIRECTIONS FOR FURTHER RESEARCH	194
8.2.1	RESEARCH ON APPLICATION OF COMPOSITE CAD PACKAGE	194
8.2.2	RESEARCH ON EXTENSION OF COMPOSITE CAD PACKAGE	194
8.2.3	RESEARCH ON EXTENDED TLM	195
8.2.4	RESEARCH ON EMISSION MEASUREMENT IN SHIELDED ROOM	196
APPENDIX A		
A1	EMISSION LIMIT FOR CLASS B DIGITAL DEVICES	198
APPENDIX B		
B1	EMISSION LIMIT FOR CLASS A DIGITAL DEVICES	199
APPENDIX C		
C1	MOMENT METHOD SOLUTION FOR INTEGRODIFFERENTIAL EQUATION	200
C2	FORMULA TO COMPUTE NEAR FIELD COMPONENTS IN CYLINDRICAL CO-ORDINATE SYSTEM	202
C3	COMPUTER PROGRAMME LISTING FOR SUBROUTINE "SPECTRA"	204
C4	FUNCTION OF EACH SUBROUTINE IN NEC PROGRAMME	206
C5	IMPLEMENTATION OF GEOMETRICAL MODELLING RULE	208
APPENDIX D		
D1	DISTANCE BETWEEN SOURCE AND OBSERVATION POINT	210
D2	EXACT EXPRESSIONS FOR ELECTRIC FIELD COMPONENTS DUE TO FUNCTIONAL CURRENTS	210
D3	EXACT EXPRESSIONS FOR MAGNETIC FIELD COMPONENTS DUE TO FUNCTIONAL CURRENTS	213
D4	GEOMETRY INVOLVED TO COMPUTE VECTOR POTENTIAL DUE TO DISPLACEMENT CURRENT	213

D5	FIELD COMPONENTS DUE TO DISPLACEMENT CURRENT	214
D6	CLOCK OR DATA SIGNAL	216
D7	COMPUTER PROGRAMME LISTING FOR RADIATED FIELD DUE TO FUNCTIONAL CURRENTS	218
D8	COMPUTER PROGRAMME LISTING FOR RADIATED FIELD DUE TO DISPLACEMENT CURRENT	228
APPENDIX E		
E1	BATCH ROUTINE	233
E2	COMPUTER PROGRAMME LISTING FOR IFGR	234
E3	COMPUTER PROGRAMME LISTING FOR EXTRACTION OF GEOMETRICAL AND LOAD DATA	238
E4	LINE FORMAT FOR FILE CREATED BY SUBROUTINE "COMV"	261
E5	COMPUTER PROGRAMME LISTING FOR EXTRACTION OF ELECTRICAL DATA	262
E6	CORNER CO-ORDINATES OF A SHIELDED SECTION	265
E7	COMPUTER PROGRAMME LISTING FOR SUBROUTINE "SHIELD"	266
E8	COMPUTER PROGRAMME LISTING FOR SUBROUTINE "ASSC"	267
E9	DETERMINATION OF OPTIMUM LAYOUT	269
E10	COMPUTER PROGRAMME LISTING TO FIND OPTIMUM LAYOUT	270
APPENDIX F		
F1	PROBE PERFORMANCE FACTOR (PF)	277
F2	ANTENNA FACTOR (AF) FOR BCA AND LPA	278
F3	SHIELDING EFFECTIVENESS OF SHIELDING BLOCK	279
F4	DEVELOPMENT OF FIELD EXPRESSIONS IN AN EMPTY ROOM DUE TO TE WAVES	281
F5	DEVELOPMENT OF FIELD EXPRESSIONS IN AN EMPTY ROOM DUE TO TM WAVES	285

F6	DOWNHILL SIMPLEX METHOD	286
F7	COMPUTER PROGRAMME LISTING FOR THE FIELD MAXIMA	287
F8	PERFORMANCE OF ECCOSORB AN 79	292
F9	ABSORPTION CHARACTERISTIC OF FERRITE ABSORBER	293
APPENDIX G		
G1	SIZE OF A PCB	294
G2	LIST OF PUBLICATIONS OUT OF THIS RESEARCH	295
REFERENCES		296

LIST OF SYMBOLS

c	Speed of light ($=3 \times 10^8$ m/s)
f	Frequency, Hz
ω	Angular frequency, rad/s
λ	Wavelength, m
λ_0	Wavelength in free space, m
β	Phase constant ($=2\pi/\lambda$), rad/m
β_0	Phase constant in free space ($=2\pi/\lambda_0$)
μ	Permeability, H/m
μ_0	Permeability of free space ($=4\pi \times 10^{-7}$ H/m)
ϵ	Permittivity, F/m
ϵ_0	Permittivity of free space ($=8.854 \times 10^{-12}$ F/m)
ϵ_r	Dielectric constant of PCB substrate ($=4.7$)
ϵ_r'	Effective dielectric constant of the medium surrounding the PCB track
τ	Pulse width, second
T	Pulse period, second
t_r	Pulse rise time, second
t_f	Pulse fall time, second
V_{ns}	Amplitude of the n th harmonic of the pulse, volt
t	PCB track thickness ($= 35 \mu\text{m}$)
w	PCB track width, m
h_t	PCB substrate thickness ($=1.45$ mm)
a	Wire radius, m
h	Distance between the wire (simulated PCB track) and an imperfect ground, m
C	Transmission line capacitance, F/m
L	Transmission line inductance, H/m
Z_s	Source impedance, ohms
Z_1	Load impedance, ohms
\vec{A}	Vector magnetic potential
Φ	Scalar potential
\vec{F}	Vector electric potential
E	Electric field, dB $\mu\text{V/m}$
H	Magnetic field, dB $\mu\text{A/m}$
SE	Shielding effectiveness, dB

LIST OF ACRONYMS

BCA	Bi-conical antenna
CAD	Computer aided design
CM	Common mode
DM	Differential mode
EM	Electromagnetic
EMC	Electromagnetic compatibility
EMI	Electromagnetic interference
EDER	Electrical data extraction routine
IFGR	Input file generating routine
LDER	Layout data extraction routine
MoM	Method of moment
NEC	Numerical electromagnetic code
PCB	Printed circuit board
PUL	Per unit length
TLM	Transmission line modelling

Chapter 1

EQUIPMENT AND PCB EMC

- ❑ EMC AND EMI
- ❑ EQUIPMENT EMC
- ❑ WAYS TO ACHIEVE EMC REQUIREMENTS
- ❑ DESIGN PCB WITH EMC
- ❑ PROBLEM STATEMENT AND SOLUTION
- ❑ AIM AND OBJECTIVES
- ❑ CONTRIBUTIONS
- ❑ ORGANISATION OF THIS THESIS

1.1 INTRODUCTION

Recent studies [1, 2] show that the effective use of electromagnetic compatibility (EMC) can bring benefits for every electronic industry in the areas of design and development, production, marketing and sales, service and financial performance. Hence, elimination or minimisation of EMC problems should be a major design objective of a circuit designer. Marvin *et al.* [134] described the requirements for a computer aided design package to predict radiated emissions from electronic equipment and to aid their reduction. Since a printed circuit board (PCB) is an integral part of electronic equipment, it is advisable for a circuit designer to consider the EMC problem in the design cycle of a PCB.

Various methods [3-7, 14-20, 25, 27, 41, 46, 49, 131] are available to predict PCB radiation. In all cases, prediction is outside the design process. The aim of this research was to develop a composite CAD package for predicting and reducing PCB radiation at the design stage. Such a package is considered to be particularly important for product compliance with mandatory EMC requirements, in effecting considerable saving in hardware cost for enclosing the PCB and in the time required for redesign of the circuit in the event of final product failing to meet requirements. It could also confirm reliable operation of the circuit itself.

Prior to entering the main topics of PCB radiation, the general background to EMC research is discussed in section 1.2. Sources of EMC problems in a piece of electronic equipment are discussed in section 1.3. Section 1.4 discusses various ways of achieving EMC requirements by reducing or minimising the different EMI problems in equipment. PCBs play a vital role in achieving EMC performance of the equipment. The design of a PCB with EMC is described in section 1.5. The problem of verifying the PCB EMC in the design process of equipment is highlighted and a solution is presented in section 1.6. The benefits of the proposed solution are given in section 1.7.

The aim and objectives of this research are described in section 1.8 and the achievements from the work are given in section 1.9. At the end of this chapter, in section 1.10, the organisation of this thesis is summarised.

1.2 EMC : AN OVERVIEW

EMC is defined by the IEEE [100] as "the ability of a device, equipment or system to function satisfactorily in its electromagnetic environment without introducing intolerable electromagnetic disturbance to anything in that environment" and EMI is defined as "the degradation of the performance of a device, equipment, or system caused by an electromagnetic disturbance." Therefore the purpose of EMC practices is to ensure system or subsystem compatibility. Various aspects of EMC and EMC requirements are discussed in the following subsections.

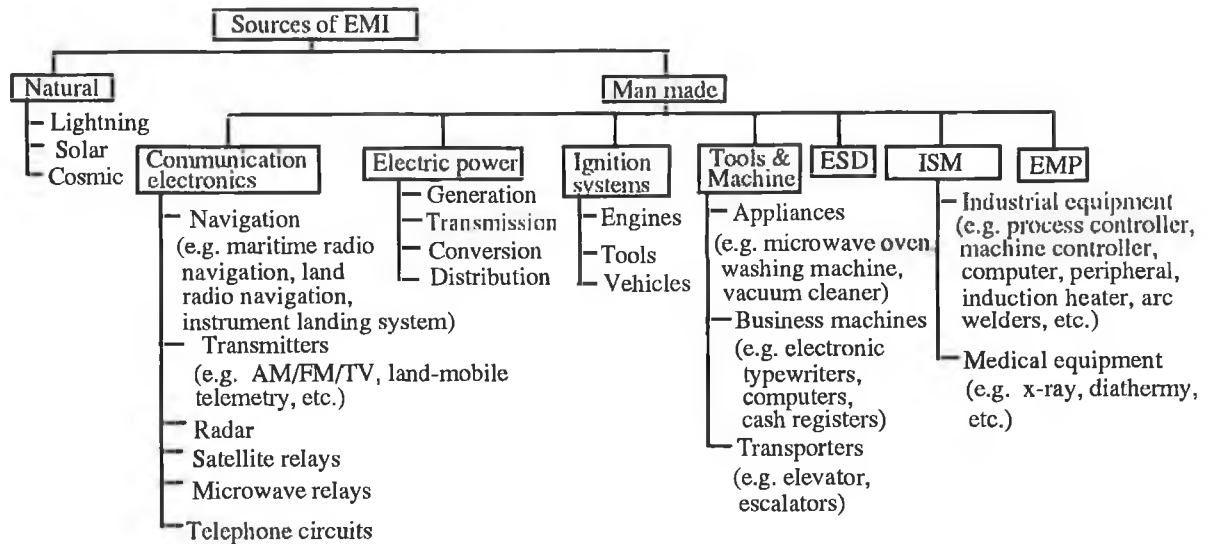
1.2.1 ASPECTS OF EMC

The three main factors to be discussed under the heading of EMC are the source, the transfer and the receptor of electromagnetic energy. A source (also referred as emitter) produces the emission. A transfer or coupling path transfers the electromagnetic energy to a receptor (receiver) where it is processed, resulting in either desired or undesired behaviour. The interference occurs if the received energy causes the receptor to behave in an undesired manner. Thus any man-made device or apparatus that transmits, distributes, processes or otherwise utilises any form of electrical energy can be a source of EMI if any aspect of its operation generates electromagnetic signals that can cause a degradation of performance of any other equipment or system (victims) that shares the same environment [58].

Other man-made sources of EMI are electrostatic discharge (ESD) and an electromagnetic pulse (EMP). ESD results from the accumulation of static charge on objects due to contact with any other object moving relative to it. Such charging can create an intense electric field and consequently a voltage difference between two objects [97]. This voltage can be as high as 10-25 kV with stored energies of 20-30 mJ [107, 156]. The discharging of this energy can produce fast rising current pulses which can damage electronic circuits.

EMP is the electromagnetic pulse which radiates from nuclear detonation. EMP results from electron scattering due to the collision of emitted gamma rays with molecules of the media exposed to the gamma flux. The pulse strength may be of the order of 10 kV/m at a distance of 1.6 km from a one-megaton detonation, with accompanying magnetic fields of the order of 260 A/m [54]. It may cause severe EMI problems for electronic circuits.

Electromagnetic energy associated with natural phenomena, such as lightning or cosmic noise, is also a source of EMI. Sources of EMI for various natural and man made categories are illustrated in Fig. 1.1.



Note: ISM - Industrial, scientific and medical equipment

Fig. 1.1 Sources of EMI. Adapted and modified from [58].

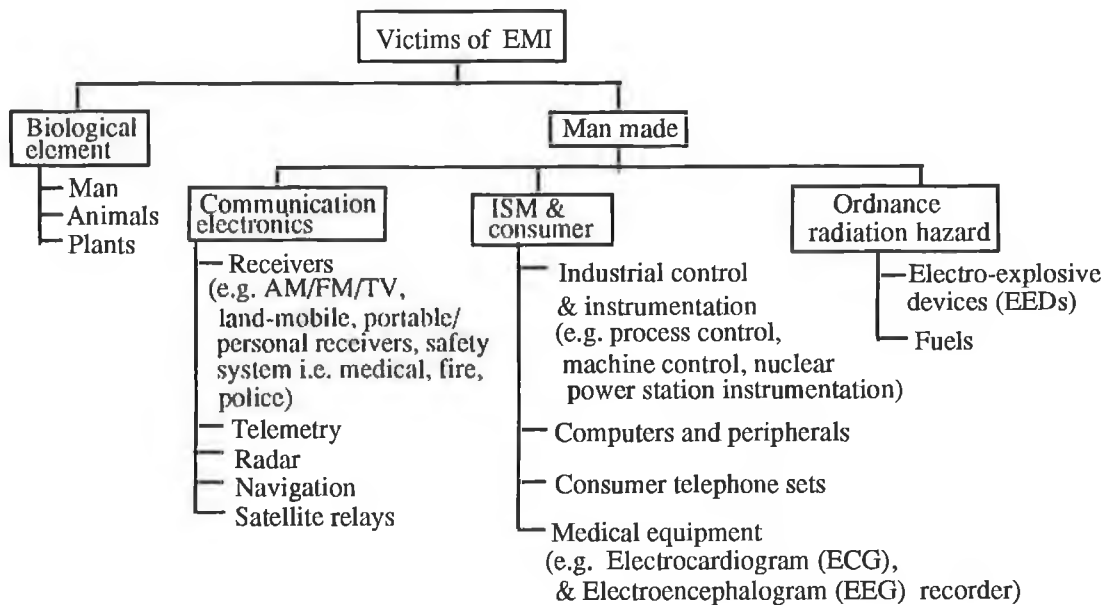


Fig. 1.2 Receptors (victims) of EMI. Adapted and modified from [58].

It is very difficult to separate the sources of EMI from its receptors. Probably most of the sources (except the natural sources of EMI) are also victims of EMI generated by other sources. In some cases the same system is defined both as a source and as a receptor of EMI. Examples of natural and man-made receptors of EMI are illustrated in Fig. 1.2.

1.2.2 EMC REQUIREMENTS

In order to control EMC problems, various governmental and international bodies have responded by introducing stringent regulations. Regulations cover both the emission and susceptibility limits of various types of equipment, and also define the guidelines for measurement systems to show conformance with the standards.

A large number of bodies such as the British Standards Institute (BSI) and the Department of Trade and Industry (DTI) in the UK, the Federal Communications Commissions (FCC) and the Department of Defence (DoD) in USA, and the Verband Deutscher Elektrotechniker (VDE) in Germany specify the EMC requirements for various types of electronic equipment. The requirements are based on recommendations from the International Special Committee on Radio Interference (CISPR), a section of the International Electrotechnical Commission (IEC). The conformity of equipment with the EMC requirement is obligatory before it can be put on sale on national or international markets [103].

Since October 1983, any computing device or equipment, manufactured in or outside the USA, must conform to the FCC legislation (FCC docket no. 20780 part 15J) before being marketed in USA. Prior to the FCC issuing its rule, the DoD imposed emission limits on electronic systems to prevent EMI through MIL-STD-461. In 1985, CISPR also published a set of emission standards (referred to as CISPR 22) that concern information technology equipment (ITE) which includes digital devices. Both documents cover two classes of equipment Class A (i.e. commercial, business and industrial equipment) and Class B (i.e. home and residential equipment). CISPR radiated emission limits for Class A and Class B equipment are given in Appendix A and B respectively.

In May 1989, the European committee for electrotechnical standards (CENELEC) issued a directive 89/336/EEC (based on the recommendations of CISPR) to which all member states have to comply. The directive is due to be enforced by January, 1996 [103]. It states that all electrical and electronic equipment to be marketed in the member countries of

the European Union affixing a *CE* mark on them, must satisfy the emission and susceptibility limits.

In addition to the EMC limits, the recommendations on standard test methods and instruments are made by the regulating bodies such as American Society for Tests and Measurements (ASTM) in USA, National Electrical Manufacturers Association (NEMA), the National Measurement Accreditation Service (NAMAS) and DTI in UK, and the Japanese Standard Organisation (JIS) in Japan.

1.3 EQUIPMENT EMC

Various sources of EMC problems in a piece of electronic equipment are for examples:

- cables
- PCB
- connectors
- components
- power supplies
- enclosure
- relays, switches, and motors

Eliminating or minimising EMC problems associated with these sources can help reduce EMC problems in the equipment.

1.3.1 CABLES

Two pieces of equipment (or two PCBs within a single piece of equipment) may communicate with each other through cable. A cable may consist of two or more conductors. If the cable is not shielded, it may act as a transmitting antenna (i.e. an emitter) or a receiving antenna (i.e. a receptor). Thus a cable can create serious EMI problems (both conducted and radiated) in equipment. For example, the use of unshielded cables in local area networks (LANs), intended to support digital data transmission, often causes severe EMC problems [102]. One effect is system lockup or freezeup, where the user's equipment fails to communicate with other system components because it cannot transfer data without errors. Multiconductor cable causes crosstalk problems. Such problems can degrade the functional performance of a circuit. A powerline cable causes conducted EMI problem in equipment.

1.3.2 PCB

PCBs present two major EMC problems: the on-board problems associated with crosstalk and ground coupling, and the off board problems from radiated and conducted emission and susceptibility [29, 136, 138].

1.3.2.1 Grounding

The conventional notation of "Ground" is a zero impedance, equipotential surface. However, at a high frequency (above 30 MHz), this definition is no longer valid as the inductance of a ground conductor (track) provides a significant amount of ground impedance [97, 139]. Therefore, any current flowing through this impedance produces ground noise that eventually increases the noise coupling and the radiated emission from a cable shield or a PCB track connected to the ground.

1.3.2.2 Crosstalk

Tracks on a PCB are generally routed in close proximity to each other to make maximum use of available board space. Signals on a pair of tracks (or between a track and a ground plane) are electromagnetically coupled to adjacent tracks, inducing signals onto the circuits connected to the adjacent tracks. This coupling is referred to as crosstalk. High levels of induced signal (crosstalk) can degrade functional performance of the circuits that are on the board or attached (via cables) to the board.

1.3.2.3 Susceptibility

Susceptibility is the inability of a device, equipment, or system to perform without degradation in the presence of electromagnetic disturbance [100]. The coupling of external EM fields onto a victim circuit is a function of the polarisation, strength and wavelength of the incident field, and the loop area and characteristic impedance of the circuit, as well as its loads [29]. This coupling can cause serious EMI problems which result in improper functioning of the circuit itself.

1.3.2.4 Radiated emission

A PCB track acts as a bare wire, thus any RF current flowing in a track can produce spurious radiated emission. Two types of radiated emission, differential mode (DM) and common mode (CM) radiation, are generally found in a PCB. DM radiation is the result of current flowing around a loop formed by tracks in a PCB. This type of radiation depends on the loop area, loop currents and frequency [5, 7, 97].

CM radiation is due to CM current. The CM current is due to the undesired voltage drops in the circuit and the asymmetrical placement of the voltage source between two parallel tracks in a PCB [20, 41]. This causes some parts of the system to be at a common mode potential above the true ground. CM radiation also depends on the frequency and track length [5, 97].

1.3.3 CONNECTORS

Connectors are the interfacing and mating device between cables and other devices or equipment. Connectors can cause EMI by circuit geometric discontinuities because of the following [58]:

- (i) poor mating contact, which develops varying contact potentials with resulting broadband noise;
- (ii) formation of local circuits of inductance and capacitance having natural resonant and anti resonant frequencies in the passband of other circuits;
- (iii) formation of lumped impedance discontinuities at certain points in the circuit, which cause reflection and standing waves.

Thomas [83] has shown experimentally that the coupling between connector pins is a significant source of EMI.

1.3.4 COMPONENTS

Fundamental passive elements such as capacitors, inductors and resistors of an electronic circuit do not perform their intended functions at high frequency. This non-ideal behaviour arises because of their parasitic inductance and capacitance as illustrated by their frequency responses. For an example, a capacitor giving low impedance path at high frequency, is often

used to bypass or divert the undesired high frequency signal from a PCB track or from a cable where the signal may radiate efficiently. If the undesired signal frequency is above the self resonant frequency¹ of the capacitor then the capacitor behaves as an inductor. Thus the desired low impedance path will not be realized [97]. These elements produce potential EMI problems.

The discrete active components of an electronic circuit may be classified into three groups namely the bipolar transistor, the operational amplifier and the field effect transistor (e.g. CMOS and MOSFET). All such components have inherent noise generation mechanisms such as shot noise, popcorn noise and thermal noise. In semiconductors, shot noise is due to random diffusion of carriers through the base of a transistor and the random generation and recombination of hole electron pairs whereas the popcorn noise is caused by a defect in the junction usually a metallic impurity of a semiconductor device [139]. They adversely affect the EMC characteristics of the equipment [29].

In a digital circuit, all integrated circuit (IC) logics are potential EMI sources [58]. The characteristics of various logic families are given in Table TB2 of Appendix B.

1.3.5 POWER SUPPLIES

Power supplies, particularly switched mode power supplies (SMPS) often present EMC problems. For example, the normal switching frequency of a SMPS varies from 20 kHz to 200 kHz. Unwanted EMI may be generated at the switching frequency and its numerous harmonics, up to several hundred MHz. Bowles and Paul [76], for example, have shown that the spikes caused by reflections on long length PCB tracks, attached to a SMPS, produce high frequency signals that may radiate and cause interference with other electronic subsystems.

1.3.6 ENCLOSURE

An electronic circuit is generally housed in a shielded enclosure in order to avoid any unwanted interference to or from the circuit. Enclosures may have many apertures for ventilation, power lines, connectors, front panel seams and for various other reasons [119]. These apertures degrade the shielding performance of the enclosure and consequently increase EMI problems (both emission and susceptibility) in the equipment.

¹Self resonant frequency (f_{rc}) is expressed as: $f_{rc} = 1/2\pi(L_{lead}C)$, where L_{lead} is the lead inductance and C is the capacitance.

On the other hand a metallic or a metallised plastic enclosure acts as a cavity resonator whose resonance frequency depends on size and shape of the enclosure. Within the enclosure, the radiated EM field from the circuit will be reflected backwards and forwards. As a result a standing wave pattern will be set up. At resonance it may become strong and increase the EMI problems in the equipment [157].

1.3.7 RELAYS, SWITCHES AND MOTORS

Electromagnetic relays and switches are capable of generating EMI problems in equipment. For an example, during the de-energising of a relay, an arc developed at the switch contact may conduct or radiate broadband transient noise [54].

The use of brushes and a commutator in a motor produces broadband EMI problems (up to 100 MHz or higher). It is caused by the transient developed as a result of an arc discharge upon the separation of the rotating brush-commutator interface [54, 58].

1.4 WAYS TO ACHIEVE EMC REQUIREMENTS

Once the emissions and susceptibility standards of electronic equipment are specified, manufacturers can achieve the required level of EM compliance of their product by reducing or controlling EMI problems at the source level. For example,

- the use of shielded cable could reduce radiated emission from the equipment;
- filtering could attenuate the conducted EMI problems through a cable (e.g. powerline cable, DC power cords);
- the common impedance coupling between two subsystems in the equipment can be avoided by the use of a common mode choke, an isolation transformer or an optical coupler [107];
- the use of twisted-pair wire could decrease the crosstalk problem in a cable [97];
- suppression of EMI problems in the design process of components such as ICs, transistors, op-amplifier [139];
- in case of a PCB, proper design of the signal flow path (i.e. track routing), the PCB layout (component placement), the grounding as well as the

application of multilayer techniques could improve EMC performance of the equipment [97, 107, 58, 54];

- proper choices of logic families could minimise emission from the equipment;
- EMI problems due to SMPS can be controlled by the use of a filter at the main inlet of the circuit. Enclosing the SMPS within a shielded box is also advisable [107];
- the use of a solid-state switch or a solid-state relay could eliminate the arc effect in a switch or a relay and hence decrease EMI problems in the equipment [54];
- the low resistivity brush material, the provision of shielding in brushes and brush lead and the frequent replacement of brush could reduce EMI problems in a motor [58];
- the proper choice of enclosure material, and aperture planning (i.e. size, shape and relative position of the aperture) improves the shielding performance of an enclosure and consequently reduces EMI problems in the equipment [102]. At the enclosure resonances the radiation could be reduced by the use of lossy material (electric or magnetic field absorber) within the enclosure to dampen the enclosure resonance [157].

Obviously, many EMC problems can be effectively tackled during the design process. This research addressed the PCB as a source of EMC problems and attempted to produce a computer-aided **design** package that incorporated EMC factors alongside electrical and layout considerations.

1.5 PCB DESIGN WITH EMC

Various factors that affect the radiated emission from a PCB are: (i) layout (ii) dimensions of a track and its routing on the board (iii) grounding and (iv) the characteristics of the propagating signal (e.g. clock or data signal) along the track.

Designing a PCB layout with EMC in mind is a first and obvious step. In designing the circuit layout on the board, analogue circuits should be separated from digital circuits as much as possible to avoid common impedance coupling and spurious radiation. The use of different places on the PCB for high, medium and low speed logic circuits is also recommended [54, 107]. A clock oscillator should be placed as close as possible to the logic circuit so that the track carrying clock signal will be short. Connectors should be separated as far as possible

from the clock oscillator. If a clock oscillator is located near a cable connector on a PCB then the radiated EM fields from the clock signal may be incident on the cable wires causing radiated emission from the cable. Thus simply moving the connector away from the oscillator or the oscillator away from the connector may reduce the radiated emission.

PCB radiation (both DM and CM radiation) depends among other factors on the track routing and track size. Track separation to width ratio also plays an important role in minimising the radiated emission [17]. Efficient track routing is therefore essential. The circuit loop should also be minimised. Routing a dedicated ground track very close to the signal track can reduce the loop area because the majority of the signal current will return on the track closest to the signal track [54, 97, 138].

In a real PCB, routing the return track for every signal track in this manner may not be possible. However a ground grid or ground plane can solve this problem. A ground grid or ground plane provides a large number of alternative paths, so that the signal can choose a return path closest to the signal path, thereby reducing the return path inductance [138]. Thus a well-designed ground grid or a ground plane can reduce the radiated emission from a PCB [74, 138, 151].

High speed logic families are generally used in present day digital circuits. In such circuits, the waveforms of primary importance are those which represent clock or digital signals. These signals are represented in the form of pulses. The transition between each state (i.e. the pulse rise and fall times) tends to be extraordinarily fast (of order of 1 to 20 ns). These fast transitions generate high frequency (HF) spectral content in the frequency domain representation of such signals and contribute to the radiated emissions. The radiated emission due to the HF spectral content could be reduced by controlling or properly choosing the pulse rise time and fall times without disturbing the functional performance of the circuit. The designer can reduce the emission by increasing the rise and fall times of the clock signal (e.g. by inserting a resistor in series with the clock oscillator output [97]). In the design process, the designer can make provision (e.g. pads or holes may be placed in series with a track which is connected to clock output) for later insertion of a series resistor.

On the other hand, for 50 % duty cycle of a pulse, there will be no even harmonics of the pulse and therefore no emission at these harmonic frequencies [97]. However in practice it is not possible to produce an exact 50 % duty cycle. To minimise the radiated emission due to even harmonics of a clock or digital signal one should keep the duty cycle close to 50 %.

The suppression of harmonics generated by the clock signal may be necessary for the product to comply with the EMC limit and this can be done by placing a filter at the output of the clock oscillator. During the PCB design, the designer can keep provisions to insert a filter at the output stage of the oscillator.

1.6 PROBLEM STATEMENT AND PROPOSED SOLUTION

EMC problems can cause delays in a product's development schedule if one does not pay attention to these problems during the design process. Generally, at the end of the development schedule the product is tested for its compliance with the mandatory EMC requirements.

Section 1.3 outlined the various sources of EMI problems in a piece of electronic equipment where the PCB is one of the significant sources. EMI problems due to such a source can be reduced in the design process so that the designer can achieve a sufficient level of compliance with mandatory EMC requirements for the equipment. Hence pre-compliance "testing" of a PCB is necessary. Two possible routes for this testing are: (1) prototype without hardware (soft) and (2) prototype with hardware. Routes are shown in Fig. 1.3.

Route 2 as shown in Fig. 1.3 (b) involves measurement of radiation from a PCB. If radiation exceeds the acceptable limit, the PCB has to be redesigned and rebuilt to bring the radiation within the mandatory limit. This causes delay in the product's development schedule and also increases the product's development cost as it involves: (i) repetitive measurements of PCB radiation, (ii) redesigning of the circuit and the PCB and (iii) rebuilding of the PCB.

Moreover it is very difficult to diagnose the source of the problem while performing the test. Thus manufacturers are now very interested in incorporating PCB EMC verification with the soft design process of their products. In this thesis a solution, using route 1, is proposed, investigated and described.

Route 1 (Fig. 1.3 (a)) is a soft design iterative process towards achieving mandatory EMC performance of electronic product. If the predicted radiation exceeds the mandatory EMC requirement then the designer can modify the design where this requirement has not been met.

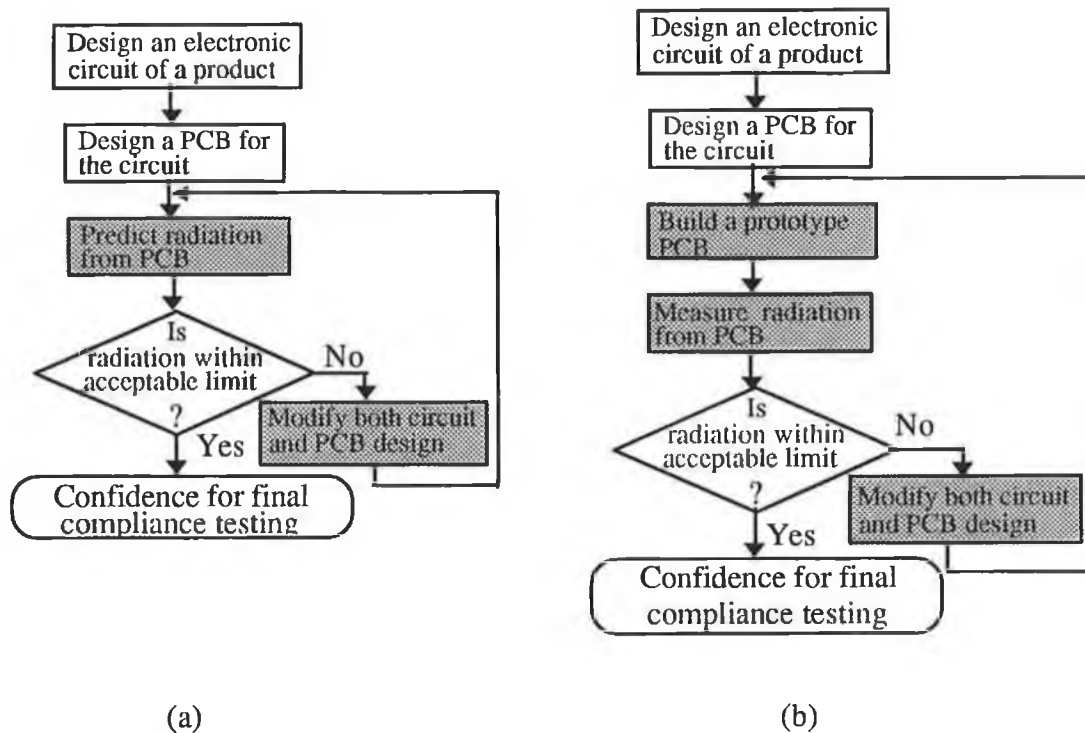


Fig. 1.3 Pre compliance "test" routes: (a) without hardware (soft) and (b) with hardware.

1.7 BENEFITS

Route 1 can be viewed as a supporting tool for EMC verification for the design engineer having only a little EMC background. Moreover it will be helpful to the experienced design engineer.

Also early and continuous EMC verification has many advantages such as:

- (i) minimising the additional cost which would be required to redesign the circuit in order to meet the mandatory EMC requirement;
- (ii) maintaining the product development schedule;
- (iii) ensuring satisfactory operation of the circuit itself.

1.8 AIM AND OBJECTIVES OF THIS RESEARCH

This work was primarily aimed at predicting and reducing PCB radiation in the design process of electronic products. In order to fulfil the aim, the following objectives were envisaged :

- development of a composite CAD package by combining an EM computation tool (Numerical electromagnetic code (NEC version 2)) with other circuit design packages;
- modification of the existing NEC-2;
- extraction of geometrical and electrical data from circuit design packages;
- automating the preparation of input files for a circuit simulation package;
- automating the implementation of geometrical modelling rules and segmentation schemes;
- incorporation of various techniques to reduce PCB radiation with the composite CAD package;
- theoretical validation of the use of NEC-2 for the present application;
- experimental validation of the composite CAD predicted radiation.

Other objectives which arose in the course of the work were as follows:

- extension of the use of transmission line modelling (TLM) for predicting PCB radiation;
- reduction of PCB radiation by providing shielding in an appropriate section of the PCB;
- finding a optimum layout which could minimise EM radiation from a PCB;
- finding the field maximum position in a shielded room.
- measurement of EM radiation from a PCB in a shielded room by damping room resonance;

1.9 CONTRIBUTION FROM THIS RESEARCH

The following contributions were made in this research :

- a composite CAD package by combining NEC-2, ORCAD™(a schematic design package), Boardmaker™ (a PCB layout design tool) and PSPICE™ (a circuit simulation tool);

- geometrical and electrical data (node voltage, frequency) extraction algorithm;
- algorithm to automate the geometrical modelling rules and segmentation schemes for EM analysis of a radiating structure with NEC-2;
- algorithm for incorporating various techniques intended to reduce or minimise EM radiation with the composite CAD package;
- algorithm to find an appropriate section of the PCB where shielding would be necessary;
- exact expressions for the radiated fields (electric and magnetic), in the extended TLM;
- a guideline for optimum layout;
- theoretical formulation to find the field maximum position in a shielded room.

1.10 ORGANISATION OF THIS THESIS

This thesis is organised into eight chapters, the layout of which is shown in Fig 1.4. The background to the work has been described briefly in this introductory chapter.

Chapter 2 presents a critical survey in quest of a suitable technique and an EM computation tool for predicting PCB radiation. Various software tools for EM analysis of a radiating structure are studied with a view to determining their applicability for this work. Various techniques for predicting PCB radiation are also reviewed in this chapter. Emission measurement techniques are reviewed to find a suitable technique for measurement of PCB radiation.

Chapter 3 contains the theoretical background of the EM computation tool (NEC-2). To predict EM radiation from a PCB using this tool, the simulation of a PCB as a loaded wire structure is described. To automate the geometrical modelling and segmentation schemes of a wire structure, an algorithm is proposed and discussed. The predicted EM radiation from a sample PCB using NEC-2 is presented.

Theoretical validation of the EM computation tool used for this work is presented in chapter 4. The well known transmission line modelling (TLM) technique was extended for this application and is described here. The effect of displacement current in PCB radiation is presented. The TLM predicted radiation is then compared with that obtained from NEC-2.

Chapter 5 describes the proposed composite CAD package. It was necessary to extract the geometrical, load and electrical data from circuit design packages (e.g. ORCAD™, PSPICE™ and Boardmaker™) and data extraction algorithms are presented. By providing shielding in some part of the PCB, radiation can be reduced. An algorithm is described to find the part of a circuit where shielding is necessary. An analysis to minimise EM radiation from a PCB with respect to s/w ratio is also presented.

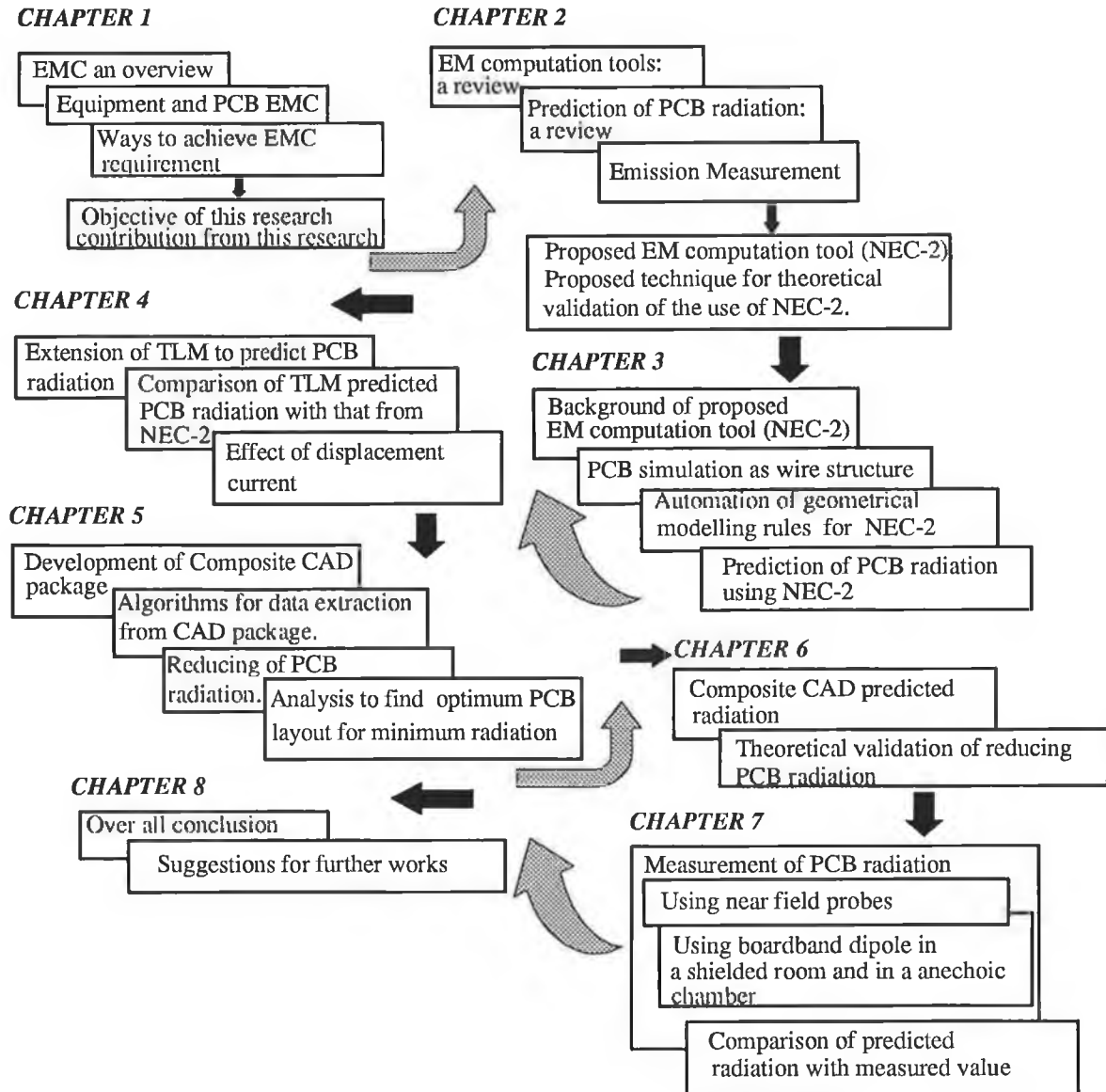


Fig. 1.9 The scope of this work and the layout of the thesis.

Chapter 6 presents the composite CAD predicted EM radiation from different PCBs. It also contains theoretical validations of the reduction/ minimisation of PCB radiation.

Chapter 7 presents the experimental validation for: (i) the composite CAD package described in this work (ii) the extended TLM used to predict PCB radiation and (iii) the optimum layout for minimum radiation. Radiation measurements were performed by near field probes and broadband dipoles with different PCBs and methods of measurement are described. The experimental results are then compared with the theoretical results obtained in chapters 4 and 6 respectively.

Chapter 8 contains the overall conclusions. Future development and the extension of the current work are also discussed.

Chapter 2

PCB RADIATION: PREDICTION TECHNIQUES AND MEASUREMENT

- ❑ EM COMPUTATION SOFTWARE TOOLS
- ❑ VARIOUS TECHNIQUES FOR PREDICTING PCB RADIATION
- ❑ CIRCUIT DESIGN PROCESS AND SOFTWARE
- ❑ PROPOSED TECHNIQUE TO PREDICT PCB RADIATION
- ❑ VARIOUS METHODS FOR MEASUREMENT OF PCB RADIATION

2.0 INTRODUCTION

This chapter describes various EM computation software tools, techniques for predicting PCB radiation, circuit design process and standard emission measurement methods.

The distinction between near and far field regions is described in section 2.2. EM computation software tools and techniques are reviewed in sections 2.3 and 2.4 respectively. A brief description of the circuit design process is given in section 2.5.

Since no software package is available for prediction of PCB radiation in the design process of an electronic circuit, a rationalised approach is presented in section 2.6. This section describes the proposed technique and its theoretical validation. In order to validate the predicted PCB radiation experimentally various emission measurement techniques are described in section 2.7.

2.2 FIELD REGION

In antenna theory, the space surrounding an antenna or a radiator is usually divided into three regions: (a) reactive near field, (b) radiating near-field (referred to as Fresnel region) and (c) radiated far field (referred to as Fraunhofer region) region. These regions are illustrated in Fig. 2.1. Various criteria have been given to define the boundaries separating these regions [98].

The boundaries are based on the radial distance (R) from the source (radiator) to an observation point as

$$\text{reactive near field region : } R < 0.62 \sqrt{\frac{D^3}{\lambda}} \quad (2.1a)$$

$$\text{radiating near field region : } \frac{2D^2}{\lambda} > R \geq 0.62 \sqrt{\frac{D^3}{\lambda}} \quad (2.1b)$$

$$\text{radiating far field region : } \infty \geq R \geq \frac{2D^2}{\lambda} \quad (2.1c)$$

where, D is the largest dimension of the radiator (or antenna) and λ is the wavelength.

These boundaries for separating the field region are valid for $D \gg \lambda$.

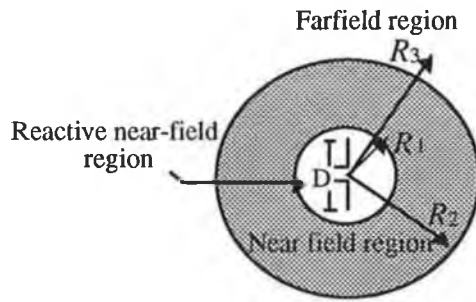


Fig. 2.1 Field regions of a radiator (e.g. an antenna) [98].

Radiated near field and far field regions are also of common interest in EMC problems. Some EMC handbooks [58] often use a boundary line for separating these regions based on the value of $\lambda / 2\pi$ as

$$\text{radiated near field region} \quad : \quad R \leq \lambda / 2\pi \quad (2.2a)$$

$$\text{radiated far field region} \quad : \quad R \geq \lambda / 2\pi \quad (2.2b)$$

The region around the boundary ($R = \lambda/2\pi$) should be considered as a transition region and the regions known as "near" and "far field" are considered to be at some distance away from the boundary. For example, Chatterton [107] conservatively defines the regions (see Fig. 2.2) as

$$\text{radiated near field region} \quad : \quad R \leq 0.1 \lambda / 2\pi \quad (2.3a)$$

$$\text{radiated far field region} \quad : \quad R \geq 10 \lambda / 2\pi \quad (2.3b)$$

with the transition region:

$$0.1 \lambda / 2\pi < R < 10 \lambda / 2\pi \quad (2.3c)$$

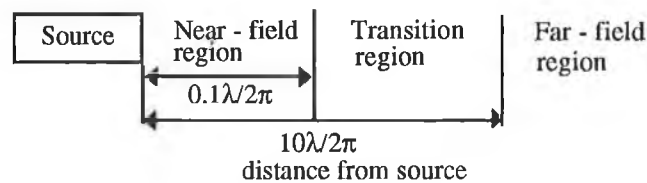


Fig. 2.2 Distinction of field regions.

These divisions are important when making approximations for calculating the shielding behaviour of a material.

2.3 EM COMPUTATION SOFTWARE TOOLS

The development of software tools for EM computation and analysis is an ongoing activity within the area of EMC research. Both new requirements and improved computational techniques contribute to the proliferation of software tools. A few software tools that are commonly used in EM analysis of an electronic system are described briefly in the following subsections.

2.3.1 GEMACS

GEMACS [114] is an acronym for "general electromagnetic model for the analysis of complex systems". It was originally developed at Rome Air Development Center, New York, USA. GEMACS uses the method of moments (MoM) technique to solve Maxwell's equations for an arbitrary geometry of radiators and scatterers. It provides for the modelling and characterisation of large systems in terms of near-field and far-field radiation patterns. GEMACS allows one to predict the coupling between a large number of collocated antennas, and the input impedances of antennas in large radiating systems. In this model the actual geometry is represented by thin wires. The model considers that current exists only on the wire axis; the azimuthal variation of current or radial component of current has been neglected. Currents can be determined only at specific points along conductors.

2.3.2 SEMCAP AND IEMCAP

SEMCAP [54, 55] is an acronym for "system and electromagnetic compatibility analysis programme" and IEMCAP is an acronym for "intrasystem electromagnetic compatibility analysis programme". SEMCAP was originally developed at TRW System Group, USA and IEMCAP was developed at Rome Air Development Center, USA. These programs analyse the coupling on a wire, due to "wire to wire" and "field to wire" interaction in several different configurations.

The process to determine the total system compatibility using either SEMCAP or IEMCAP is described in Fig. 2.3. In the software, the interference sources are analysed by calculating their spectrum and the EM energy transferred from them through transfer functions to the victims (i.e. receptor circuit). The received spectrum is limited by the receptor bandwidth. This spectrum is integrated over the frequency range in question. The integral then represents the voltage available at the receptor terminals. The received voltage is then

compared to the threshold of the particular receptor circuit to determine compatibility. Both programs utilise transfer functions which describe the received voltage at the receptor terminals in terms of the source interference output. Source outputs are described as E-field, H-field, current and voltage of the source [55]. Both programs are system oriented programs and do not analyse down to the circuit level. The capabilities of these programs and a guide to the selection of programs that are best suited to a user's requirements are summarised by Keiser [54].

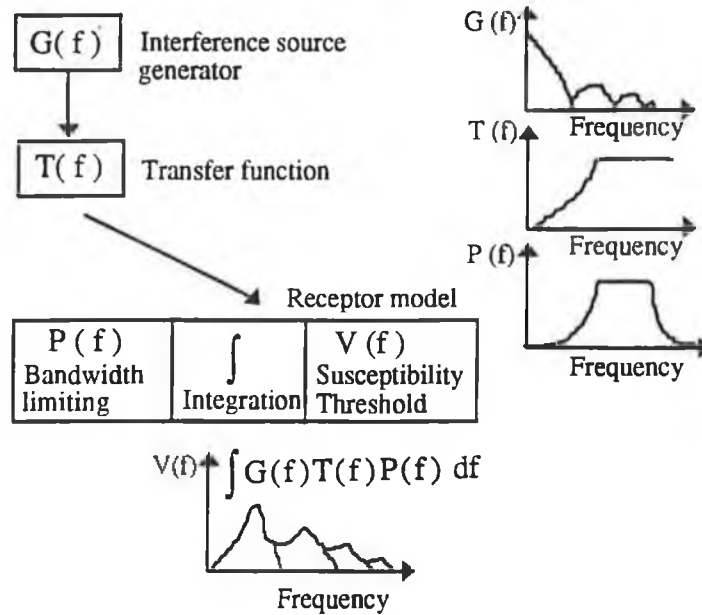


Fig. 2.3 Transfer function model used in SEMCAP and IEMCAP. Adapted from [55].

2.3.3 NEC PROGRAMME

NEC [111] is an acronym for "numerical electromagnetic code". This programme was originally developed at Lawrence Livermore Laboratory, USA. It is based on a numerical solution of integro-differential equations for the currents induced on a wire structure or a scattering object. The MoM is used to reduce the integro-differential equation to matrix equations. Excitation may be an applied voltage source or an incident plane wave. NEC provides outputs such as induced currents and charges, near or far zone electric or magnetic fields, and input impedance or admittance of an antenna. Other commonly used parameters such as gain, directivity and power budget (i.e. input power, radiated power, structure loss, network loss and efficiency) are also available. NEC can include non-radiating networks and

transmission lines, perfect and imperfect conductors, lumped element loading and a ground plane. The ground plane may be a perfect or an imperfect conductor. This programme has a facility to analyse a radiating structure very close to an imperfect ground.

2.3.4 MININEC

MININEC [56] is the PC version of NEC. The MININEC system can be used to model any arbitrary configuration of a thin wire radiating structure. The numerical solution in MININEC is somewhat different from the approach used in the NEC system. Here the MoM with the Galerkin procedure [56] is applied. In the Galerkin procedure the expansion or basis function is equal to the testing or weighting function. The calculated currents are then used to compute the near electric and magnetic fields and radiated far fields. The excitation can be an applied voltage source or an incident field. The MININEC can include a perfect or an imperfect ground. This programme uses the image method for evaluating the effect of an imperfect ground in radiation patterns of a wire antenna.

2.3.5 WIRE PROGRAMME

Wire programme [51, 52] was originally developed at Syracuse University, USA. This programme is based on the MoM to solve the integro-differential equation for determining the current distribution on a thin wire structure in free space. This method differs from the NEC programme in choosing the expansion and testing function of the MoM solution. The programme accepts wire configurations with voltage sources and loads as input and then calculates the radiation pattern, input impedance and near electric or magnetic fields.

2.4 METHODS TO PREDICT PCB RADIATION

Various methods are available to predict radiation from a PCB. Methods are divided into two categories: (i) analytical models, (ii) numerical models. Both methods are discussed in the following subsections.

2.4.1 ANALYTICAL MODELS

Analytical models for predicting the PCB radiation make many simplifying approximations to reduce the complexity of the problem. The models use antenna theory. They can be

subdivided into three groups: (i) simplified method, (ii) circuit concept approach and (iii) transmission line modelling (TLM).

2.4.1.1 Simplified method

This method is based on the field equations for a short dipole, monopole or a small loop antenna [4-8]. The following conditions have to be satisfied for predicting PCB radiation using this method,

- (i) PCB track length should be electrically short (i.e. less than one quarter wavelength at frequency of interest);
- (ii) track separation should be very short so that the loop perimeter becomes less than one quarter wavelength;
- (iii) current along the track should be uniform.

The DM radiation is modelled using a small circular loop. A simple equation (see Eqn. 2.4) that was originally developed for a small round loop carrying uniform current (see Fig. 2.4 (a)), is used to determine the magnitude of the radiated far electric field (E). Although Eqn. 2.4 was derived for a circular loop, it can be used for any shape, since "for a small loop the maximum radiation is insensitive to the shape but depends only on the area of the loop" [12].

$$E = 131.6 \times 10^{-16} \left[\frac{f^2 AI}{r} \right] \sin \theta \quad \text{V/m} \quad (2.4)$$

where,

- f – the frequency, [Hz]
- A – the area of a loop, [m²]
- I – the loop current, [A]
- r – the distance from loop to observation point, [m]

The CM radiation is modelled using a short monopole antenna driven by a voltage (i.e. the ground potential). The magnitude of the far electric field of such an antenna at a distance r (see Fig. 2.4 (b)) is given in [5] as

$$E = 4\pi \times 10^{-7} \left[\frac{f I_c l}{r} \right] \sin \theta \quad \text{V/m} \quad (2.5)$$

where,

I_c – the common mode current, [A]

l – the length of the monopole antenna (length of PCB track), [m]

When currents (i.e. differential and common mode currents) are known at a particular frequency of interest, Eqns. 2.4 and 2.5 can then be used to predict the radiation from a particular PCB. The DM current can be computed using a transmission line model (as well as lumped circuit model), whereas the CM current is not easy to compute. However, if one amends Kirchhoff's current law (KCL) to include displacement current, it can apply to CM current. The "return path" for CM current is through displacement current [6]. Here the common mode model solely depends on the measurement of CM current.

Both DM and CM radiation models are limited to far field conditions and the frequencies below 200 MHz [140]. Moreover a real PCB is a complex structure that may have a number of loops. In such cases the simplified method cannot be applied.

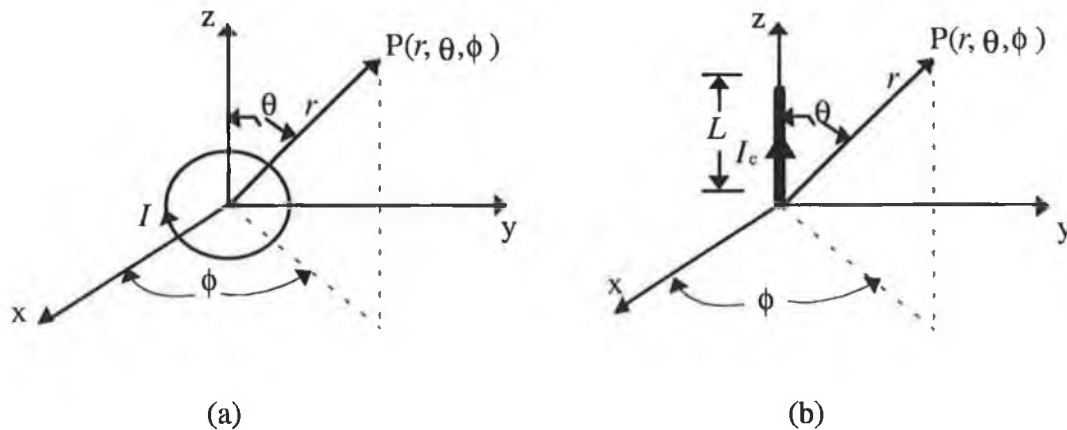


Fig. 2.4 Geometry of the field observation point: (a) a small circular loop in the x-y plane; (b) a z-directed short monopole over a ground plane.

2.4.1.2 Circuit concept approach

A circuit concept approach is presented by Kami and Sato [30-33] to predict radiation from a transmission line. This approach can be applied to predict radiation from PCB tracks that form a transmission line structure. This technique is based on the assumption of reciprocity

between coupling phenomena of an external plane wave and the radiation to and from the transmission line. The coupling phenomena can be expressed by the line equation (i.e. a set of differential equations, for line voltage and line current) [30]. A radiation model and its equivalent three port network is depicted in Fig. 2.5.

The impedance matrix of the network may then be determined by coupling analysis which in turn defines the radiation impedance matrix (reciprocity). Thereafter the radiated far field may be obtained. The same formulation can be applied for the analysis of a single cascaded bent line in both the frequency and time domains [30]. This model does not consider the effects of dielectric and the radiation due to the singularities at the bends. Thus the model is limited to two wire transmission lines or a single wire over a ground plane (as return path) in an homogeneous medium and far field radiation.

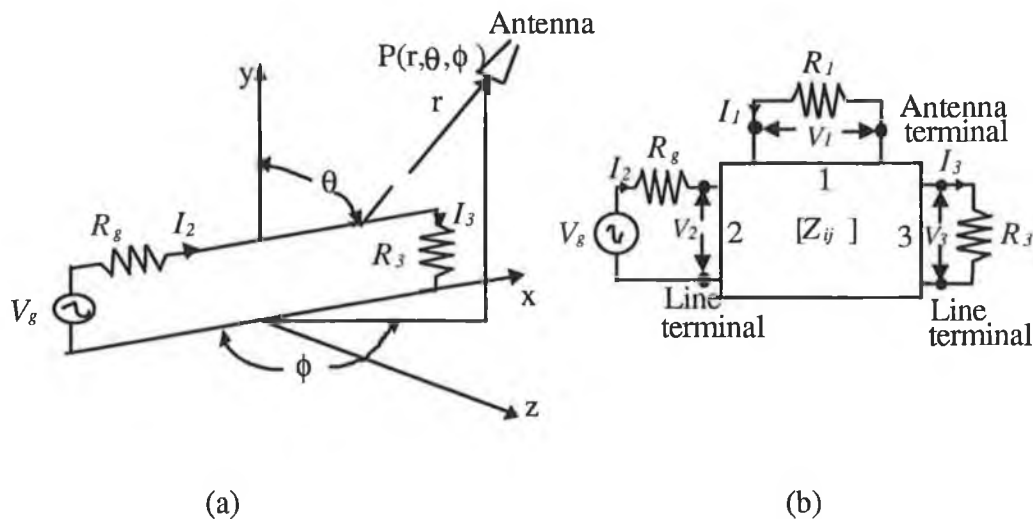


Fig. 2.5 Two wire transmission lines : (a) Radiation model ; (b) Equivalent three port network for the radiation model. Adapted from [30].

2.4.1.3 Transmission line modelling (TLM)

Researchers [16-20] have developed different models to predict radiation from a pair of tracks or a single track over a ground plane using TLM. Using TLM one computes the current distribution along a PCB track for a given source and load. The computed current is then used to calculate the magnetic vector potential at a distant point in free space. The radiated EM fields are then determined from the spatial derivative of the vector potentials. Different

approaches have been taken by researchers to cover different track configurations, termination and computational techniques.

Raut [16] presented an analysis to compute the radiated field from a pair of tracks running between two pairs of pins of two devices (e.g. integrated circuit (IC) chips) laid out on a PCB. In his formulation the devices are characterised by the output impedance of the driving device (source) and the input impedance of the driven device (load). The tracks are modelled as two wire transmission lines. The characteristic impedance (Z_0) of the transmission line is computed using the formula given in [21] as

$$Z_0 = \frac{120}{\sqrt{\epsilon_r}} \log_e \left[\frac{s}{w} + \left\{ \left(\frac{s}{w} \right)^2 - 1 \right\}^{\frac{1}{2}} \right] \quad \Omega \quad (2.6)$$

where,

- s - the track separation
- w - the track width
- ϵ_r - the relative dielectric constant of PCB substrate

Currents (i.e. source end current, load end current and current along track) are computed from transmission line equations. Later Raut proposed a numerical technique and developed computer code to compute radiated fields from the net vector potentials due to these currents at high frequencies.

Raut's method is limited to straight PCB track, wide separation between tracks and the EM radiation due to DM currents. It is widely accepted [5-7, 20, 46] that the radiated emission solely based on DM currents can severely underpredict the radiated emission. Raut used the free space propagation constant in the transmission line equations. However, since the dielectric is inherently present in a PCB, the effect of dielectric should not, and cannot be ignored for near field radiation.

Costa *et al.* [20], on the other hand considered both the DM and the CM radiated emission in his model. A formula given by Schelkunoff [22] was used to compute radiated field due to DM currents. Schelkunoff's formula for the radiated EM field in a cylindrical coordinate system was expressed in terms of track current and its derivatives at both ends of the track. The PCB tracks were divided into electrically small segments to compute the CM radiation. The length of each segment had to be very small compared to the wavelength and to

the distance from its centre to the observation point. This segment was then modelled as a Hertzian dipole carrying a uniform current that was obtained from the measurement of CM current.

Costa's model is limited to straight PCB track, measurement of common mode current and singlesided PCB. This model also assumes that the PCB track is immersed in an homogeneous medium. Unfortunately, this assumption is not valid as the PCB track is immersed in an inhomogeneous medium (i.e. PCB substrate and air).

A method for computing electric and magnetic fields from a PCB using TLM was also presented by Sistino [18]. Sistino's model considers the displacement current as well as the currents in the (source and load) end segments of the PCB track, the track current and its image. In a transmission line structure the displacement current is confined to the region between the two lines or a line and its image as shown in Fig. 2.6. All these currents are assumed to be known. The model computes the radiated field due to these currents under far field conditions. In the reference [18], radiated electric field was computed from a microstrip structure (a PCB track above ground plane as shown in Fig. 2.6) at frequencies 350 MHz and 701 MHz at a distance of 0.9 m ($> \lambda / 2\pi$, for both frequencies). It was found that at 350 MHz, the radiated electric field due to displacement current is larger than the field due to the track current and its image. On the other hand at 701 MHz, the main contributor to the radiated field was the track current and its image. Sistino explained that the radiation at far distances due to displacement current and due to the two end currents cancel each other because of the equation of current continuity. However the range of frequencies or distance within which the above observation remains valid is not apparent from the reference [18].

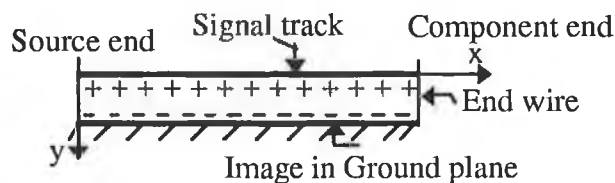


Fig. 2.6 A track in a PCB having a ground plane [18].

Sistino's model is limited to the far field condition, the known currents and the size of the loop. This model is not applicable to non-parallel PCB tracks.

Daijavad *et al.* [23] developed a model to predict the radiation from a multilayer PCB. Their model is based on TLM which they use to find the amplitude and spatial distribution of

currents in PCB tracks. Lumped equivalent circuit models based on full wave electromagnetic analysis are used to represent the bends, vias¹, and the circuit loads of a complex structure. The radiated far field is computed using Green's function for a current element just above or inside a thin dielectric sheet. Green's function was derived by adding the solution of the homogeneous Helmholtz equation to the free space Green's function, and then demanding continuity of the magnetic and tangential electric fields, as well as the normal component of electric displacement, on crossing the dielectric interface.

2.4.2 NUMERICAL MODELS

Numerical models solve Maxwell's equations with boundary condition to predict PCB radiation. Various numerical techniques include: the finite element method (FEM), the method of moments (MoM) and the finite difference time domain (FDTD) method.

2.4.2.1 Finite element method (FEM)

A simple radiation model for a PCB having a number of parallel tracks and ground plane was reported by Khan *et al.* [25]. In this model, the FEM is applied to determine the per unit length (PUL) inductance and capacitance matrices of a number of PCB tracks in multilayer dielectric regions. In FEM, the total region is subdivided into triangular shaped sub regions in which the field is approximated by first, second or higher order polynomial expressions. The simultaneous solution of these equations gives the field distribution from which the inductance and capacitance matrices can be calculated. Once these matrices are known, the currents along the tracks can be derived by modal analysis of transmission line equations in the frequency domain. The transmission line equations are generally described in terms of currents, voltages and PUL parameters. From the calculated currents, Khan *et al.* developed a simple far field radiation model over a frequency range of 30-1000 MHz. This model is limited to the computation of far field radiation and is not valid if the PCB has no ground plane.

2.4.2.2 Finite difference time domain (FDTD) method

An approach to predict the radiation from a digital circuit was presented by Railton *et al.* [27]. In computing the radiated field, the FDTD is applied to solve Maxwell's equations with boundary conditions. The FDTD method solves Maxwell's time-dependent curl equations

¹A via is simply a metallised hole through the board substrate.

directly in the time domain by converting them into finite-difference equations that are then solved in a time marching sequence by alternately calculating the electric and magnetic fields in an interlaced spatial grid [141].

The main difference between the FDTD method and the TLM method is that the FDTD method directly uses a finite difference form of Maxwell's equations, whereas the TLM method replaces the actual problem by an approximation, based on a network of transmission lines. This approximate problem is then solved exactly.

2.4.2.3 Method of moments (MoM)

The MoM is a numerical technique for solving complex integro-differential equations. This technique essentially transforms a general operator equation into a matrix equation which can be solved easily on a computer. There are many PCB radiation models based on this technique [36, 38, 40-42, 46-49]. Each model is discussed in the following paragraphs.

A mixed (scalar and vector) potential surface integral formulation, recently developed for microstrip antenna [42] was employed by Krishna and Berry [40, 41] to compute radiation from an arbitrarily shaped printed circuit track. The MoM is used to solve the integral equation. This technique is based on the dyadic vector potential Green's functions and Lorentz-gauge related scalar potential. These Green functions are simplified by near field approximation of vector and scalar potentials [40]. In order to compute the radiated field, the track current is modelled as a continuous array of x or y directed elemental dipoles. The radiated far-field from these elemental dipoles is determined from the expression of radiated field given by (Eqn.10, [40]). Since a PCB substrate is electrically thin, the surface wave is tightly bound to the air-dielectric interface and therefore does not contribute much to the total radiation. Therefore Krishna [41] computes the far field radiation due to the space wave. This type of formulation is most suitable for microstrip-like structure. The method does not consider the effect of components that are commonly found in a practical PCB.

An analysis to compute radiation from high frequency printed circuits, such as a microstrip circuit was presented by Gardiol [36]. This analysis is also based on the mixed potential integral equation (MPIE) formulation, with Green's function provided by Sommerfeld integrals. The use of this Green's function in the MPIE formulation gives an exact evaluation for the PCB radiation at high frequencies. Currents flowing in circuits are

developed over subsectional basis functions and computed by the MoM. This model is suitable for micro-strip like structure.

Cerri *et al.* [46] presented a rigorous model to compute both DM and CM radiation from a PCB. Regarding the DM radiation the analysis, is carried out using Green's function for a stratified medium [47, 48]. An integral equation for the evaluation of current distribution along the track is obtained by imposing the condition of a vanishing tangential component of the total electric field on the track. The solution of this integral equation is achieved by MoM. After determining the current distribution, the radiated far fields are computed by means of the stationary phase method². Regarding the CM radiation, the same analysis is carried out by the proper Green's function in free space. Cerri applied his formulation to a rectangular loop on a grounded dielectric substrate with particular attention to corners of the loop to assure the continuity of current at the edge.

Ungvichian and Perez-Rodriquez [38] proposed a wire modelling technique based on MoM to determine the EM radiation from a multilayer PCB in the frequency range 30-200 MHz. In this method a portion of the rectangular track carrying the high frequency clock signal, board ground plane and reflecting ground plane is modelled using several straight round wires. These wires form a radiating structure. The components connected to the clock tracks are represented by their input capacitances. Since the effect of dielectric is neglected, the model is limited to predicting the far field radiation from a PCB.

Hubing and Kaufman [49] presented an end driven wire modelling technique to determine the EM radiation from an electrically small table-top product (e.g. video display terminal). This technique is based on the use of moment method programs (e.g. NEC, WIRE) which were originally developed for wire antenna modelling. The analysis of electrically small table-top product using this technique involves a two step process. In the first step, the product has to be reduced to its end driven wire equivalent, complete with lumped-element components and shields. In the second or last step, the equivalent end driven wire model is analysed using a MoM technique. This model cannot be used to analyse a product that is not electrically small at the frequency of interest, a product without a cable, a floor-standing product or a well-shielded product [49].

²The principle of stationary phase is the assertion that the major contribution to the integral (e.g. $\int_a^b g(t)e^{j\phi(t)} dt$) comes from points where the phase function ($\phi(t)$) is stationary i.e. where $\phi'(t)$ vanishes [158].

2.5 CIRCUIT DESIGN PROCESS

A circuit design is both science and art. A circuit design process may be represented as in Fig. 2.7, with three stages namely schematic design, circuit analysis and layout design.

Generally one starts with the schematic of a circuit produced using a CAD package. Several schematic design packages are now commercially available. Examples of such packages are Mentor™, Schema™, Easy-PC professional™, Ranger-1™ and ORCAD™. These packages can be used in conjunction with other design packages such as circuit simulation tools and PCB layout tools.

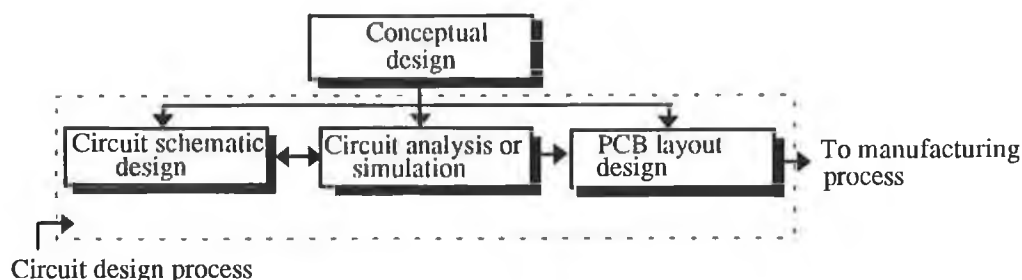


Fig. 2.7 Circuit design process.

Circuit analysis is the heart of designing a circuit. Computer-aided circuit analysis became popular in the mid 1960s. IBM³ developed the first Electronic Circuit Analysis Program (ECAP™). Other well-known circuit analysis programs are SPICE™, PSPICE™ (PC version of SPICE™), Mentor™ and ASTP™. All are capable of analysing an analogue circuit. An electronic circuit may have both analogue and digital parts. Two types of circuit simulation software packages are obviously required to analyse such a circuit: (i) analogue simulation for analogue part and (ii) digital simulation for digital part of the circuit. An example of a digital circuit simulation is PULSAR™ developed by Number One Systems Ltd. UK [137].

A number of software packages are commercially available for PCB layout (i.e. component placement and track routing). Some examples are ULTIboard™, Easy-PC professional™, Ranger 1™ and Boardmaker™ (BM).

³International Business Machine.

2.6 PROPOSED TECHNIQUE AND THEORETICAL VALIDATION

A thorough review of the existing EM computation tools as mentioned in section 2.3 reveals that none of these tools is related to the circuit design packages such as schematic design, circuit simulation and PCB layout design packages. From the review it was seen that various analytical models as well as numerical models (stated in section 2.4) used for predicting the PCB radiation are also not related to the circuit design packages. Moreover none of the aforementioned circuit design packages considers EMC verification at the design stage.

On the other hand, inclusion of PCB EMC verification in the circuit design process is necessary as stated in section 1.6. Thus this research proposed a technique to predict PCB radiation using an EM computation tool with other circuit design packages. This approach is illustrated in Fig. 2.8.

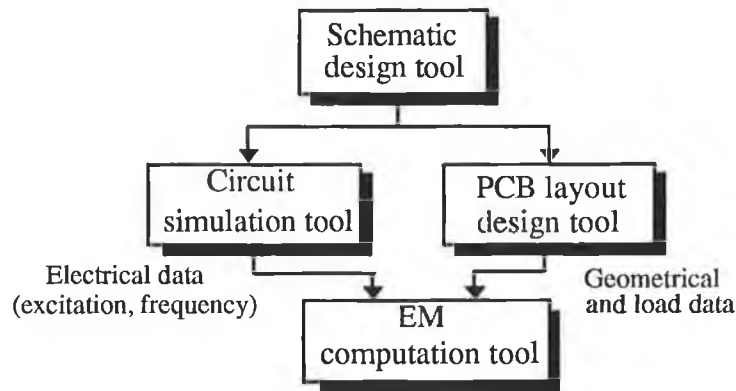


Fig. 2.8 Block diagram to predict PCB radiation using an EM computation tool with other circuit design packages.

From the review of the existing PCB radiation prediction techniques (section 2.4.2.3, paragraph 5), it is known that a PCB track can be modelled as an equivalent round wire. The components connected to the track can be replaced by their input and output impedance (refer to sections 2.4.1.3 (paragraph 2), and 2.4.2.3 (paragraph 5)).

In this work, NEC (version 2) was the only software package for EM computation of a radiating structure available to the author. Moreover from the review of the existing EM computation tools (refer to section 2.3) it was concluded that NEC is suitable for EM analysis of an arbitrarily shaped wire structure very close to an imperfect ground. Therefore

this research study simulates the PCB (singlesided PCB) as a loaded thin wire structure just above (but not contacting) the surface of an imperfect ground.

Input data files for NEC-2 consist of geometrical data of a radiating structure, structure environment, loading data and electrical parameters (i.e. excitation and frequency). All the data required by NEC-2 can be obtained from circuit design packages. It is necessary to extract these data. By transferring these data to NEC-2, the radiation from a proposed PCB of an electronic circuit could be obtained.

It is necessary for some degree of theoretical validation of the use NEC-2 in this manner (as stated earlier). This can be done by comparing the NEC-2 predicted radiation with that obtained from a suitable analytical technique for predicting PCB radiation.

The comprehensive review of current techniques reveals that the TLM method although not analytically rigorous, provides good accuracy for EM computation. For this reason the TLM was employed as a second technique to predict PCB radiation. The existing TLM technique has been extended in this work. However the major weakness of TLM for predicting PCB radiation is in the application of complex geometries such as bends and vias in a PCB.

2.7 EMISSION MEASUREMENT

Measurement of radiated EMI from a piece of equipment is referred to as emission measurement. The purpose of such a measurement is necessary to validate the predicted emission.

Every standard that sets out limits on radiated emission (FCC, CISPR, MIL-STD-461 and EU Directive) has a related standard that clearly defines how the emission measurement has to be performed. These measurement standards include test procedures, instrumentation (test equipment and test antennas), and test methods. The emission measurement procedures that apply to the FCC and CISPR 22 requirements are described in [97]. Instrumentation and various recommended test methods are described briefly in the following subsections.

2.7.1 INSTRUMENTATION

Emission measuring systems generally use antennas and an EMI receiver or a spectrum analyser.

Various antennas are available for emission measurement such as dipole, biconical, log periodic, horn and loop antennas. These antennas are mainly employed for open field testing although they may also be used for measurement inside a shielded enclosure by taking certain precautions [58]. The selection of antenna depends on the type of field (i.e. electric or magnetic field) to be measured and the test frequency.

A spectrum analyser or an EMI receiver is primarily used for intercepting, displaying and examining a signal, or electrical noise activity over a wide frequency spectrum (e.g. the harmonic generated by an oscillator, RF heating or a digital signal). EMI measurement error can arise due to the spectrum analyser being driven into compression by high energy signals. This error can be lessened by placing a preselector in front of spectrum analyser [104]. A preselector has a tracking filter to reject the out of band interference significantly. Thus this enables the low-level signal to be monitored in the presence of high level ambient. A preamplifier can be used in conjunction with the EMI receivers or a spectrum analyser to amplify the received signal for better indication.

Automatic data acquisition in emission measuring system can increase the measurement accuracy and reduce the testing time and efforts [149]. This can be done by interfacing the test instruments with a computer through the IEEE-488 general purpose interface bus.

2.7.2 MEASUREMENT METHODS

Numerous standard measurement methods are available for performing EMC/EMI tests (e.g. emission measurement) depending on the following considerations [69]:

- (i) size of the test equipment;
- (ii) frequency range;
- (iii) test limits;
- (iv) types of field to be measured (electric or magnetic);
- (v) polarisation of the field;
- (vi) electrical characteristics of the test signal (frequency or time domain).

It is essential for valid measurement that it be carried out in a known EM environment. Three common test environments that are being employed for radiated emission (or susceptibility) measurements are as (i) open-field, (ii) shielded-anechoic chamber and (iii)

shielded room. Various methods which are commonly used for performing the radiated emission tests under these environments are as follows,

- (i) open area test site;
- (ii) shielded room;
- (iii) hooded antenna;
- (iv) transverse electromagnetic (TEM) cell;
- (v) reverberating chamber;
- (vi) anechoic chamber.

Each of these test methods has its own advantages and disadvantages, both technical and economical. Each method is described briefly in the following subsections.

2.7.2.1 Open area test site (OATS)

Open site measurement provides a straightforward approach for evaluating the EMI performance of electronic equipment. It is a convenient method for performing far field radiated emission measurement for a large system over a wide frequency range. A suitable test site will be clear of obstructions such as trees, metal fences, buildings and any reflecting object within an elliptical boundary. The area within the ellipse should be flat [60]. The regulating bodies such as CISPR, FCC and VDE have standardised a boundary for such a test site and the recommended dimensions of the site are shown in Fig. 2.9.

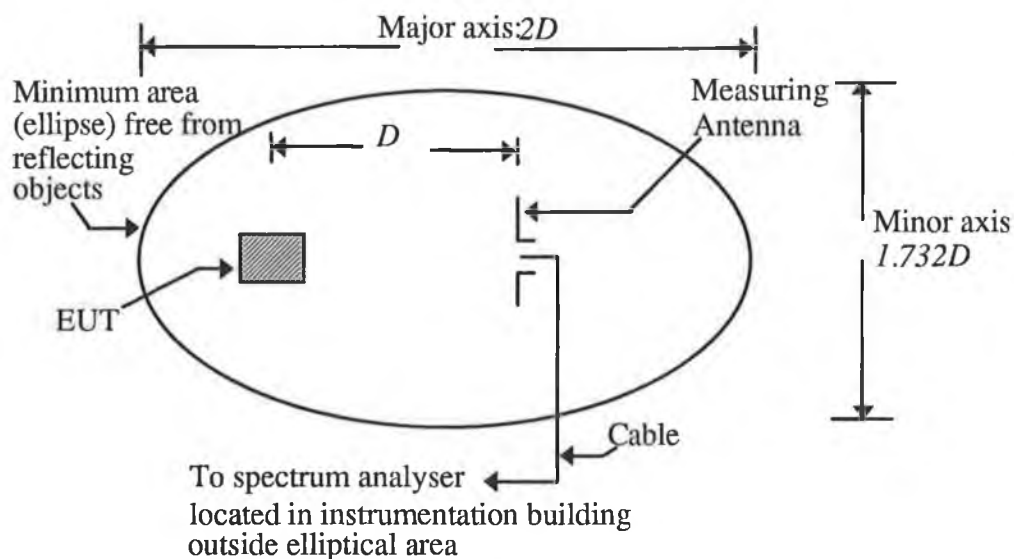


Fig. 2.9 Standardised test site for the measurement of radiated emission in OATS.

The recommended measuring distance (D) between equipment under test (EUT) and measuring antenna for different frequency range are described in [58]. The EUT is at a fixed height of 1 m or 2 m and the height of the measuring antenna varies from 1 to 6 m to obtain the maximum reception level.

2.7.2.2 Shielded room

To meet the specifications and standards for measurements of EMI characteristics, the test environment must be isolated from the EM environment. A shielded room can provide a high degree of isolation from the EM environment and local sources of interference. However the multiple paths of reflections from the room walls significantly affect the radiated measurement. A typical measurement set up in a shielded room depicting the multiple reflection from walls is shown in Fig. 2.10.

Due to the multiple reflection from the walls, the radiated measurement may be higher or lower than the actual measurement. This disagreement is due to the reflected field being added to or subtracted from the desired emission path from the source. Results from experimental investigations [62] have shown that errors in radiated measurement in a shielded room as great as ± 40 dB are possible at frequencies greater than 50 MHz.

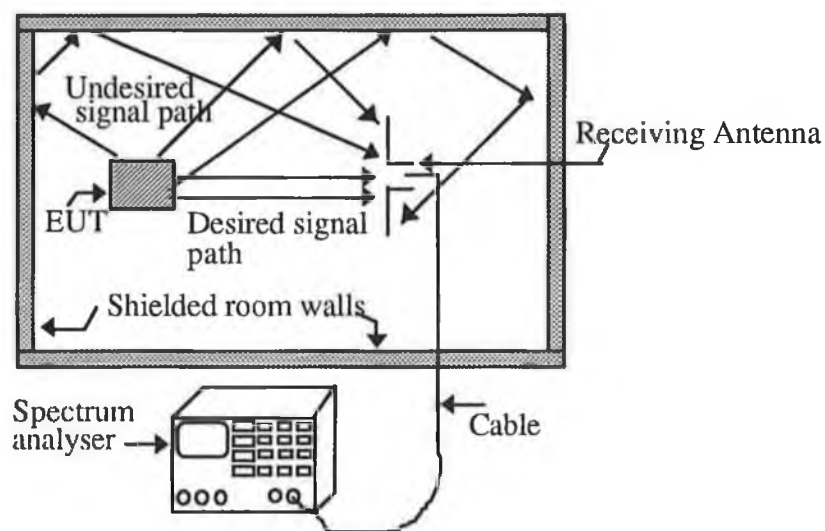


Fig. 2.10 Radiated EMI measurement set-up in a shielded room depicting the undesired reflection from room walls.

Two methods of improving the accuracy of measurement made in a shielded enclosure for frequency above 200 MHz are hooded antenna techniques [62] and room perturbation techniques [64]. A new method of measurement in a screened room by damping room resonance was recently recommended by Dawson [59] over the frequency range of 30 to 200 MHz.

2.7.2.3 Hooded antenna technique

In this method the emission measurement is also performed in a shielded room. The main difference between this method and shielded room measurement is that it can avoid the multiple reflection paths from room walls. This can be done by shielding the receiving antenna in all directions except the desired signal path from the EUT. From this concept a hooded antenna technique was developed and evaluated [62]. A hooded antenna measurement technique in a shielded room is shown in Fig. 2.11.

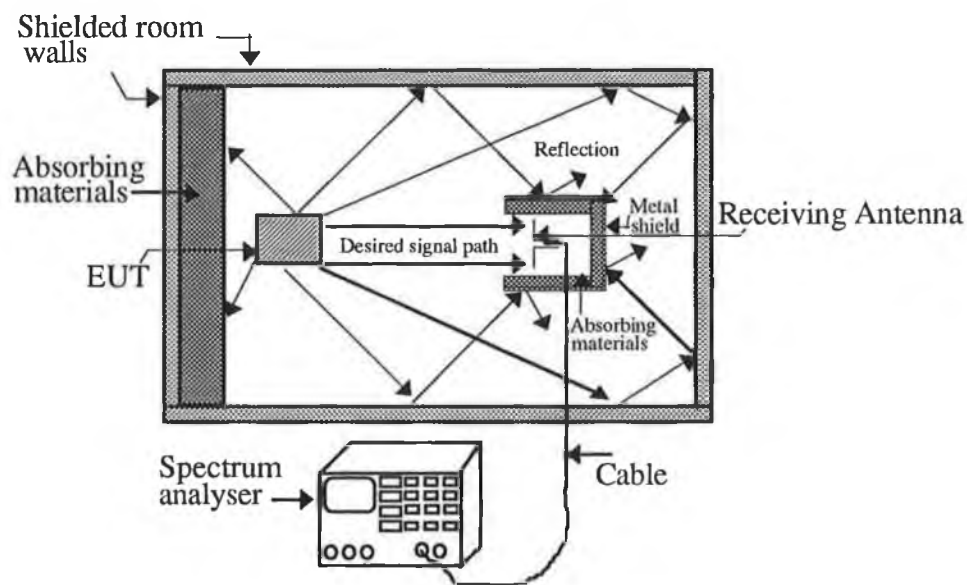


Fig. 2.11 Hooded antenna measurement set-up in a shielded room.

The receiving antenna hood is also a metal enclosure in which one end is open and the inside walls are lined with absorbing material to reduce reflection from the metal hood to the receiving antenna. The shielded room wall behind the EUT is also covered with absorbing material to prevent reflections from the back wall of the EUT to the receiving antenna.

2.7.2.4 TEM cell

A TEM cell typically consists of a section of rectangular coaxial transmission line tapered at each end to adapt to standard co-axial connectors as shown in Fig. 2.12. This cell also provides a high degree of isolation from the EM environment and local sources of interference but does not introduce the multiple reflection problems associated with the conventional shielded room.

Emission measurements in a TEM cell are made on the assumption of reciprocity [57]. The emissions from the EUT are coupled to the TEM mode of the cell and propagated to the cell's port. The RF energy at the port of the cell is used to determine the relative emission (as a function of frequency) of the EUT based on the receiver characteristic, and the impedance and coupling properties of the cell.

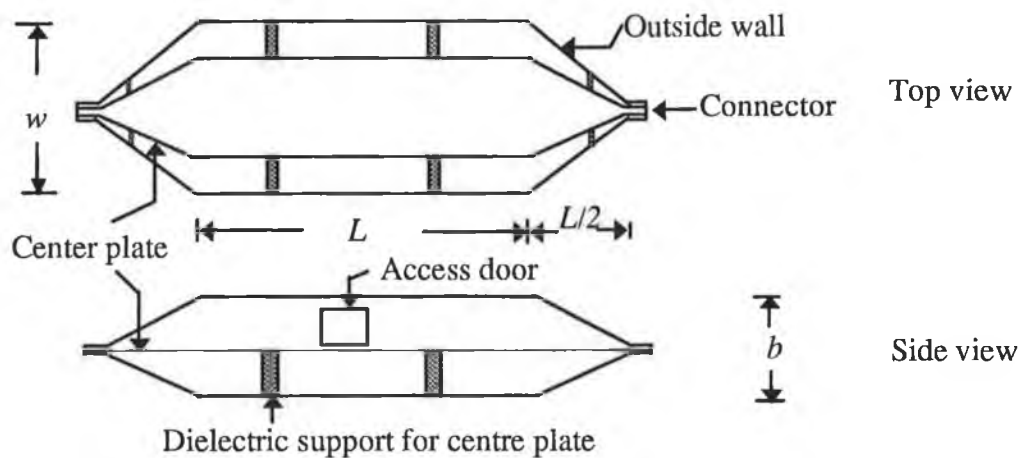


Fig. 2.12 Geometry of the cell, where $2L$ = length, w = width of the cell, and $0.5b$ = distance between the center plate and outer wall of the cell [57].

When the EUT is placed in a TEM cell, its radiation resistance is changed relative to its free-space radiation resistance. Thus a correction factor must be applied to determine the absolute magnitude of the emission from the EUT relative to free space [57].

To measure radiated emission in a TEM cell, an electrically small source (EUT) can be modelled by an equivalent dipole system consisting of three orthogonal electric dipoles and three orthogonal magnetic dipoles. The detailed radiation pattern and total power radiated from the EUT in free space can then be computed from the measured powers and phase by the

use of an algebraic relation as given by Sreenivasiah *et al.* [68]. The method requires a complicated measurement procedure which may not be practical in case of some EUT.

The major limitations of the TEM cell for emission measurement from an EUT are: (i) the inverse proportionality between the cell size and its upper frequency limit; (ii) size of the EUT and (iii) physical rotations (or different orientations) of the EUT.

2.7.2.5 Reverberating chamber

A reverberating chamber is a modified shielded room with a paddle wheel (perturbator) in the ceiling or in the wall as shown in Fig. 2.13. The perturbator may be turned continuously (i.e. stir mode) or in a small discrete step (i.e. tuned mode) [69]. As a result the perturbator tunes the room through many resonant modes at the test frequency.

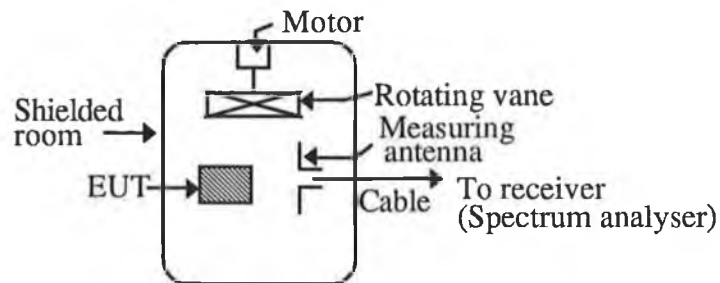


Fig. 2.13 Measurement set-up in stirred mode chamber.

The purpose of the perturbator is also to adjust the positions of field maxima so that the average of the radiated power received by the measuring antenna is proportional to the power radiated by the EUT into the room [59]. It is assumed that this is the same as the power which would be radiated by the EUT into free space. The power measured in the chamber depends on room dimensions and its geometry [66].

For EMC purposes one is interested in field intensity under free space condition. The radiated far field can be determined from the power received by the measuring antenna [64, 69].

2.7.2.6 Anechoic chamber

An anechoic chamber is an enclosure whose metallic walls, ceiling and floor are lined by anechoic material that has a high absorption co-efficient. The anechoic material absorbs the incident EM energy on the wall, ceiling and floor from a source within the enclosure and provides a nearly reflection-free enclosure. Therefore no resonance exists during the EMI/EMC measurement. Such a chamber provides a quasi free space environment.

Generally anechoic material will be at least one quarter wavelength deep to absorb any appreciable amount of EM energy. Since the wavelength is inversely proportional to frequency, the depth of absorber will be increased with decreasing the lower frequency limit of the chamber. The lower frequency limit of most existing anechoic chambers is 200 MHz or above.

2.8 SUMMARY

A general description of EM computation tools is given and various circuit design packages are discussed. Existing PCB radiation prediction techniques are reviewed. A technique is proposed to predict the PCB radiation using NEC-2 with other circuit design packages. For some degree of theoretical validation for the use of NEC-2 in this manner TLM was proposed (in a modified form).

Various emission measurement techniques are described considering their merits and demerits with regard to technical and economical aspects. It is noted that an anechoic chamber measurement is suitable and straightforward. However emission measurement can be carried out in a screened room by damping resonance over the frequency range of 30 to 200 MHz.

Chapter 3

USE OF NEC-2 FOR THE PREDICTION OF PCB RADIATION

- ❑ THEORETICAL BACKGROUND OF THE NEC PROGRAMME
- ❑ SIMULATION OF PCB AS LOADED WIRE STRUCTURE
- ❑ MODIFICATION OF THE NEC PROGRAMME
- ❑ AUTOMATION OF SEGMENTATION SCHEME AND
IMPLEMENTATION OF GEOMETRICAL MODELLING RULES

3.1 INTRODUCTION

Section 2.6 outlined how PCB radiation could be computed using an EM computation tool (NEC-2). A theoretical background of NEC-2 is presented in section 3.2. Section 3.3 describes the modelling guidelines for EM analysis of a wire structure using NEC-2.

Basically a PCB is composed of a dielectric substrate onto which conductors of rectangular cross-section are etched for component interconnections. Section 3.4 describes the simulation of a PCB.

It was necessary to modify NEC-2 with a view to the development of the composite CAD package. The modification of this tool is presented in section 3.5. Wire segmentation plays an important role in making an accurate and efficient prediction of EM radiation from a complex structure such as a PCB. The effect of segmentation schemes is illustrated in section 3.6.

The PCB is simulated as a loaded thin wire structure just above (non contacting) the surface of an imperfect ground. The effect of the interaction distance between a wire structure and an imperfect ground is presented in section 3.7. The effect of the dielectric substrate in far field radiation is illustrated in section 3.8.

3.2 THEORETICAL BACKGROUND OF THE NEC PROGRAMME

The NEC programme uses an electric field integro-differential equation (EFIE) and magnetic field integro-differential equation (MFIE) to model the EM response of a general radiating structure or a scatterer. The EFIE is suited to a thin wire structure whereas the MFIE is used for surfaces. In NEC, the EFIE can also be used to model a surface as a wire grid structure. Since a PCB track (see section 2.6, paragraph 3) of rectangular cross-section is to be modelled as a thin round wire, only the EFIE is presented here. The numerical methods for solving the integro-differential equation (i.e. EFIE), the treatment of ground effects and the capabilities of this programme are described in the following subsections.

3.2.1 THE EFIE

The EFIE, an integro-differential equation, is derived from Maxwell's equations and their boundary conditions. The form of this equation used in NEC follows from an integral

representation for the electric field of a volume current distribution \vec{J} . The EFIE is given by Burke [111] as,

$$\vec{E}(\vec{r}) = \frac{-i\eta}{4\pi k} \int_V \vec{J}(\vec{r}') \cdot \vec{G}(\vec{r}, \vec{r}') dv' \quad (3.1)$$

where,

$$\vec{G}(\vec{r}, \vec{r}') = (k^2 \vec{I} + \nabla\nabla) g(\vec{r}, \vec{r}') \quad (3.1.1)$$

$$g(\vec{r}, \vec{r}') = \frac{e^{(-ik|\vec{r}-\vec{r}'|)}}{|\vec{r}-\vec{r}'|} \quad (3.1.2)$$

$$k = \omega \sqrt{\mu_0 \epsilon_0} \quad (3.1.3)$$

$$\eta = \sqrt{\frac{\mu_0}{\epsilon_0}} \quad (3.1.4)$$

where

- k = the free space propagation constant
- η = the wave impedance in free space ($\eta = 377 \Omega$)
- ω = the angular frequency [rad/s]
- μ_0 = the free space permeability ($\mu_0 = 4\pi \times 10^{-7}$ H/m)
- ϵ_0 = the free space permittivity ($\epsilon_0 = 8.854 \times 10^{-12}$ F/m)
- \vec{I} = the identity dyad ($\hat{x}\hat{x} + \hat{y}\hat{y} + \hat{z}\hat{z}$)
- $g(\vec{r}, \vec{r}')$ = the free space Green's function
- \vec{r} = the position vector of the observation point (see Fig. 3.1)
- \vec{r}' = the position vector of the source point (see Fig. 3.1)

The thin wire approximations are applied to Eqn. 3.1 to reduce it to a scalar integro-differential equation. The approximations are as follows [111]:

- (i) transverse current can be neglected relative to axial currents on the wire;
- (ii) the circumferential variation in the axial current can be neglected;
- (iii) the current can be represented by a filament on the wire axis;
- (iv) the boundary condition on the electric field need be enforced in the axial direction only.

Fig. 3.1 shows the geometry of the arbitrarily oriented straight wire of radius a . With the thin wire approximations, the EFIE for the wire takes the scalar form which is expressed by Burke [111] as,

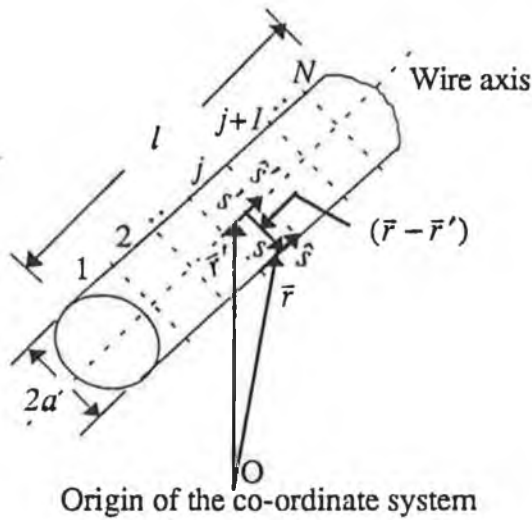


Fig. 3.1 Geometry of the arbitrarily oriented wire.

$$-\hat{s} \cdot \bar{E}^i(\vec{r}) = \frac{-i\eta}{4\pi k} \int_l I(s') \left(k^2 \hat{s} \cdot \hat{s}' - \frac{\partial^2}{\partial s \partial s'} \right) g(\vec{r}, \vec{r}') ds' \quad (3.2)$$

where I is the induced current, \bar{E}^i is the exciting field, \hat{s} and \hat{s}' are unit vectors tangent to the wire axis at s and to the wire surface at s' respectively, j is the wire segment number and $j=1,2,\dots,N$.

It should be noted here that the prime represents the source point and the unprimed represents the observation point. The integration is carried out over the length of the wire.

The NEC computes the radiated field after determining the unknown current I by solving the integral equation for a known excitation.

3.2.2 NUMERICAL TECHNIQUE FOR SOLVING THE EFIE

In the NEC programme the integral equation (Eqn. 3.2) is solved for the unknown current by a form of the method of moments (MoM). The MoM involves expanding the unknown current in a summation of basis functions (also known as expansion functions) and enforcing

equality of the weighted integral of the fields to reduce the integral equation to a matrix equation. The detail of reducing an integral field equation into a matrix equation is given in Appendix C1. In NEC a wire is divided into a number of segments, therefore Eqn. 3.2 takes the form [112]:

$$[Z_{mn}] [I_n] = [V_m] \quad (3.3)$$

where,

- m = 1,2 ... N
- n = 1,2 ... N
- N = total number of wire segments
- Z_{mn} = the impedance matrix
- I_n = the unknown current vector
- V_m = the known excitation vector

The first index (m) refers to the observation points on the m th segment where the second index (n) is associated with the field from the n th segment or the n th source.

The selection of the basis function is very important for accurate and efficient numerical computation. In the NEC programme, the expansion function for the current is chosen so that the total current on a wire segment j has the form [111] :

$$I_j = a_j + b_j \sin\{k(s - s_j)\} + c_j \cos\{k(s - s_j)\} \quad (3.4)$$

where,

- j = 1,2 ... N
- s_j = the value of s at the center of segment j
- a_j, b_j and c_j = constants

Eqn. 3.4 is valid for $(s-s_j) \leq (\Delta_j/2)$, where Δ_j is the length of the j th segment. Two of the three constants of Eqn. 3.4 are eliminated by applying the continuity condition on current and charge at the segment ends. The linear charge density (q) is related to the current by the equation of continuity

$$\frac{\partial I(s)}{\partial s} = -j \omega q \quad (3.5)$$

Current is continuous and satisfies Kirchhoff's current law (KCL) at multiple wire junctions. Charge is also continuous on uniform wires. At a junction of n wires with different radius, the NEC imposes an additional condition related to the charge per unit length which was given by Wu and King [159] as:

$$q_1 \Psi_1 = q_2 \Psi_2 = q_3 \Psi_3 = \dots = q_i \Psi_i = \dots = q_n \Psi_n \quad (3.6)$$

where

- q_i = the charge per unit length on the i th wire;
- a_i = the radius of the i th wire;
- Ψ_i = the proportionality factor = $2[\ln(2/ka_i) - 0.5772]$;
- i = 1,2,... n .

The one unknown associated with the basis function is determined by solving the integral equation.

In MoM, it is necessary to determine a suitable inner product which is a scalar quantity and then to define a set of weighting functions (refer to Appendix C1). NEC chooses weighting functions ($W_i(\vec{r})$) as a set of delta functions, where $\delta(\vec{r} - \vec{r}') = 0$ for ($\vec{r} \neq \vec{r}'$), otherwise $\delta(\vec{r} - \vec{r}') = 1$.

3.2.3 GROUND EFFECT

Three options are available in the NEC programme for the EM analysis of a wire structure above or near the ground. The options are described in the following paragraphs.

A perfectly conducting ground is modelled by including the image field in the kernel of the integral equation [Eqn. 3.1].

An approximate model for a wire structure over a finitely conducting ground uses the image modified by the Fresnel plane-wave reflection co-efficient. This approximate model is applicable for a wire structure at least 0.1 to 0.2 times the wavelength (λ) above the ground [111].

NEC uses the Sommerfeld integral formulation for a wire structure very close to an imperfect ground. However in this situation, NEC restricts the interaction distance (h , see

Fig. 3.2) between a wire structure and an imperfect ground by a relation that is expressed in terms of λ at the frequency of interest. For a horizontal wire of radius a , this relation is given as

$$(h^2 + a^2)^{1/2} > 10^{-6} \lambda \quad (3.7)$$

Since the evaluation of the Sommerfeld integral is very time consuming, a separate programme known as SOMNEC was developed by Burke [111]. SOMNEC uses the bivariate interpolation in a table of pre-computed Sommerfeld integral values to obtain the field values required for integration over current distributions.

For a wire structure above or near a ground NEC computes the radiated space wave with the direct and reflected wave (from ground) and can also include the surface wave with the space wave.

3.2.4 EVALUATION OF RADIATED FIELD

The NEC programme evaluates the radiated near field and the radiated far field due to the induced current on a wire structure. The radiated field from a PCB is evaluated from the near field formulation used in the NEC programme for a wire structure. The formulae that have been used in NEC to compute the near field components in the cylindrical co-ordinate system are given in Appendix C2.

The radiated far electric field from a wire structure due to the induced current is computed using Eqn. 3.1 and by considering the far field approximation as described in section 2.2 [111]. Computation of these radiated fields is necessary to find the radiation pattern of an antenna (an intentional radiator).

The total radiated field is of common interest in EMI problems. NEC-2 outputs the radiated near field components in the rectangular co-ordinate system. The total radiated field from a PCB can be determined from the field components obtained from near field computation.

3.3 MODELLING GUIDELINES

There are a number of rules which must be followed in order to obtain accurate results from an EM computation tool such as NEC. If these rules are ignored while solving an EMC problem, incorrect results may be achieved. Therefore it is necessary to become familiar with the modelling guidelines before using NEC for EM analysis of a complex structure such as a PCB. Some modelling guidelines for a wire structure that are particularly important for predicting the PCB radiation are described in the following subsections.

3.3.1 SEGMENT LENGTH

The length of the wire segment (Δ) should be less than or equal to 0.1λ , where λ is the wavelength at the desired frequency. However a longer segment of length about 0.14λ may be considered for long straight wire or a non critical part of a wire structure. Recently Jian *et al.* [110] proposed that a longer wire segment could be of 0.2λ if the wire is not directly illuminated by a source.

On the other hand, a shorter segment is needed for modelling the critical region of a wire structure (such as a bent wire). The NEC programme does recommend the length of a short segment to be greater than or equal to 0.001λ . This is due to the degeneracy of the basis function used in NEC. Jian *et al.* [110] found good accuracy by considering a segment length as small as 0.04λ to model a simple structure.

3.3.2 WIRE RADIUS

Wire radius plays an important role in the geometrical modelling of a wire structure for EM analysis. The wire radius a relative to λ is limited by the approximation used in the kernel of EFIE of the NEC programme. Two options are available in NEC, the thin wire kernel (TWK) and extended thin wire kernel (EWTk). The TWK is considered here because this work simulates the rectangular PCB track as an equivalent round wire whose radius is small compared to the wavelength at the frequency of interest (30 to 1000 MHz). The validity of the thin wire approximation depends on the value of the a/λ ratio. The thin wire approximations as mentioned earlier will be valid when $(2\pi a/\lambda) \ll 1$. In rare cases, the maximum track width is of the order of 10 mm [142]. The equivalent wire radius will then be of the order of 2.5 mm (see Eqn. 3.9) and thus $(2\pi a/\lambda)_{\min} = 0.0523$.

The accuracy of the numerical solution for the axial current along a wire is also dependent on Δ/a . In this context a general guideline is given in NEC, according to which the ratio of the length of a wire segment to its radius (i.e. Δ/a) must be greater than 8 for errors of less than 1%. Segments with small Δ/a should be avoided at bends of a wire.

3.3.3 SEGMENT CONNECTION

Wire segments that are electrically connected must have coincident end points. In NEC programme, a wire segment will be treated as connected if the separation of their ends is less than about $(0.001 \Delta_{\min})$. In this context a guideline is given in the NEC programme, according to which identical co-ordinates should be used for the connected segments.

3.3.4 WIRE SEGMENTATION

In addition to the selection of segment size and wire radius, the segmentation scheme is also important because it may noticeably affect the predicted current distribution which in turn influences the radiated fields. A recent study [110] has shown that a better numerical result could be achieved by using a uniform segmentation near a source segment¹ (i.e. the adjacent segment on either side of the source segment should have equal length) in the geometrical modelling of a wire structure.

3.4 SIMULATION OF A PCB

Current distribution over a PCB track cross-section behaves in a manner that is quite similar to that of a wire [97]. Therefore in applying the NEC-2 programme for predicting PCB radiation, the track is modelled as a round wire that forms a radiating structure (stated in section 2.6). The equivalent wire radius (a) can be obtained from the cross-section of the rectangular track and is given by Springfield [39] as,

$$a = 0.335 w \left(0.8 + \frac{t}{w} \right) \quad (3.8)$$

where, w is the track width and t is the track thickness.

Eqn. 3.8 is valid for $0.1 < t/w < 0.8$. Typical track thicknesses are 35 μm and 70 μm . The most common thickness, 35 μm is considered in this work [142, 143], so the restriction is

¹ A source segment is the segment of a wire where excitation is applied.

satisfied as long as $43 \mu\text{m} \leq w \leq 350 \mu\text{m}$. For a very thin rectangular track (i.e. $0 \leq t/w \leq 0.1$), the wire radius can be determined from the following expression [148].

$$a \approx 0.25w \left[1 + \frac{t}{\pi w} \left(1 + \log_e \left(4\pi \frac{w}{t} \right) \right) \right] \quad (3.9)$$

For a PCB where the tracks are very wide, a single wire would not be sufficient to model a rectangular track because the first two conditions of the thin wire approximation method (described in section 3.2) are no longer valid. In such cases each track should be represented by a rectangular patch. In NEC-2 a rectangular patch can be modelled as a wire grid.

In NEC-2 programme a lumped load such as resistance, inductance and capacitance may be specified on a wire structure. The components connected to a PCB track are replaced by their input and output impedances. The PCB is then simulated as a loaded thin wire structure just above (but not contacting) the surface of an imperfect ground. A real PCB track and a simulated PCB track are illustrated in Fig. 3.2.

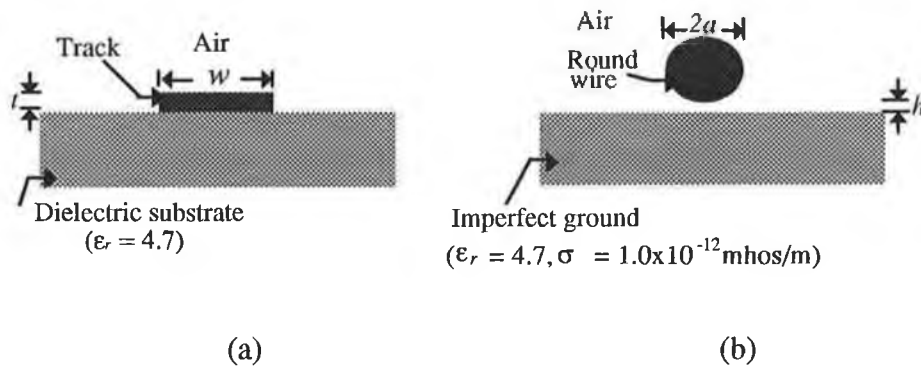


Fig. 3.2 (a) A real PCB track; (b) a simulated PCB track (i.e. a round wire).

The minimum value of h (ideally $h = 0$) is desirable. In this work h is set to $1 \mu\text{m}$ because it is observed that NEC-2 requires this as a minimum value. Typical minimum values of a are of the order of $20 \mu\text{m}$. The range of frequencies is typically 30 -1000 MHz and thus $(10^{-6}\lambda)_{\text{max}} = 10 \mu\text{m}$. Therefore the condition (Eqn. 3.7) is always satisfied. The effect of h on the predicted PCB radiation will be discussed later in this chapter.

A double sided or a multilayer PCB is generally used for a complex electronic circuit. In such a PCB, a signal path may follow a PCB track on the top side of the board and then move to the bottom side of the board using a via. In simulating such a PCB, a via is modelled as a short segment of solid wire.

3.5 MODIFICATION OF NEC-2 PROGRAMME

The original version of NEC-2 runs on a VAX/VMS computer. NEC-2 was modified for near field computation by discarding some subroutines that are not required for such an application. The modified version runs on a personal computer (PC) with a "386" processor, running at 33 MHz. A flow diagram of the modified NEC-2 main programme is shown in Fig. 3.3. The main programme is divided into two sections: (i) input section and (ii) solution section. The function of the main programme is to handle input and output and to call the appropriate subroutines. In the flow diagram *IFLOW* and *IGO* are the two integer flags. *IFLOW* distinguishes the various input sections and *IGO* indicates the stage of completion of the solution as given in [111]. The modifications which have been carried out in the input and solution sections are described in the following paragraphs.

The original NEC-2 programme reads input data (such as the geometry, load, excitation, frequency, etc.) from a common input file. In developing a composite CAD package it is necessary to read this data separately as NEC-2 must obtain this data from the output files of various circuit design packages.

NEC-2 performs the EM analysis of a wire structure in the frequency domain. Therefore any time domain signal has to be converted into a frequency domain signal and this can be done using the Fourier transform. An example of this time domain signal is a clock or data signal in a digital circuit. The subroutine SPECTRA computes the amplitude of harmonics generated by a clock or data signal. In case of a digital circuit NEC-2 calls subroutine SPECTRA to obtain the amplitude and frequency data of a clock or a data signal. A computer program listing for subroutine SPECTRA is given in Appendix C3.

In this work NEC-2 was modified to automate the segmentation scheme of a wire structure. NEC-2 calls the subroutine WSN to determine the number of segments in a wire. The subroutine WSN also verifies all the geometrical modelling rules for the geometrical modelling of a wire structure.

The subroutine DATAGN from the original NEC-2 programme was used to read the structure input data (geometrical data) and set segment and patch data. Since the PCB is simulated as a wire structure, this subroutine was modified by discarding parts of the routine that are not required for such an application. The modified DATAGN sets the segment data for a wire structure.

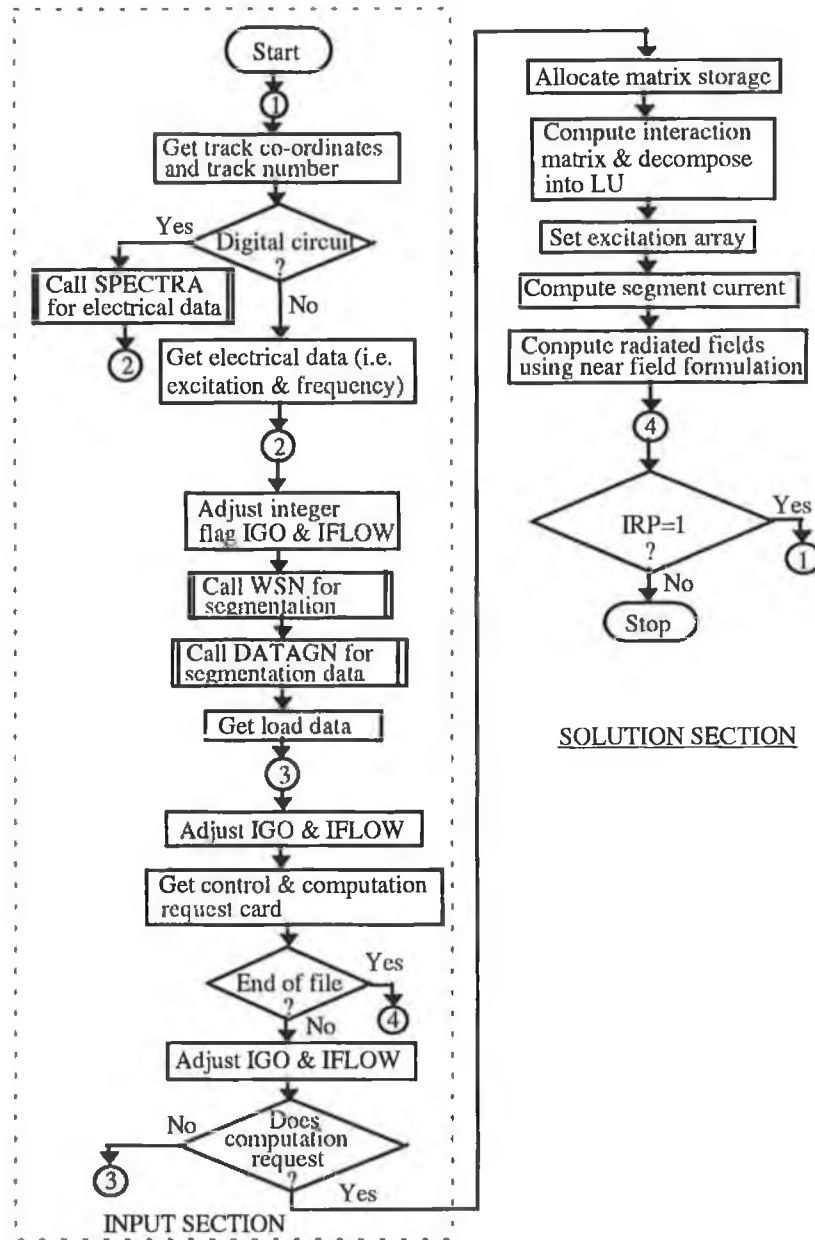


Fig. 3.3 Flow diagram of main programme of NEC-2. Modified and adapted from [111].

The solution part of the NEC-2 programme was modified for near field computation. The subroutine linkage chart of the solution part of the modified NEC-2 programme is shown in Fig. 3.4. The function of each subroutine is summarised in Appendix C4. The detail of each routine is available in [111].

NEC-2 outputs the field components (electric and magnetic) in the rectangular co-ordinate system. The magnitude of the resultant electric field (E) and magnetic field (H) can be obtained from the expressions as given in Eqns. 3.10 and 3.11 respectively.

$$|E| = \sqrt{|E_x|^2 + |E_y|^2 + |E_z|^2} \quad (3.10)$$

$$|H| = \sqrt{|H_x|^2 + |H_y|^2 + |H_z|^2} \quad (3.11)$$

Once the radiated EM field has been computed the modified NEC-2 requests the next prediction from the designer. The integer flag ($IRP=1$) indicates the next computation for the radiated fields.

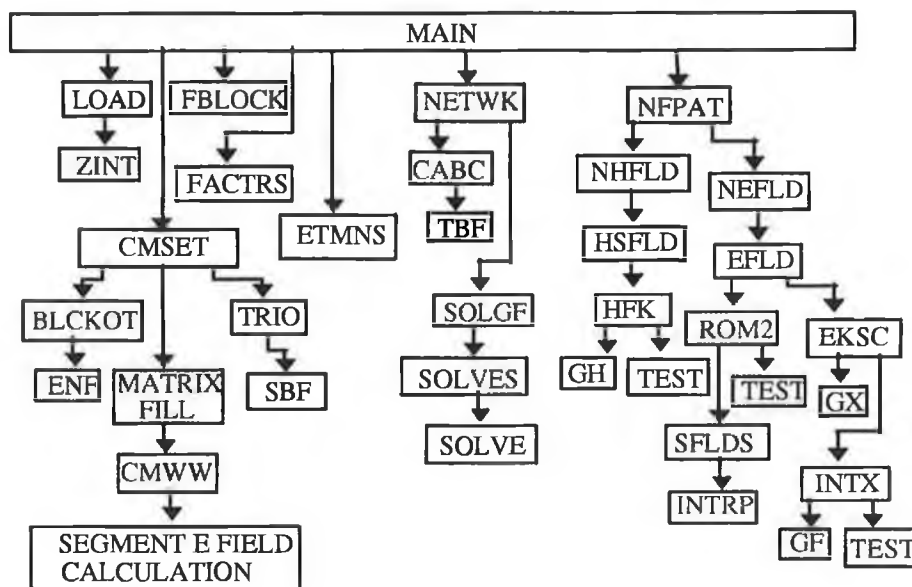


Fig. 3.4 A subroutine linkage chart for near field computation.

3.5.1 AUTOMATION OF SEGMENTATION SCHEME

It is difficult to obey the geometrical modelling rules of NEC-2 in order to make an accurate and efficient prediction of EM radiation from a complex structure such as a PCB. The accuracy of the tool depends on the segmentation of the wire and the wire radius. Some modelling guidelines for segmentation have already been discussed in section 3.3. On the basis of these guidelines, an algorithm was developed to automate the generation of segment size at the frequency of interest. A flow chart of this algorithm is shown in Fig. 3.5. The developed algorithm was implemented in Fortran and a computer programme listing is given in Appendix C5.

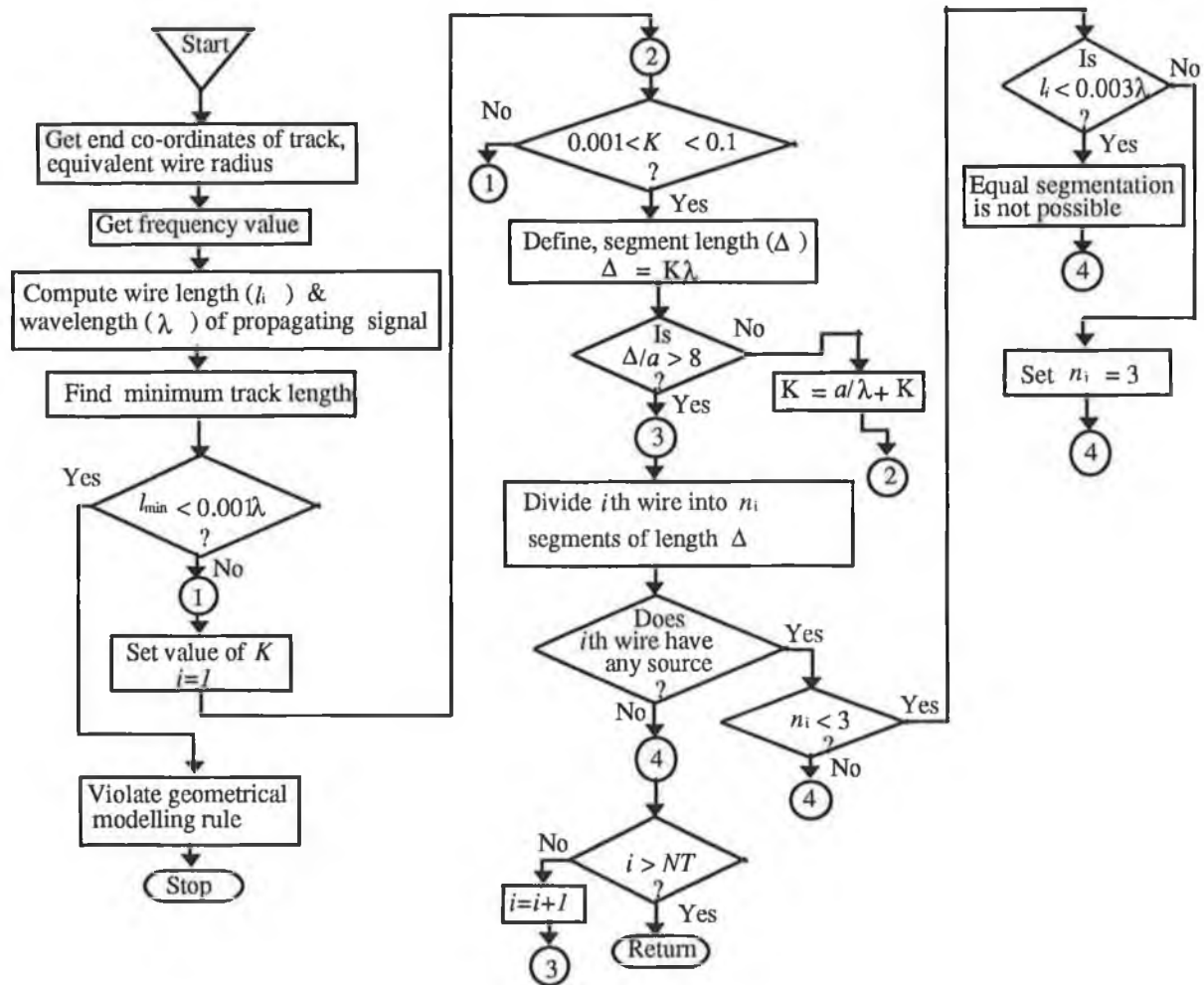


Fig. 3.5 Flow diagram for automating the segmentation scheme of a wire structure.

In Fig. 3.5, K is the user's defined multiplication factor for setting the segment size, l_i is the length of the i th wire (simulated track), n_i is the number of segments of the i th wire, Δ is the segment length and NT is the total number of wires.

The input parameters to generate a number of segments for a wire are as follows: frequency, segment size, end co-ordinates of a wire and wire radius. The developed algorithm performs the following tasks:

- implementation of geometrical modelling rules as described in section 3.3;
- division of a wire into a number of segments;
- checking the equality of source and adjacent segment lengths.

3.6 ANALYSIS OF SEGMENTATION SCHEME

A smaller segment usually increases the accuracy but significantly decreases the computational efficiency. A very small segment also causes the degeneracy of the constant and cosine term (i.e. the constant and the cosine term of the basis function as given in Eqn. 3.4 are no longer sufficiently different). The degeneracy of the basis function results in the loss of numerical precision and shows up as random noise in the currents and consequently causes inaccurate prediction of EM radiation.

In addition to the segment size, the segmentation scheme is also important as described in section 3.3.4. Jian *et al.* [110] predicted the current distribution of a center fed dipole with three different schemes to show the effect of the segmentation scheme. It was shown that the maximum difference of current between the uniform and non uniform scheme is about 11% while that between the uniform and slightly non uniform case is around 2 to 3%.

In this work the effect of segment size and segmentation scheme is illustrated by predicting the radiation patterns of a short circuited track configuration and a center-fed dipole.

3.6.1 A SHORT CIRCUITED TRACK CONFIGURATION

The radiated far field from a short-circuited track configuration on a grounded dielectric substrate (i.e. a rectangular loop on a grounded substrate) was computed with three different schemes. The rectangular loop is shown in Fig. 3.6. The first scheme was a uniform segmentation scheme where the loop was divided into 126 segments of equal length. The

second case was a non uniform scheme which used 26 segments of unequal length. The third scheme used 26 segments where only the source and adjacent segments were of equal length. The segmentation schemes are shown in Fig. 3.7. In all cases the segment size satisfies the length requirement and thin wire approximation of NEC-2 as described in section 3.3.

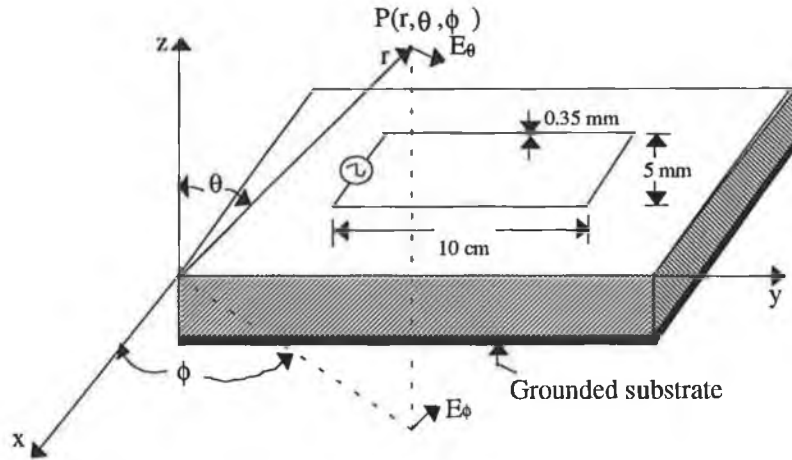


Fig. 3.6 A rectangular loop on a ground plane formed from a short circuited track configuration on a grounded substrate.

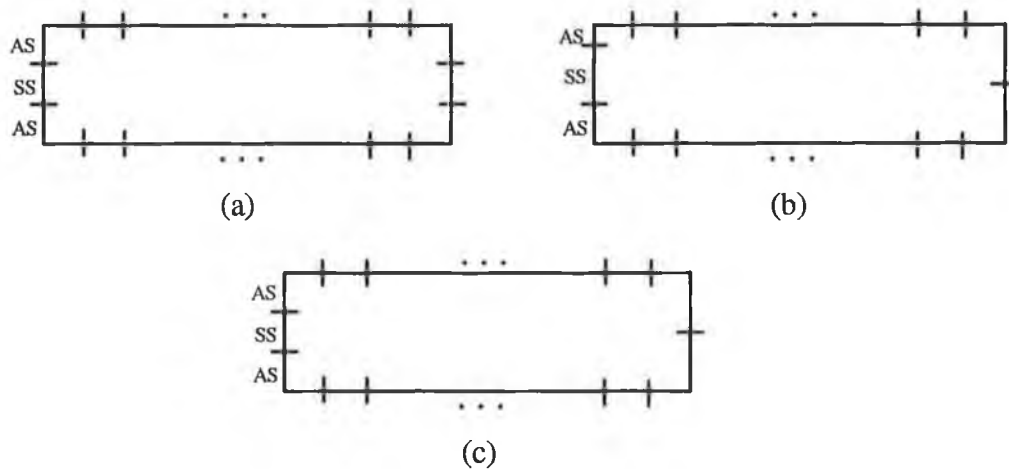
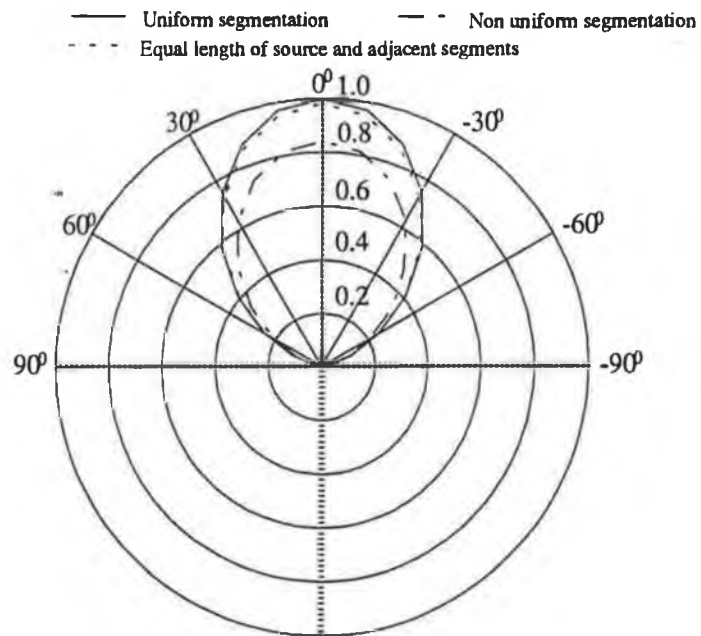


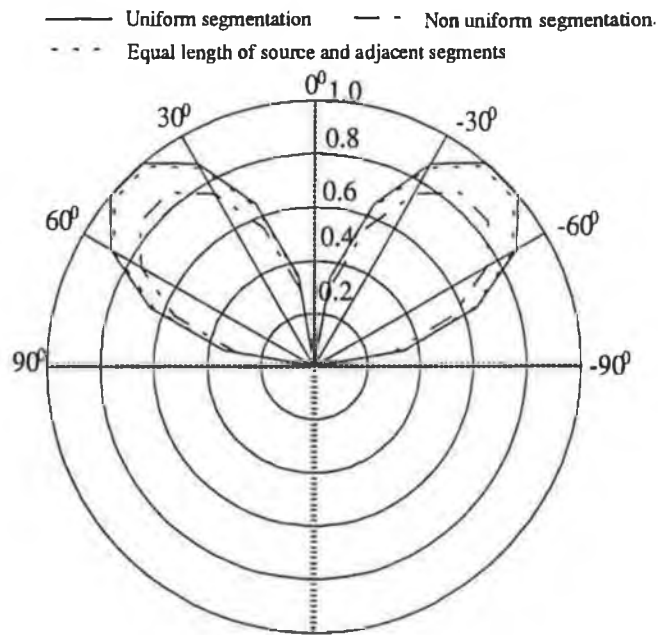
Fig. 3.7 A rectangular loop: (a) uniform segmentation scheme (126 segments); (b) non uniform segmentation (26 segments); (c) source segment (SS) and adjacent segments (AS) are of equal length (total 26 segments).

The radiated electric field at 400 MHz is computed using the original NEC-2 in the x - z plane (i.e. azimuth angle $\phi=0$) at a radial distance (r) of 3 m. The effect of dielectric substrate is neglected by considering the far field approximations. A plot of the radiation pattern for three

different cases is shown in Fig. 3.8. The plot resembles the radiation pattern of a loop over a ground plane.



(a)



(b)

Fig. 3.8 Radiation pattern of a short circuited two parallel track configuration on $\phi = 0^\circ$ plane with θ varying from -90° to 90° : (a) E_θ pattern; (b) E_ϕ pattern.

It is evident from the plot that the maximum difference in radiated field between the uniform segmentation and non uniform segmentation is around 12-13%, while that between the second scheme (i.e. source and adjacent segment of equal length) and the uniform segmentation is around 2-3%.

3.5.2 A CENTRE FED DIPOLE

The radiated electric field at 200 MHz from a short centre fed dipole of length 0.1λ over a ground plane has been predicted with three different segmentation schemes as described in the previous section. The geometry of the dipole and the segmentation schemes are shown in Fig. 3.9. In all cases the segment length satisfies the length requirement and thin wire approximation of NEC-2.

The radiated electric field was computed in the x - z plane at a 3 m distance. As the dipole is in the y direction of the rectangular co-ordinate system (i.e. a horizontal dipole), only the ϕ component of the radiated field will be present. A plot of the radiation pattern is shown in Fig. 3.10. The plot reveals that the maximum difference in radiated field between the uniform and non uniform scheme is about 7-8% while that between the uniform and slightly uniform schemes (i.e. source segment and adjacent segment are of equal length) is about 1%.

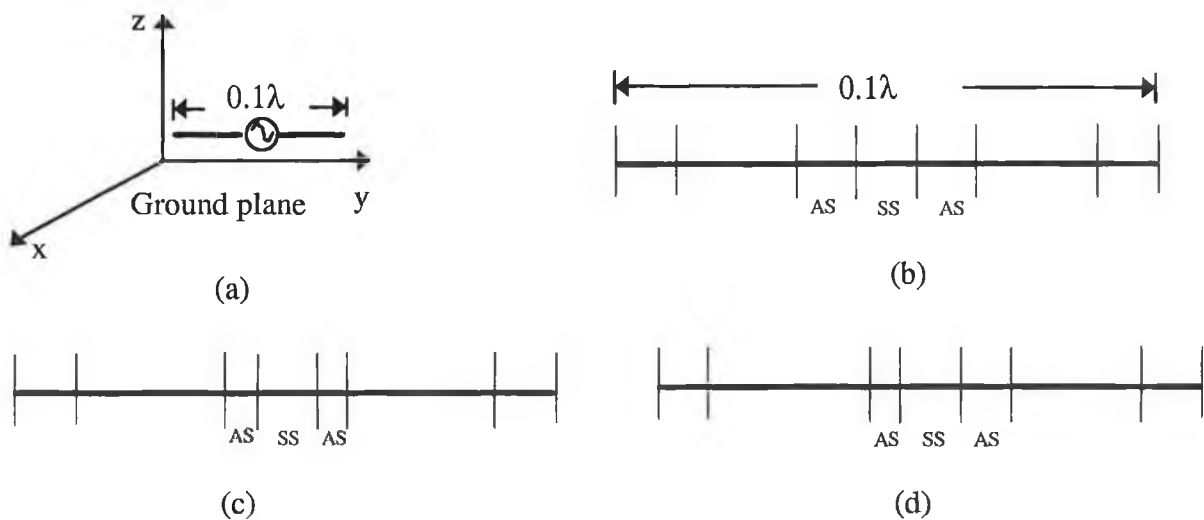


Fig. 3.9 A centre fed dipole of length 0.1λ : (a) geometry of the dipole; (b) uniform segmentation scheme (15 segments); (c) source segment and adjacent segment are of equal length (9 segments); (d) non uniform segmentation (11 segments).

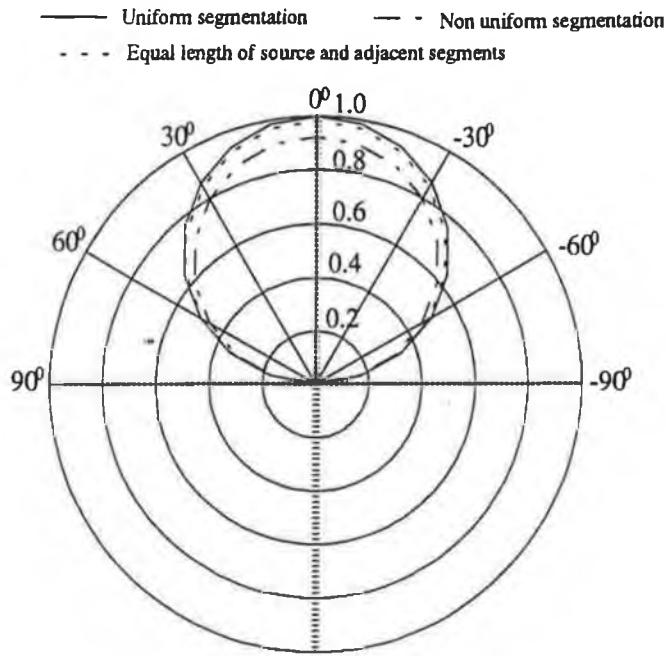


Fig. 3.10 The E_θ radiation pattern of a short horizontal dipole on $\phi=0^\circ$ plane with θ varying from -90° to 90° .

3.7 EFFECT OF h

The effect of h on the prediction of radiated field is observed theoretically. In the cartesian co-ordinate system, the geometry of a simple test circuit is shown in Fig. 3.11. The radiated electric fields were predicted at $r = 0.1\text{m}$, $\theta = 0^\circ$ and $\phi = 90^\circ$.

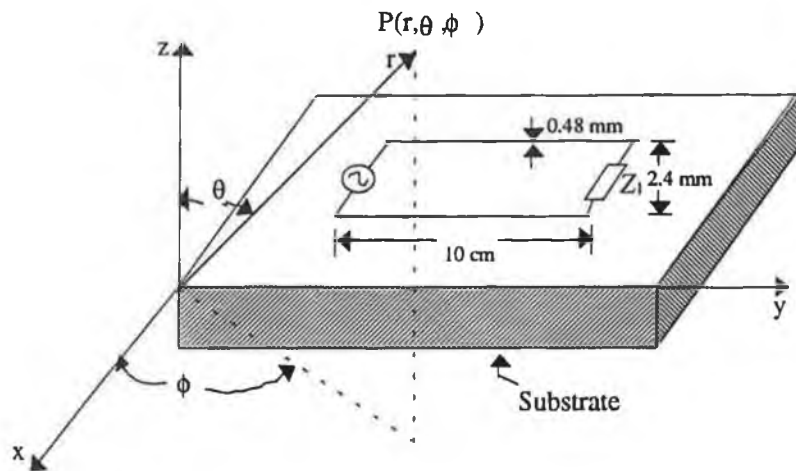


Fig. 3.11 Geometry of a simple test circuit.

The predictions were performed at the third, seventh and the ninth harmonic of the 50 MHz pulse generated by a crystal oscillator.

A plot of the radiated electric field as a function of h is shown in Fig. 3.12. The plot shows that for h less than 50 μm the variation of the radiated field is not significant. As h goes above 50 μm the radiated field drops rapidly. Therefore the choice of h as 1 μm is seen to be justified.

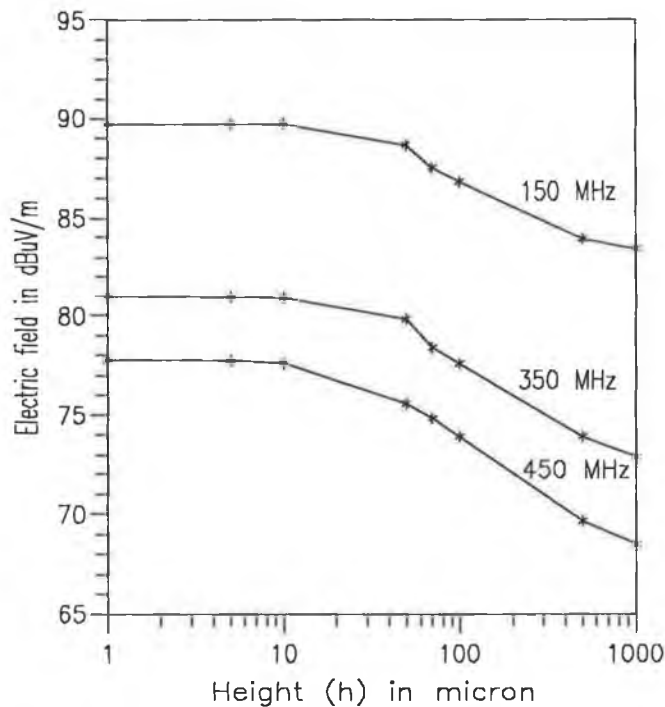


Fig. 3.12 Radiated electric field as function of h .

3.8 EFFECT OF DIELECTRIC SUBSTRATE AT FAR FIELD REGION

The effect of a dielectric has been investigated by predicting the electric far fields from a short circuited microstrip structure using NEC-2. This structure is shown in Fig. 3.13 (a). The predicted field was compared with that computed by Daijavad *et al.* [23] and Rubin *et al.* [37]. It should be noted here that both references [23, 37] are from the same group of researchers. Daijavad's method has already been described in section 2.4 (see last paragraph). Rubin *et al.* also included the effect of dielectric by considering the polarisation currents in their model, which was based on the MoM. In NEC-2, a microstrip structure is simulated as a short circuited wire above a ground plane as shown in Fig. 3.13 (b) and it was assumed that $\epsilon_r = 1.0$ (i.e. absence of dielectric substrate).

All dimensions of the microstrip structure as used in [23, 37] are considered for comparison and the fields are also computed at the same observation point (i.e. $r = 3$ m, $\theta = 0$, $\phi = 0$). A source voltage of 1 V and source impedance of 50Ω were assumed for all frequencies (100 to 1000 MHz). Rubin *et al.* [37] also computed radiated electric field for the same source and at the same observation point for $\epsilon_r = 1.0$. A plot of the NEC-2 predicted electric field and that computed by the two methods [23], [37] is shown in Fig. 3.14. Data points for curve #1, curve #2 and curve #3 (see Fig. 3.14) have been taken from the reference [23, Fig. 4].

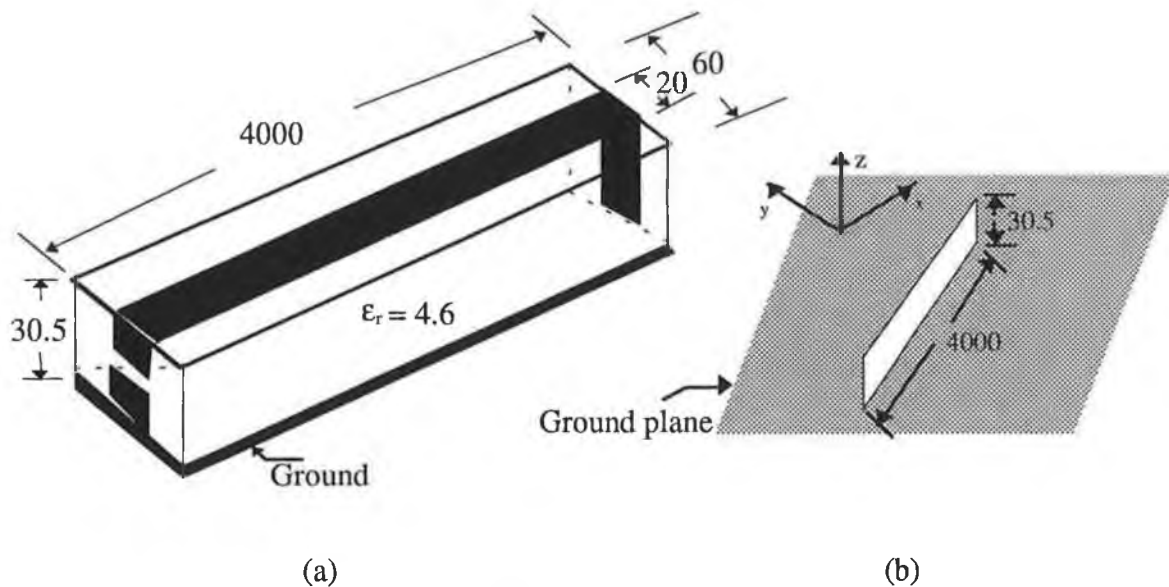


Fig. 3.13 (a) A microstrip structure adapted from [23]; (b) simulated microstrip. All dimensions are given in mil (1 mil = 0.001 in).

The plot shows a good agreement between the NEC-2 predicted value and that computed by Rubin *et al.* [37] for $\epsilon_r = 1.0$. It is also evident from the plot that the difference between the NEC-2 predicted value and that computed by Daijavad *et al.* [23] and Rubin *et al.* [37] (for $\epsilon_r = 4.6$) is about 4 to 5 dB at all frequencies except 800 MHz. This difference may be due to the presence of a finite size dielectric in the y-direction [23, 37] and also due to the use of an infinite ground plane in case of NEC-2. The large discrepancy at 800 MHz is most likely due to the resonance occurring in the microstrip structure. The authors [23, 37] do not comment on this resonance which they predict. Attempts to compute a resonant frequency for the structure yielded a value of around 440 MHz. It is not known to this author how their computations yielded a value of 800 MHz. As the effect of dielectric is not significant (except at 800 MHz) it is neglected in predicting the PCB radiation in far field region.

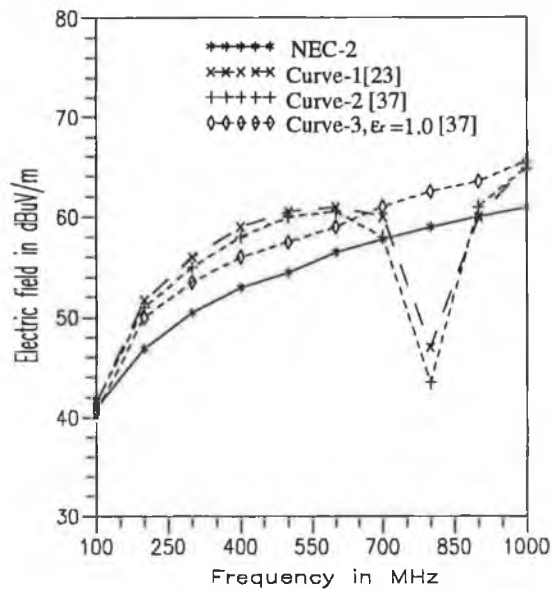


Fig. 3.14 Radiated electric field from a short circuited microstrip structure.

3.9 CONCLUDING REMARKS

An EM computation software tool is essential for EMC verification of electronic equipment at the design stage. Here NEC-2 was employed for such an application as described in section 2.6. The theoretical background of NEC-2 was described. The simulation of a PCB as a loaded thin wire structure was proposed.

Geometrical modelling of a wire structure is very important for an accurate and efficient prediction of EM radiation from a PCB. Automation of geometrical modelling and the segmentation scheme of a wire structure was elucidated. The effect of the segmentation scheme was illustrated by predicting the radiation pattern of a short-circuited parallel track configuration and a centre fed dipole with three different segmentation schemes. It was concluded that in addition to meeting the geometrical modelling rule of NEC-2, a uniform segmentation scheme (equal length source and adjacent segment) was preferable for predicting the EM radiation from a PCB.

The effect of interaction distance (i.e. h) between the wire structure and an imperfect ground was investigated and the value of h chosen was justified. The effect of a dielectric on the fields in the far field region was investigated and it was found that a dielectric material that is inherently present in a PCB has a minimal effect on the radiated field.

Chapter 4

THEORETICAL VALIDATION

- ❑ EXTENSION OF TLM
- ❑ ANALYTICAL BACKGROUND OF EXTENDED TLM
- ❑ COMPARISON OF NEC PREDICTED PCB RADIATION WITH THAT FROM TLM COMPUTATION
- ❑ EFFECT OF DISPLACEMENT CURRENT

4.1 INTRODUCTION

The use of NEC-2 for predicting PCB radiation at design level is based on some approximations as mentioned in the previous chapter. Therefore theoretical validation of this tool was necessary. This was done by comparing NEC-2 predicted radiation with that from a TLM computation. A simple PCB having two parallel tracks running between two devices was chosen for the comparison.

Other researchers [14,16,17] have used the TLM technique to predict PCB radiation. In their models, they assumed that PCB tracks are immersed in an homogeneous medium. This is not the real case as a PCB track is generally immersed in an inhomogeneous medium (i.e. air and dielectric substrate). Moreover the previous models were limited to far field conditions and large track separation.

An extended TLM method is proposed to cover the real cases and is described in section 4.2. Section 4.3 presents the numerical methods and software for computing the PCB radiation using the extended TLM.

Section 4.4 presents the comparison of NEC-2 predicted EM radiation with that from a TLM computation. This comparison is made for three different cases: (i) various frequencies, (ii) different observation points and (iii) different driven devices or components (i.e. loads).

The extended TLM method considers the displacement current along with the functional currents of a circuit. The displacement current is generally confined between two parallel tracks or between a track and ground plane. The effect of displacement current in PCB radiation is elucidated in section 4.5.

4.2 TLM

The EM radiation from a PCB was predicted using the TLM method (as described in section 2.4.1.3) which was extended by considering the following:

- (i) effective dielectric constant of the medium surrounding PCB tracks;
- (ii) the exact velocity of a propagating wave along the PCB track;
- (iii) exact expressions of per unit length (PUL) parameters to compute the characteristic impedance of two parallel tracks;

(iv) the displacement current.

A singlesided PCB having a pair of tracks running between two devices was chosen as an example.

4.2.1 EFFECTIVE DIELECTRIC CONSTANT

Having two parallel tracks running between two devices on the same side of a board is quite similar to a coplanar strip configuration. In this configuration, the medium surrounding the track is referred to as an inhomogeneous medium because the electric field exists partly in the board substrate and partly in the air surrounding the board. The electric flux density will be maximum in the board substrate because of higher permittivity of the substrate material than that of air. The cross-sectional electric field distribution for this configuration is shown in Fig. 4.1(a). The dielectric of the board does not affect the magnetic field as the board permeability is the same as that of free space (μ_0). The inhomogeneous medium (air and dielectric) can be replaced as an homogeneous medium having the effective dielectric constant, ϵ_r' [97].

The electric field lines for two parallel tracks immersed in that homogeneous medium is shown in Fig. 4.1(b). The effective dielectric constant (ϵ_r') is considered to be that of a fictitious dielectric material. Therefore if the original tracks are immersed in the homogeneous medium as shown in Fig. 4.1(b), the corresponding tracks would exhibit the same characteristic impedance and would have the same velocity of propagation as that of tracks shown in Fig. 4.1(a).

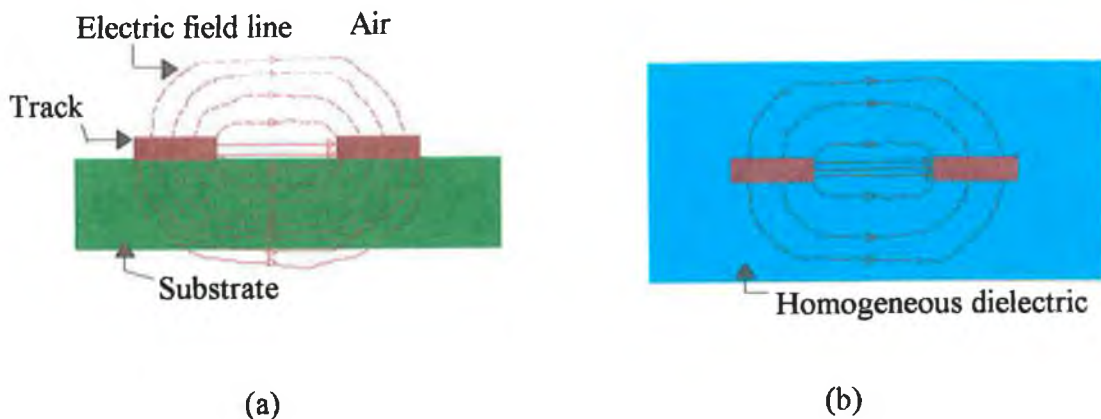


Fig. 4.1 (a) Cross-sectional field distribution for two parallel tracks in an inhomogeneous dielectric (i.e. air and substrate); (b) electric field lines in an homogeneous dielectric having an effective dielectric constant (ϵ_r').

The velocity of propagation is given by

$$v = \frac{1}{\sqrt{\mu_0 \epsilon_0 \epsilon'_r}} \quad \text{m/sec} \quad (4.1)$$

where, μ_0 (H/m) and ϵ_0 (F/m) are the free space permeability and permittivity respectively.

The exact expression for the effective dielectric constant originally developed [97, 101, 123, 153] for coplanar strip configuration has been used here. The expression is given in terms of cross-sectional dimensions of the PCB tracks, the dielectric constant of the substrate material and the substrate thickness. The cross-sectional dimensions of two parallel tracks (i.e. coplanar strip configuration) is shown in Fig. 4.2.

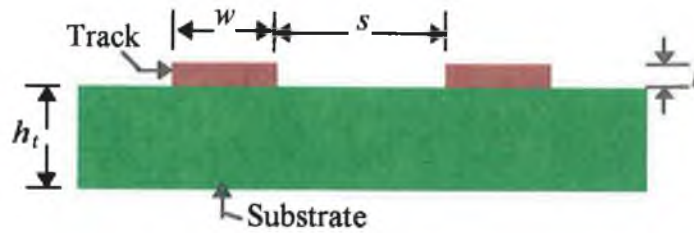


Fig. 4.2 Cross-sectional dimension of two parallel tracks on a PCB.

The effective dielectric constant is given [97] as

$$\epsilon'_r = \frac{\epsilon_r + 1}{2} \left\{ \tanh \left[0.775 \ln \left(\frac{h_t}{w} \right) + 1.75 \right] + \frac{kw}{h_t} \left[0.04 - 0.7k + 0.01(1 - 0.1\epsilon_r)(0.25 + k) \right] \right\} \quad (4.2)$$

where k is given by,

$$k = \frac{s}{s + 2w} \quad (4.3)$$

The expression for ϵ'_r was derived using quasi-TEM approximation [97]. This is valid for low ranges of microwave frequencies (< 3 GHz) and therefore its use for the current work is justified.

4.2.2 PUL PARAMETERS

Approximate expressions for the PUL parameters originally developed for microwave circuit applications have been used here. Various computational methods for finding the PUL parameters are: (i) the method of conformal transformations, (ii) the finite element method, and (iii) the integral equation method (method of moments).

The methods (ii) and (iii) are applicable if the PCB has a ground plane [25, 90]. The PUL parameters of two parallel tracks on a PCB without any ground plane can be obtained from the method of conformal mapping [101, 106]. An analysis of this first method is given in the literature [106]. Risaburo's [106] formulas have been used here to find the PUL capacitance and inductance of two parallel tracks.

The PUL capacitance of two parallel tracks is given by

$$C = \epsilon_0 \epsilon_r \frac{K'(k)}{K(k)} \quad (4.4)$$

where,

$K(k)$ – the complete elliptic function of the first kind with modulus k (as given in Eqn. 4.3)

$K'(k)$ – the complementary function of $K(k)$, and $K'(k) = K(k')$, with $k' = \sqrt{1 - k^2}$.

The PUL inductance can be obtained from the capacitance calculated with the dielectric removed. The expression for the PUL inductance is given by

$$L = \epsilon_0 \mu_0 (C_0)^{-1} \quad (4.5)$$

where, $C_0 = \epsilon_0 \frac{K'(k)}{K(k)}$, the PUL capacitance of two parallel track in the absence of the dielectric.

Thus,

$$L = \mu_0 \frac{K(k)}{K'(k)} \quad (4.6)$$

In this work, the dielectric constant (ϵ_r) was replaced by the effective dielectric constant (ϵ_r') to find the PUL capacitance of two parallel tracks using the above formulations.

4.2.3 CHARACTERISTIC IMPEDANCE

In the absence of a ground plane, the characteristic impedance of two parallel tracks (as shown in Fig. 4.2) was determined using Eqn. 2.6 by previous researchers [14, 16-17]. Eqn. 2.6 was originally developed for large track separation [21]. Therefore determining the characteristic impedance using Eqn. 2.6 for short track separation, which is generally found in a real PCB, will not be accurate.

The characteristic impedance of two parallel PCB tracks was determined here from the exact expressions of the PUL parameters of these tracks. The characteristic impedance (Z_0) in terms of PUL is given by

$$Z_0 = \sqrt{\frac{L}{C}} \quad \Omega \quad (4.7)$$

Substituting the expressions for L (Eqn. 4.4) and C (Eqn. 4.6) in Eqn. 4.7 gives,

$$Z_0 = \sqrt{\frac{\mu_0}{\epsilon_0}} \frac{1}{\sqrt{\epsilon_r'}} \frac{K(k)}{K'(k)} \quad (4.8)$$

An exact and accurate expression for $K(k)/K'(k)$ is given by Paul [97] as:

$$\frac{K(k)}{K'(k)} = \frac{1}{\pi} \ln \left(2 \frac{1 + \sqrt{k}}{1 - \sqrt{k}} \right) \quad \text{if } 0.707 \leq k \leq 1.0 \quad (4.9a)$$

$$\frac{K(k)}{K'(k)} = \frac{\pi}{\ln \left(2 \frac{1 + \sqrt{k'}}{1 - \sqrt{k'}} \right)} \quad \text{if } 0.0 \leq k \leq 0.707 \quad (4.9b)$$

The characteristic impedance of two parallel tracks was calculated using both Eqn. 2.6 (as given in chapter 2) and Eqn. 4.8 for various s/w ratios. Raut *et al.* [17] also calculated

these values using the software package based on the boundary element method. Table 4.1 shows a comparison of these values.

Table 4.1 Characteristic impedance (Z_0)

s/w ratio	Z_0 using Eqn. 2.6 (Ω)	Z_0 using Eqn. 4.8 (Ω)	Z_0 [17] (Ω)
1.1	26.614	123.932	68.330
1.2	37.342	127.320	79.320
2.0	79.070	147.351	121.110
3.0	105.765	165.397	147.770
5.0	137.540	190.267	179.500

Table 4.1 shows that for large s/w ratio, the difference among Z_0 values (Eqn. 2.6, Eqn. 4.8 and reference [17]) becomes small.

4.2.4 COMPUTATION OF CURRENT AND VOLTAGE

Currents and voltages along the PCB tracks are computed using TLM under the following assumptions:

- (i) short track separation as compared to the wavelength;
- (ii) lossless track (i.e. track should be a perfect conductor);
- (iii) the propagating mode is only the TEM wave.

Two parallel tracks of length l running between the two pairs of pins of two devices are considered. These two tracks constitute a two wire transmission line. The driving device (i.e. source) is replaced by its input impedance and the driven device (i.e. load) is replaced by its output impedance. The transmission line structure is illustrated in Fig. 4.3(a) and its geometry is shown in Fig. 4.3(b). In Fig. 4.3(a), Z_s is the source impedance and Z_l is the load impedance.

The source end current, load end current and currents along the tracks are determined from transmission line equations. These equations can be written as a pair of second-order differential equations in terms of voltage and current.

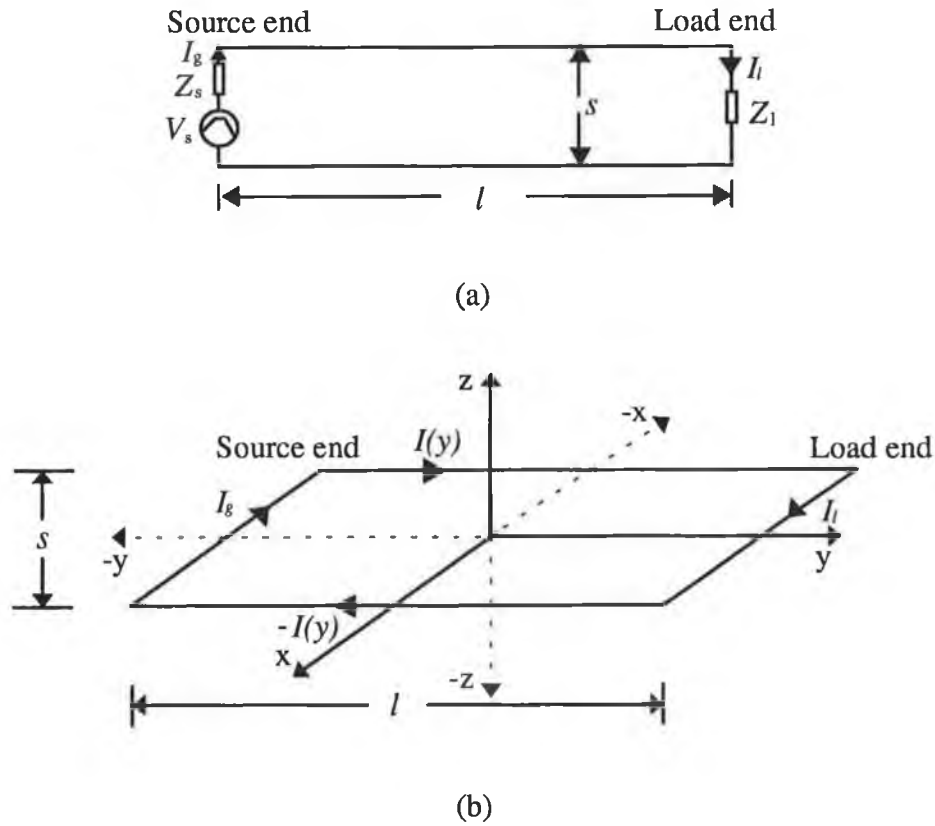


Fig. 4.3 A schematic of two parallel track running between two devices, (a) circuit configuration ; (b) geometry of the circuit.

These equations for a two conductor transmission line in the x - y plane of a rectangular coordinate system depicted in Fig. 4.3(b) are given by

$$\frac{\partial^2 V(y)}{\partial y^2} = -\beta^2 V(y) \quad (4.10)$$

$$\frac{\partial^2 I(y)}{\partial y^2} = -\beta^2 I(y) \quad (4.11)$$

where, β is the propagation constant, $V(y)$ is the voltage on the line and $I(y)$ is the current along the line.

The solutions of Eqns. 4.10 and 4.11 are determined by enforcing the line termination conditions and are given in [26, 95, 115]. The current distribution $I(y)$ along the line is determined by the following equation.

$$I(y) = \frac{V_s [Z_0 \cos\{\beta (l - y)\} + j Z_l \sin\{\beta (l - y)\}]}{D} \quad (4.12)$$

Similarly,

$$V(y) = \frac{V_s Z_0}{D} [Z_l \cos\{\beta (l - y)\} + j Z_0 \sin\{\beta (l - y)\}] \quad (4.13)$$

where D is a complex quantity and is given as

$$D = Z_0 (Z_s + Z_l) \cos(\beta l) + j (Z_0^2 + Z_s Z_l) \sin(\beta l) \quad (4.14)$$

The source end current (I_s) is obtained by putting $y = 0$ in Eqn. 4.12 and is given as

$$I_s = \frac{V_s (Z_0 \cos(\beta l) + j Z_l \sin(\beta l))}{D} \quad (4.15)$$

Similarly by substituting $y = l$ in Eqn. 4.12, the load end current (I_l) is obtained as

$$I_l = \frac{V_s}{D} Z_0 \quad (4.16)$$

These currents are sinusoidally distributed and therefore the radiated EM field due to these currents can be easily computed.

4.2.5 DISPLACEMENT CURRENT

Physically, there are equal and opposite alternating charges on the line as shown in Fig. 4.4(a), and these produce a displacement current (I_d)¹ in a capacitor. The displacement currents or fluctuating electric fields are confined to the region between the lines. In this case the displacement currents exist only in the x -direction as depicted in Fig. 4.4(b). These currents are not necessary for the functional performance of the electronic devices that the track connects and are substantially smaller than the track ends current and current along the track.

To find the displacement current between the two parallel tracks, consider a differential length (Δy) of the transmission line (i.e. track) shown in Fig. 4.4(b). Since the displacement current is virtually the capacitance current of the line, it can be determined using the following expression,

¹Subscript d is for displacement current.

$$I_d = j \omega C' V(y) \quad (4.17)$$

where,

C' – the capacitance of the differential length (Δy) and $C' = C\Delta y$

$V(y)$ – the line voltage

The line voltage is obtained from Eqn. 4.13.

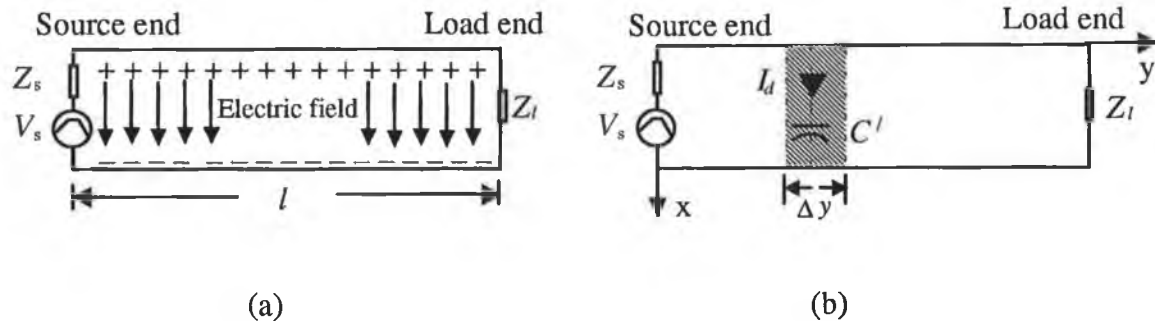


Fig. 4.4 Two wire transmission line (a) showing the equal and opposite charge on the line; (b) the path of displacement current through capacitance.

4.2.6 RADIATED FIELDS DUE TO FUNCTIONAL CURRENTS

The currents I_g , I_p and $I(y)$ are the functional currents of the circuits as shown in Fig. 4.3(b). A model of the radiation due to these currents is developed here. The computation of the radiated EM field involves two steps: (i) computation of the vector potential at a distant point from the PCB tracks and (ii) derivation of radiated field from the vector potentials. The radiated electric fields (\vec{E}) and magnetic fields (\vec{H}) are spatial derivative of the vector potentials [16].

The current at any point along a long track of length l in the y direction (as shown in Fig. 4.3(b)) is represented by $I(y')^{\#}$. The source and load ends are short in length in the x direction and therefore, the corresponding current is assumed uniform. The source end and load end currents are represented by I_g and I_l respectively.

[#] The prime represents the source co-ordinate.

4.2.6.1 Vector and scalar potentials

The magnetic vector potential (\vec{A}) due to the electric current density (\vec{J}) and vector electric potential (\vec{F}) due to magnetic current density (\vec{M}) of a conductor can be expressed [98] as:

$$\vec{A} = \frac{\mu}{4\pi} \iiint_{v'} \vec{J}(x', y', z') \frac{e^{-j\beta_0 R}}{R} dv' \quad (4.18)$$

$$\vec{F} = \frac{\epsilon}{4\pi} \iiint_{v'} \vec{M}(x', y', z') \frac{e^{-j\beta_0 R}}{R} dv' \quad (4.19)$$

where,

R – the distance from source to observation point

β_0 – the free space propagation constant and $\beta_0 = \frac{2\pi}{\lambda}$

λ – the wavelength in free space

x', y', z' – the source co-ordinates in rectangular co-ordinate system.

The scalar potential (Φ) due to electric charge density (ρ) of a conductor is given [112] as

$$\Phi = \frac{1}{4\pi\epsilon} \iiint_{v'} \rho(x', y', z') \frac{e^{-j\beta_0 R}}{R} dv' \quad (4.20)$$

This scalar potential is expressed in terms of vector potential using the Lorentz gauge relation [96]. This relation is given by

$$\nabla \cdot \vec{A} = -j\mu\epsilon\omega\Phi \quad (4.21)$$

Since the transmission line contains only the electric current source (i.e. $\vec{M}=0$), the contribution of vector electric potential to radiated field will be zero. From Fig. 4.3(b), it is evident that \vec{J} is a line source. There are two line sources: (i) the x -directed line source and (ii) the y -directed line source. The magnetic vector potential due to a line source reduces to

$$\vec{A}_\alpha = \frac{\mu}{4\pi} \int I(\alpha') \frac{e^{-j\beta_0 R}}{R} d\alpha' \quad (4.22)$$

where, α is either x or y depending on whether the line source is x or y directed respectively.

As there is no line source along the z -direction, the z component of the vector potential will be zero. Therefore the net vector potential (\vec{A}) due to these line sources can be written as

$$\vec{A} = A_x \vec{x} + A_y \vec{y} \quad (4.23)$$

where \vec{x} and \vec{y} are unit vectors oriented along the x and y axis respectively.

To compute the vector potential for the circuit shown in Fig. 4.3.(a), the geometry of the field point is illustrated in Fig. 4.5. The origin of rectangular co-ordinate system is in the middle of the circuit shown in Fig. 4.5.

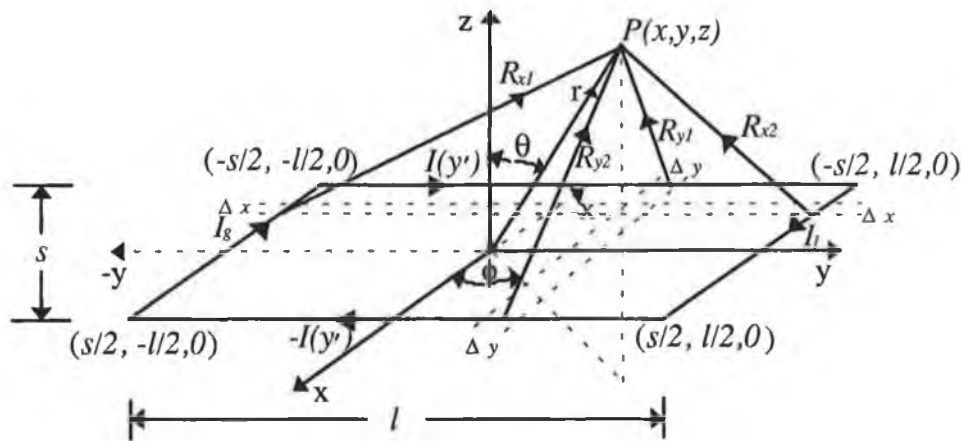


Fig. 4.5 Geometrical parameters for computing the vector potentials and radiated fields at the observation point $P(x, y, z)$ ².

The x component of the vector potential is due to currents I_g and I_l . The elemental vector potential (ΔA_x) at point $P(x, y, z)$ due to these currents is written as

$$\Delta A_x = \frac{\mu}{4\pi} \Delta x \left[I_g \frac{e^{-j\beta_0 R_{x1}}}{R_{x1}} - I_l \frac{e^{-j\beta_0 R_{x2}}}{R_{x2}} \right] \quad (4.24)$$

where,

Δx — the differential length of x -directed line source;

²The unprimed co-ordinates represent a observation point.

- R_{x1} – the distance from the x -directed line source at source end to observation point;
 R_{x2} – the distance from the x -directed line source at load end to observation point.

The net x -component (A_x) of vector potential (\vec{A}) can be obtained by integrating the elemental vector potential over the length of x -directed line source i.e. the separation between the two tracks:

$$A_x = \frac{\mu}{4\pi} \int_{-\frac{s}{2}}^{\frac{s}{2}} \left[I_g \frac{e^{-j\beta_0 R_{x1}}}{R_{x1}} - I_l \frac{e^{-j\beta_0 R_{x2}}}{R_{x2}} \right] dx' \quad (4.25)$$

The currents along the same cross-sectional position of a transmission line are equal in magnitude but opposite in direction. Thus the y component (A_y) of vector potential (\vec{A}) due to y -directed line sources shown in Fig. 4.5 can be written as,

$$A_y = \frac{\mu}{4\pi} \int_{-\frac{l}{2}}^{\frac{l}{2}} I(y') \left[\frac{e^{-j\beta_0 R_{y1}}}{R_{y1}} - \frac{e^{-j\beta_0 R_{y2}}}{R_{y2}} \right] dy' \quad (4.26)$$

where,

- $I(y')$ – the current along the y -directed track;
 R_{y1} – the distance from the y directed line source along top track to observation point ;
 R_{y2} – the distance from the y directed line source along bottom track to observation point.

The expressions for R_{x1} , R_{x2} , R_{y1} and R_{y2} are given in Appendix D1. A numerical integration technique (such as Simpson's rule) can be employed to obtain the vector potentials.

4.2.6.2 Radiated electric field

The electric field is expressed in terms of the vector and scalar potentials [98] as:

$$\vec{E} = -j\omega\vec{A} - \nabla\Phi - \frac{1}{\epsilon} \nabla \times \vec{F} \quad (4.27)$$

Substituting Eqn. 4.21

$$\vec{E} = -j\omega\vec{A} - \frac{j}{\omega\mu\epsilon} \nabla(\nabla \cdot \vec{A}) - \frac{1}{\epsilon} \nabla \times \vec{F} \quad (4.28)$$

The last term of Eqn. 4.28 vanishes due to the absence of a magnetic current source in a transmission line. Therefore the resultant electric field is

$$\vec{E} = -j\omega\vec{A} - \frac{j}{\omega\mu\epsilon} \nabla(\nabla \cdot \vec{A}) \quad (4.29)$$

Substituting Eqn. 4.23 in Eqn. 4.29 one obtains the orthogonal components of \vec{E} :

$$E_x = -j\omega A_x - \frac{j}{\omega\mu\epsilon} \left(\frac{\partial^2 A_x}{\partial x^2} + \frac{\partial^2 A_y}{\partial x \partial y} \right) \quad (4.30)$$

$$E_y = -j\omega A_y - \frac{j}{\omega\mu\epsilon} \left(\frac{\partial^2 A_y}{\partial y^2} + \frac{\partial^2 A_x}{\partial y \partial x} \right) \quad (4.31)$$

$$E_z = -\frac{j}{\omega\mu\epsilon} \left(\frac{\partial^2 A_x}{\partial z \partial x} + \frac{\partial^2 A_y}{\partial z \partial y} \right) \quad (4.32)$$

The exact expressions for the electric field components are derived by substituting the expression for A_x from Eqn. 4.25 and the expression for A_y from Eqn. 4.26, in Eqns. 4.30, 4.31 and 4.32. The spatial derivatives of the vector potential are evaluated analytically and these derivations are given in Appendix D2.

The last term of the Eqn. 4.29 is known as the scalar potential term. Under far field conditions, the contribution of this term to the radiated field is negligible and the effect of dielectric could be neglected under this condition. As a result, the field equation would take a simple form. However this form has not been considered here.

4.2.6.3 Radiated magnetic field

The radiated magnetic field from a current carrying conductor can be expressed in terms of the vector potential. The magnetic field (\vec{H}) is given by

$$\vec{H} = \frac{1}{\mu} (\nabla \times \vec{A}) \quad (4.33)$$

Substituting Eqn. 4.23 in Eqn. 4.33 allows the expressions of the magnetic field components to be written as

$$H_x = -\frac{1}{\mu} \frac{\partial A_y}{\partial z} \quad (4.34)$$

$$H_y = \frac{1}{\mu} \frac{\partial A_x}{\partial z} \quad (4.35)$$

$$H_z = \frac{1}{\mu} \left(\frac{\partial A_y}{\partial x} - \frac{\partial A_x}{\partial y} \right) \quad (4.36)$$

The exact expressions of the magnetic field components are given in Appendix D3.

4.2.7 RADIATED FIELD DUE TO DISPLACEMENT CURRENT

Radiated electric field (\vec{E}_d) and magnetic field (\vec{H}_d) due to displacement current are computed using Eqn. 4.29 and Eqn. 4.33 respectively. For electrically short track separation, the vector potential due to I_d can be computed by using the formula for a Hertzian dipole. The geometry involved in the computation of the radiated field due to I_d is given in Appendix D4. Since the displacement currents are x -directed shown in Fig. 4.4, only the x component of the vector potential due to I_d (i.e. A_{xd}) must be found.

$$A_{xd} = \frac{\mu s}{4\pi} I_d \frac{e^{-j\beta R_d}}{R_d} \quad (4.37)$$

where, R_d is the distance between the displacement current element to the observation point.

For large track separation, the Hertzian formula for a dipole cannot be applied to find the vector potential. In such cases, Eqn. 4.22 is used and A_{xd} is given by

$$A_{xd} = \frac{\mu}{4\pi} \int_s I_d \frac{e^{-j\beta R_d(x')}}{R_d(x')} dx' \quad (4.38)$$

where,

$R_d(x')$ – the distance between the displacement current element along the x -axis and observation point. The expression for R_d has been given in Appendix D4.

Thus the field components of \vec{E}_d due to I_d can be expressed in terms of vector potential (A_{xd}). The field components are given by

$$E_{xd} = -j\omega A_{xd} - \frac{j}{\omega\mu\epsilon} \frac{\partial^2 A_{xd}}{\partial x^2} \quad (4.39)$$

$$E_{yd} = -\frac{j}{\omega\mu\epsilon} \frac{\partial^2 A_{xd}}{\partial y\partial x} \quad (4.40)$$

$$E_{zd} = -\frac{j}{\omega\mu\epsilon} \frac{\partial^2 A_{xd}}{\partial z\partial x} \quad (4.41)$$

Since the magnetic vector potential due to displacement current is only in the x -direction for the circuit shown in Fig. 4.3, the x -component of magnetic field (\vec{H}_d) will be zero (i.e. $H_{xd} = 0$). The y and z component can be obtained from Eqns. 4.42 and 4.43 respectively as:

$$H_{yd} = -\frac{1}{\mu} \frac{\partial A_{xd}}{\partial z} \quad (4.42)$$

$$H_{zd} = \frac{1}{\mu} \frac{\partial A_{xd}}{\partial y} \quad (4.43)$$

Electrically small track separation was assumed in evaluating the spatial derivatives of the vector potentials due to displacement current. The expressions for radiated electric and magnetic fields due to displacement current are given in Appendix D5 and D6 respectively.

4.2.8 TOTAL RADIATED FIELD

The total radiated electric field (\vec{E}_t) can be obtained from the vector addition of \vec{E} and \vec{E}_d .

$$\vec{E}_t = \vec{E} + \vec{E}_d \quad (4.44)$$

Similarly the total radiated magnetic field is written as

$$\vec{H}_r = \vec{H} + \vec{H}_d \quad (4.45)$$

4.3 NUMERICAL METHOD AND SOFTWARE

The driving source is assumed to be a crystal oscillator. This oscillator generates a train of periodic trapezoidal pulses (as illustrated in Fig. D7.1 of Appendix D). The amplitude (V_{ns}) of the n th harmonic of the pulse is obtained using Eqn. D7-1.

The flow chart of a programme developed to compute radiated field is shown in Fig. 4.6. The computer programme listing is given in Appendix D8 and D9.

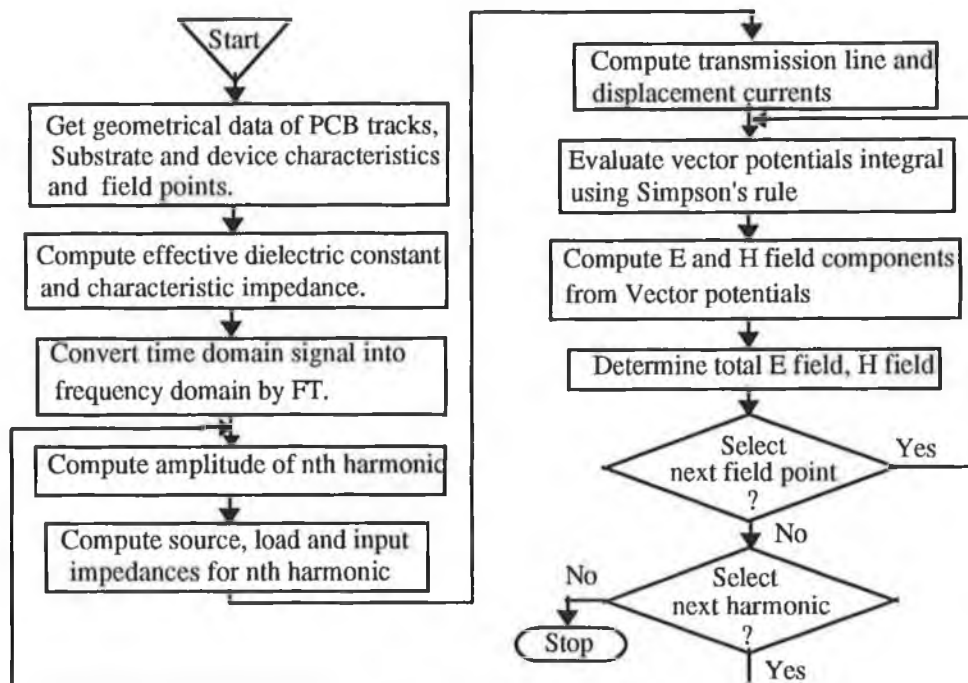


Fig. 4.6 A schematic flow chart to predict EM radiation from a PCB using the extended TLM.

The input data of this programme are: (i) cross-sectional dimension of PCB track, (ii) track length and track separation, (iii) characteristics of PCB substrate (iv) input impedance of the driven device (v) output impedance of driving device, (vi) characteristics of driving signal (refer to Appendix D7) and (vii) field observation point.

4.4 RESULTS AND COMPARISON

The radiated EM fields (from a test circuit such as that shown in Fig. 4.3(a)) were computed using the proposed TLM techniques. The predicted field using TLM was compared with that from NEC-2. Two parallel tracks laid down on a glass epoxy substrate were used for the test. Geometrical data were as follows: track length (l) = 10.0 cm, track width (w) = 0.048 cm, track separation (s) = 0.24 cm and track thickness (t) = 35 μm .

The characteristics of the substrate were: (i) dielectric constant (ϵ_r) = 4.7, (ii) substrate thickness (h_s) = 1.45 mm and relative permeability (μ_r) = 1.0.

The effective dielectric constant (ϵ'_r) of the medium surrounding the track was computed using Eqn. 4.2 from the above mentioned data. The value of ϵ'_r was found to be 2.5. The velocity of the propagating wave along the track was computed using Eqn. 4.1, and the characteristic impedance of two parallel tracks was determined using Eqn. 4.8.

The tracks were excited by a crystal oscillator (several choices of crystal: 6 MHz, 10 MHz, 24 MHz, 40 MHz and 50 MHz). The pulse characteristic of a crystal oscillator is given in Table TD1 of Appendix D7.

The comparison was then made by determining the radiation, (using both methods), for the following situations:

- (i) at different observation points (e.g. different points in the x - z plane at a radial distance of 0.1 m from the PCB) at a particular frequency;
- (ii) at various frequencies;
- (iii) using several choices of load impedance.

4.4.1 DIFFERENT OBSERVATION POINTS

The radiated electric field from a sample PCB as illustrated in Fig. 4.3 was determined at different points in the x - z plane (i.e. the azimuth angle $\phi = 0^\circ$) of a rectangular co-ordinate system. The load as depicted in Fig. 4.3 was replaced by a resistance of value 1.2 k Ω . A

crystal oscillator that generates a trapezoidal pulse of frequency 40 MHz was used as a source. The predictions were also repeated for a crystal oscillator of 24 MHz.

A plot of the radiated electric fields predicted by TLM and NEC-2 at a radial distance (r) of 0.1 m from the PCB is shown in Fig. 4.7, at different values of polar angle θ . The comparison is presented for the third, fifth and the seventh harmonics of the pulses. The NEC-2 predicted values are found to be within ± 4 dB of TLM computed values. This variation is not significant compared to total radiation.

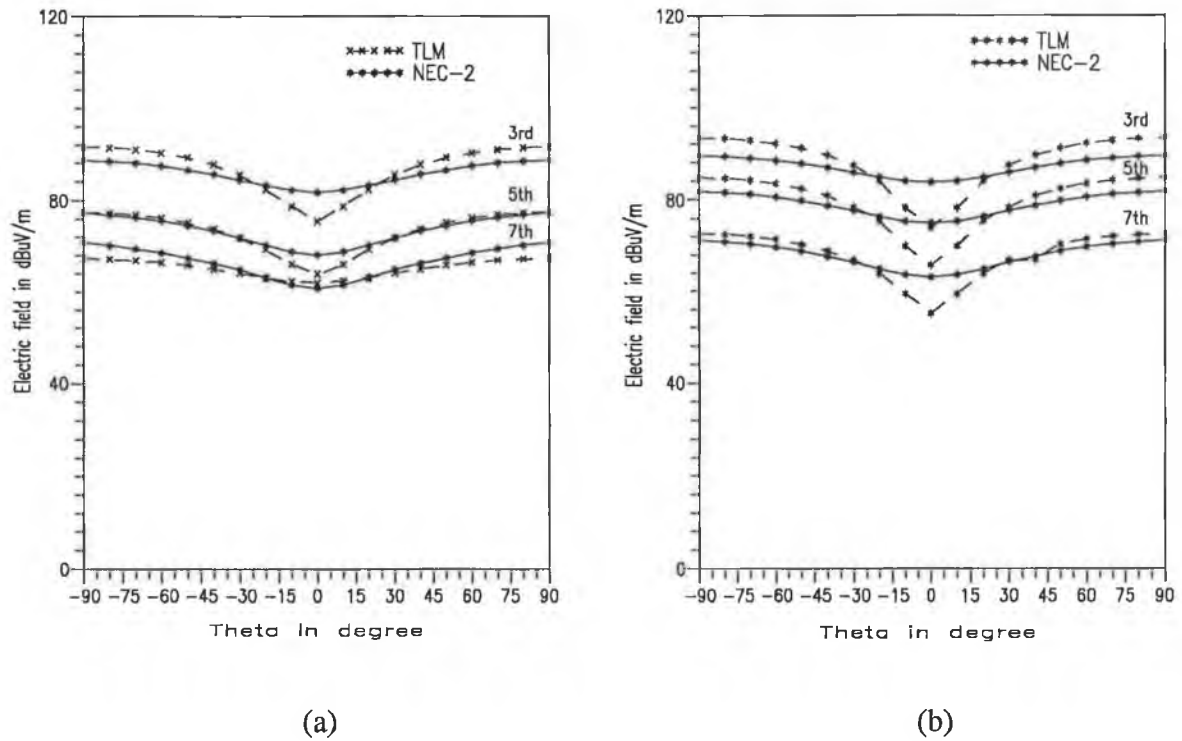


Fig. 4.7 Radiated electric field as a function of θ : (a) 24 MHz crystal; (b) 40 MHz crystal.

The radiated magnetic fields were also determined for the same PCB. In this case a crystal oscillator of 6 MHz was used as a source. The radiated fields were predicted at fundamental frequency, and the third and the fifth harmonics of the source. Fig 4.8 (a) shows a plot of the radiated magnetic fields obtained from TLM and NEC-2 at $r = 0.1$ m and $\phi = 90^\circ$. The prediction was repeated for a crystal oscillator of 10 MHz. These results are shown in Fig. 4.8 (b).

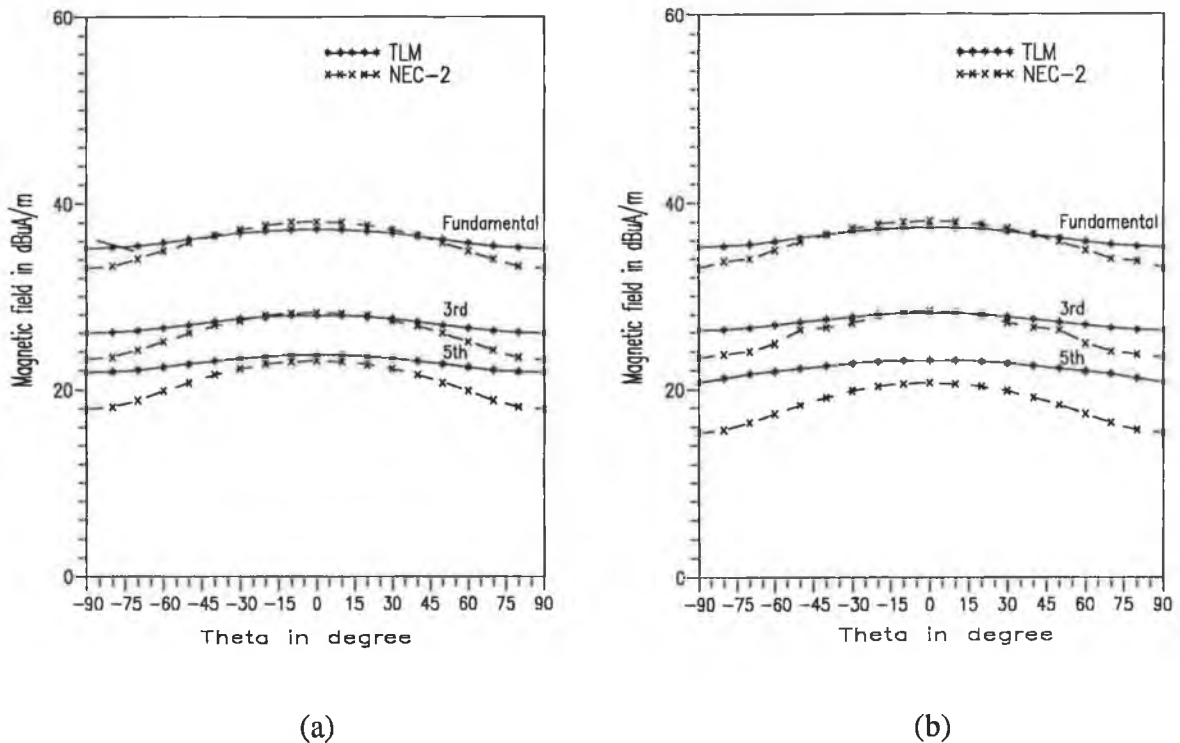


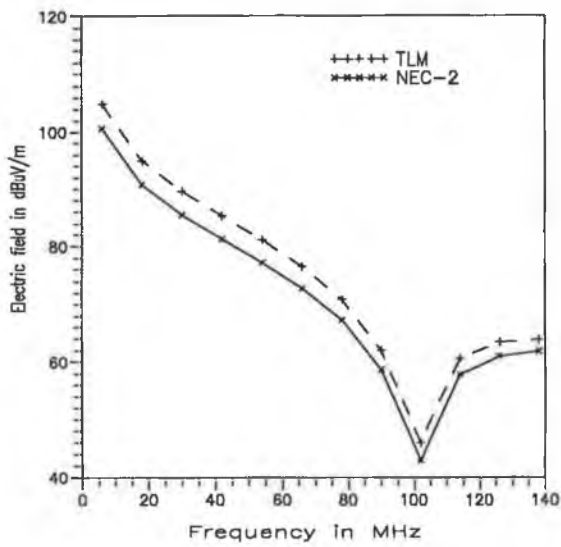
Fig. 4.8. Radiated magnetic field as a function of θ : (a) 6 MHz crystal; (b) 10 MHz crystal.

The TLM predictions are found about 1 to 4 dB higher than those of NEC-2.

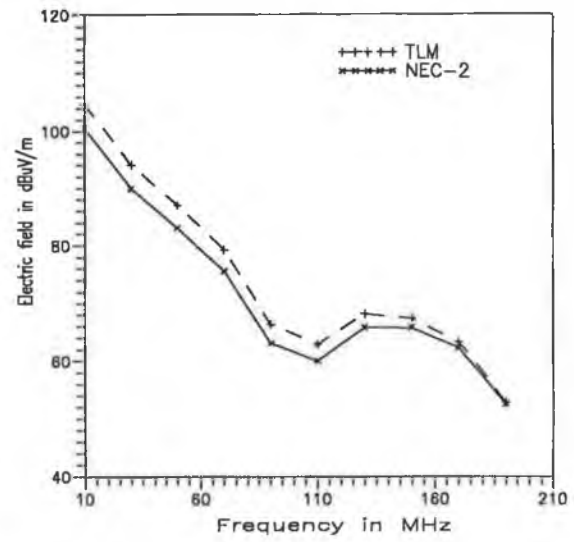
4.4.2 DIFFERENT FREQUENCIES

The radiated electric fields were also computed at different frequencies corresponding to odd harmonics of a pulse (i.e. a clock or a data signal) generated by a crystal oscillator. The fields were predicted at a distance of 0.1 m from the PCB. The maximum field is of most interest in EMI problems. Therefore the maximum radiated electric field was computed. The maximum field occurs in the x - z plane (i.e. the azimuth angle $\phi = 0^\circ$) at $\theta = 90^\circ$ for the PCB shown in Fig. 4.3(b).

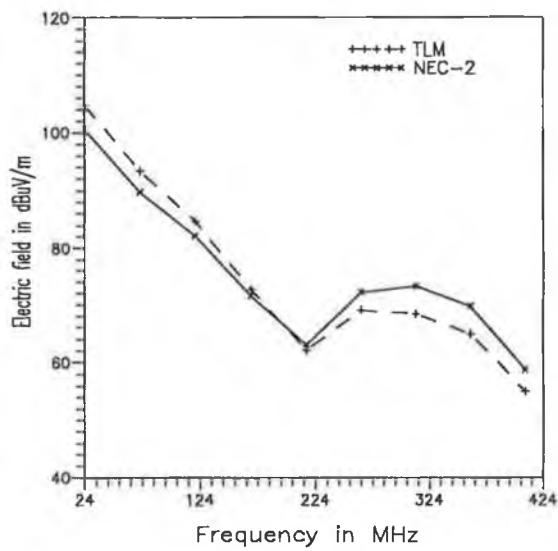
A plot of the radiated electric fields as a function of frequency corresponding to odd harmonics of clock signal, predicted using TLM and NEC-2 is shown in Fig. 4.9. It is found that in all cases, the TLM predictions are about 2 to 4 dB higher than those of NEC-2.



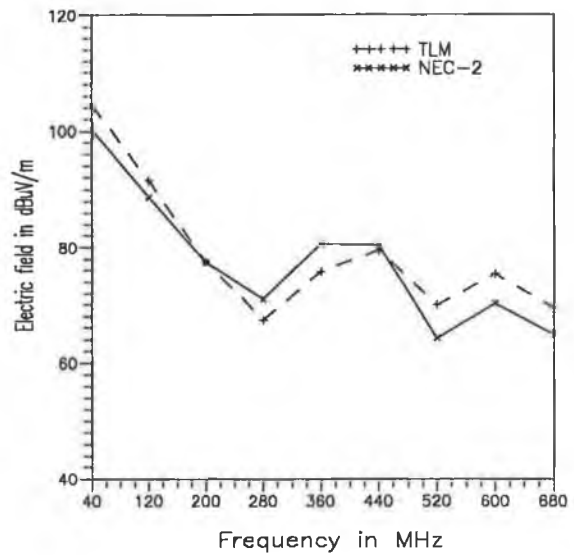
(a)



(b)



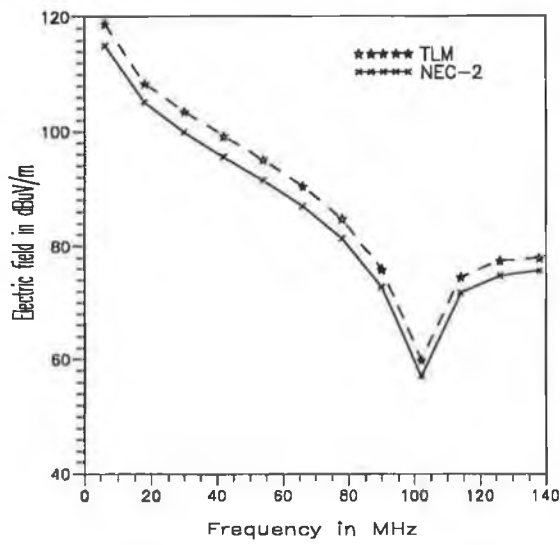
(c)



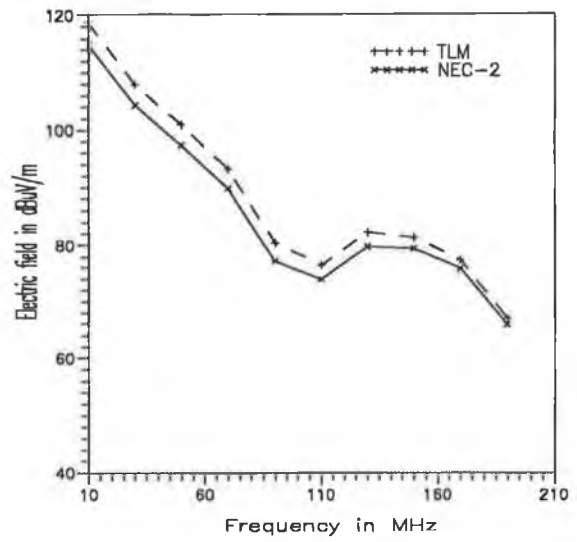
(d)

Fig. 4.9. Radiated electric field as a function of frequency at a radial distance of 0.1 m from PCB: (a) 6 MHz crystal; (b) 10 MHz crystal ; (c) 24 MHz ; (d) 40 MHz crystal oscillator.

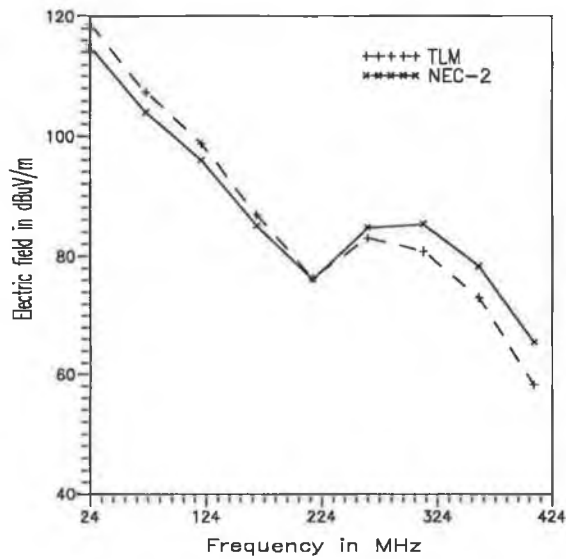
The radiated electric fields were also computed at a distance of 0.05 m from the PCB. The plot of predicted field as a function of frequency is shown in Fig. 4.10. This plot also reveals a good agreement between the NEC-2 predicted results and TLM computed values.



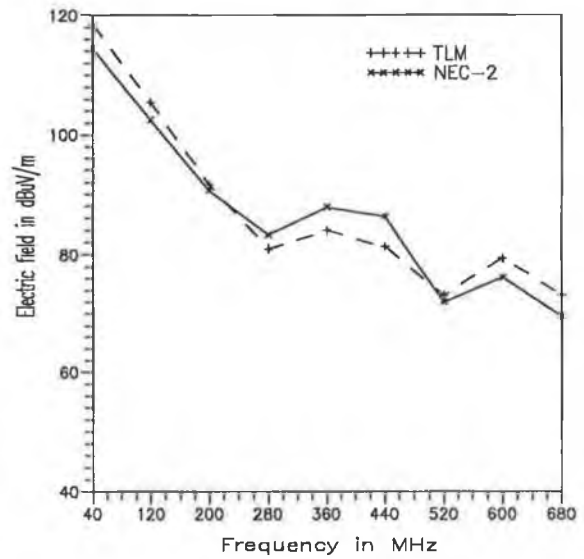
(a)



(b)



(c)



(d)

Fig. 4.10. Radiated electric field as a function of frequency at a radial distance of 0.05 m from PCB: (a) 6 MHz crystal ; (b) 10 MHz crystal ; (c) 24 MHz ; (d) 40 MHz crystal oscillator.

4.4.3 DIFFERENT LOAD IMPEDANCES

The radiated electric fields were computed for two different load values using NEC-2 and TLM: (i) a resistive load ($Z_l = 100 \Omega$) and (ii) a complex load ($R_l = 1.2 \text{ k}\Omega$ and $C_l = 5.7 \text{ pF}$). A plot of the radiated electric fields as a function of frequency corresponding to odd harmonics of the 40 MHz pulse at a distance of 0.1 m from the PCB is shown in Fig. 4.11.

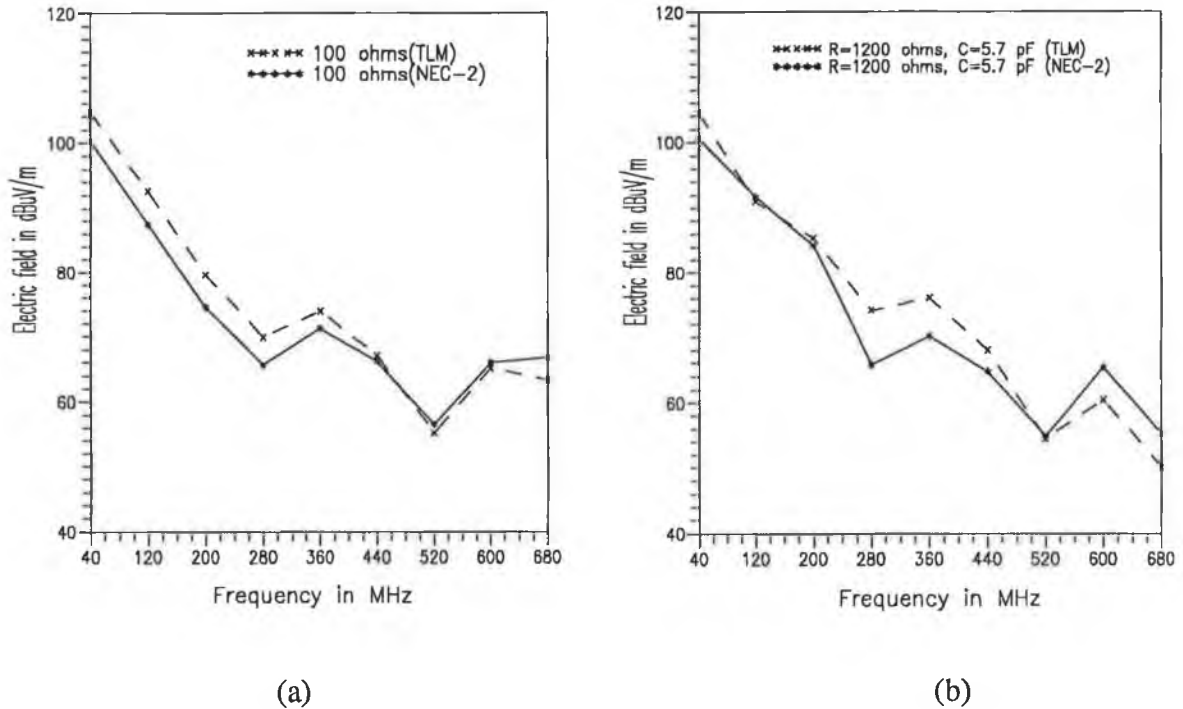


Fig. 4.11. Radiated electric field as a function of frequency at a radial distance of 0.1m from PCB: (a) resistive load ($Z_l = 100 \Omega$); (b) complex load ($R_l = 1.2 \text{ k}\Omega$, $C_l = 5.7 \text{ pF}$). 40 MHz crystal oscillator was used.

The plot shows a very good agreement between the NEC-2 predicted value and the TLM computed value.

4.5 EFFECT OF DISPLACEMENT CURRENT

The radiated electric fields due to functional (i.e. desired) currents and displacement current were computed separately using TLM. The total radiated electric fields were obtained from the vector addition of the individual field components. The radiated electric fields were predicted at different frequencies corresponding to odd harmonics of a pulse generated by a

crystal oscillator (two choices of crystal of 10 MHz and 50 MHz) at a distance of 0.1 m from the PCB.

A plot of the radiated electric fields as a function of frequency is shown in Fig. 4.12. The plot shows that the radiated electric fields due to displacement current is larger than that due to functional currents. Thus in predicting the radiated field under near field regions, it is necessary to consider the displacement current with the functional currents.

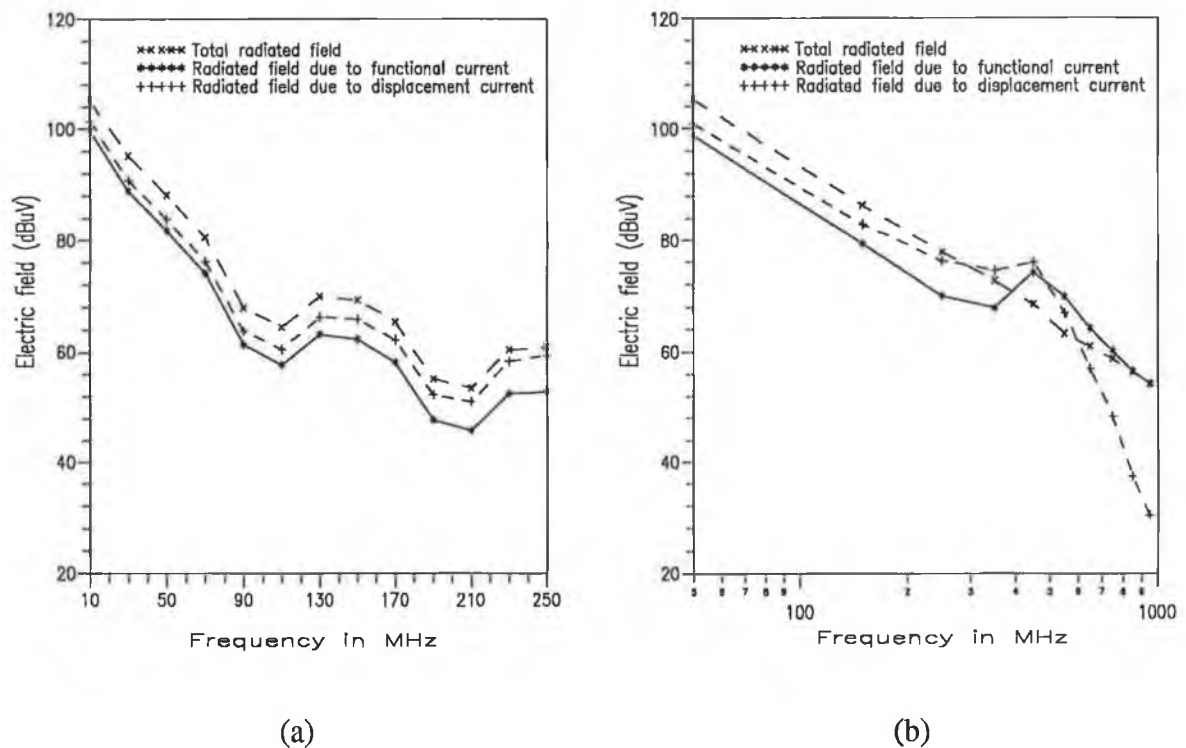


Fig. 4.12 Diagram shows the effect of displacement current in PCB radiation (a) 10 MHz ; (b) 50 MHz crystal oscillator.

The effect of displacement current at far field region was also observed. A plot of predicted radiation as function of radial distance from the PCB to observation point is shown in Fig. 4.13. The plot clearly shows that the radiated field due to displacement current falls more rapidly than that due to functional currents when the radial distance is greater than 0.16λ (i.e. far field region), which is approximately 0.32 m for a 150 MHz signal (e.g. the 15th harmonic of 10 MHz pulse).

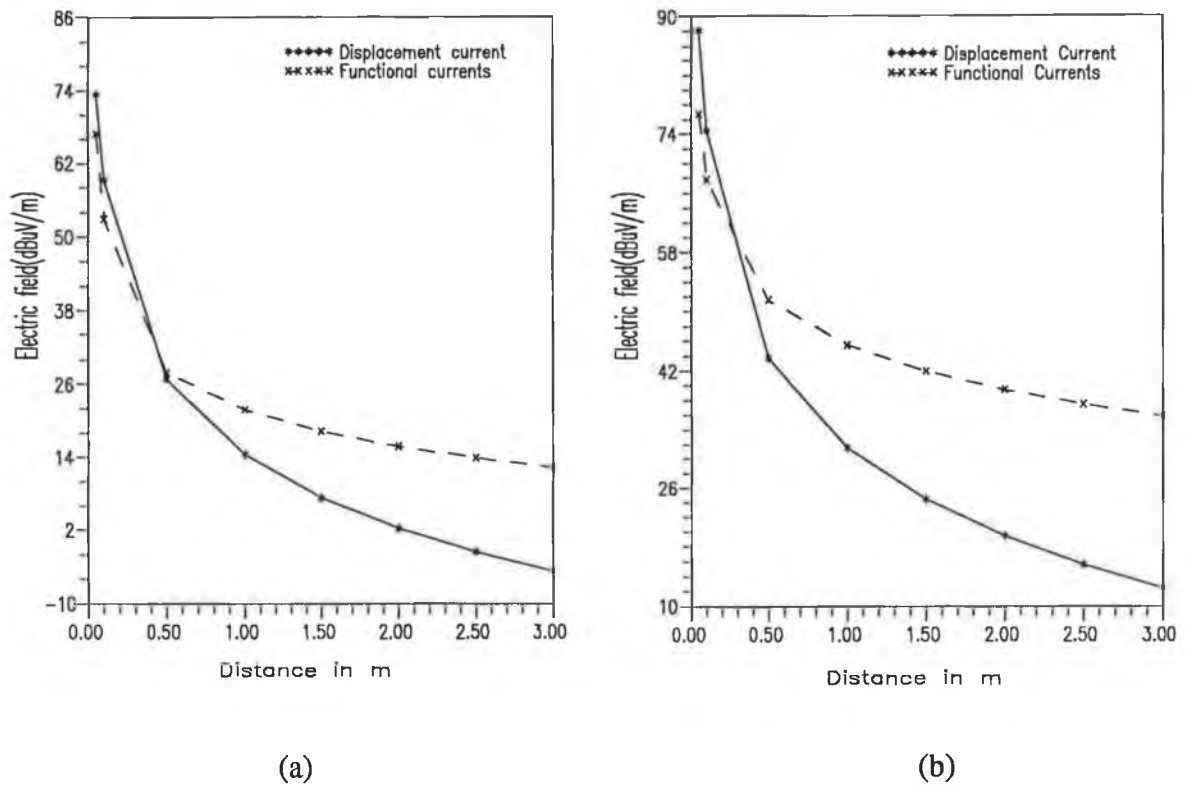


Fig. 4.13 Radiated electric fields due to displacement and functional currents as function of radial distance from PCB to observation point: (a) 150 MHz (i.e. 15th harmonic of 10 MHz crystal) ; (b) 350 MHz (i.e. 7th harmonic of 50 MHz crystal).

It is also evident from Fig. 4.12(b) that at frequencies above 550 MHz, the radiated field due to displacement current is less than that due to functional currents. The total radiated field is also very close to the radiated field due to functional currents because the radial distance (i.e. 0.1 m in this case) is greater than 0.16λ for frequencies above 550 MHz. Therefore in the far field region the radiated field due to displacement current can be neglected.

4.6 CONCLUDING REMARKS

The use of TLM in predicting EM radiation from a complex circuit is very difficult. Thus a simple circuit was chosen as an example for comparison of NEC-2 predicted radiation with that from TLM computation. In this case, the results from NEC-2 and TLM were in good

agreement. Thus it is assumed that the same agreement would also be found for a complex circuit.

The effect of displacement current in radiated emission has been described. It is concluded that the displacement current produces a larger radiation than that due to the functional currents at near field region.

Chapter 5

COMPOSITE CAD PACKAGE

- ❑ DEVELOPMENT OF COMPOSITE CAD PACKAGE
- ❑ GEOMETRICAL AND LOAD DATA EXTRACTION ALGORITHM
- ❑ ELECTRICAL DATA EXTRACTION ALGORITHM
- ❑ INCORPORATING RADIATION REDUCING TECHNIQUES INTO THE COMPOSITE CAD PACKAGE
- ❑ DETERMINATION OF OPTIMUM LAYOUT

5.1 INTRODUCTION

A composite CAD package has been proposed in this project to predict and reduce the PCB radiation during the design process of an electronic product. The development of this CAD package is described in section 5.2.

The use of a composite CAD package to predict and reduce PCB radiation depends on data sharing among the various circuit design packages (CDPs) and an EM computation tool (NEC-2). According to the needs of CDPs and NEC-2, data extraction and preparation of data files are essential. The salient features of various CDPs used in this work are discussed in section 5.3. Section 5.4 describes the data extraction algorithms.

Various techniques which can be employed to reduce the PCB radiation during the design process were described in the introductory chapter. Section 5.5 presents an algorithm for incorporating these techniques into the composite CAD package. An analysis to determine the optimum layout which could minimise PCB radiation is presented in section 5.6.

5.2 DEVELOPMENT OF A COMPOSITE CAD PACKAGE

The developed composite CAD package is based on the combination of circuit design packages and an EM computation tool. A block diagram of this package is shown in Fig. 5.1.

The circuit design packages that have been used in conjunction with the EM computation tool NEC-2 are : (i) ORCADTM [109] as a schematic design tool , (ii) PSPICETM [118] as a circuit simulation tool and (iii) BoardmakerTM (BM) [108] as a PCB layout tool. The modified NEC-2 (as described in section 3.5) is used here.

Within the process of designing an electronic circuit with EMC verification, a schematic is developed with the aid of the schematic tool ORCAD. From this tool one obtains a netlist that can be passed to a circuit simulation package PSPICE which yields electrical data (node voltages and frequency). The netlist can also be passed to a board layout tool BM for component placement and track routing. BM prepares an output file containing the geometrical data of a PCB.

All the data required by NEC-2 would therefore be available. By transferring the data to NEC-2, the radiation from a proposed PCB could be obtained and compared with the pre-

defined EMC requirements. Design engineers could also "close the loop" and modify the design where these requirements have not been met. EMC could thus become an integral part of the "soft" design process (i.e. prototyping without hardware).

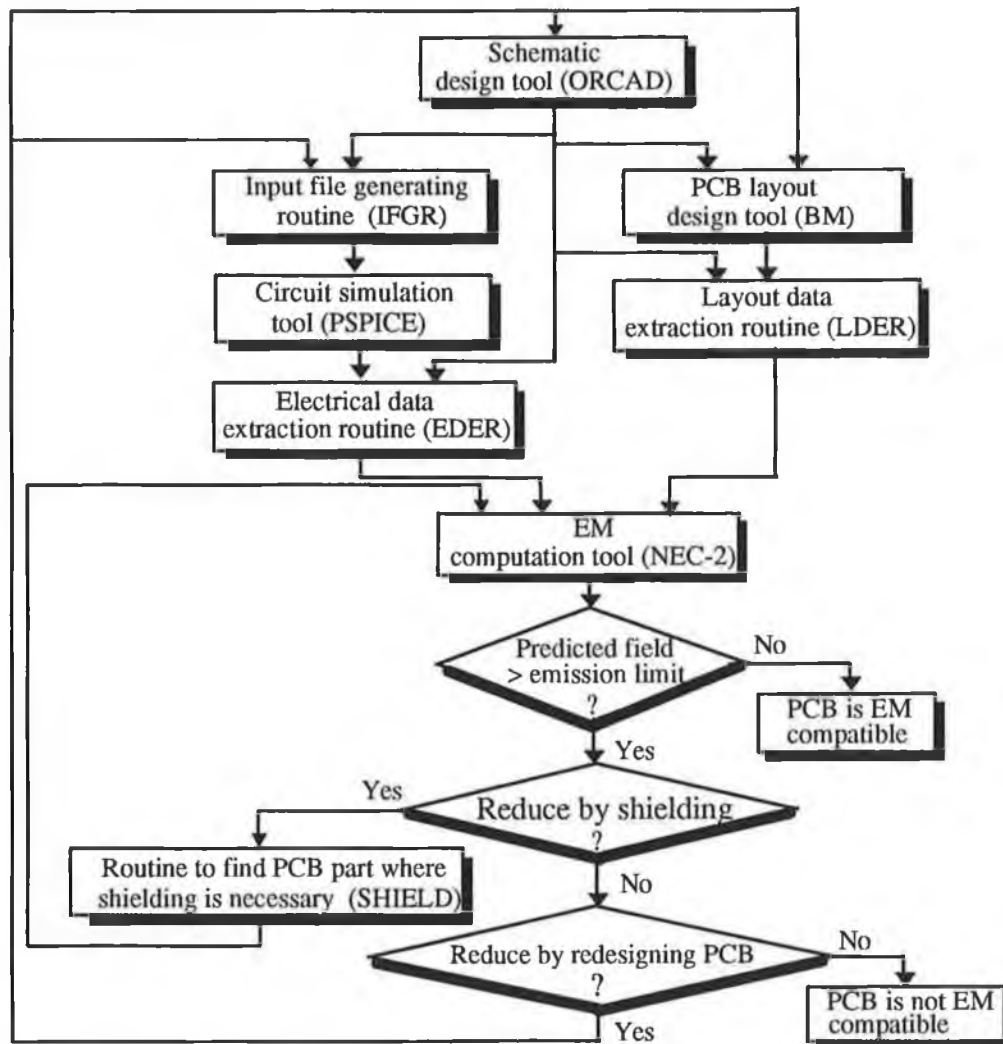


Fig. 5.1. Overall structure of a composite CAD package for predicting and reducing PCB radiation at design stage.

The netlist created by ORCAD is not a complete input file for PSPICE, hence the necessity for the input file generating routine (IFGR) in Fig. 5.1.

The original NEC-2 programme requires the user to enter all input data. This involves human effort and hence it is both time consuming and prone to errors, especially in the case of a complex structure such as a PCB. Extracting all the required data from the circuit design

tools is also not a straightforward task. Therefore a data extraction algorithm was developed. The extraction of data is divided into two parts:

- (i) extraction of geometrical and load data ;
- (ii) extraction of electrical data.

The layout data extraction routine (LDER) extracts the geometrical and load data of a PCB from the layout tool. The electrical data extraction routine (EDER) is used to extract the electrical data from the circuit simulation tool. The data extraction algorithms will be discussed later in this chapter.

If the predicted radiation exceeds the radiation limit, the composite CAD package requests the circuit designer to reduce EM radiation in two different ways as follows: (i) by providing shielding in some section of the PCB and (ii) by employing a reducing technique (e.g. by changing PCB layout, track size and separation, filtering the higher harmonics). The designer can choose either or both. To reduce the radiation using the first method, the designer has to find the section of the PCB where shielding is required. The developed programme SHIELD and ASSC (not shown in Fig. 5.1) can perform this function.

It is necessary to link all the packages and developed software. A batch routine to accomplish the links was written and is given in Appendix E1.

5.3 CIRCUIT DESIGN PACKAGES

Various CAD packages used in the design of electronic circuits from schematic to PCB layout are commercially available, as mentioned in section 2.5. The salient features of circuit design packages that have been used in this work are described in the following subsections.

5.3.1 SCHEMATIC DESIGN TOOL

ORCAD/SDT-III¹ (version 3.2) was used as a schematic design tool. ORCAD™ was originally developed by OrCAD system corporation, Oregon, USA. This schematic design

¹This was the latest version of this software that was available to the author.

tool can run on an IBM personal computer or its compatibles. ORCAD [109] provides many facilities such as:

- (i) drafting a circuit schematic;
- (ii) extensive part libraries (e.g. TTL, CMOS, analogue, device) which are most commonly used for circuit design;
- (iii) editing a part of any library in the library editor;
- (iv) creating a part which is not available in the standard libraries;
- (v) generating a netlist (a list of connections) in various formats depending on the use of the netlist in other circuit design packages (e.g. SPICETM, EDIFTM, PCADTM, TANGOTM);
- (vi) design checking and part listing.

These facilities were exploited in the development of a composite CAD package.

5.3.2 CIRCUIT SIMULATION TOOL

A circuit simulation tool such as SPICE is used to analyse an electronic circuit. SPICE is a general-purpose analogue circuit simulation software package that was originally developed at the University of California, Berkeley, USA. PSPICE is a PC version of SPICE. The commercial version of PSPICE comes with a library of models for about 100 standard devices (diodes, bipolar transistors, power MOSFET's, operational amplifiers, comparator). The restricted version of PSPICE is used in this work. All the features of the commercial PSPICE are available in this version except the circuit size which is restricted to a maximum of about 10 transistors.

The circuit under analysis using PSPICE may contain resistors, capacitors, inductors, mutual inductors, independent voltage sources, four types of dependent sources, transmission lines and semiconductor devices. PSPICE (restricted version) has built-in models for four types of semiconductor devices such as diodes, bipolar junction transistors (BJTs), junction field effect transistors (JFETs) and metal oxide semiconductor field effect transistors (MOSFETs). The circuit designer only has to specify the appropriate model parameters. For example, the SPICE model for a BJT has 40 parameters including forward beta, reverse beta (i.e. current gain when one interchanges the collector and emitter of a transistor) and emitter resistance.

PSPICE allows one to analyse a circuit for non-linear DC, non-linear AC and non-linear transient analysis. The DC analysis portion of PSPICE determines the DC operating point of a circuit with inductors shorted and capacitors opened. A DC analysis is automatically performed prior to (i) a transient analysis to determine the initial conditions, and (ii) an AC small-signal analysis to determine the linearised small -signal models for non-linear devices.

PSPICE computes the output variables (node voltages) as functions of frequencies in an AC small signal analysis of a circuit. This programme first computes the DC operating point of a circuit and then determines linearised small-signal models for all non-linear devices in the circuit. The resultant linear circuit is then analysed over a user-specified range of frequencies.

In the transient analysis of a circuit, PSPICE computes the transient output variables as functions of time over a user-specified time interval. The initial conditions are automatically determined by DC analysis of the circuit. All time independent sources (e.g. power supplies) are set to their DC value.

A Fourier analysis is required in conjunction with a transient analysis to obtain the Fourier-coefficients of the transient's output in the frequency domain. PSPICE performs a Fourier analysis of a transient output variable and gives the amplitude and phase of the first nine harmonics and the DC component.

On the basis of designer's choices, PSPICE prepares an output file in a tabular form to provide the results of an analysis.

5.3.2.1 Preparation of an input file for PSPICE

The input file of a circuit simulation package generally contains the circuit design netlists, device model parameters, analysis statements, control and output options. The structure of this file for PSPICE is shown in Fig. 5.2. The circuit design netlist is described in terms of circuit nodes. The description of each component in a circuit should be given in a single line. Each power supply or signal input should also be described in a single line. The ground connection in the circuit is designated as node zero.

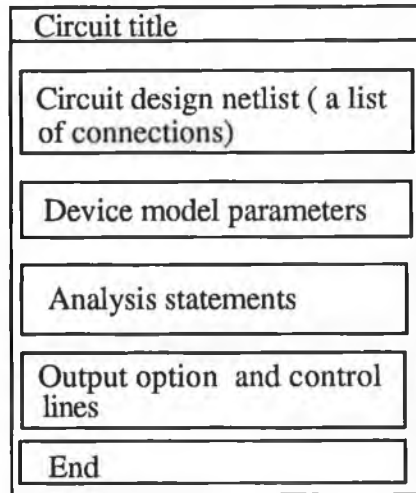


Fig. 5.2 Input file structure of a circuit simulation package (PSPICE).

PSPICE can get a device model name from the netlist created by ORCAD. Using this name, PSPICE can obtain model parameters from its own device library. However this facility is not available in the restricted version.

Fig. 5.2 shows that the netlist created by ORCAD is not a complete input file for PSPICE. An algorithm has been developed to prepare the input file and a flow chart for this algorithm is shown in Fig. 5.3.

The developed algorithm requires the following information from the designer:

- data for the power supply;
- device model parameters;
- type of analysis (e.g. transient, AC, Fourier analysis);
- data for analysis;
- output options for PSPICE.

After getting the above information, the algorithm performs the following tasks:

- getting the netlist from the output file created by ORCAD for SPICE;

- getting the signal node number;
- creating a file in a format that is similar to the input file for PSPICE.

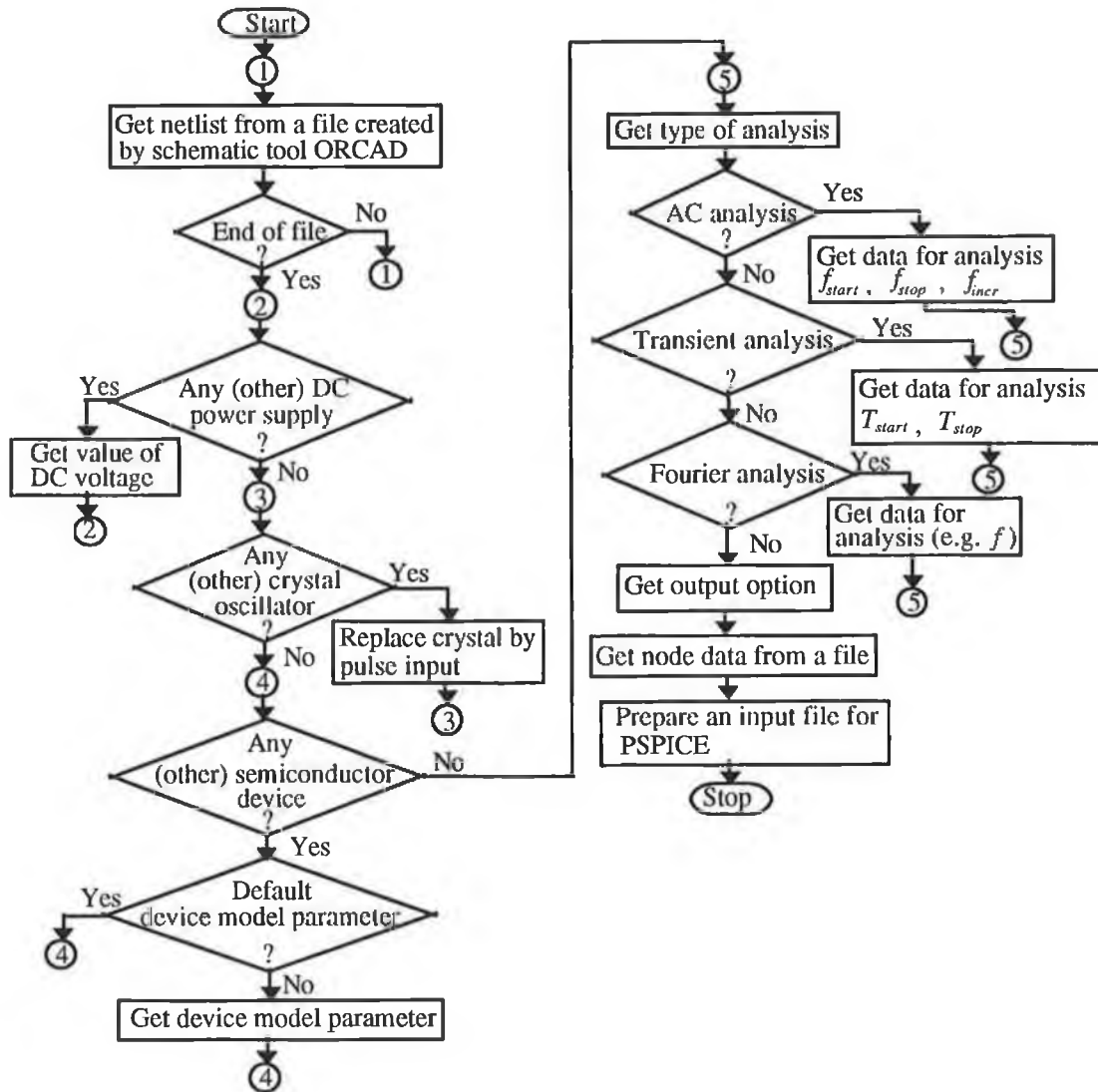


Fig. 5.3 Flow chart to prepare an input file for PSPICE.

The algorithm is implemented using a Fortran programme (IFGR) which is user interactive. A computer programme listing is given in Appendix E2.

5.3.3 PCB LAYOUT DESIGN TOOL

Boardmaker™ (BM version 2#), a PCB design tool has been used in this work for component placement and track routing. BM was originally developed by Tsien Ltd. UK. The following paragraphs discuss some salient features of this tool.

BM offers integrated utilities that allow a designer to translate the netlist created by some schematic design tools (Tango™, Mentor™, Schema™ and Protel™ formats are supported) into BM format [108]. Thus BM can read, translate and validate the netlist created by ORCAD. A circuit designer can easily and quickly map the schematic components (as described in the netlist) to a PCB layout symbol. BM is capable of performing an extensive pin name validation to reduce the possibility of errors in the mapping of a component. After mapping the symbols for components listed in a netlist, BM automatically creates a PCB and places the components on the board. The designer can also edit the location of a component in the PCB editor of this tool.

In considering the board structure, there is a choice of single layer, double layer and multilayer PCB. BM can provide up to 10 layers and also has the auto-via facility for interconnections among the layers [108].

Once the components have been located on the PCB, the designer can route the board by laying tracks for the interconnection of components. A track may be made of a series of track sections as shown in Fig. 5.4 (a) [108]. For the current work each track section is represented as a single track (shown in Fig. 5.4 (b)) because BM outputs the geometrical data for individual track sections.

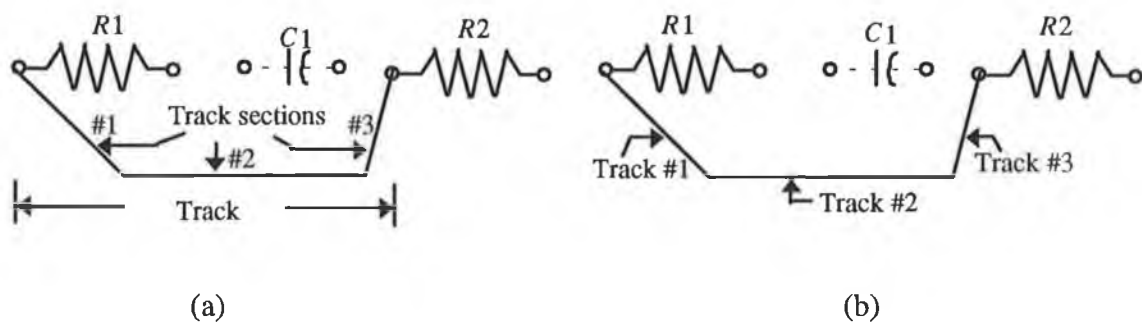


Fig. 5.4 (a) In case of BM; (b) for the current work.

Latest version available to the author.

The board can be routed both manually and automatically. Autorouting is not possible for designing a singlesided PCB using this tool. In auto routing the nets are generally routed in the following order: bus, power, signal and then unspecified net. One can change this order either in the netlist or by editing the net in BM. After completing the board routing, BM can also perform checking of the designed PCB to ensure the correct placement of tracks and pads.

BM provides eight different track width numbers, each of which can be assigned a width in the range of 0.05 to 13.5 mm. BM also has sixteen different pad width numbers, each of these can be assigned in the range of 0.16 to 13.5 mm for outside pad diameter and 0.05 to 13.39 mm for inside pad diameter [108]. Therefore, the designer can change the track width and pad size according to his/her requirements. For example, since PCB radiation depends on the cross-sectional dimension of a PCB track and PCB layout, the designer can vary the track size and layout where required, to reduce the EM radiation.

BM can generate an output file for various output devices such as dot-matrix printer, laser printer or a pen plotter. For a laser printer, BM produces an output file in Postscript™ format. It is possible to extract the geometrical data of a PCB from such an output file.

5.4 DATA EXTRACTION ALGORITHMS

The input data for NEC-2 can be obtained from the aforementioned circuit design packages. Data extraction algorithms were developed by exploiting the facilities of the various circuit design packages described in the previous sections. The following subsections discuss the data extraction algorithms.

5.4.1 EXTRACTION OF GEOMETRICAL AND LOAD DATA

Geometrical data for a PCB describes the end co-ordinates of a PCB track in the rectangular co-ordinate system and load data describes the impedance loading on a PCB track. All geometrical and load data are available in the output file and the netfile created by BM and ORCAD respectively. The units of all geometrical data in the BM output file are given in thousandths of an inch (i.e. mil).

The BM Postscript output file was used to extract the geometrical and load data of a PCB. It has been observed that BM follows a fixed format for creating such an output file. The file format is shown in Fig. 5.5.

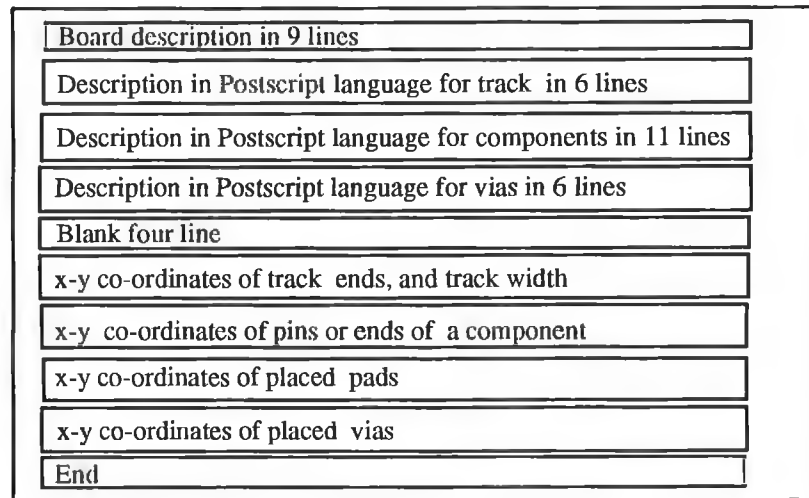


Fig: 5.5 BM output file format for laser printer (Postscript).

5.4.1.1 Layout Data Extraction Routine (LDER)

The LDER is the main programme used for extraction of the geometrical and load data of a single or double sided PCB. This routine consists of eight subroutines to implement data extraction algorithms. A subroutine linkage chart and a flow chart of this routine are shown in Fig. 5.6 and 5.7 respectively.

Prior to reading the geometrical data from the BM output file, this routine issues a request for the type of PCB (e.g. singlesided, doublesided or multilayer PCB). Once the type of PCB has been specified, the LDER sets an integer flag (*PCBTF*) to indicate the type of a PCB and then sets the z co-ordinate of a PCB track, component and placed pad. The dielectric substrate of a PCB is assumed to be situated in the x - y plane, at $z = 0$ in the rectangular co-ordinate system (see Fig. 3.6). Since a PCB is simulated as a loaded wire structure just above (but not contacting) an imperfect ground (dielectric substrate), the z co-ordinates of a track, component, or a pad should not be equal to zero. For an example, in case of singlesided PCB the value of the z co-ordinate is equal to h ($h = 1 \mu\text{m}$, stated in section 3.4).

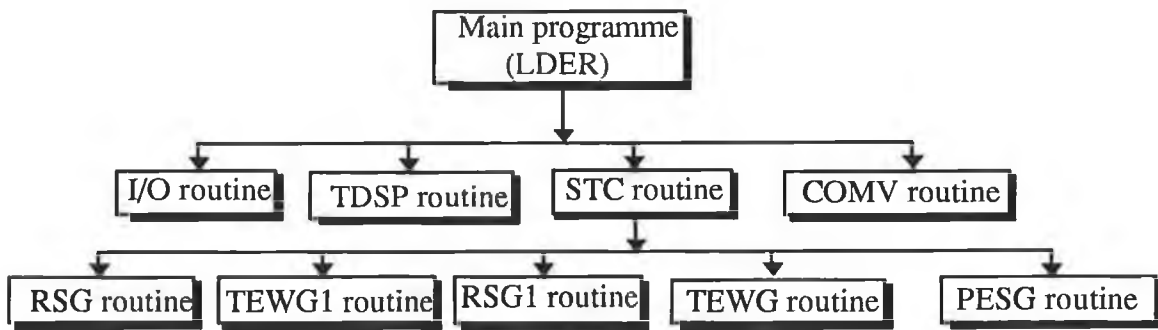


Fig. 5.6 Subroutine linkage charts of main programme (LDER) for the extraction of geometrical and load data.

The extraction of the geometrical data begins with the omission of the first thirty-six lines of the BM output file because these lines do not contain any geometrical or load data for a PCB. The LDER will then start to read geometrical data (i.e. x-y co-ordinates) for the following:

- both ends of the PCB tracks;
- pins or ends of components in the PCB;
- placed pads;
- placed vias.

Prior to storing the geometrical data from a BM output file, the LDER first checks the thirty-seventh column of each line of the output file. If this column value is equal to "u", it means that the line contains a PCB track geometry (i.e. co-ordinates of both ends of a track, and its width). The LDER will then store the track geometry in a temporary file. If this column value equals "r", then it indicates that the line is the beginning line of a DIL package of rectangular shape where an integrated circuit (IC) is housed and the line contains the first pin co-ordinate of an IC. Otherwise the reading line contains the geometrical data of a discrete component (e.g. transistors, diode, resistors, inductors and capacitors), a pad or a via.

Once the first pin co-ordinate of an IC in a PCB has been identified, the LDER stores the pin co-ordinates of the IC in a temporary file. Generally IC pins are located on the two sides of DIL packages. In some cases, where an IC has a large number of pins (e.g. 64 pins for 32-bit microprocessor), the IC pins are located on the four sides of a package. The geometry of a DIL package is shown in Fig. E3-1 of Appendix E. Though a general case has been

considered in this work the routine can be extended to handle other cases. The LDER performs the following tasks to check the termination of pin co-ordinates of an IC:

- task 1: Determination of the status of the thirty-seventh column of each line. If the column value is equal to "r" then it indicates the first pin co-ordinates of the next IC and skips tasks 2 and 3.
- task 2: Computation of the difference of x co-ordinates ($Difx$) between the probable pin (current pin) and last pin. If $Difx = 0$ then it indicates the pin co-ordinates of the same IC and skips task 3.
- task 3: Computation of the difference of y co-ordinates ($Dify$) between the probable pin (current pin) and last pin. If $Dify = 0$ then it also indicates the pin co-ordinate of the same IC.

If neither $Difx$ nor $Dify$ equals zero then the LDER assumes it is at the start of geometrical data for a discrete component, a placed pad or a placed via, and then stores the following geometrical data in a temporary file :

- x - y co-ordinates of component ends;
- x - y co-ordinates of a placed pad or a via;
- inner diameter of a placed pad or a via;
- pads inner diameter of a component ends.

After storing the geometrical data, the LDER calls subroutine TDSP (refer to section 5.4.1.2) to identify the components (e.g. transistor (Q), resistor (R), inductor (L), capacitor (C), diode (D), etc.), pads and vias.

Subroutine COMV (refer to section 5.4.1.3) is called to find the value of passive components such as resistors, inductors and capacitors. COMV also finds node data for LDER from the netfile created by ORCAD. The LDER calls subroutine STC (refer to section 5.4.1.4) to find those PCB tracks that are the likely sources of EM radiation and then the load that connected to those track.

The co-ordinates of both ends of all tracks, track width, loads and node data are then available. Since a PCB track is being modelled as a round wire, the LDER determines the equivalent wire radius from the cross-sectional dimension of the track. Finally the LDER prepares input files for the modified NEC-2 programme (as described in section 3.5). The

prepared files then contain descriptions of the geometrical data of a wire, the load connected to it, and the wire number².

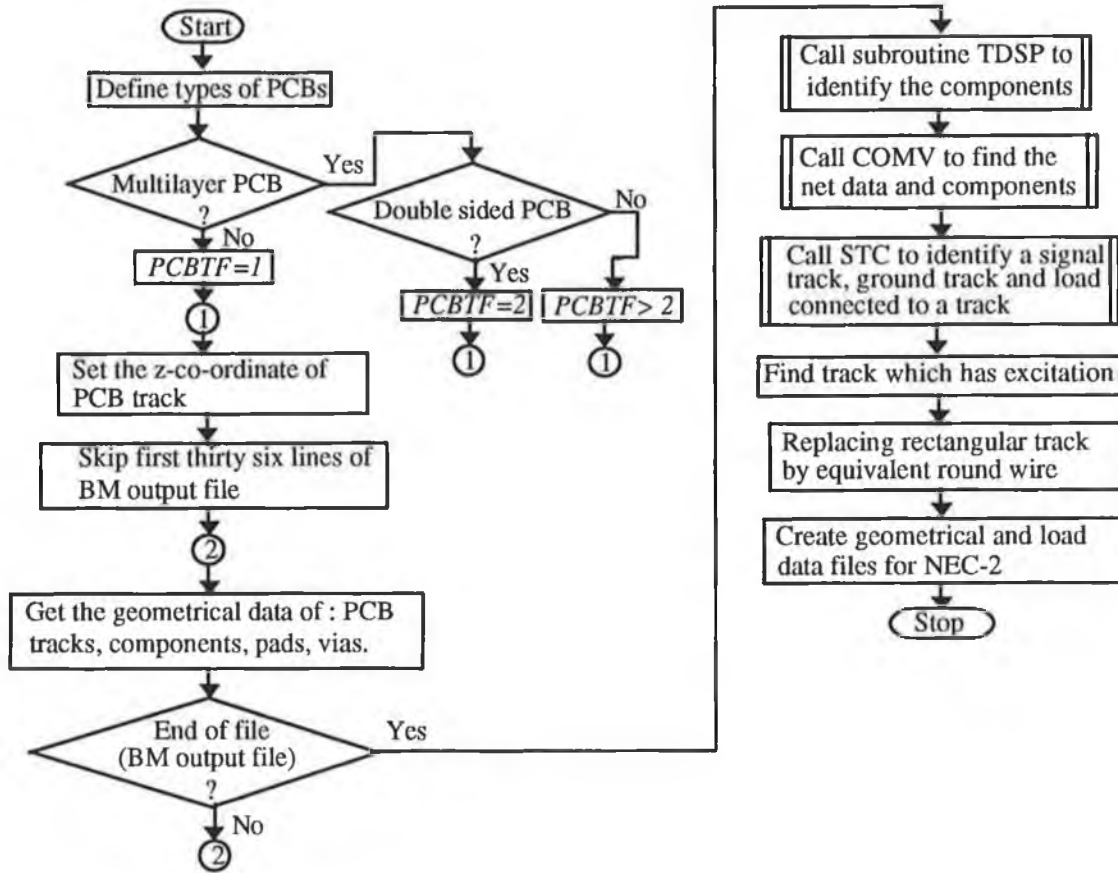


Fig. 5.7 Flow chart for layout data extraction routine (LDER).

The algorithm was implemented using Fortran programme. A computer programme listing of this routine and all subroutines are given in Appendix E3.

5.4.1.2 Subroutine TDSP

The LDER stores the geometrical data for all discrete components, all sources (i.e. signal generator) and all placed vias (as placed pads). An algorithm was developed to separate these data. The algorithm is based on the default geometrical dimensions (i.e. axial length (*AL*) and inner pad diameter (*IPD*)) of the discrete components, the signal generator (*SG*), the placed

²Tracks in a PCB are distinguished by different indices. These indices are referred to as wire number.

pad and the placed via. The default dimensions for all these are given in Table TE1 of Appendix E. A flowchart of this algorithm is shown in Fig. 5.8.

The various steps of this routine are described below :

Step 1 : Get the default geometrical dimension of discrete components (Q , D , R , L and C), SG , placed pad and via.

Step 2 : Get the inner pad diameter (IPD) of the i th pad.

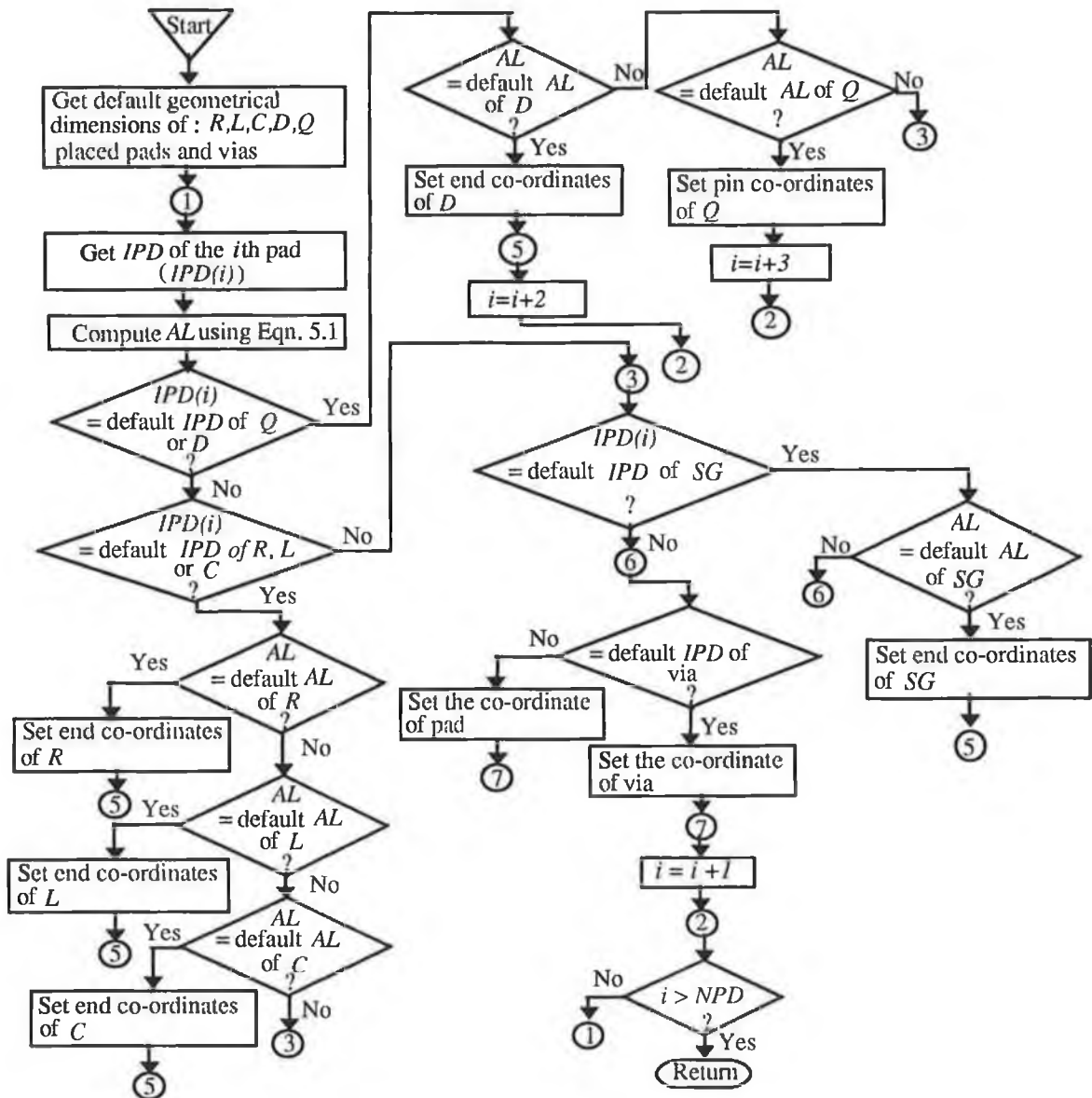


Fig. 5.8 Flow chart of subroutine TDSP to identify the component.

Step 3 : Compute the axial length (AL). This is given by,

$$AL = \sqrt{(PADx(i) - PADx(i+1))^2 + (PADy(i) - PADy(i+1))^2} \quad (5.1)$$

where,

$PADx(i)$ – x -co-ordinate of the i th pad;

$PADy(i)$ – y - co-ordinate of the i th pad.

Step 4 : Compare the IPD of the i th pad with that of a Q or a D .

Step 5 : If they are equal, then do the following tasks, otherwise go to step 6,

task 1 : Compare the AL with the default AL of Q . If they are equal, set the followings and go to step 11, otherwise go to task 2;

– the pin co-ordinates of a Q ;

– $i = i + 3$;

task 2 : Compare the AL with that of D . If they are equal, set the following and go to step 11, otherwise go to step 8;

– the pin co-ordinates of a D ;

– $i = i + 2$.

Step 6 : Compare the IPD with that of R , L or C .

Step 7 : If they are equal then do the following task otherwise go to step 8.

task : Compare the AL with that of R . If they are equal, set the following and go to step 10;

– the ends co-ordinates of R ;

– $i = i + 2$;

If they are not equal repeat task for L and C otherwise go to next step.

Step 8 : Compare the IPD with that of SG . If they are equal, perform the following task otherwise go to step 9.

task : Compare the AL with that of SG . If they are equal, set the following and go to step 10 otherwise go to next step;

– the ends co-ordinates of a SG ,

– $i = i + 2$.

Step 9 : Compare IPD with that of via, if they are equal, perform task 1 otherwise task 2;

task 1 : Set the following and then go to step 10;

– the co-ordinates of a via;

– $i = i + 1$.

task 2 : Set the following and then go to step 10;

- the co-ordinates of a pad;
- $i = i + 1$.

Step 10 : Compare i with the NPD ,

where, NPD is the total number of pads.

If i is greater than NPD , then go to step 11, otherwise go to step 2.

Step 11 : Return to the main programme LDER.

The described algorithm is capable of handling other components which are not shown in the Table TE1 of Appendix E. A computer programme was written in Fortran to implement the described algorithm.

5.4.1.3 Subroutine COMV

The function of this subroutine is to extract the following data from a netfile (myfile.net) created by ORCAD for BM:

- the types and values of passive components (e.g. R , L , C);
- the types and model name of active components (e.g. Q , IC (U^3));
- the signal nodes (see Fig. 5.9) and their netlist (list of connections);
- the ground node (see Fig. 5.9) and its netlist;
- the power supplies (dc power) for active devices and their netlist.

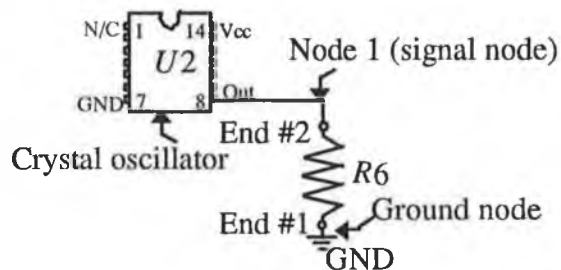


Fig. 5.9 A schematic of a simple circuit consisting of a crystal oscillator ($U2$) and a resistor ($R6$).

It was observed that in creating a netfile ORCAD follows a fixed format. The algorithm to extract the mentioned data was developed based on this format. A flow chart of this routine is

³In a netlist, an IC is represented by U .

shown in Fig. 5.10. This routine begins with the checking of the first column of each line of myfile.net and performs the following tasks at different steps:

Step 1 : Get the character of the first column of a line of the myfile.net.

Step 2 : If the character is "[" (indicates the beginning of component list), then go to next step, otherwise go to step 5.

Step 3 : Check the character of the first column of the next line. This character indicates the types of components (active or passive). If it is a passive component, then get the type (i.e. R , L , or C) and value of the passive component. If it is an active component then get the type (i.e. Q , or U) and model name.

Step 4 : Skip the next 6 lines of the file (myfile.net) and go to step 1.

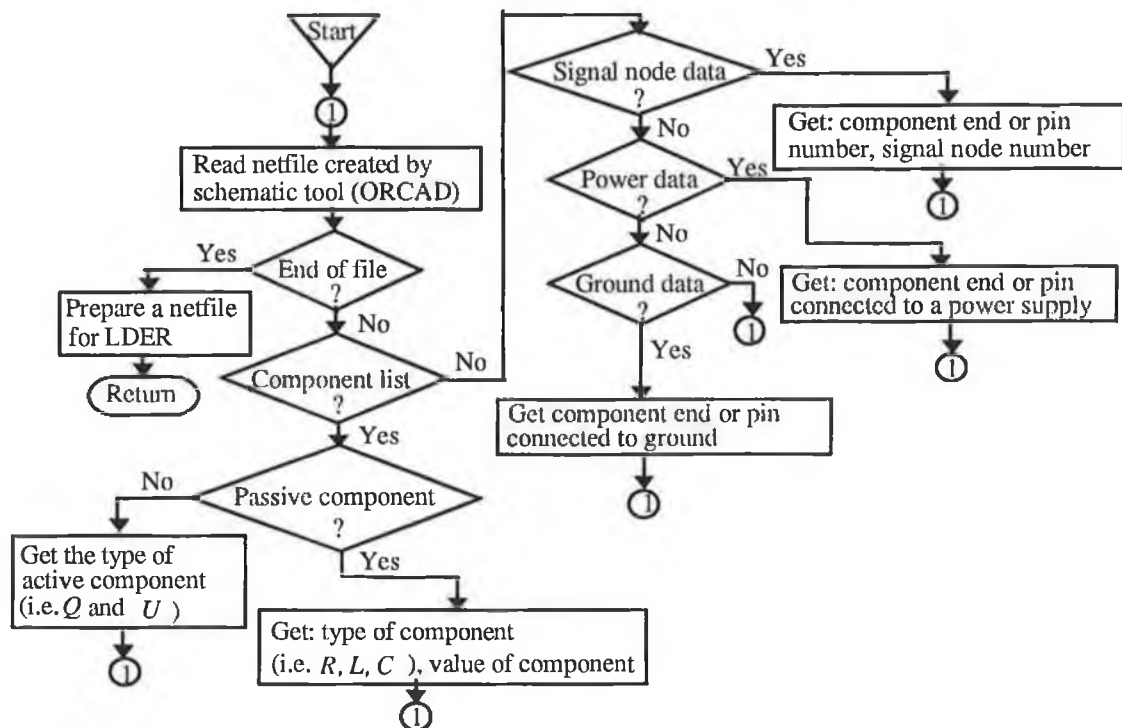


Fig. 5.10 Flow diagram of subroutine COMV.

Step 5 : If this character is "(" (indicates the beginning of a signal node, a power supply or a ground netlist), then go to step 6 otherwise go to 7.

Step 6 : Get the character of the first column of the next line and perform the following tasks:

task 1 : If the character is "N" (indicates the beginning of a signal node), then get the signal netlist and go to step 1.

task 2 : If the character is " V" (indicates the beginning of a power supply), then get the power supplies netlist and go to step 1.

task 3 : If the character is "G" (indicates the beginning of a ground node), then get the ground netlist and go to step 1, otherwise go to step 7.

Step 7 : If the character is ")", it indicates the end of any netlist and the end of netfile (myfile.net). To find the end of the file "myfile.net", check whether the previous node was a ground node or not. If it was a ground node, go to step 8, otherwise go to step 1.

Step 8 : Return to main programme LDER.

After extracting the data as described in this section, this routine prepares a file (myfile.nod) that contains a netlist in a specified format for LDER. The line format of the prepared file is shown in Appendix E4 and an example (for a signal node in the simple circuit shown in Fig. 5.9) of this file is given as:

```
N    U    1    2    8
N    R    1    6    2
```

A computer programme was written in Fortran to implement this algorithm.

5.4.1.4 Subroutine STC

The three main tasks of this subroutine are: (i) finding the signal tracks and (ii) finding the ground tracks and (iii) determining the impedance loading on a track. A track connected to a signal node is referred to as signal track, for example, in Fig. 5.12 (b) the signal track is a combination of tracks #1, #2, #3, #4 #5, #6 and #7. Ground track can also be defined in the same manner. The input data for this routine are:

- the x - y co-ordinates of both ends of tracks in a PCB;
- the x - y co-ordinates of all pins of an IC;
- the x - y co-ordinates of both ends of discrete components;
- the node data.

The routine consists of five subroutines. A flow chart of this routine is shown in Fig. 5.11 where,

$(TPSx, TPSy) =$ the x - y co-ordinates of a signal node;

- $(TPGx, TPGy)$ = the x - y co-ordinates of a ground node;
 (Px, Py) = the x - y co-ordinates of an IC pin connected to a signal node or a ground node;
 (Qx, Qy) = the x - y co-ordinates of any pin of a transistor connected to a signal or a ground node;
 (Dx, Dy) = the x - y co-ordinates of either end of a diode connected to a signal or a ground node;

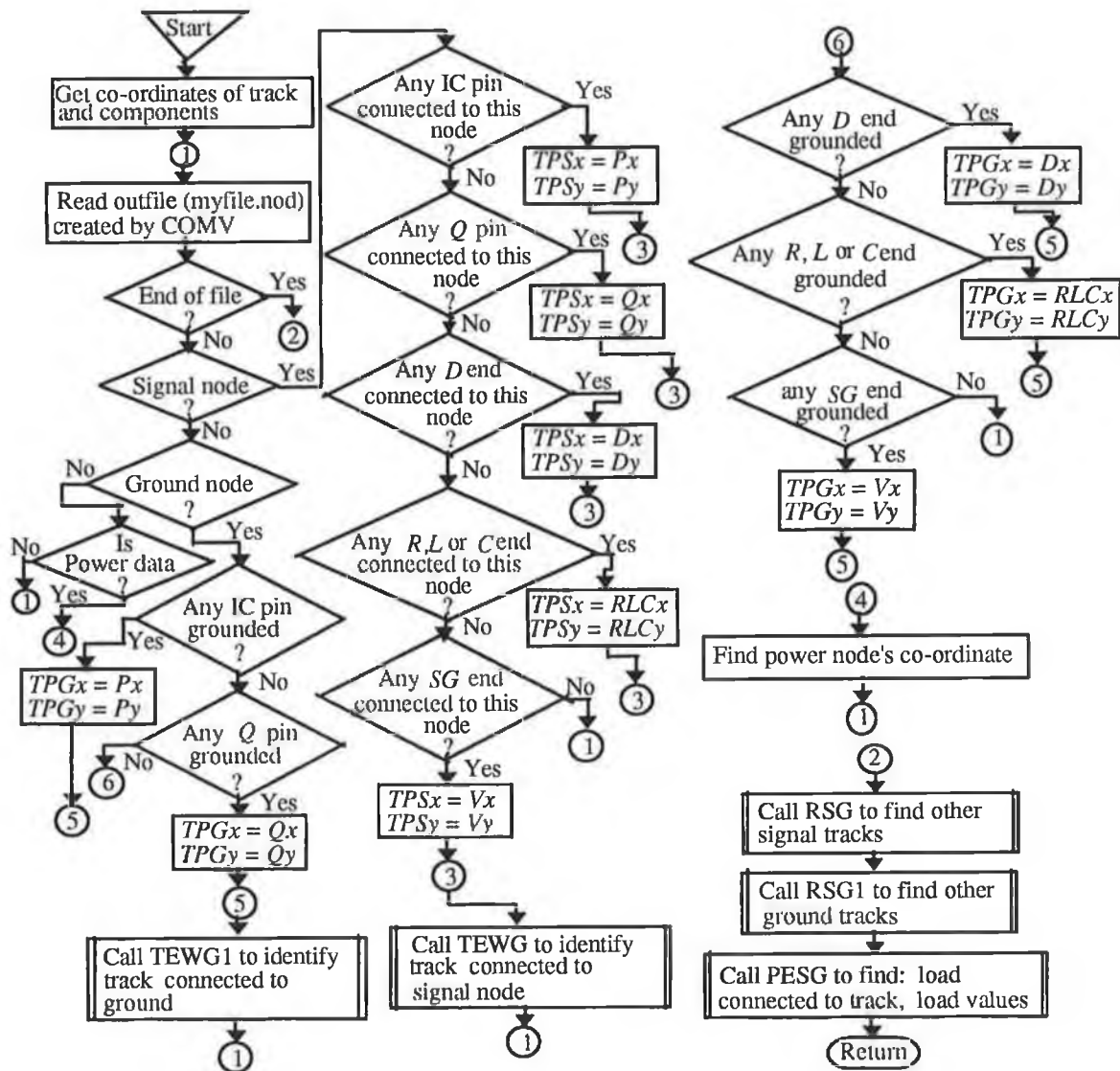


Fig. 5.11 Flow chart for subroutine STC.

- $(RLCx, RLCy) =$ the x - y co-ordinates of either end of a load (e.g. R , L , or C) connected to a signal or a ground node;
- $(Vx, Vy) =$ the x - y co-ordinates of either end of a signal generator connected to a signal or a ground node.

To find the signal tracks STC performs the following tasks:

- Task 1 : Searches file (myfile.nod) for the signal node (see Fig. 5.12).
For the example given in section 5.4.1.3, STC finds node #1 (as signal node) which starts at pin #8 of $U2$ (could also have started at end #2 of $R6$) as shown in Fig. 5.12.
- Task 2 : Set the co-ordinates of the signal node. For this example,
 $TPSx = Px$ (x co-ordinate of pin #8 of $U2$)
 $TPSy = Py$ (y co-ordinate of pin #8 of $U2$)

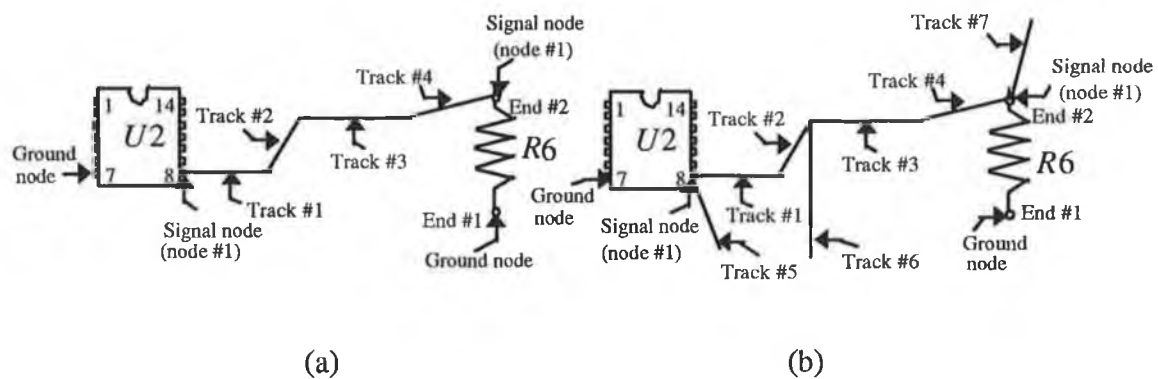


Fig. 5.12 A portion of PCB layout for simple circuit shown in Fig. 5.9: (a) Tracks running between pin #8 of $U2$ and end #2 of $R6$; (b) other tracks connected to tracks running between pin #8 of $U2$ and end #2 of $R6$.

- Task 3: Calls subroutine TEWG to find track that is directly connected to a signal node. For an example, the PCB as shown in Fig. 5.12 (a), TEWG routine finds track #1 that is connected to pin #8 of $U2$.
- Task 4: Calls subroutine RSG to find the remaining tracks. For the example RSG finds the remaining tracks (i.e. track #2, track #3 and track #4) that eventually arrives at end #2 of $R6$. A numerous number of tracks

may be connected to the tracks running between pin #8 of $U2$ and end #2 of $R6$ (as shown in Fig. 5.12 (b)). RSG could also find those tracks (i.e. track #5, track #6 and track #7).

The STC calls subroutines TEWG1 and RSG1 to identify ground tracks. Prior to calling these subroutines STC repeats tasks 1 and 2 (stated in this section) for ground node. These tracks are then combined with signal tracks to obtain a total number of tracks.

Finally the STC calls subroutine PESG to find the tracks which are loaded. The PESG also determines the type and value of a load .

5.4.1.5 Subroutine TEWG

The function of this routine is to find the track that is directly connected to the signal node as stated in the previous section. The inputs of this routine will be the co-ordinates of both ends of PCB tracks and a signal node. The flow chart of this routine is shown in Fig. 5.13. The routine follows the algorithm as described below:

Step 1 : Get x - y co-ordinates of the j th end of the i th track in a PCB, and that of a node, where, $1 \leq i \leq M$, M is the total number of tracks, and $1 \leq j \leq 2$.

Step 2 : Set $i = 1$.

Step 3 : Set $j = 1$.

Step 4 : Compute the difference between the x co-ordinates of the j th end of the i th track and that of a signal node. The difference ($DIFFS_x$) is defined by,

$$DIFFS_x = (TPS_x - x(i, j)) \quad (5.2)$$

where,

TPS_x – the x co-ordinates of a signal node;

$x(i, j)$ – the x co-ordinate of the j th end of the i th track.

Step 5 : Repeat step 4 for the y co-ordinate and this difference ($DIFFS_y$) is defined by,

$$DIFFS_y = (TPS_y - y(i, j)) \quad (5.3)$$

where,

TPS_y – the y co-ordinate of a node;

$y(i, j)$ – the y co-ordinate of the j th end of the i th track.

Step 6 : Check the following cases:

Case 1 : If both $DIFFS_x$ and $DIFFS_y$ are not equal to zero and j is not equal to 2, then repeat step 4 and 5 for $j = 2$. If j is equal to 2 and i is less than M then repeat step 3 to step 5 for $i = i+1$, otherwise go to step 9.

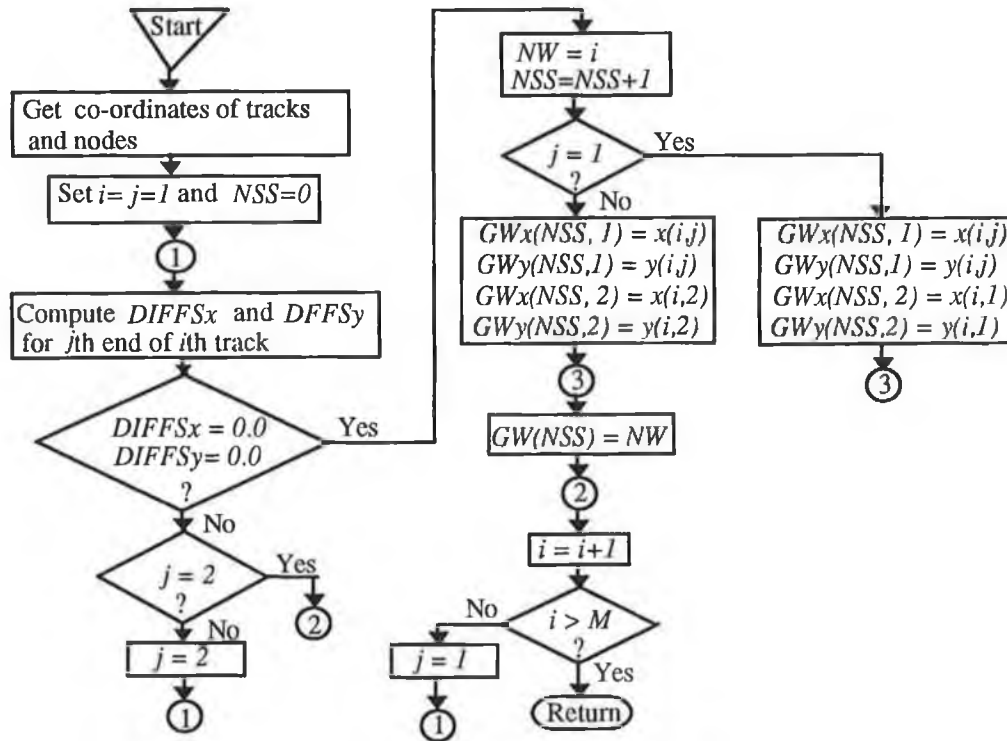


Fig. 5.13 Flow chart for subroutine TEWG.

Case 2 : If both $DIFFS_x$ and $DIFFS_y$ are equal to zero and j is equal to 1 then set the co-ordinates of a signal track.

$$NSS = NSS + 1 \quad (5.4)$$

$$GW(NSS) = i \quad (5.9)$$

For $j = 1$, the x - y co-ordinates of both ends of this track are given by,

$$GW_x(NSS, 1) = x(i, j) \quad (5.5)$$

$$GW_y(NSS, 1) = y(i, j) \quad (5.6)$$

$$GW_x(NSS, 2) = x(i, 2) \quad (5.7)$$

$$GWy(NSS, 2) = y(i, 2) \quad (5.8)$$

where,

$GWx(NSS, j)$ – the x co-ordinate of the j th end of the NSS th signal track;

$GWy(NSS, j)$ – the y co-ordinate of the j th end of the NSS th signal track;

NSS – the total number of signal track number;

$GW(NSS)$ – the tag number of the NSS th signal track.

If j is not equal to 1 then the x - y co-ordinates of both ends of signal track will be:

$$GWx(NSS, 1) = x(i, j) \quad (5.10)$$

$$GWy(NSS, 1) = y(i, j) \quad (5.11)$$

$$GWx(NSS, 2) = x(i, 1) \quad (5.12)$$

$$GWy(NSS, 2) = y(i, 1) \quad (5.13)$$

Step 7 : Set $j = 1$ and $i = i + 1$.

Step 8 : If, $i \leq M$, then go to step 3, otherwise go to step 9.

Step 9 : Return to called subroutine (STC).

A computer programme was written in Fortran to implement this algorithm.

5.4.1.6 Subroutine RSG

The function of this routine has already been stated in section 5.4.1.4. The inputs of this routine will be: (i) the x - y co-ordinates of both ends of all tracks, (ii) the x - y co-ordinates of both ends of all tracks those are identified by TEWG, and (iii) the track tag number. A flow chart of this routine is shown in Fig. 5.14. The routine performs the following tasks at different steps:

Step 1 : Get the x - y co-ordinates of the jj th end of the ii th track in a PCB, where, $1 \leq ii \leq M$ and $1 \leq jj \leq 2$.

Step 2 : Get the x - y co-ordinates of the j th end of the i th signal track in a PCB, and the tag number of a signal track ($GW(LL)$), where, $1 \leq i \leq NSS$, $1 \leq LL \leq NSS$, and $1 \leq j \leq 2$.

Step 3 : Set $TWN = NSS$,

where, TWN is the total number of signal tracks.

Step 4 : Set $ii = 1$, and $i = 1$.

Step 5 : Set $LL = 1$.

Step 6 : Compare $GW(LL)$ with ii .

Step 7 : Check the following cases:

Case 1 : If $GW(LL) = ii$, then set $ii = ii + 1$. If $ii \leq M$, then go to step 4, otherwise set $i = i + 1$. If $i \leq NSS$, then set $ii = 1$ and go to step 4, otherwise go to step 12.

Case 2 : If $GW(LL) \neq ii$, then set $LL = LL + 1$. If $LL \leq NSS$, then repeat step 5, otherwise go to step 8.

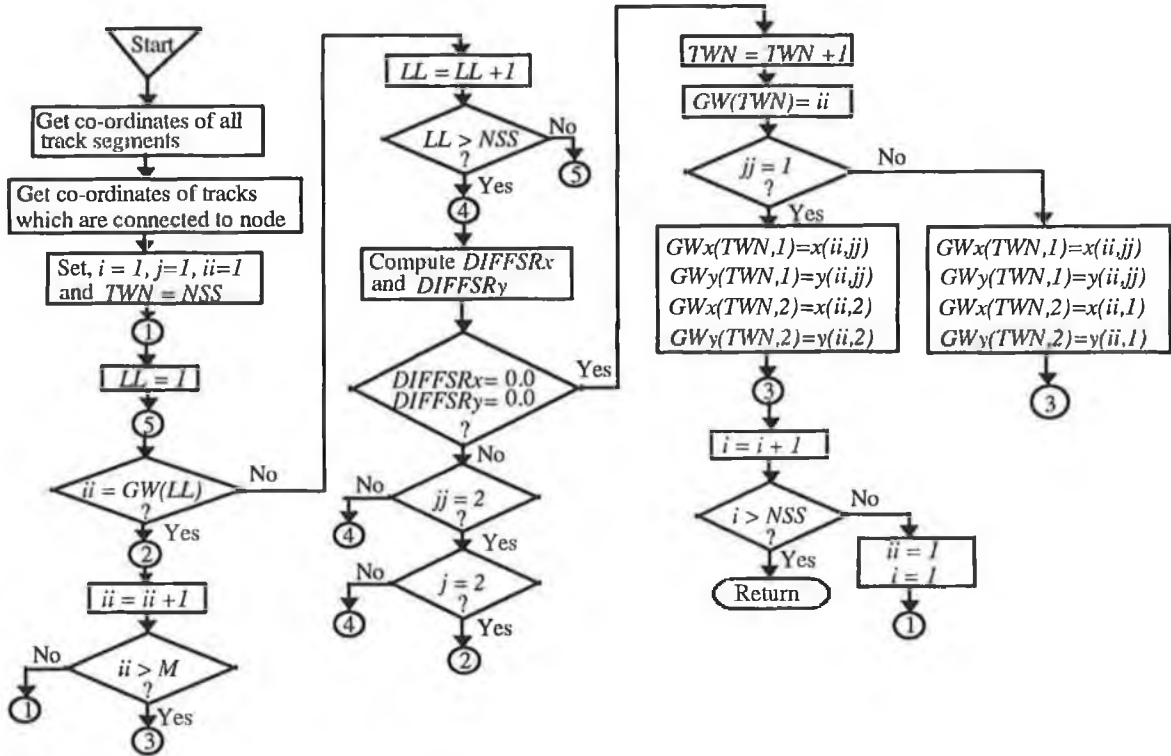


Fig. 5.14 Flow chart for subroutine RSG.

Step 8 : Compute the difference between the x co-ordinates of the jj th end of the ii th track and that of the j th end of the i th signal track. This difference ($DIFFSRx$) is defined by,

$$DIFFSRx = (GWx(i, j) - x(ii, jj)) \quad (5.14)$$

Step 9 : Repeat step 8 for the y co-ordinates and the difference ($DIFFSRy$) is defined by,

$$DIFFSRy = (GWy(i, j) - y(ii, jj)) \quad (5.15)$$

Step 10 : If both $DIFFSR_x$ and $DIFFSR_y$ are not equal to zero, perform the following tasks otherwise go to task 4:

task 1 : If $jj \neq 2$ then repeat step 8 and 9 for $jj = 2$.

task 2 : If $j \neq 2$ then repeat step 8 and 9 for $j = 2$.

task 3 : If both jj and j are equal to 2 then set $ii = ii + 1$. If $ii \leq M$ then go to step 5, otherwise go to step 11.

task 4 : If either $DIFFSR_x$ or $DIFFSR_y$ is equal to zero then go to step 11, otherwise set the x - y co-ordinates of both ends of the additional signal track.

$$TWN = TWN + 1 \quad (5.16)$$

$$GW(TWN) = ii \quad (5.17)$$

For $jj = 1$, the x - y co-ordinate of both ends of the additional signal track are given by,

$$GW_x(TWN, 1) = x(ii, jj) \quad (5.18)$$

$$GW_y(TWN, 1) = y(ii, jj) \quad (5.19)$$

$$GW_x(TWN, 2) = x(ii, 2) \quad (5.20)$$

$$GW_y(TWN, 2) = y(ii, 2) \quad (5.21)$$

where,

$GW_x(TWN, j)$ – the x co-ordinate of the j th end of the TWN th signal track;

$GW_y(TWN, j)$ – the y co-ordinate of the j th end of the TWN th signal track.

For $jj \neq 1$, then x - y co-ordinates of both ends of the additional signal track will be:

$$GW_x(TWN, 1) = x(ii, jj) \quad (5.22)$$

$$GW_y(TWN, 1) = y(ii, jj) \quad (5.23)$$

$$GW_x(TWN, 2) = x(ii, 1) \quad (5.24)$$

$$GW_y(TWN, 2) = y(ii, 1) \quad (5.25)$$

Step 11 : Set $i = i + 1$. If $i > NSS$ then go to step 12, otherwise set $ii = 1$ and go to step 5.

Step 12. Return to called subroutine (STC).

This routine was implemented by a Fortran programme.

5.4.1.7 Subroutines TEWG1 and RSG1

The subroutines TEWG1 and RSG1 are called by STC, for finding the ground tracks in a PCB. The TEWG1 and RSG1 follow the same algorithm as described in the subroutines TEWG and RSG respectively.

The only difference between the subroutines TEWG and TEWG1 is that the TEWG1 considers the ground node instead of a signal node as used in TEWG. This ground node will be a pin of an IC or any end of a discrete component. For an example (shown in Fig. 5.12), ground node starts at pin #7 of *U2* (could also have started at end #1 of *R6*).

The difference between the RSG and RSG1 is that the RSG1 uses the co-ordinates of both ends of a ground track instead of a signal track as used in RSG.

5.4.1.8 Subroutine PESG

The function of this routine is to find a track that has an impedance loading (e.g. *R*, *L*, *C*). The input of this routine will be the following:

- *x-y* co-ordinates of : (i) both ends of passive component, (ii) both ends of a signal track, (iii) both ends of a ground track and (iv) placed pad in a PCB;
- node data.

The node data is available from a file that is created by subroutine COMV. A flow chart of this routine is shown in Fig. 5.15. The developed algorithm is described below:

Step 1 : Get the *x-y* co-ordinates of the *j*th end of the *i*th signal track in a PCB, where, $1 \leq i \leq TWN$ and $1 \leq j \leq 2$.

Step 2 : Get the *x-y* co-ordinates of the *j*th end of the *ii*th ground track in a PCB, for $1 \leq ii \leq TWNG$ and $1 \leq j \leq 2$, where, *TWNG* is the total number of ground tracks. The ground node is represented by zero.

Step 3 : Get the *x-y* co-ordinates of the *l*th pad for $1 \leq l \leq NPD$, where, *NPD* is the total number of pads in a PCB.

Step 4 : Set *NPSG* = 0, where *NPSG* is the total number of signal and ground pads.

Step 5 : Set *l* = 1, and *j* = 1.

Step 6 : Determine the difference ($DIFFSP_x$) between the x co-ordinates of the j th end of the i th signal track, and the x co-ordinate of the l th pad. The $DIFFSP_x$ is defined by,

$$DIFFSP_x = (GW_x(i, j) - PAD_x(l)) \quad (5.26)$$

where $PAD_x(l)$ is the x -co-ordinate of the l th pad.

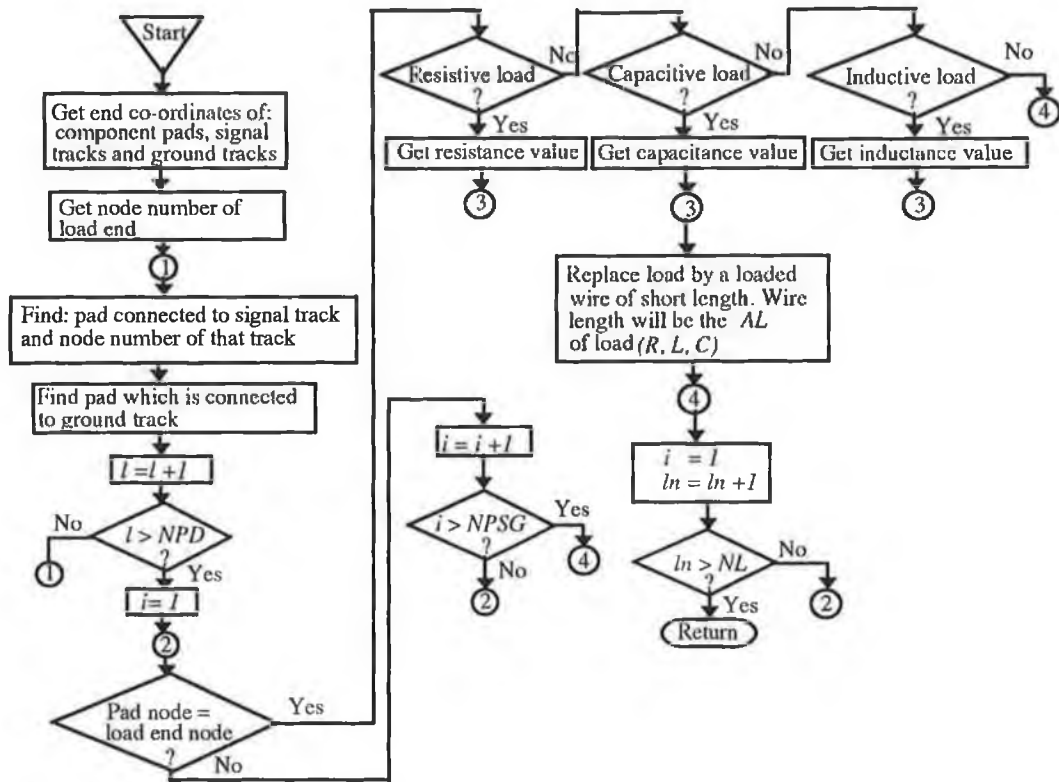


Fig. 5.15 Flow chart for subroutine PESG to find load.

Step 7 : Repeat step 6 for the y co-ordinate. The difference ($DIFFSP_y$) is defined by,

$$DIFFSP_y = (GW_y(i, j) - PAD_y(l)) \quad (5.27)$$

where, $PAD_y(l)$ is the y - co-ordinate of the l th pad.

Step 8 : If both $DIFFSP_x$ and $DIFFSP_y$ are not equal to zero, then the routine performs the following tasks:

task 1 : If $j \neq 2$, then repeat step 6 and 7 for $j=2$ otherwise performs task 2.

task 2 : Set $i = i + 1$. If $i > TWN$, then go to step 10 otherwise set $j=1$ and go to step 6.

Step 9 : If both $DIFFSP_x$ and $DIFFSP_y$ are equal to zero then set the node number of the l th pad to the node number of the i th signal track . Set, $NPSG=NPSG+1$.

Step 10 : Set $l = l + 1$. If l is greater than NPD , then go to step 11. Otherwise set $j=1$, $i = i + 1$ and then go to step 6.

Step 11 : Repeat step 5 to step 10 with the taking of the x - y co-ordinates of both ends of the i th ground track instead of signal track to determine the $DIFFSP_x$ and $DIFFSP_y$. In step 9, set the node number of the l th pad to zero.

Step 12 : Set $ln = 1$ for $1 \leq ln \leq NL$, where NL is the total number of loads.

Step 13 : Compare the node number of the i th pad with that of the j th end of the ln th load.

Step 14 : If they have the same node number then go to step 15. Otherwise do the following tasks:

task 1 : If j is not equal to 2 then repeat step 13 for $j = 2$ otherwise perform task 2.

task 2 : Set $i = i + 1$. If i is greater than $NPSG$ then perform task 3. Otherwise go to step 13.

task 3 : Set $ln = ln + 1$. If ln is greater than NL then go to step 17. Otherwise set $j = 1$, $i = 1$ and go to step 13.

Step 15 : Identify the load as being resistive, inductive or capacitive and its value.

Step 16 : Replace the load by a loaded track. The track length will be equal to the axial length of a passive component. The type and value of loading on the track will be obtained from step 15.

Step 17 : Return to called subroutine.

A computer programme was written in Fortran to implement the described algorithm.

5.4.2 EXTRACTION OF ELECTRICAL DATA

In NEC-2, electrical data defines the excitation on the radiating structure and a frequency at which the radiated EM field has to be computed. All electrical data are available in an output file of the circuit simulation tool PSPICE.

In this work, the radiating structure is a PCB that is simulated as a loaded thin wire structure as stated in section 2.6. This radiating structure may have many excitation sources. A circuit node is assumed as an excitation point of this structure. Therefore it is necessary to

extract the node voltage of the circuit. For a complex circuit, extracting and transferring the electrical data to NEC-2 programme involves considerable user intervention. Therefore automating the extraction and transfer of electrical data (node voltage and frequency) to NEC-2 programme is desirable.

PSPICE follows a fixed format for preparing an output file. An algorithm for extracting the electrical data from an output file of PSPICE was developed on the basis of this format. A flow chart of the electrical data extraction routine (EDER) is shown in Fig. 5.16.

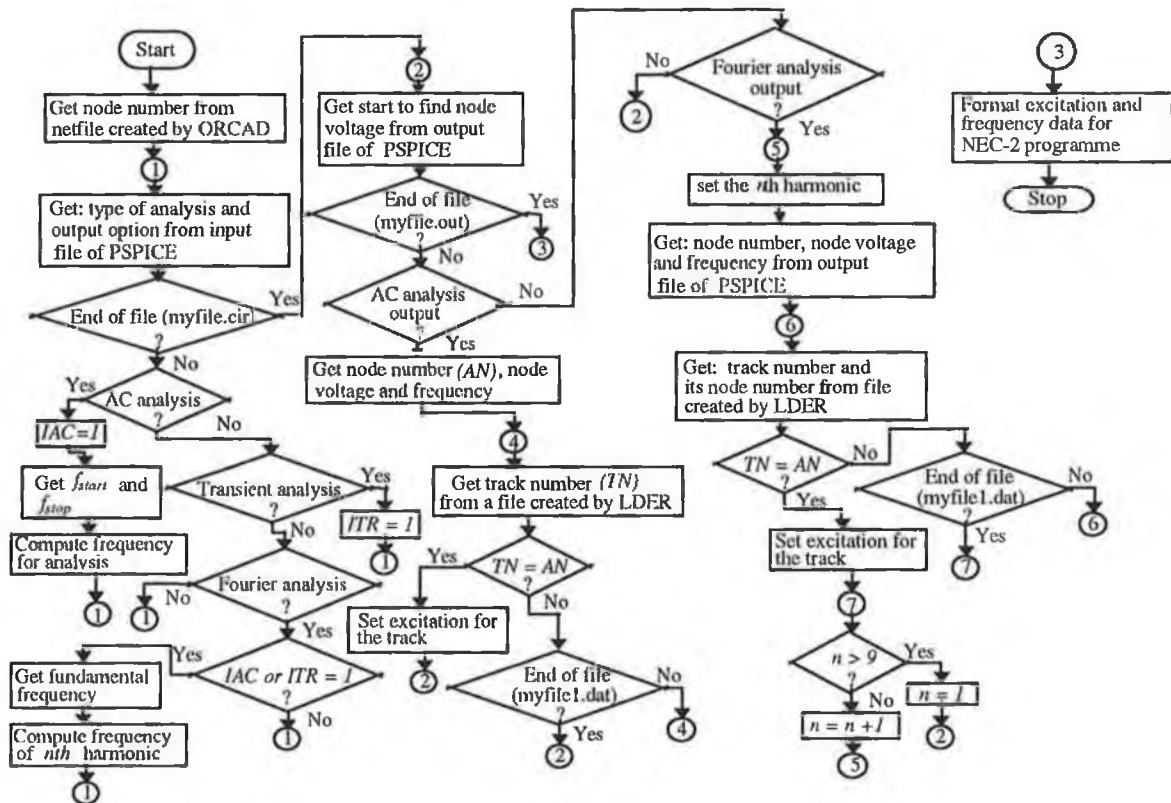


Fig. 5.16 A flowchart to extract electrical data from circuit design package.

The developed algorithm is described below:

Step 1 : Get circuit node numbers from the netfile (myfile1.net) created by ORCAD for PSPICE.

Step 2 : Extract the type of analysis from a file (myfile.cir) which is created by IFGR.

Step 3 : Check the end of myfile.cir. If the file (myfile.cir) ends then go to step 4 otherwise check the following cases:

Case 1 : Identify the type of circuit analysis. If it is an AC analysis, then set the *IAC* to 1 and find frequency otherwise go to case 2.
where, *IAC* is an integer flag to indicate the AC analysis.

For finding the various frequencies at which the AC analysis is performed, let:

f_1 = the start frequency;
 f_2 = the stop frequency;
 Δf = the frequency step size.

The total number of frequency steps (m) and the value of the N th frequency are given by Eqns. 5.28 and 5.29 respectively.

$$m = \frac{f_2 - f_1}{\Delta f} \quad (5.28)$$

$$f(N) = f_1 + N \Delta f, \quad \text{for } N = 0, 1 \dots m \quad (5.29)$$

After determination of frequency data, go to step 2.

Case 2 : If it is transient analysis then set *ITR* to 1 and go to step 3, otherwise go to next case. *ITR* is an integer flag to indicate the transient analysis.

Case 3 : If it is Fourier analysis then go to next case otherwise go to step 3.

Case 4 : If either *IAC* or *ITR* is equal to zero then find frequency of the n th harmonic from the given data of Fourier analysis, otherwise go to step 3.

If f_0 is the specified fundamental frequency, then the frequency of the n th harmonic is given by,

$$f_n = n f_0, \quad \text{for } n = 1, 2 \dots n \quad (5.30)$$

For PSPICE (restricted version), the default value of n is 9. After the determination of frequency, go to step 3.

Step 4 : Read the output file (myfile.out) which is created by PSPICE.

Step 5 : Check the end of this output file. For the end of this file go to step 8, otherwise go to next step.

Step 6 : Check the types of output options. If it is an AC analysis then do the following tasks otherwise go to step 7.

task 1 : Get node number (AN), node voltage and frequency from the file (myfile.out).

task 2 : Get node number (TN) of PCB track from a file (myfile1.dat) which is created by LDER.

task 3 : Compare AN with TN . If both are equal then set the excitation for the PCB track having node number TN and go to step 4. If both are not equal, repeat task 2 for all signal tracks in a PCB.

Step 7 : Check the output option for Fourier analysis output. For Fourier analysis, perform task 1 to task 3 of step 6 for the n th harmonic, otherwise go to step 4.

Step 8. Format the electrical data and then prepare a file for NEC-2.

A computer programme was developed in Fortran for this routine. A computer programme listing of this routine is given in Appendix E5.

5.5 INCORPORATING RADIATION REDUCING TECHNIQUES INTO THE COMPOSITE CAD PACKAGE

In cases where NEC-2, linked with the other CDPs, predicts a level of PCB radiation that exceeds pre-defined limits (e.g. those mentioned in section 1.2.2 for class A or class B equipment) it would be very useful to have aids or techniques available that would allow the designer to reduce the level. Such a facility was incorporated into the composite CAD package.

The process of comparison is summarised in the flow chart in Fig. 5.17. The radiated emission limits are given at the required distance (distance from the product to observation points) shown in Tables TA1 and TB1 (see Appendix A and B). For example FCC emission limits are at 3 m distance for class "B" and at 10 m distance for class "A" equipment. If the prediction is not performed at the required distance for the emission limits, then for comparison, the predicted radiation has to be translated to a required distance (RD) from the distance (R) by adding a factor of $20\log(R/RD)$. This factor is valid only for the far field region.

If the predicted radiation exceeds the emission limit, the designer can reduce the EM radiation by modifying the design (both circuit and PCB) or by providing shielding in some part of the PCB where it is necessary. Various techniques to reduce EM radiation from a PCB are discussed in the following subsections.

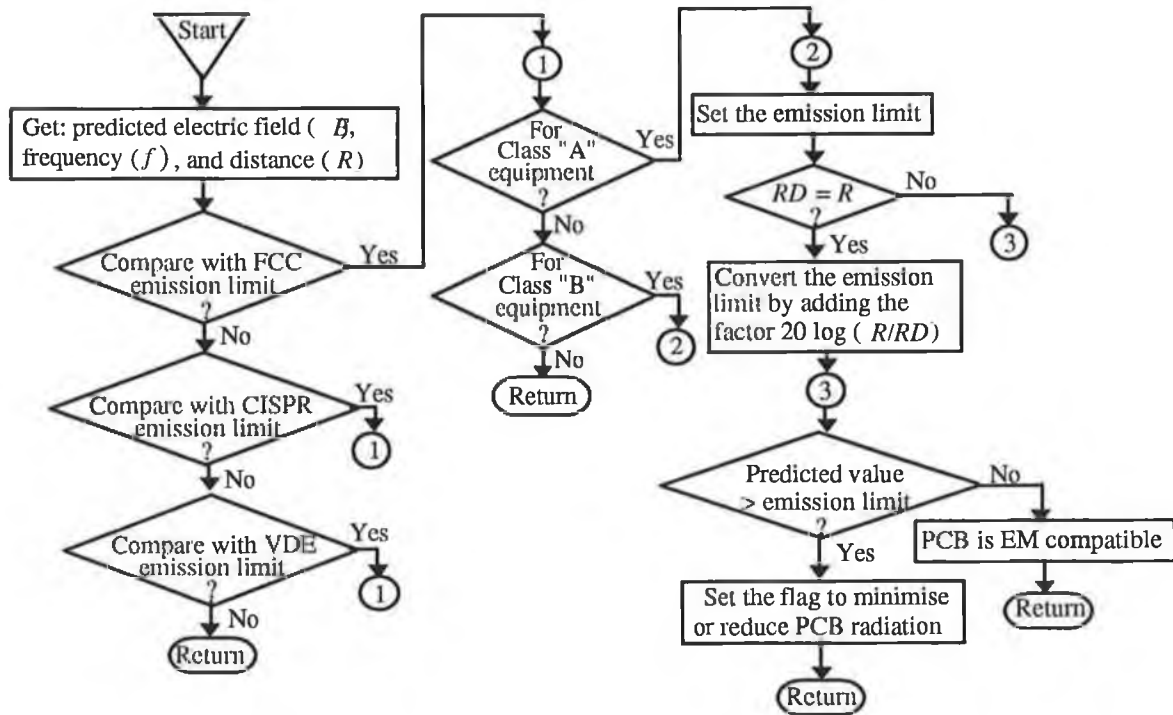


Fig. 5.17 Flow chart to compare the composite CAD predicted PCB radiation with the emission limit set by the regulating bodies.

5.5.1 REDUCING PCB RADIATION BY MODIFYING DESIGN

Various factors that influence the EM radiation from a PCB have been mentioned earlier in section 1.5. EM radiation from a PCB can be reduced by the factors such as:

- (i) better PCB layout (i.e. component placement);
- (ii) shorter track length and smaller track separation;
- (iii) placing a ground grid or a ground plane to reduce the loop area and common mode impedance;
- (iv) proper choices of logic families;
- (v) filtering the higher harmonics of clock or data signal (for digital circuits) and unwanted RF signal;

- (vi) increasing the rise or fall times of a clock or data signal;
- (vii) making pulse duty cycle nearly 50%.

The first three factors (i-iii) do not affect the functional performance of the circuit. However the last three factors (v-vii) may affect the normal behaviour of the circuit. Therefore a designer has to reconsider these factors in such a way that EM radiation can be reduced without affecting the functional performance of the circuit.

A flowchart for incorporating these factors into the composite CAD package is shown in Fig. 5.18.

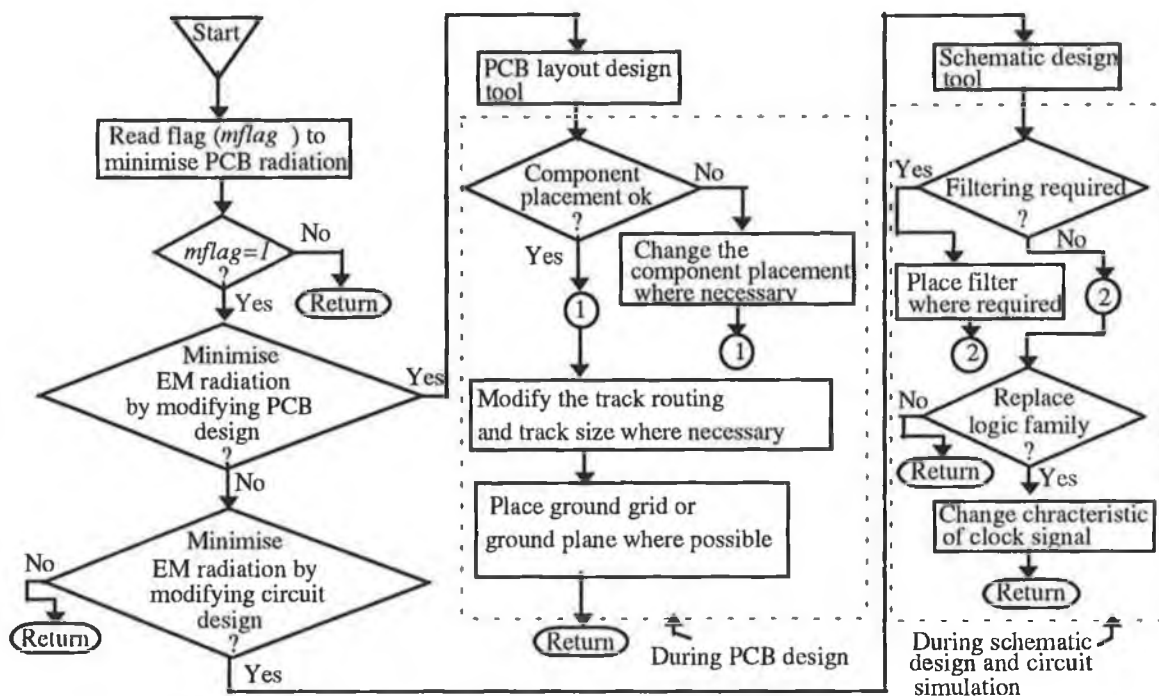


Fig. 5.18 Flow chart to incorporate the EM radiation reducing techniques into the composite CAD package.

On the basis of this algorithm the composite CAD package requests the designer to choose a method for reducing the PCB radiation. Following the designer's choice this CAD

package sets an integer flag so that he or she can go to that part of the design process and modify the design where necessary.

5.5.2 REDUCING RADIATION BY PROVIDING SHIELDING

The EM radiation from a PCB can be reduced by providing shielding in some section of the circuit. The shielding can be provided by the use of two open-ended rectangular boxes (one on the top side and one on the bottom side of the PCB (shown in Fig. 5.19)) made of a material having good shielding effectiveness (SE^4).

For the current work it was assumed that the effect of the internal reflection within the box (refer to section 1.3.6) and the imperfect shielding (due to the gap between the box and the section of the PCB to be shielded) on the radiation is negligible. Therefore it is possible to reduce EM radiation in this manner.

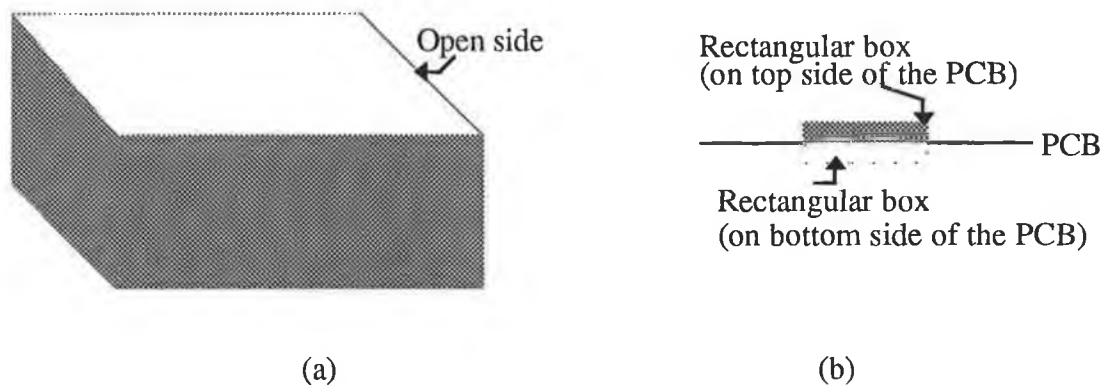


Fig. 5.19 (a) a rectangular box with one side open; (b) front view of the shielded PCB section.

It is necessary to find the section of the PCB where shielding is required. To do so a PCB is divided into a number of rectangular sub-sections to provide shielding in each sub-section separately. An algorithm was developed for finding tracks that are within shielded section. This algorithm is summarised in the flow chart shown in Fig. 5.20. The developed algorithm was implemented in Fortran and the programme is given in Appendix E7.

⁴SE usually expressed in dB, refers to ability of a material to guard against EMI, both emission and susceptibility.

In Fig. 5.20, NS is the track number, n is the rectangular sub-section number, NTS is the total number of tracks and NSP is the total number of shielded sections.

The radiating structure (track) which is within a shielded section can be identified by comparing the corner co-ordinates of the rectangular section with the end co-ordinates of the track. The x - y co-ordinates of each corner of these sections can be determined from the size of the PCB and the desired number of sections. The expressions for the corner co-ordinates are given in Appendix E6.

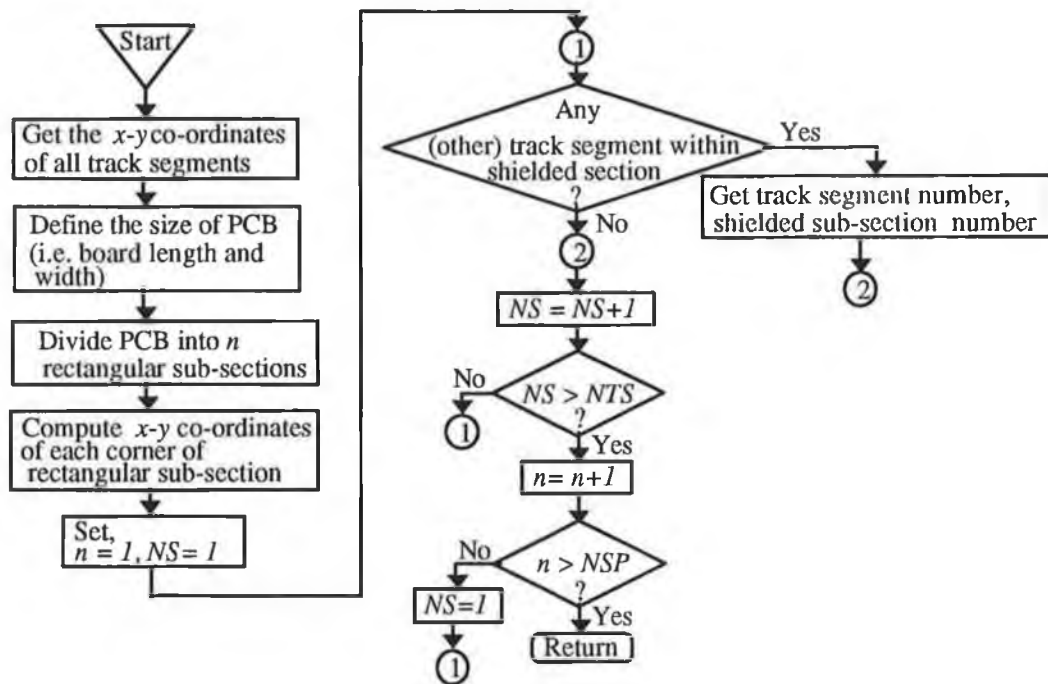


Fig. 5.20 Flow chart for finding track within a shielded section.

Prior to the prediction of radiation it is necessary to exclude the radiating structure (PCB track) which is within the shielded section. Subroutines NFPAT, NEFLD and NHFLD of original NEC-2 programme were modified so that it was possible to exclude the shielded track from the radiating structure prior to determining the radiated field.

The composite CAD package predicts the radiated field after the provision of shielding in each sub-section separately. The predicted radiated fields are then arranged in ascending order using a Fortran programme ASSC (see Appendix E8) in order to find the minimum radiated field, so that one can recognise a PCB section where shielding has to be provided.

5.6 OPTIMUM LAYOUT FOR MINIMISING PCB RADIATION

An optimum layout (i.e. track separation to track width ratio (s/w)) can minimise EM radiation from a PCB. This can be found by analysing two parallel tracks running between two devices as illustrated in Fig. 4.3. Two parallel tracks form a transmission line. As mentioned earlier in section 4.2, the PUL parameters and the characteristic impedance (Z_0) of the transmission line depend on the track size (i.e. width and thickness) and track separation. It is also obvious from the expressions of functional currents (such as I_g , I_l and $I(y)$ - refer to Eqns. 4.15, 4.16 and 4.12 respectively) and the displacement current, that Z_0 affects these currents and consequently affects the radiated fields from a PCB.

The expressions for radiated fields also reveal that a low current value leads to minimum radiation from a PCB. This can be achieved in different ways such as : (i) by reducing the source voltage (V_s) (ii) by increasing Z_0 and (iii) by changing the value of load impedance (Z_l) and source impedance (Z_s).

The expressions for Z_0 (see Eqn. 2.6 and Eqn. 4.8) reveal that the Z_0 can be increased by increasing the s/w ratio. This can be achieved by making s large and w small. However a large value of s is not desirable as it increases radiation. Therefore it is desirable to optimise the s/w ratio for reducing the PCB radiation.

Raut *et al.* [17] presented a method for finding the optimum s/w ratio. Their analysis was based on the minimisation of vector potential and some basic assumptions. In this research, the analysis is based on the minimisation of the magnitude of the total radiated field. For simplicity the far field approximation was considered so that the scalar term of the radiated electric field ($\nabla(\nabla \cdot \vec{A}) = 0$) becomes zero. After this approximation, no assumption was made in determining the field magnitude. The magnitude of the radiated electric field components due to functional currents was derived using Eqns. 4.23, 4.25, 4.26 and 4.29. This can be expressed as,

$$|E_x| = \omega \int_{\frac{s}{2}}^{-\frac{s}{2}} \left[\left\{ F_1(Z_0) \sin(\alpha_1(Z_0)) + F_2(Z_0) \sin(\alpha_2(Z_0)) \right\}^2 + \left\{ F_1(Z_0) \cos(\alpha_1(Z_0)) + F_2(Z_0) \cos(\alpha_2(Z_0)) \right\}^2 \right]^{1/2} dx' \quad (5.31)$$

where F_1, F_2, α_1 and α_2 are real functions and are given in Appendix E9.

$$|E_y| = \omega \int_{-\frac{l}{2}}^{\frac{l}{2}} \left[\frac{F_3(Z_0)}{F_4(Z_0)} \right] \sqrt{R_{y1}^2 + R_{y2}^2 - 2 R_{y1} R_{y2} \cos\{\beta (R_{y1} - R_{y2})\}} dy' \quad (5.32)$$

where, F_3 , and F_4 are real functions and are given in Appendix E9.

As the z component of the vector potential (in this case) is equal to zero, E_z is also zero.

It is evident from Eqns. 5.31 and 5.32 that the analytical minimisation of $|E_x|$ and $|E_y|$ is very difficult, so the process was tackled numerically. A computer programme listing written in Fortran is given in Appendix E10.

5.7 CONCLUDING REMARKS

The development of a composite CAD package for predicting and reducing EM radiation from a PCB has been described. Salient features of the circuit design packages that are employed for developing the composite CAD package have been discussed. Extraction of geometrical and electrical data of a PCB from circuit design packages is a key factor in predicting and reducing EM radiation from a PCB. Therefore data extraction algorithms have been developed and described.

Various techniques to reduce the PCB radiation have been incorporated along with the composite CAD package. Theoretical formulation to determine the optimum layout has been developed. This will help the designer as a guideline in the design of a PCB having parallel tracks.

Chapter 6

COMPOSITE CAD PREDICTED PCB RADIATION

- CAD PREDICTED RADIATION FROM SAMPLE PCBs
- REDUCING PCB RADIATION BY SHIELDING
- DETERMINATION OF OPTIMUM *s/w* ratio

6.1 INTRODUCTION

This chapter describes the application of the composite CAD package for predicting and reducing the PCB radiation. Three different electronic circuits have been chosen for the prediction. Section 6.2 presents the CAD predicted radiation. The provision of shielding for reducing the PCB radiation is investigated and presented in section 6.3.

The optimum layout which can minimise EM radiation (described in section 5.6) is determined in section 6.4. A guideline in designing the PCB layout is also presented in this section.

6.2 PREDICTION OF RADIATED EM FIELDS USING THE COMPOSITE CAD PACKAGE

Three circuits designed for the prediction are:

- (i) a simple digital circuit consisting of a crystal oscillator and a TTL inverter (74LS04)
- (ii) circuit consisting of a crystal oscillator and a logic inverter which was formed using discrete components
- (iii) circuit consisting of a crystal oscillator and a combinational switching network which was designed using RTL logic gates

In designing PCBs for all three circuits, PCB layout, component placement and track routing were chosen arbitrarily to prove the versatility and flexibility of the data extraction algorithms.

6.2.1 CIRCUIT #1

The schematic diagram of circuit #1 designed using ORCAD is shown in Fig. 6.1. A battery powered supply consisting of 9 V battery and voltage regulator LM 7805 provides a 5 V DC supply to the inverter and oscillator. A PCB for this circuit was designed using BM. Various configurations were chosen to design the PCB. Three configurations are shown in Fig. 6.2 and are designated as config. #1, config. #2 and config. #3. A track width of 0.48 mm was chosen arbitrarily for all three.

The input capacitance of the inverter was found to be 5 pF from the literature [29]. The capacitance was assumed to be connected between the input and ground of the inverter (not shown in Fig. 6.2). The output of the inverter was connected to a resistor of 1k Ω .

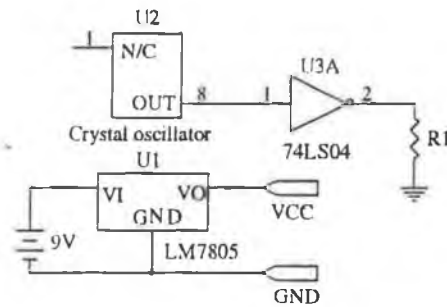


Fig. 6.1 A schematic of a digital circuit (ORCAD output).

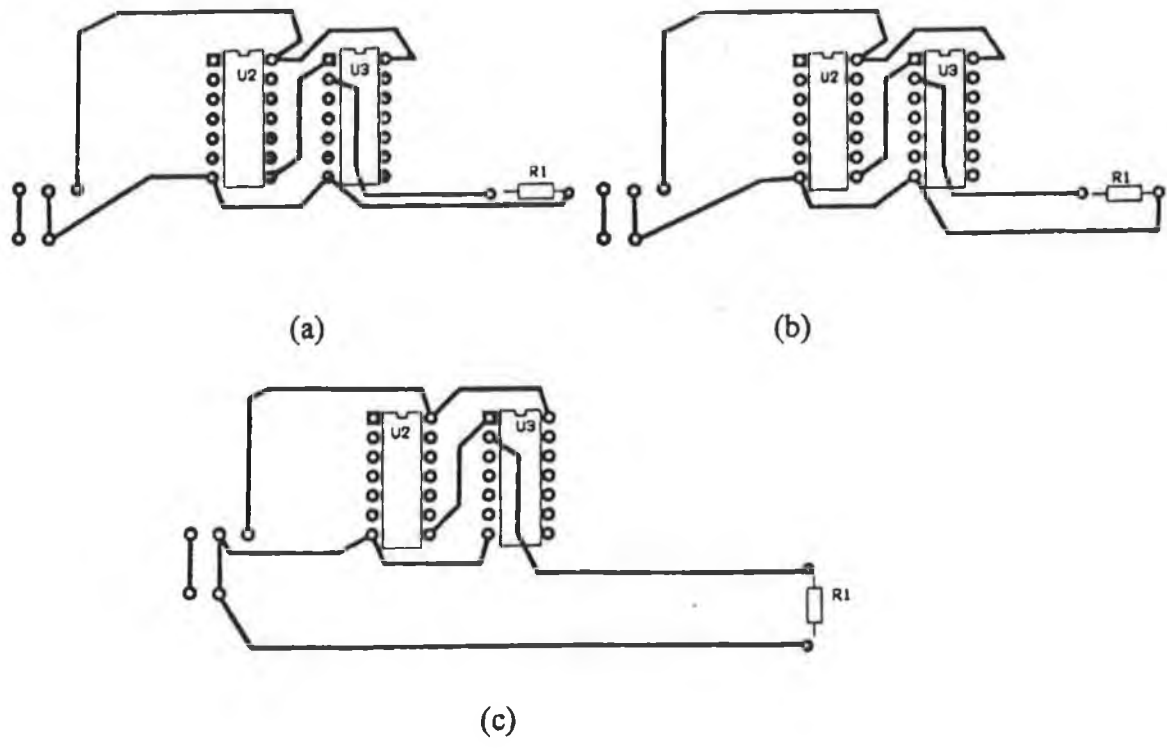


Fig. 6.2 PCB layout for circuit 1: (a) config. #1; (b) config. #2; (c) config. #3.

The radiated EM fields were computed at different frequencies corresponding to odd harmonics of a pulse generated by a crystal oscillator (two choices of crystal were available namely 24 MHz and 40 MHz). The pulse was modelled as a source with an amplitude of 5 V peak to peak. It was assumed that the source was connected between the output pin of the

crystal oscillator and ground (not shown in Fig. 6.2). The composite CAD package computes the amplitude of the harmonic from Eqn. D7-1 (given in Appendix D).

The radiated electric fields were predicted in the x - z plane at a radial distance (r) of 0.1m from the PCB at a polar angle (θ) of 90° . A plot of the predicted electric fields as functions of frequency corresponding to odd harmonics of a pulse generated by a crystal is shown in Fig. 6.3. The predictions were also repeated at a radial distance of 1 m and 3 m from the PCB. The predicted electric fields at different frequencies are shown in Fig. 6.4. It is evident from the plots that in all cases the EM radiation from config. #1 is much less than that from config. #2. This is expected because config. #1 has small track separation that results in small loop area and consequently produces low radiation.

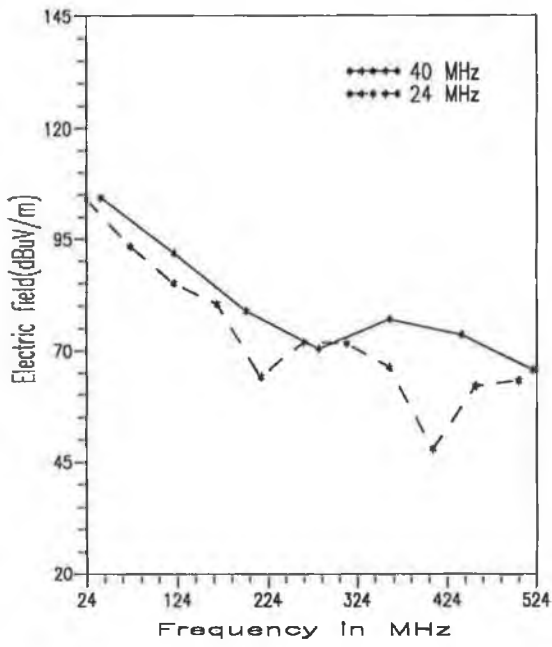
The radiated magnetic fields were computed in the x - y plane at a radial distance of 0.05 m at $\theta = 0^\circ$. In this case a crystal oscillator (two choices of crystal 6 MHz and 10 MHz) was used as a source. A plot of the radiated magnetic fields as a function of frequency corresponding to odd pulse harmonics is shown in Fig. 6.5. The plot clearly shows that config. #1 produces minimum radiation as compared to that produced by the other configurations. This is expected as stated earlier.

6.2.2 CIRCUIT #2

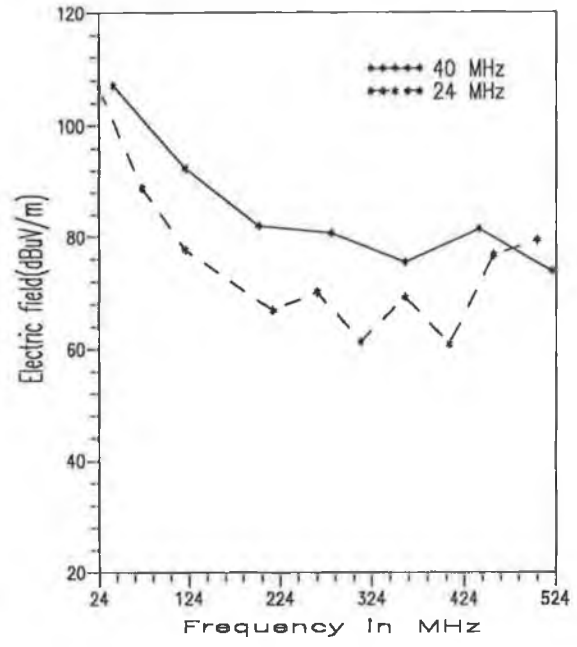
The schematic of circuit #2 again designed using ORCAD and its layout obtained from BM is shown in Figs. 6.6 (a) and 6.6 (b) respectively. The output of the inverter was connected to a pull-up resistor of 2 k Ω . The circuit was fed by a trapezoidal shaped pulse.

Each signal node was modelled as a source point of a track that was connected to the node. A Fourier analysis for every node voltage of the circuit was performed with the transient analysis using PSPICE. PSPICE yields the amplitude of the first nine frequency components (i.e. the fundamental and second through eighth harmonics of the pulse) of the pulse in the Fourier analysis. The EDER routine of the composite CAD package extracts the amplitude of the node voltage and frequency from the PSPICE output.

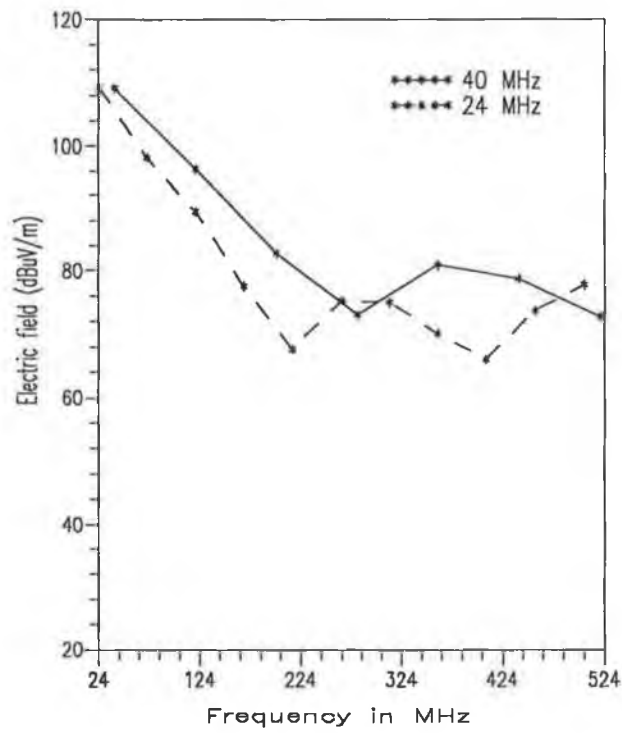
The radiated electric fields were computed at different frequencies corresponding to the fundamental and second through eighth harmonics of the generated pulse of a 24 MHz crystal. The fields were predicted at $r = 0.1$ m, $\theta = 90^\circ$ and $\phi = 0^\circ$. A plot of the predicted electric fields is shown in Fig. 6.7.



(a)

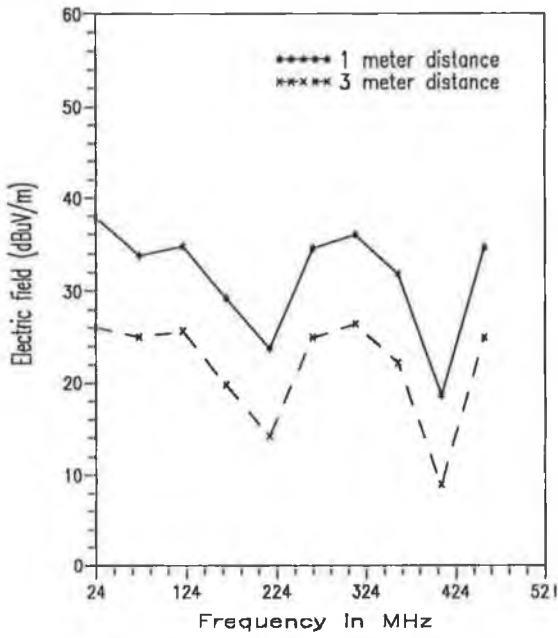


(b)

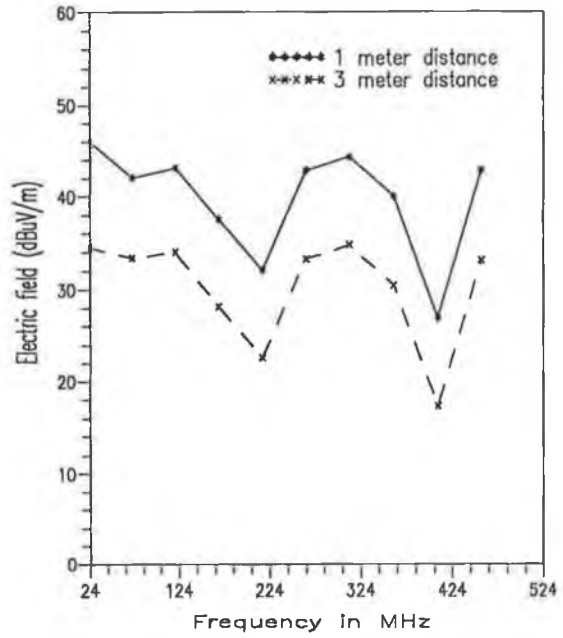


(c)

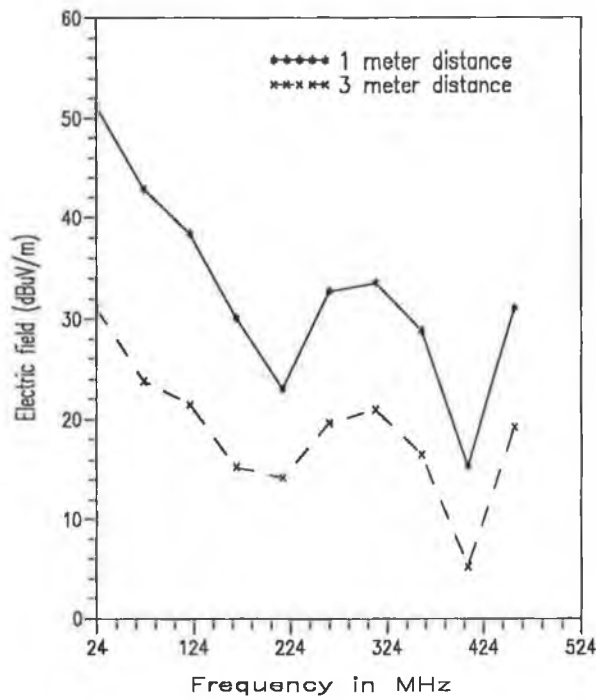
Fig. 6.3 Radiated electric field at 0.1 m distance: (a) config. #1; (b) config. #2; (c) config. #3.



(a)

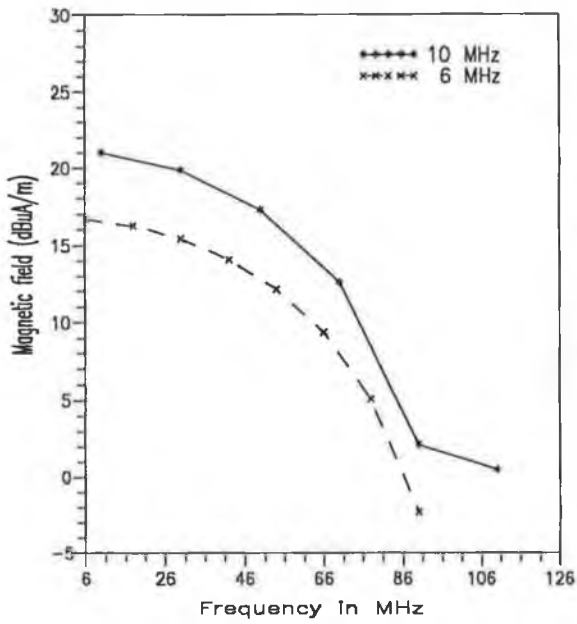


(b)

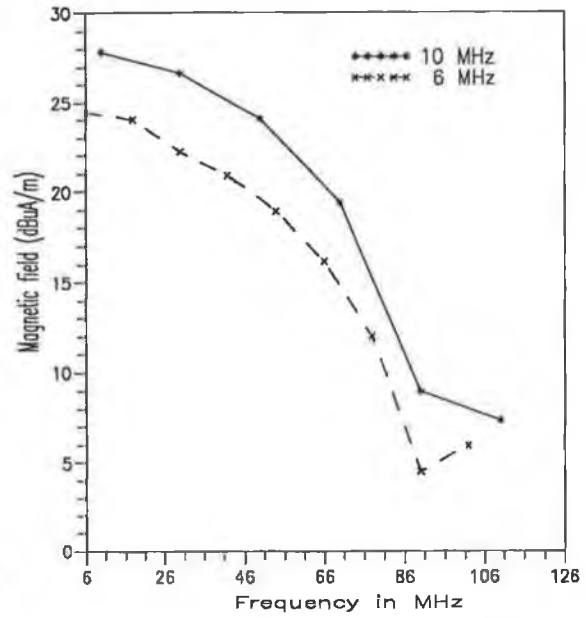


(c)

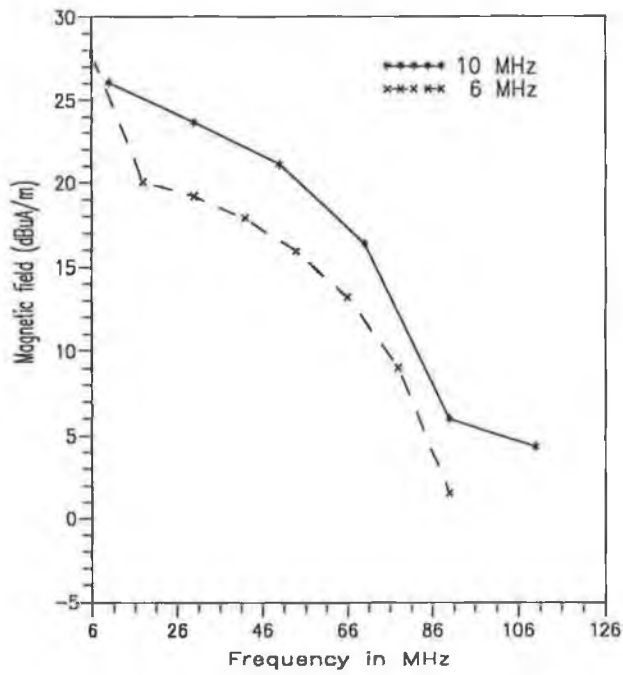
Fig. 6.4 Radiated electric field at 1 m and 3 m distance: (a) config. #1; (b) config. #2; (c) config. #3.



(a)

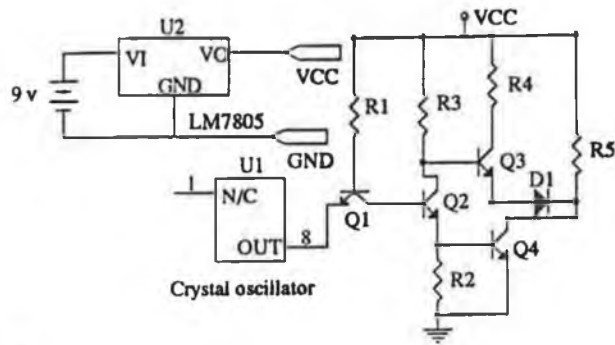


(b)

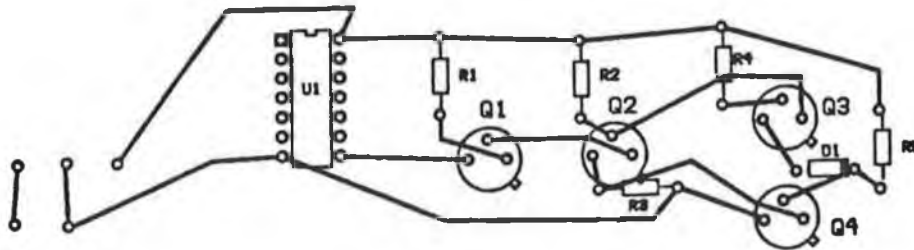


(c)

Fig. 6.5 Radiated Magnetic field at 0.05 m distance: (a) config. #1; (b) config. #2; (c) config. #3.



(a)



(b)

Fig. 6.6 A logic inverter: (a) schematic of the circuit; (b) PCB layout.

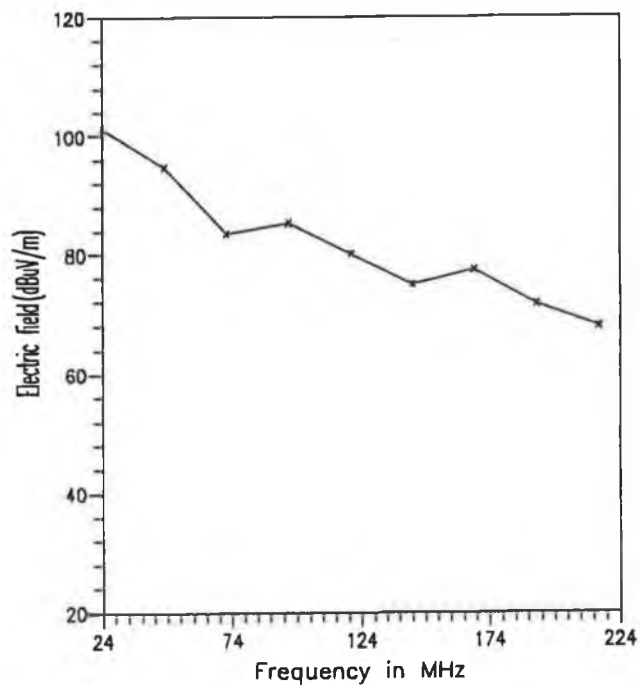


Fig. 6.7 Radiated electric field at 0.1 m distance from PCB of circuit #2.

The predictions were also repeated at a radial distance of 1 m and 3 m from the PCB. The predicted values as a function of frequency are shown in Fig. 6.8. The plot (i.e. Fig. 6.8) shows that the predicted field at a distance of 1 m from the PCB is about 10 dB (i.e. $20 \log(3)$, assuming far field) higher than those obtained at a distance of 3 m from the PCB. This difference was expected.

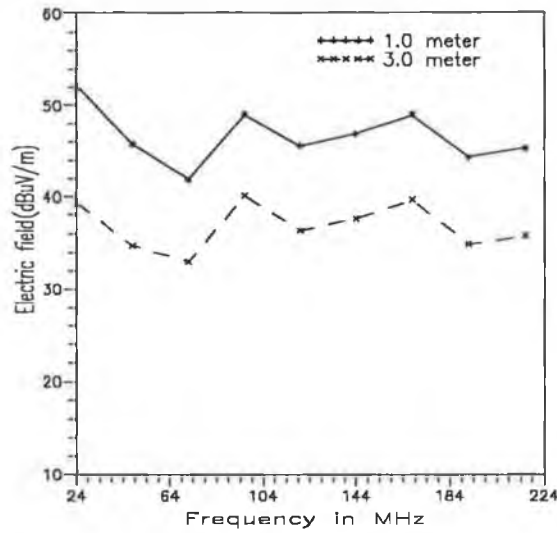


Fig.6.8 Radiated electric field at 1 m and 3 m distance from PCB of circuit #2.

The radiated magnetic fields were predicted at $r = 0.05$ m, $\theta = 0^\circ$ and $\phi = 90^\circ$. A plot of the predicted field is shown in Fig. 6.9.

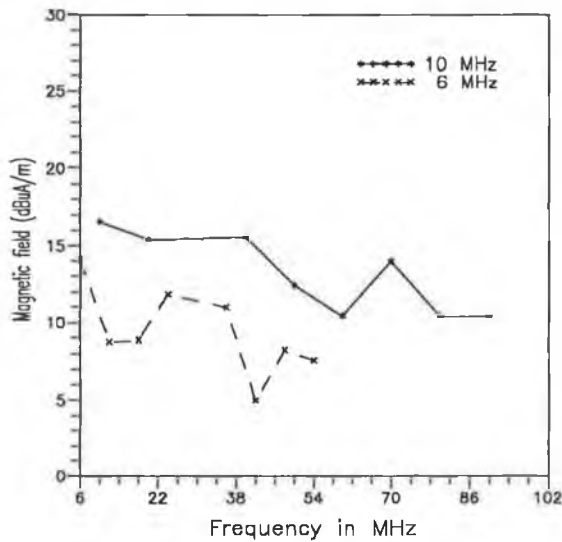


Fig. 6.9 Radiated magnetic field at 0.05 m distance from PCB of circuit #2.

6.2.3 CIRCUIT #3

A combinational switching network that was implemented using RTL gates is shown in Fig. 6.10. The schematic of the circuit that was designed using ORCAD with its layout obtained from BM is shown in Fig. 6.11.

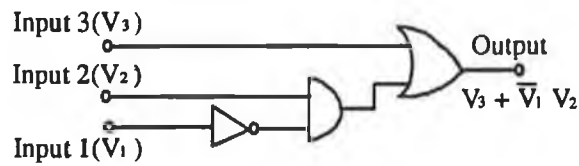
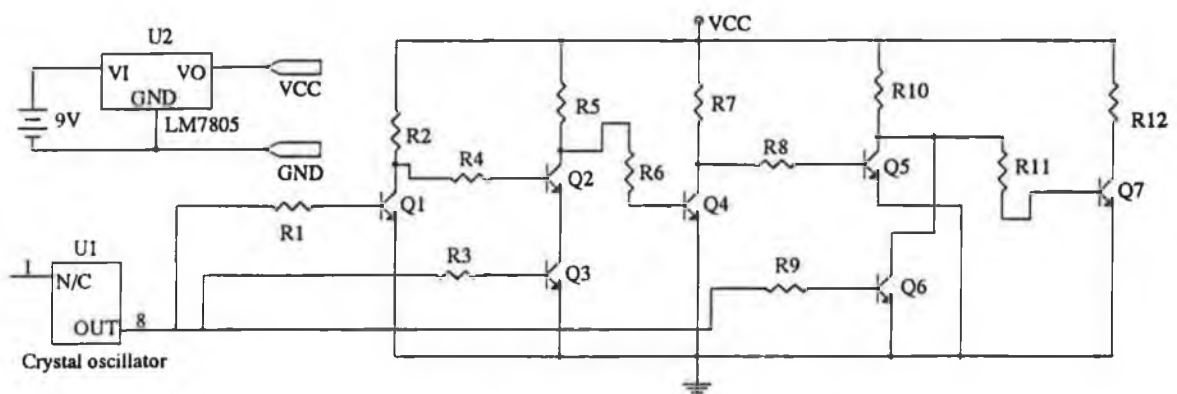
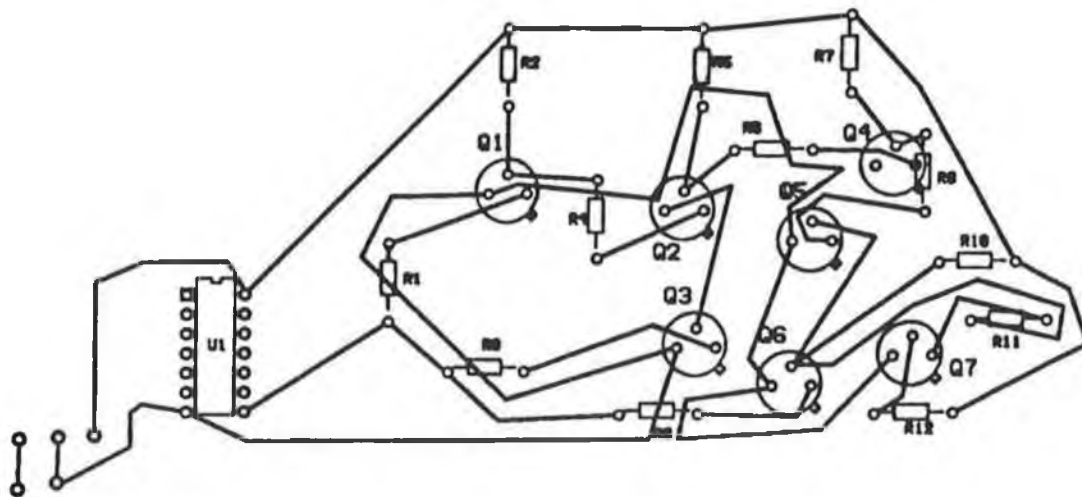


Fig. 6.10 A combinational switching network.



(a)



(b)

Fig. 6.11 Implementation of combinational switching network; (a) circuit schematic; (b) PCB layout.

Each input was a trapezoidal shape pulse that was generated by a crystal oscillator of 24 MHz. Node voltages at a frequency corresponding to a pulse harmonic were obtained from the Fourier analysis using PSPICE.

The radiated electric fields were predicted at $r = 0.05$ m, $\theta = 90^\circ$, and $\phi = 0^\circ$. A plot of the predicted electric fields as a function of frequency is shown in Fig. 6.12 (a). The predictions were repeated for $r = 1$ m and the predicted fields are shown in Fig. 6.12 (b). The radiated electric field were also computed at different positions (i.e. for different values of r) in the x - z plane ($\theta = 90^\circ$ and $\phi = 0^\circ$). A plot of the predicted field as a function of distance r is shown in Fig. 6.13. The plot shows that the field strength decreases with increasing r as expected. It may also be observed from Figs. 6.12 (b) and 6.13 that the field strength does not vary appreciably for frequencies above 72 MHz when the distance exceeds 0.7 m. This may be due to the fact that in the near field region ($r < 0.67$ m) the radiated field from the individual tracks may not cancel each other completely, although they are in close proximity and may have counter current flow. On the other hand, in the far field region ($r > 0.67$ m) the tracks may be considered as collocated because of their close proximity. This may cancel the effect of individual tracks and give a total effect which has less or no dependence on r .

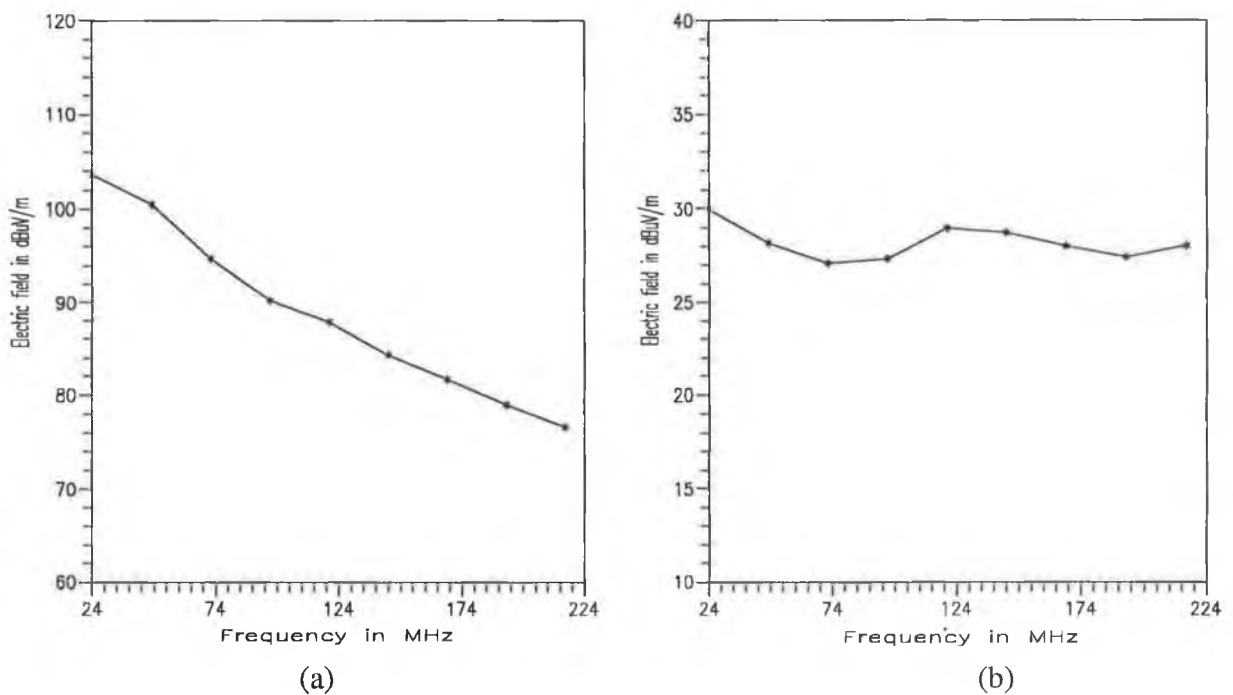


Fig. 6.12 Radiated electric field from circuit # 3 at a distance of (a) 0.05 m; (b) 1.0 m.

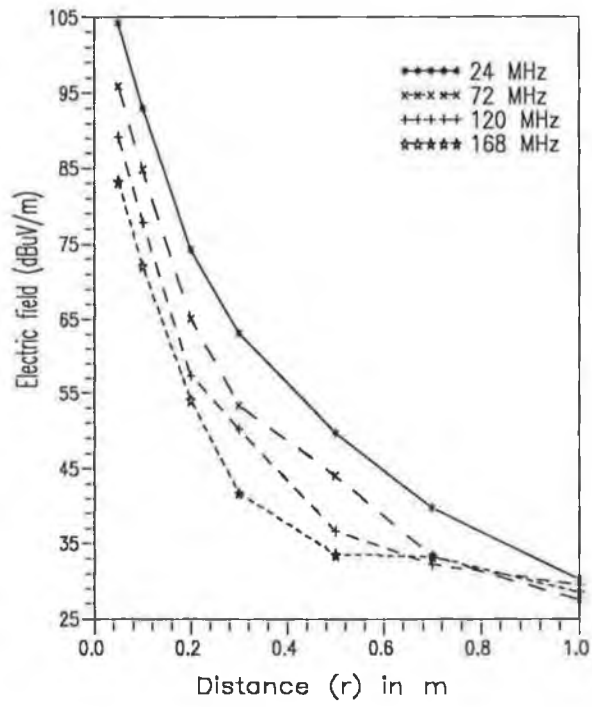


Fig. 6.13 Electric field as a function of distance (r).

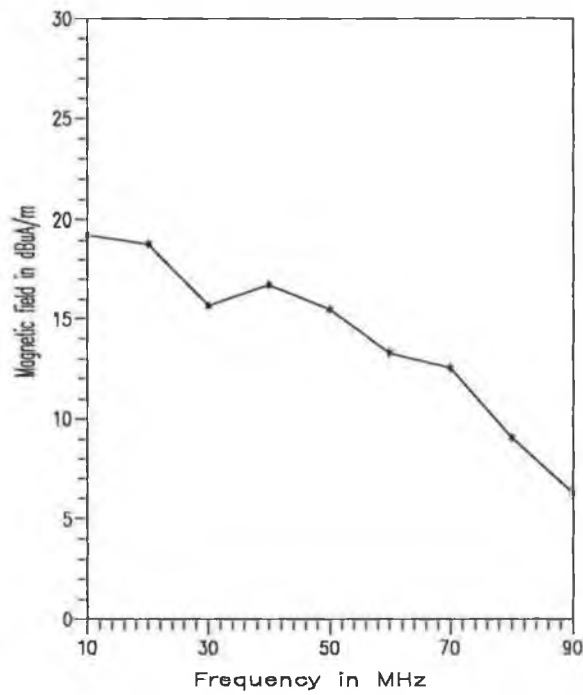


Fig. 6.14 Radiated magnetic field at a distance of 0.05 m from PCB.

The radiated magnetic fields were computed at $r = 0.05$ m, $\theta = 0^\circ$ and $\phi = 90^\circ$. A crystal oscillator of 10 MHz was used in this case. A plot of the predicted magnetic fields as a function of frequency is shown in Fig. 6.14. The predicted field will be validated later in chapter 7.

6.3 EFFECT OF SHIELDING

The effect of shielding in reducing the PCB radiation was investigated theoretically for three cases. Circuit #2 was chosen for the test. In the first case, the PCB was divided into eighteen short rectangular subsections (see Fig. E6-1, $n_x = 3$ and $n_y = 6$). A shielding block was "moved" to each section and the radiated electric fields were computed at $r = 0.05$ m, $\theta = 90^\circ$ and $\phi = 0^\circ$. Similarly the PCB was divided into six large subsections ($n_x = 2$ and $n_y = 3$) and into twelve subsections ($n_x = 3$ and $n_y = 4$) in the second and the third cases respectively. In both cases, the radiated electric field was computed in a similar way to the first case. A plot of the predicted electric fields with and without shielding is shown in Fig. 6.15.

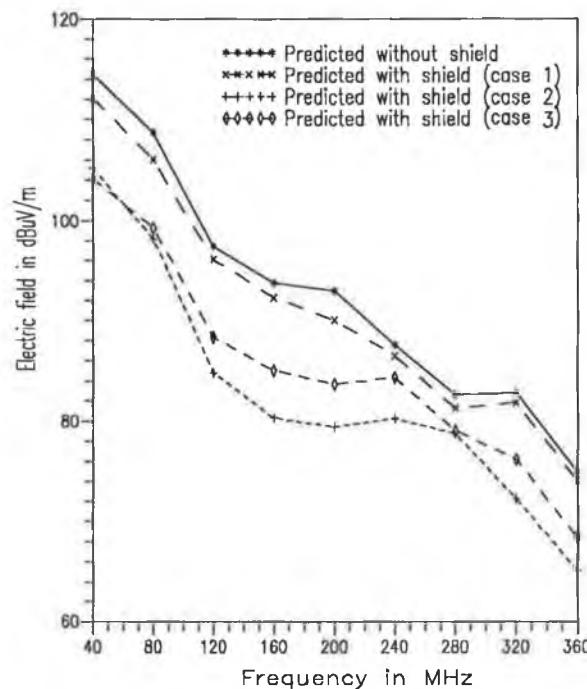


Fig. 6.15 The effect of shielding in reducing the PCB radiation.

The plot shows that in the first case radiated emission from a PCB has been reduced (but not significantly) after the provision of shielding in an appropriate section of the PCB. On

the other hand the strength of the radiated field has been decreased significantly (about 10 to 14 dB) in the other two cases. This is due to the fact that the large shielding block was chosen to cover the maximum radiating structure (PCB tracks) in the PCB. It can be anticipated that further reduction of EM radiation could be possible by providing shielding in more than one suitable section. This option could be accommodated in the developed algorithm as stated in section 5.5.2.

6.4 DETERMINATION OF OPTIMUM LAYOUT

Two parallel tracks of length 0.1 m laid on a glass epoxy substrate as illustrated in Fig. 4.3 were chosen to determine the optimum layout (i.e. s/w ratio). A source of 1 V and a source impedance (Z_s) of 50 Ω was assumed for all frequencies. The magnitudes of radiated electric fields were computed using Eqns. 5.31 and 5.32 at $r = 3$ m, $\theta = 90^\circ$ and $\phi = 0^\circ$. A plot of the predicted electric fields as a function of s/w ratio and the optimum s/w value at which the field magnitude is minimum, obtained from the minimisation routine is shown in Fig. 6.16.

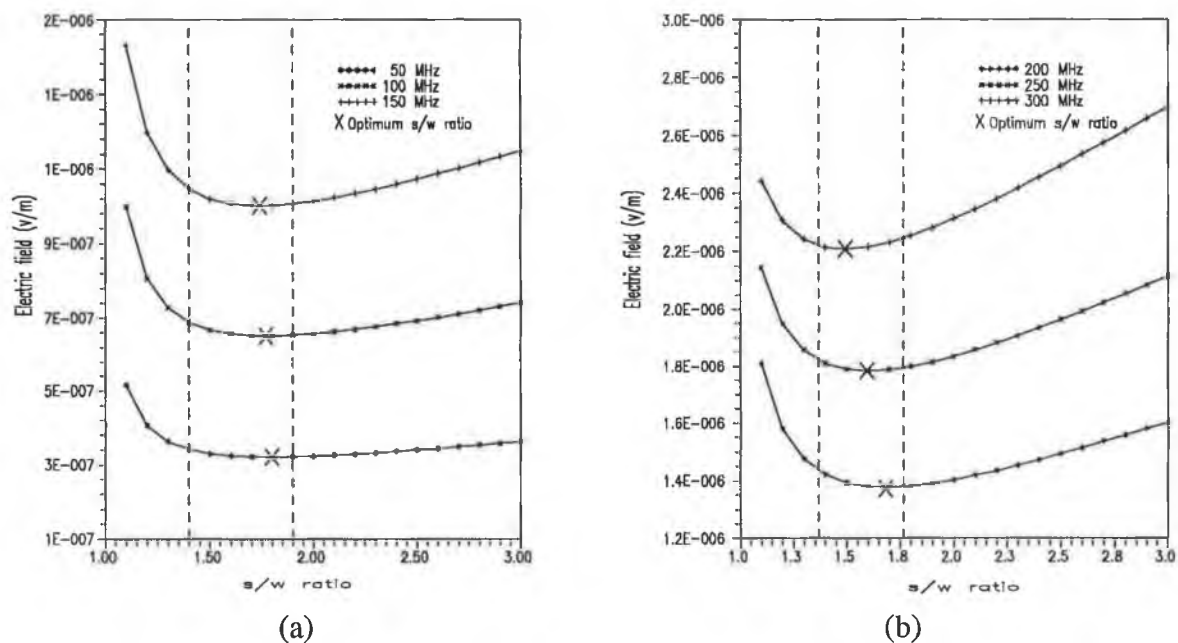


Fig. 6.16 Radiated electric field as function of s/w ratio: (a) 50 MHz, 100 MHz, and 150 MHz; (b) 200 MHz, 250 MHz and 300 MHz.

The plots exhibit that for a given layout geometry (parallel PCB tracks), physical parameters of the PCB and specified field point, an optimum spacing (i.e. s/w) that varies from

1.4 to 1.8 could minimise EM radiation from a PCB. An experimental validation of the predicted optimum layout will be presented in chapter 7.

6.5 CONCLUDING REMARKS

The radiated EM fields were predicted at different observation points and at different frequencies corresponding to the harmonics of the generated pulse of a crystal (several choices of 6 MHz, 10 MHz, 24 MHz and 40 MHz). It was observed from the prediction that in the far field regions, the difference between the predicted electric field at 1 m distance and that at 3 m distance is about 10 dB which was expected. It was also seen that the PCB radiation could be reduced by providing a shield at an appropriate section of the PCB. An investigation showed that in cases where the signal and its return path are parallel, the EM radiation from that section of the PCB can be reduced if the s/w ratio lies between 1.4 and 1.8.

Chapter 7

EXPERIMENTAL VALIDATION

- ❑ MEASUREMENT OF PCB RADIATION AT 0.1 m AND 0.05 m
- ❑ MEASUREMENT OF PCB RADIATION AT 1 m IN SHIELDED ROOM
- ❑ DETERMINATION OF FIELD MAXIMUM POSITION IN SHIELDED ROOM
- ❑ MEASUREMENT OF PCB RADIATION AT 3 m IN ANECHOIC CHAMBER
- ❑ COMPARISONS BETWEEN PREDICTED AND MEASURED VALUES

7.1 INTRODUCTION

It was necessary to validate the composite CAD predicted radiation experimentally. It would be interesting to validate the EM radiation obtained from the extended TLM computation. This was also done experimentally. This chapter details the measurement of EM radiation from various PCBs.

Various emission measurement techniques have already been described in chapter 2. Instruments and accessories which were used in the measurement of PCB radiation are described in section 7.2.

Near field measurement was performed using near field probes. Measured radiated fields were then compared with the predicted values as obtained from chapters 4 and 6. Section 7.3 describes the near field measurement and contains a comparison between the measured EM fields and the predicted EM fields.

Radiated electric field from a PCB at 1 m was measured in a small shielded room. Reflections from the room walls and room resonance may cause errors in the measured results. Thus an emission test method recently developed by Dawson [59] for use in the screened room at a frequency below 200 MHz was employed in this work. In section 7.4, the measurement of radiated EM fields is described and a comparison between the test results and the predicted results is presented.

An anechoic chamber test facility was used for the measurement of radiated electric field at a distance of 3 m from the test circuit. Section 7.5 describes the field measurement and presents a comparison between the measured radiated fields and the predicted fields obtained from the composite CAD package.

7.2 INSTRUMENTS AND ACCESSORIES

The measurement of radiated emission does not require any sophisticated instruments or accessories. The measurement system consists of the transducers (e.g. antennas, near field probes) to receive the radiated EM field and a spectrum analyser or an EMI receiver to record the received field strength.

Accessories such as an amplifier may be needed if the received signal is very weak. Some output devices such as an X-Y plotter, a pen recorder, and a memory card in an EMI receiver are also essential to display and record the radiated emission.

Some relevant features of the instruments and accessories which were employed for the measurement of PCB radiation are given in the following subsections.

7.2.1 NEAR FIELD PROBES

Antennas for near field measurement are of small dimension in order to permit fine exploration of the measurement volume. They are generally sensitive to either magnetic or electric fields. The Electro-Mechanics Model EMCO™ -7405 near field probes were used to measure the near field radiation from a PCB. Details of these probes are available from the manufacturer. However some salient features of the near field probes which are supplied by the manufacturer [118] are introduced in the following paragraphs.

The Model EMCO 7405-901, a magnetic field probe, was used to measure the near magnetic (H) field. This probe contains a single turn, shorted loop of diameter 6 cm inside a balanced electric field shield. The loop rejects electric (E) field due to the balanced shield and has E/H rejection of about 41 dB. The upper resonant frequency of this probe is about 790 MHz [118].

The ball probe EMCO 7405-904 was used to measure the near E-field. The ball probe shaft is constructed from 50 Ω coaxial cable. The coaxial cable is terminated at its end with a 50 Ω resistor in order to present a conjugate termination to a 50 Ω line. The centre conductor is extended beyond the 50 Ω termination and attached to a 3.6 cm diameter ball probe. This probe rejects the H- field due to the absence of a closed loop which prevents current flow. According to the specifications supplied by the manufacturer, the probe goes to resonance at a frequency above 1 GHz and has H/E rejection of about 30 dB.

One important parameter of these probes is the performance factor (*PF*). The *PF* is defined as the ratio of the field presented to the probe to the voltage developed by the probe at its BNC connector. The *PF* of these probes is given in Appendix F1.

7.2.2 BROADBAND ANTENNAS

Broadband antennas such as biconical, log periodic antennas are widely used to measure radiated E-fields. A biconical antenna (BCA) (Electro-Matrics, Model BIA-30) was employed to perform the emission measurement in the frequency range of 20-200 MHz. A log periodic antenna (LPA) (Electro-Matrics, Model LPA-30) was used in the frequency range of 200-1000 MHz. The input impedance of both antennas is 50 Ω . Detail specifications of these antennas are available from the manufacturer.

An important parameter when an antenna is being used to measure the radiated field is the antenna factor (*AF*). The *AF* is defined as the ratio of electric (or magnetic) field in which the antenna is located to the effective voltage appearing at the input of the measuring device (e.g. EMI receiver, spectrum analyser) which generally has an input impedance of 50 Ω . The antenna factors of these antennas at 1 m distances are given in Appendix F2.

7.2.3 EMI RECEIVER / SPECTRUM ANALYSER

An EMI test receiver (Rohde & Schwarz, Model ESVS-30) was used. This test receiver is a triple-conversion heterodyne receiver covering the frequency range from 20 to 1000 MHz. The receiver provides 100 Hz frequency resolution, fast frequency scanning and accurate level indication equally in average and quasi-peak detection. For EMI measurement, the instrument has built in facilities to compare the received signal with the EMC standards set by the regulating bodies such as CISPR, FCC, CENELAC, ETSI, and VDE. Some of the main features and facilities of this test receiver [122] are as follows:

- Wide frequency range: 20-1000 MHz
- Fast synthesiser: frequency resolution of 100 Hz, any frequency step in ≤ 30 ms, sweep mode for fast frequency scanning
- Level measurement range -17 to 137 dB μ V
- Manual or automatic test with spectrum display on screen and report on printer or plotter
- Peak, quasi-peak and average detectors operating in parallel
- Noise indication, for 10 kHz bandwidth and average indication, typically -15 dB μ V without preamplifier and -21 dB μ V with preamplifier
- 50 Ω input impedance
- Automatic calibration with the aid of a high precision built-in generator

- Parallel interface for I/O connection, IEC/IEEE -bus interface
- Built in disk drive for storing test results and receiver setting through a keyboard that can be connected.

The receiver has a built in tracking generator for two-port measurement. A logarithmic amplifier with more than 70 dB dynamic range is also available.

In addition to the EMI test receiver, a Chase ADVANTEST R3361A spectrum analyser was used for emission measurement in an anechoic chamber. This instrument uses a synthesised technique to cover a wide frequency band of 9 kHz to 2.6 GHz. The essential features of this instrument are available in the literature [102].

7.2.4 SIGNAL GENERATOR

The Hewlett -Packard Model 8657B synthesised signal generator was used. The carrier frequency range of this generator is 0.1 MHz to 2.06 GHz. The HP 8657B has precise power levels from + 7 to -143.5 dBm (114 dB μ V to 36.5 dB μ V) with overrange to +17 dBm at decreased accuracy [152].

7.2.5 PRE-AMPLIFIER

A Chase ADVANTEST preamplifier Model R14601 was used at the input of the spectrum analyser (R3361A) in order to amplify the received signal. The frequency range of this amplifier is 9 kHz to 1 GHz. The gain is 25 dB or more and almost flat. The amplifier has input and output impedances of 50 Ω .

7.3 NEAR FIELD MEASUREMENT

The radiated fields (electric and magnetic) from sample PCBs (as illustrated in chapter 4 and 6) were measured at a radial distance of 0.1 m and 0.05 m from the PCB. In an EMI problem, the maximum radiated field is of common interest. The maximum radiated fields were measured in all cases.

7.3.1 TEST SET UP

A schematic diagram of the test set-up is shown in Fig. 7.1. The near field probes (EMCO 7405-904 ball probe for electric field and EMCO 7405- 901 loop probe for magnetic field) were used to detect the radiated field. An X-Y plotter was connected to the output of the EMI receiver (ESVS-30) to plot the received signal.

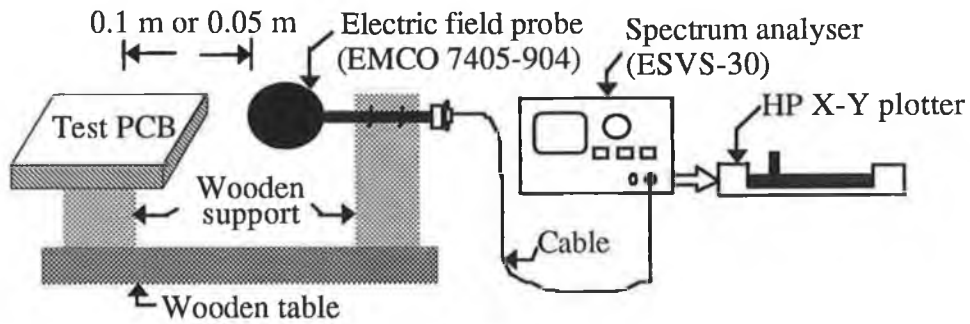


Fig. 7.1 Schematic diagram of the test setup for radiated field measurement using near field probes.

7.3.2 MEASUREMENT PROCEDURE

The PCB was placed on a wooden table in a shielded enclosure. All recording instruments such as the spectrum analyser and plotter were placed outside the enclosure, so that any emission from the recording instruments could not contaminate the radiated emission from the test PCB.

Throughout the measurement, the origin of the PCB layout in the rectangular co-ordinate system was assumed as the origin of the geometry of the field observation point. The geometry of the field observation point is shown in Fig. 7.2. The ball probe was placed in the x - z plane (i.e. azimuth angle $\phi=0^\circ$) at a polar angle θ of 90° and at a radial distance of r . Therefore the position of the field probe is $(r, 0, 0)$ in the rectangular co-ordinate system. The loop probe was placed in the x - y plane (i.e. $\phi = 90^\circ$) at an angle θ of 0° . In the rectangular co-ordinate system, the position of the loop probe is then $(0, 0, r)$. Photographs of the electric and magnetic field measurement set-up are shown in Figs. 7.3 and 7.4 respectively.

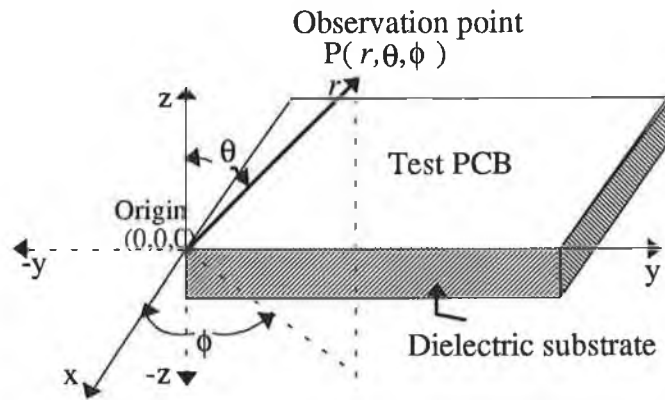


Fig. 7. 2 Geometry of field observation point.

7.3.3 TEST RESULTS & COMPARISON

The spectrum analyser recorded the voltage received by the field probe (spectrum analyser and field probe are matched with 50Ω impedance) in $\text{dB}\mu\text{V}$. Therefore it is necessary to convert the recorded voltage into field strength at the observation point.

In case of ball probe, the magnitude of the electric field at the point of observation can be obtained from the expression given below,

$$E = S_o + PF + C_l \quad (7.1)$$

where, E is the electric field strength in $\text{dB}\mu\text{V}/\text{m}$, S_o is the spectrum analyser output in $\text{dB}\mu\text{V}$, PF is the probe performance factor in dB and C_l is the cable loss in $\text{dB}\mu\text{V}$.

Similarly, the output voltage of the loop probe which was recorded by the spectrum analyser has to be corrected to obtain the magnetic field strength. The magnetic field strength (H) in $\text{dB}\mu\text{A}/\text{m}$ can be obtained from the following expression,

$$H = S_o + (PF - 51.52) + C_l \quad (7.2)$$

The constant term (i.e. 51.52) in Eqn. 7.2 arises because the loop probe PF is given for the equivalent E field [118]. The probes are also calibrated with a plane wave (i.e. $E/H = 377 \Omega$). Therefore, it is required to subtract 51.52 (i.e. $20 \log(377)$) from the given PF to obtain the equivalent H -field.

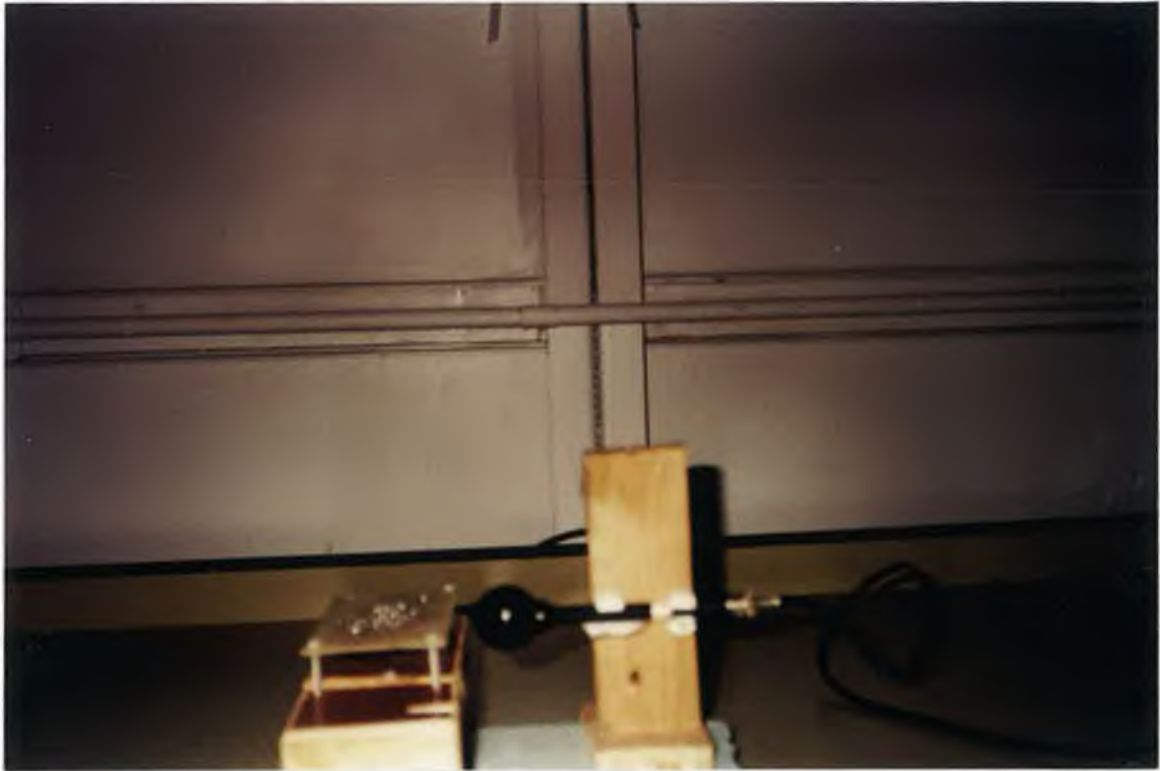


Fig. 7.3 Photograph of the near electric field measurement set-up.



Fig. 7.4 Photograph of the near magnetic field measurement set-up.

Using $C_1 = 1$ dB (see section 7.4.2.3), the spectrum analyser was offset to provide the field strength including the cable loss.

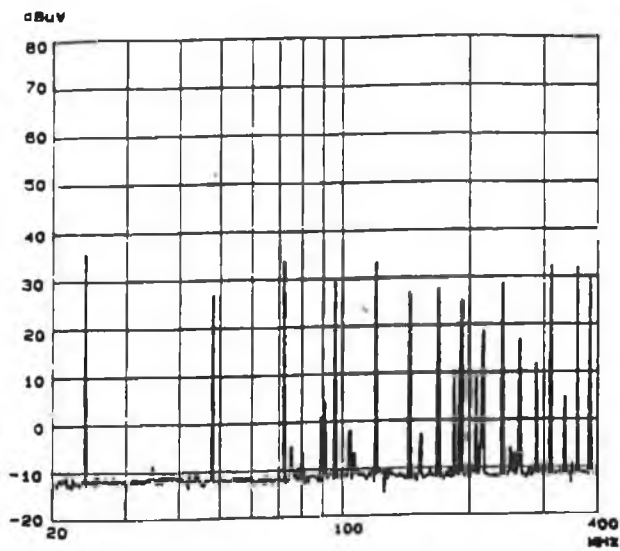
The EM radiation from sample PCBs (shown in Figs. 6.2, 6.6 and 6.11) were measured. The measured EM fields and a comparison of the measured values with the predicted values are given in the following subsections.

7.3.3.1 Circuit #1

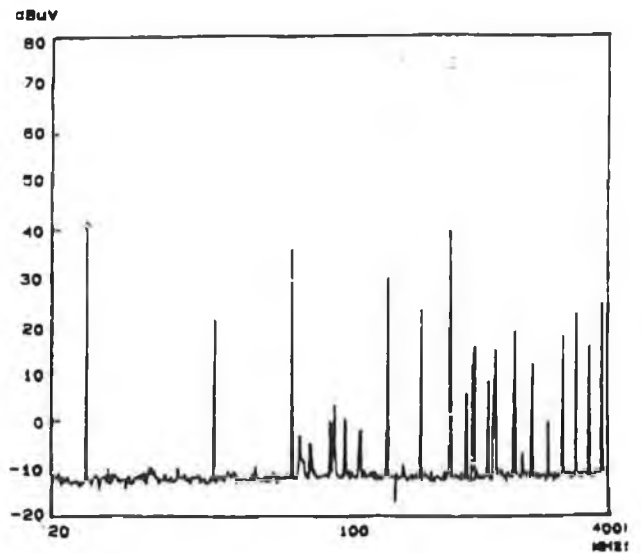
The radiated electric field from PCBs of all configurations as shown in Fig. 6.2 for circuit #1 was measured at $r = 0.1$ m, $\theta = 90^\circ$ and $\phi = 0^\circ$. A Plot of recorded field strength (PF is not included) as a function of frequency corresponding to harmonics of the pulse generated by a crystal oscillator is shown in Figs. 7.5 (for 24 MHz crystal) and 7.6 (for 40 MHz crystal). Measurement is repeated at $r = 0.05$ m for config. #1 and the recorded field strength is shown in Fig. 7.7. The corrected electric field strength at the point of observation was obtained by adding the PF to the spectrum analyser output.

A plot of the measured and predicted electric field as a function of frequency corresponding to odd harmonics of the pulse is shown in Figs. 7.8, 7.9 and 7.10. The plots clearly exhibit that in most cases, the predicted electric field is above the measured value. The maximum difference between the predicted and measured value is about ± 6 dB. It is also evident from the plots (i.e. Figs. 7.5 and 7.6) that config. # 1 produces minimum radiation as compared to that produced from config. # 2. This was expected as stated in section 6.2.1.

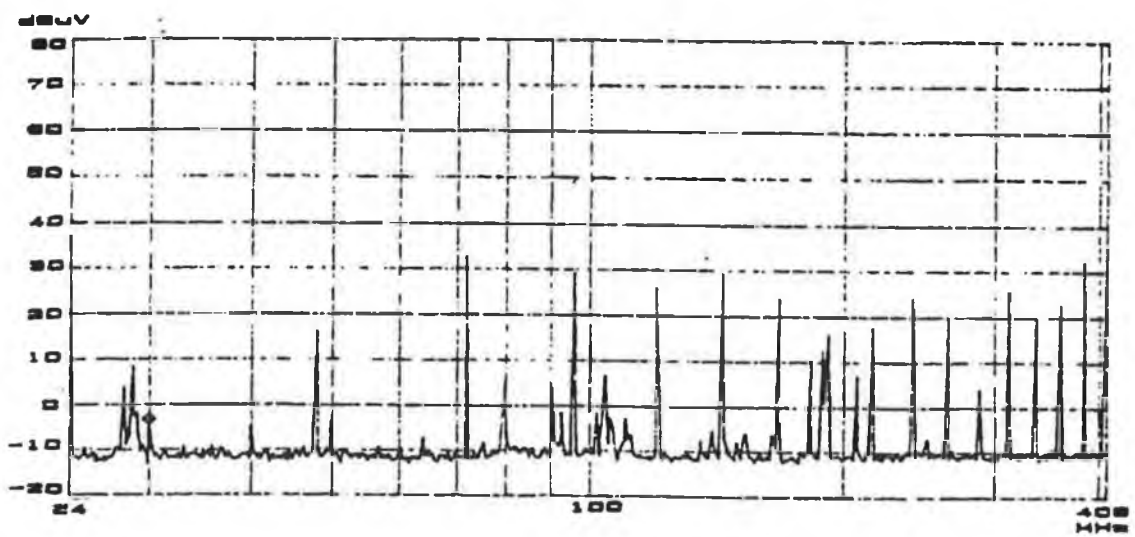
The radiated magnetic field was measured at $r = 0.05$ m, $\theta = 0^\circ$ and $\phi = 90^\circ$. The recorded field strength (excluding PF) as a function of frequency corresponding to the harmonics of the 10 MHz pulse is shown Fig. 7.11. The same measurement was repeated with the 6 MHz crystal for config. # 2. The corrected field strength at the point of observation was obtained from the expression as given in Eqn. 7.2. A comparison of the CAD predicted magnetic field and the measured field is shown in Fig. 7.12. Clearly the composite CAD predicted value is very close to the measured value and in some cases above the measured value.



(a)

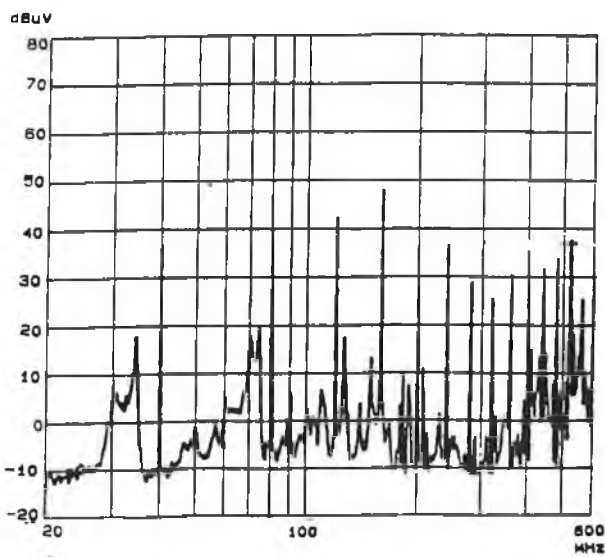


(b)

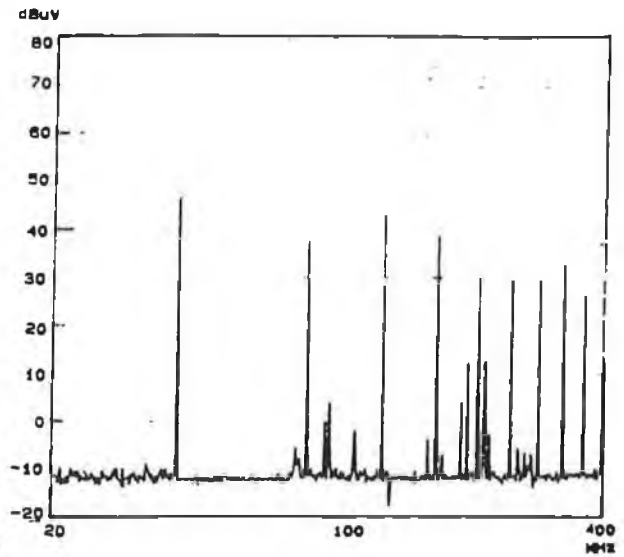


(c)

Fig. 7.5 Recorded radiated electric field at a 0.1 m distance from (a) config. #1; (b) config. #2; (c) config. #3. The 24 MHz crystal was used.



(a)



(b)

Fig. 7.6 Recorded radiated electric field at a 0.1 m distance from (a) config. #1; b) config. #2. The 40 MHz crystal was used.

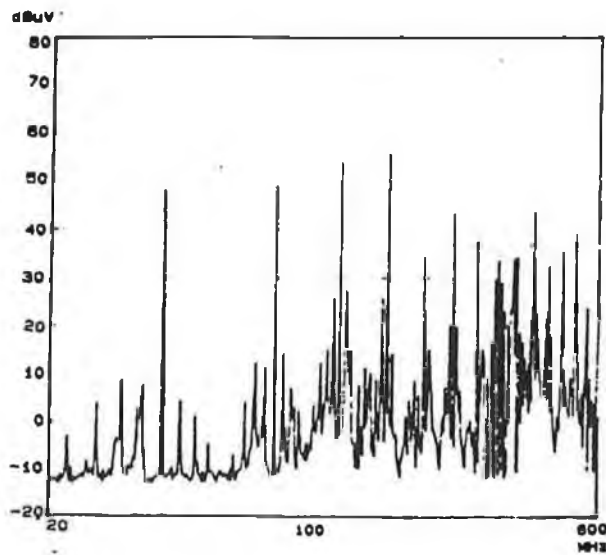
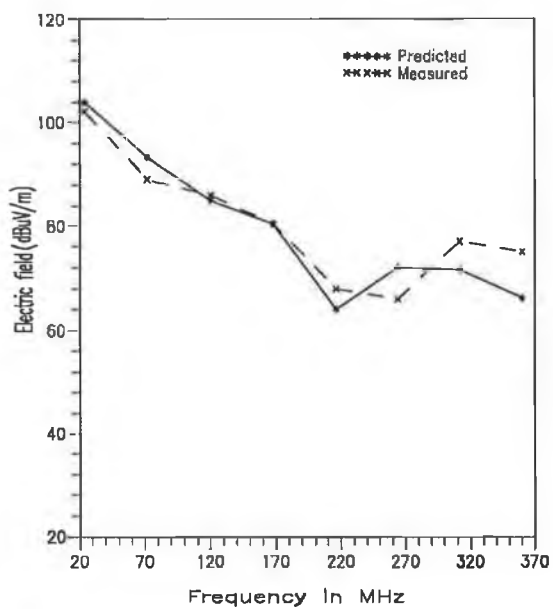
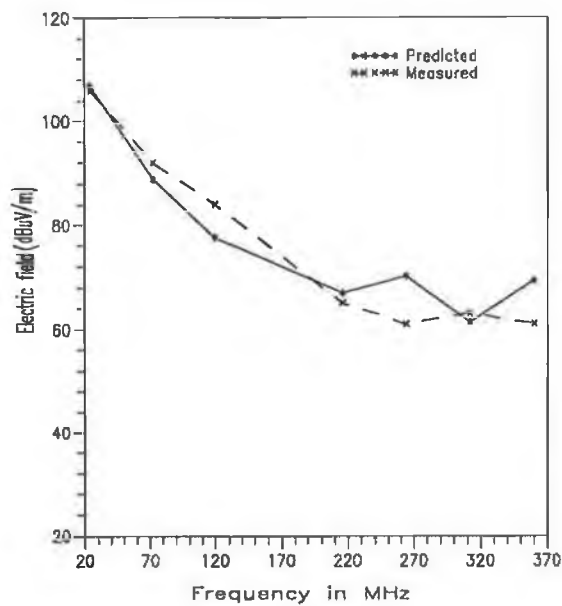


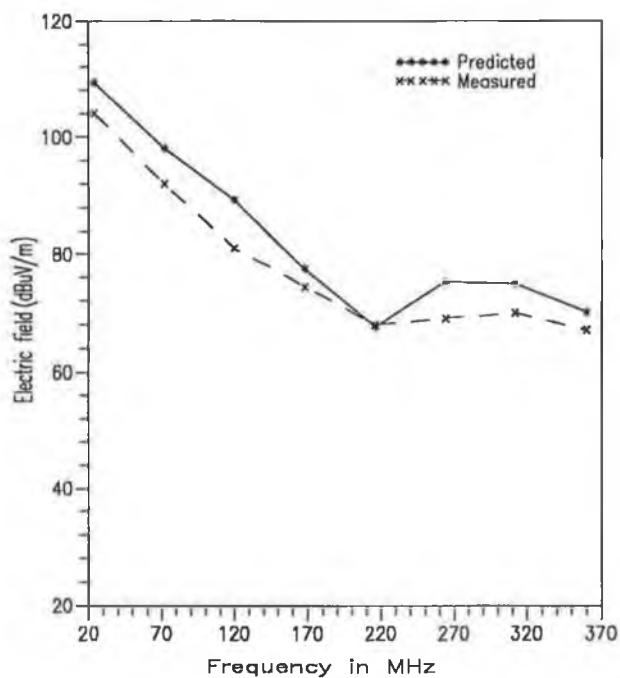
Fig. 7.7 Recorded radiated electric field from config. #1 of circuit #1 at a distance of 0.05 m for 40 MHz crystal.



(a)

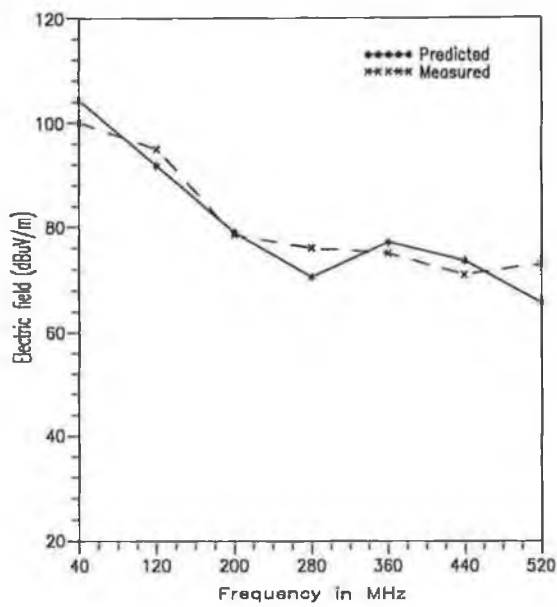


(b)

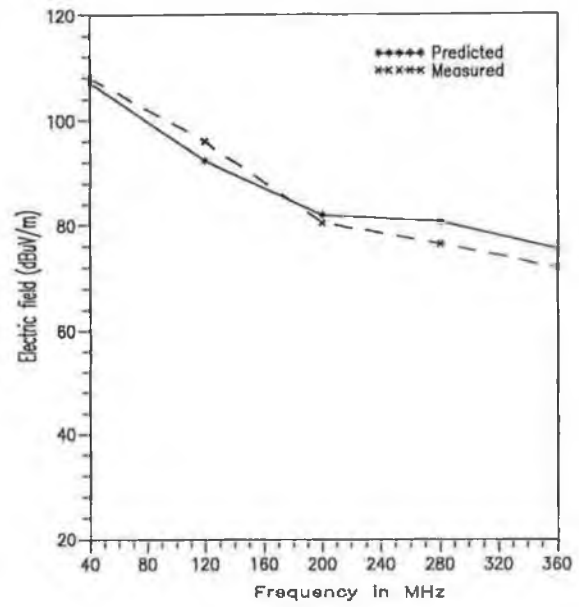


(c)

Fig. 7.8 Comparison between the predicted and measured electric field at a 0.1 m distance (a) config #1; (b) config # 2; (c) config # 3. The 24 MHz crystal was used.



(a)



(b)

Fig. 7.9 Comparison between the predicted and measured electric field at a 0.1 m distance (a) config. #1; (b) config. # 2. The 40 MHz crystal was used.

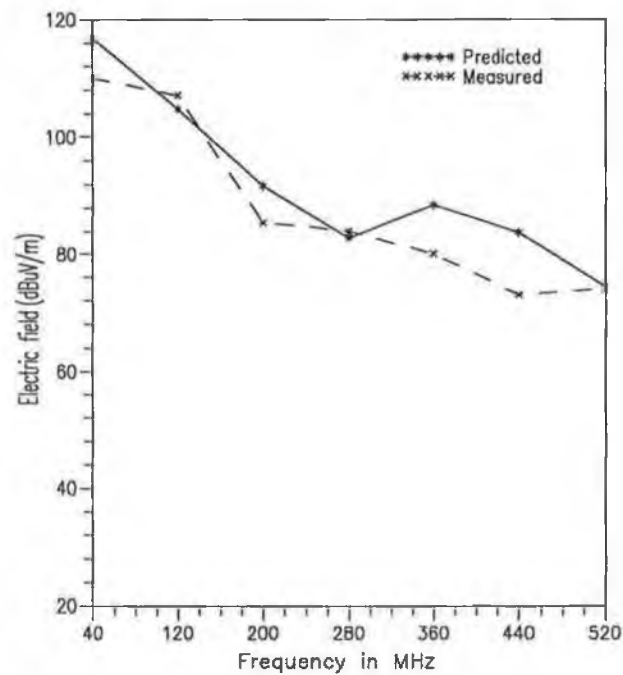
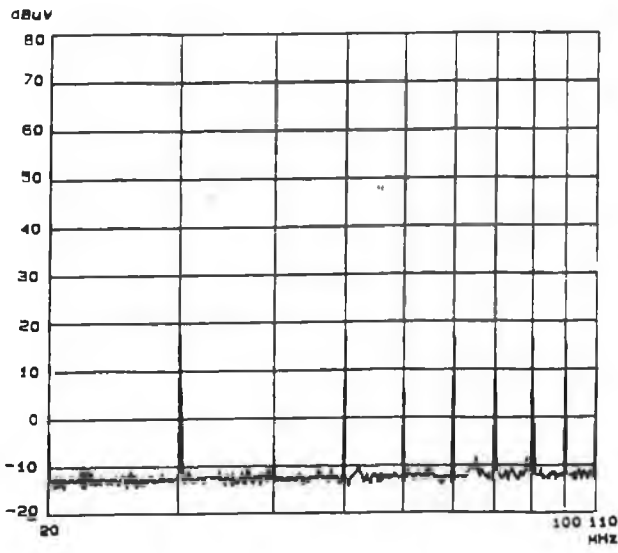
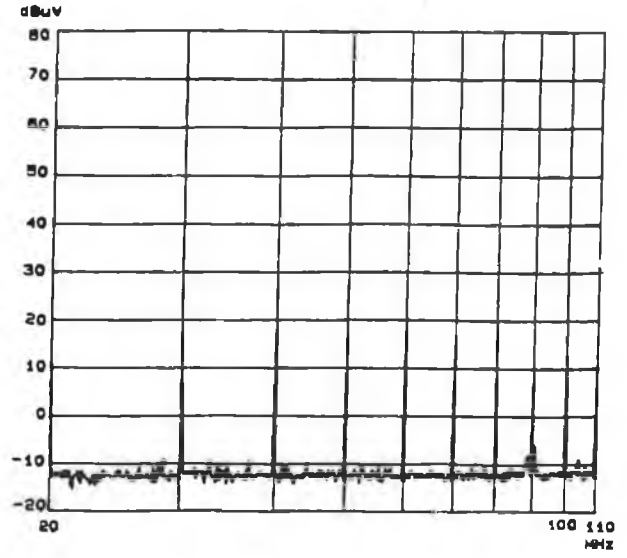


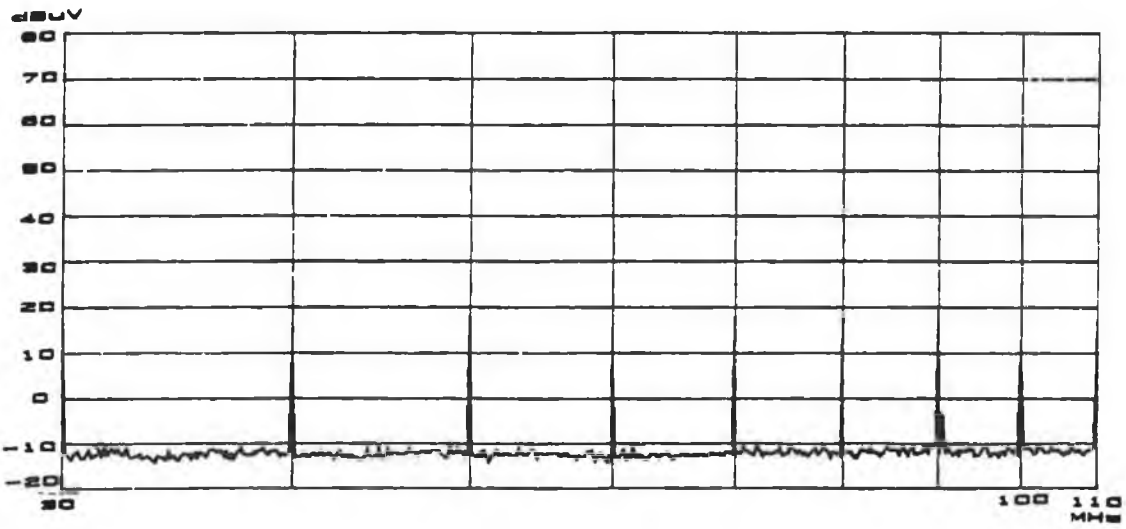
Fig. 7.10 Comparison between the predicted and measured electric field at a distance 0.05 m from config. #1 of circuit # 1. The 40 MHz crystal was used.



(a)

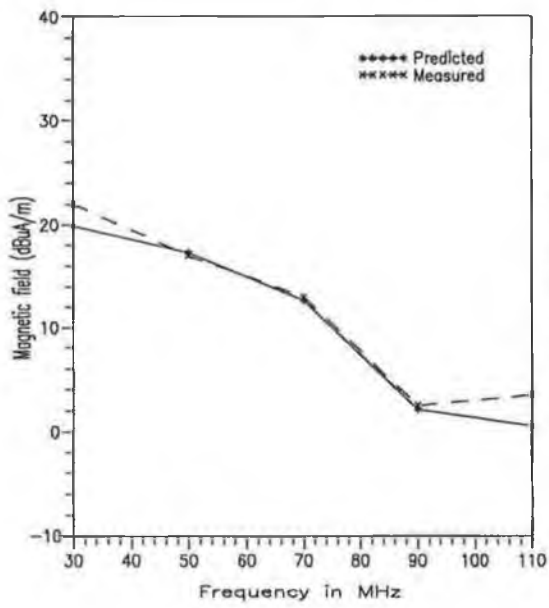


(b)

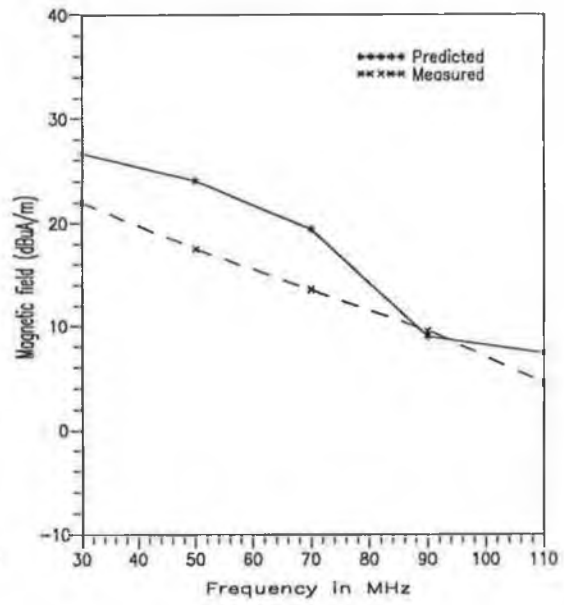


(c)

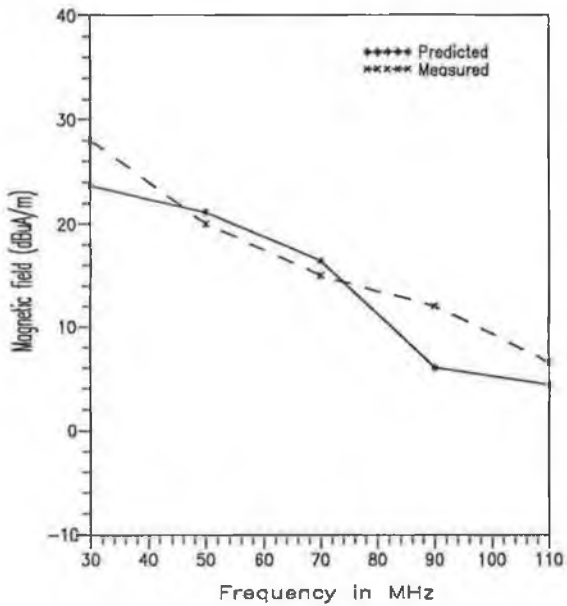
Fig. 7.11 Recorded magnetic field at a distance of 0.05 m (a) config. #1;
 (b) config. #2; (c) config. #3.



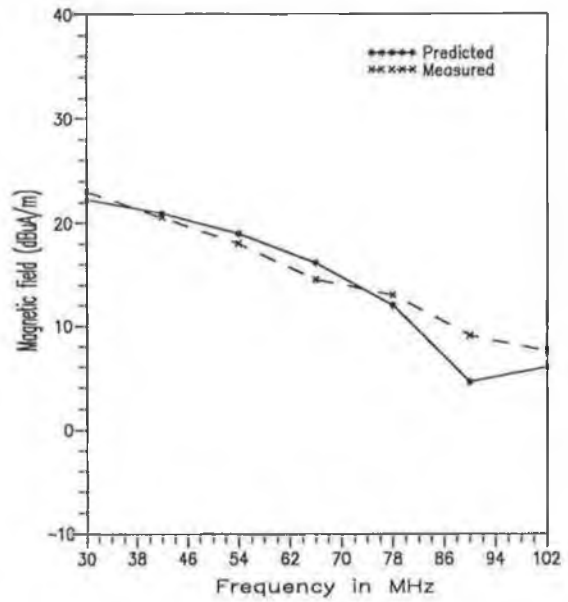
(a)



(b)



(c)



(d)

Fig. 7.12 Comparison between the predicted and the measured magnetic field: (a) config. #1; (b) config. #2; (c) config. #3; (d) config. #2, the 6 MHz crystal was used.

7.3.3.2 Circuit # 2

Measurement of the radiated electric field was carried out for circuit #2 in a manner similar to that described for circuit #1 in the previous section. A crystal oscillator of 24 MHz was used in this case. The measurement was repeated at $r = 0.05$ m. The recorded field strength is shown in Fig. 7.13. A plot of the measured electric field and the CAD predicted electric field as function of frequency is shown in Fig. 7.14. In all cases except at 48 MHz (the second harmonic of the 24 MHz crystal) the difference between the predicted value and the measured value was found to vary from ± 1 dB to ± 6 dB.

The radiated magnetic field measurement as described for circuit #1 was also carried out for circuit #2. The recorded field strength (probe PF is not included) is shown in Fig. 7.15. A plot of the measured value and the CAD predicted value is shown in Fig. 7.16. The plot exhibits a good agreement between the predicted value and the measured value of the magnetic field.

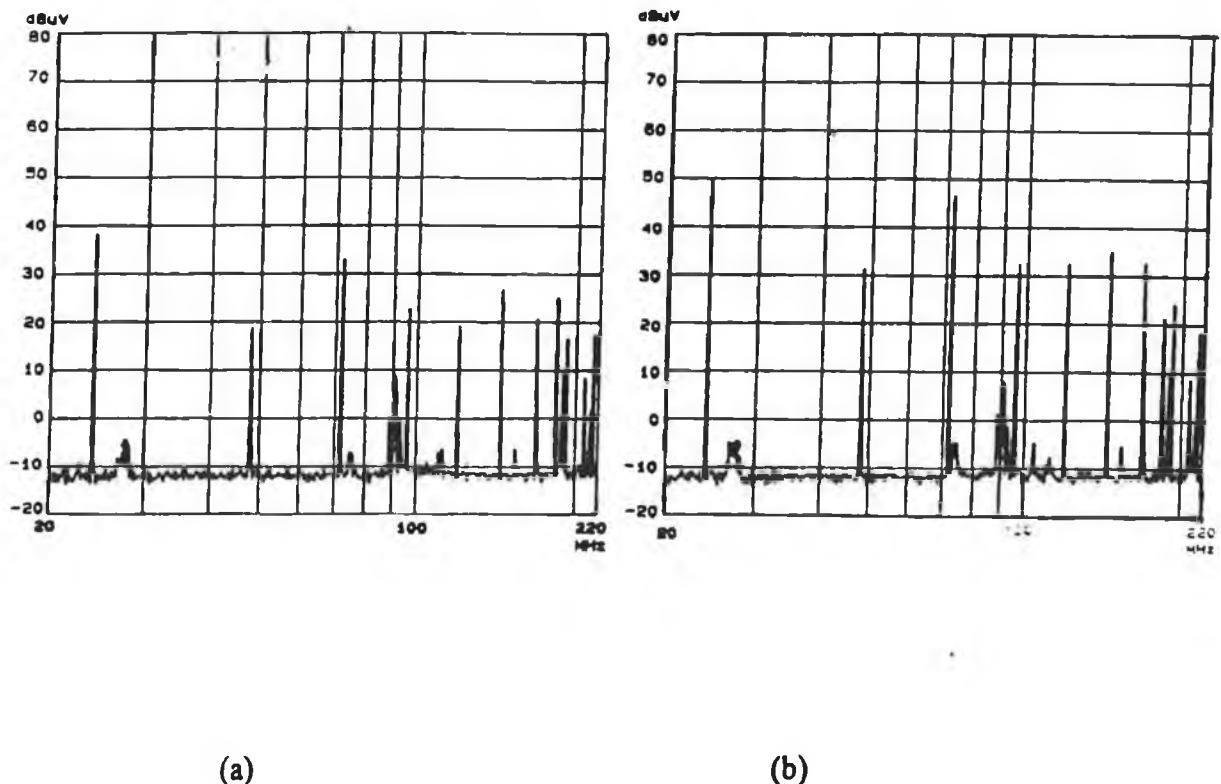
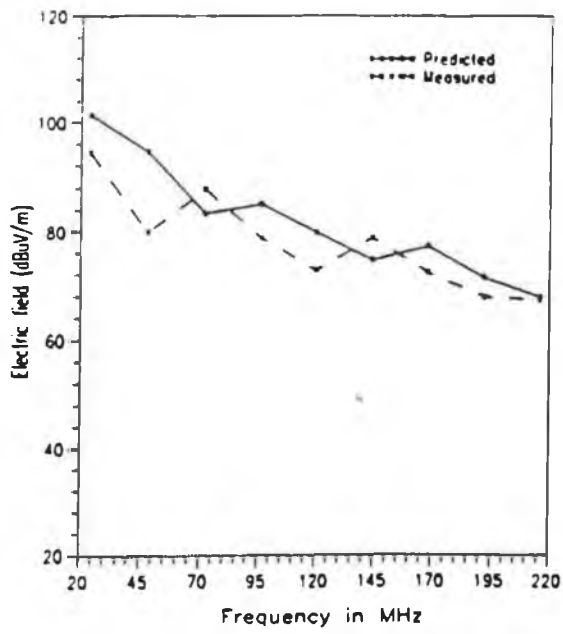
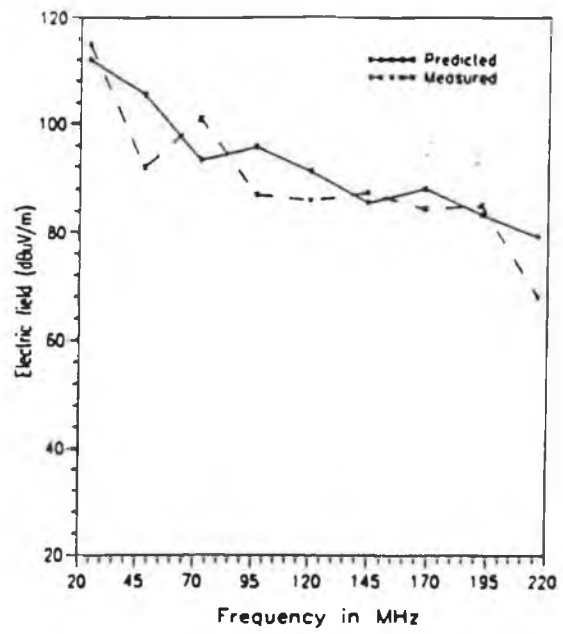


Fig. 7.13 Recorded electric field from circuit #2 at a distance of (a) 0.1 m; (b) 0.05 m.



(a)



(b)

Fig. 7.14 Comparison between the predicted and the measured electric field at a distance of: (a) 0.1 m; (b) 0.05 m.

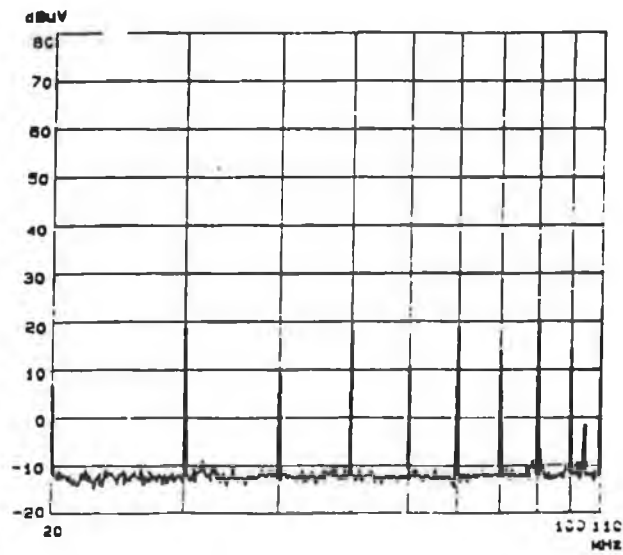


Fig. 7.15 Recorded magnetic field from circuit #2 at a distance of 0.05 m.

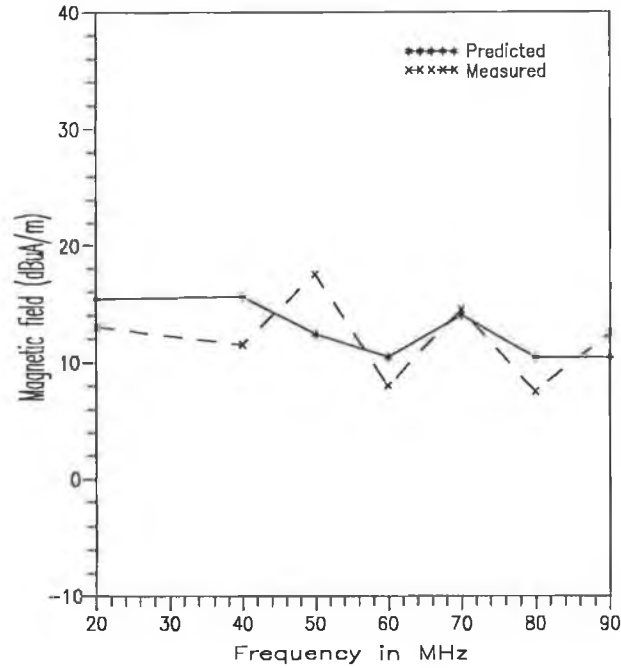
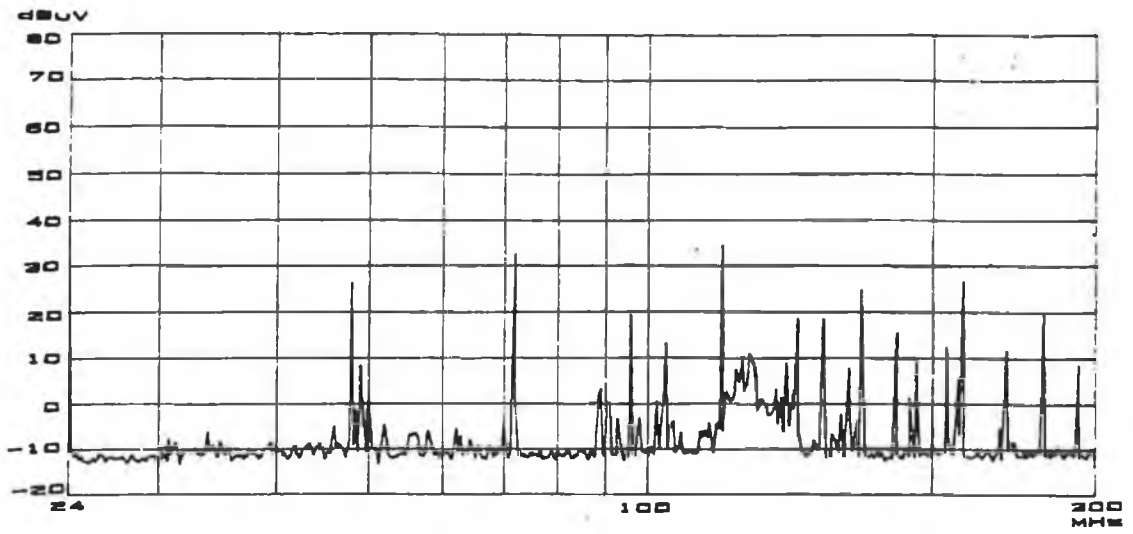


Fig. 7.16 Comparison between the predicted and the measured magnetic field.

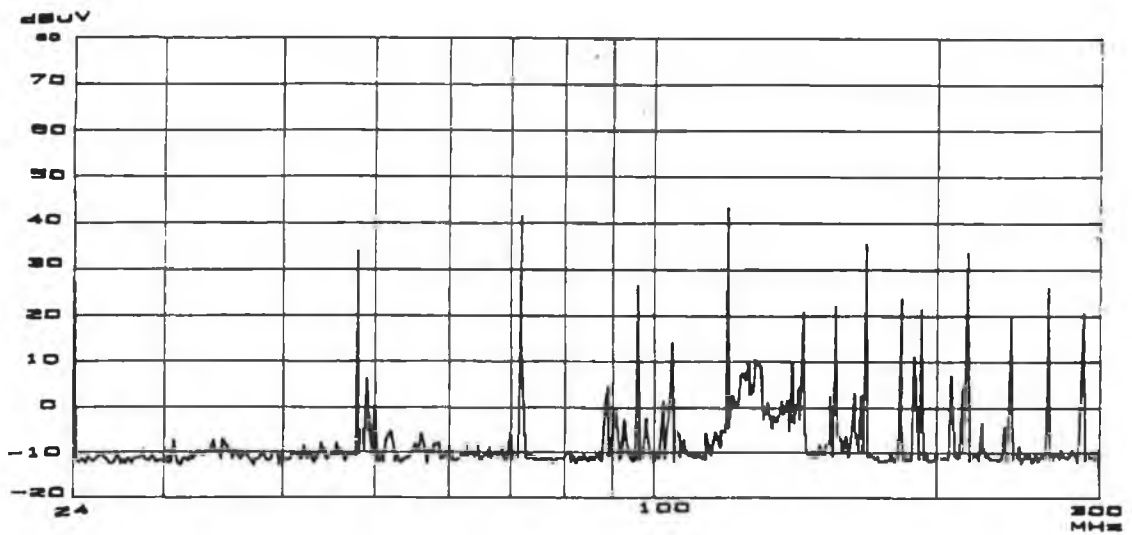
7.3.3.3 Circuit #3

The radiated electric field from circuit #3 was measured at $r = 0.05$ m, $\theta = 90^\circ$ and $\phi = 0^\circ$. A crystal oscillator of 24 MHz was used in this case. The recorded electric field strength (probe *PF* is not included) is shown in Fig. 7.17. The corrected field strength at the point of observation is obtained in a similar way to that mentioned earlier. A plot of the measured electric field and the composite CAD predicted field as a function of frequency corresponding to the first nine frequencies (fundamental and second through eighth harmonics of the pulse) is shown in Fig. 7.18.

The magnetic field measurement similar to the one mentioned for circuit #2 was also performed. The X-Y plotter output of the magnetic field strength is shown in Fig. 7.19. The measured magnetic field is compared with that obtained from the composite CAD package. A plot of the measured and composite CAD predicted magnetic field as a function of frequency is shown in Fig. 7.20. This comparison shows that the difference between the CAD predicted and the measured values is within 5 dB except at 40 MHz where the predicted value is about 8 dB higher than the measured value. This error may be due to the coupling between the PCB under test and the loop probe with its associated cabling. Furthermore

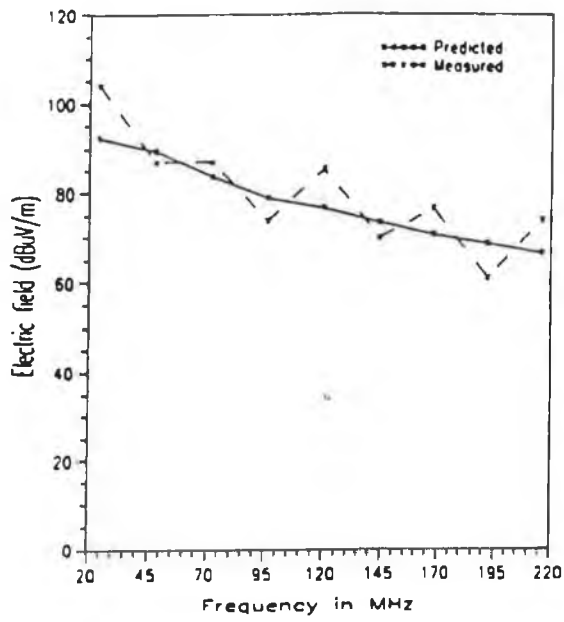


(a)

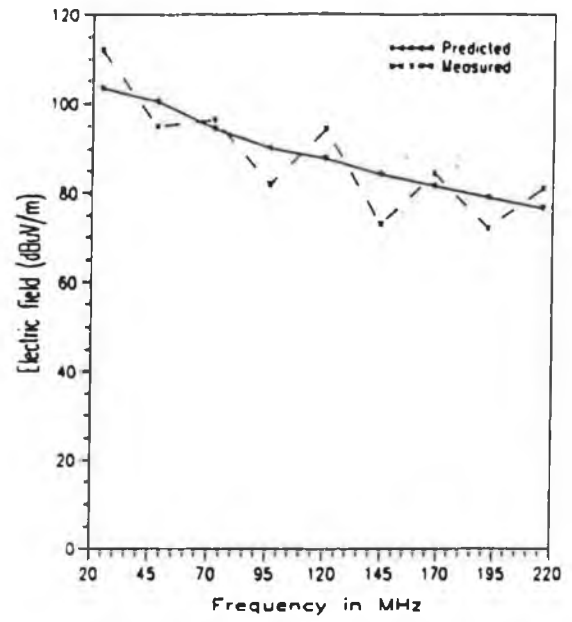


(b)

Fig. 7.17 Recorded electric field from circuit # 3 at a distance of (a) 0.10 m; (b) 0.05 m.



(a)



(b)

Fig. 7.18 Comparison between the predicted and measured electric fields at a distance of (a) 0.1 m; (b) 0.05 m.

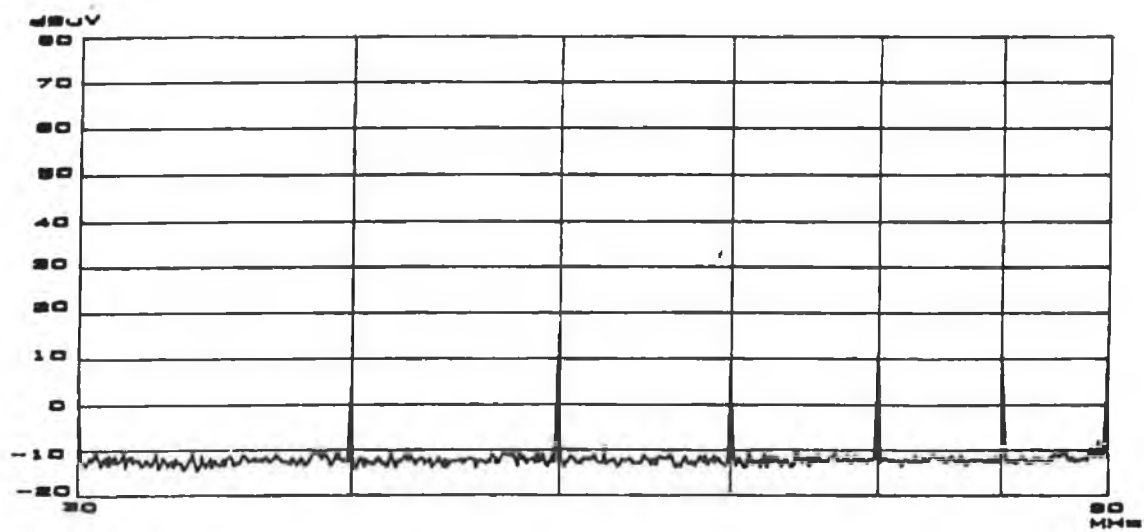


Fig. 7.19 Recorded magnetic field from circuit #3 at distance of 0.05 m.

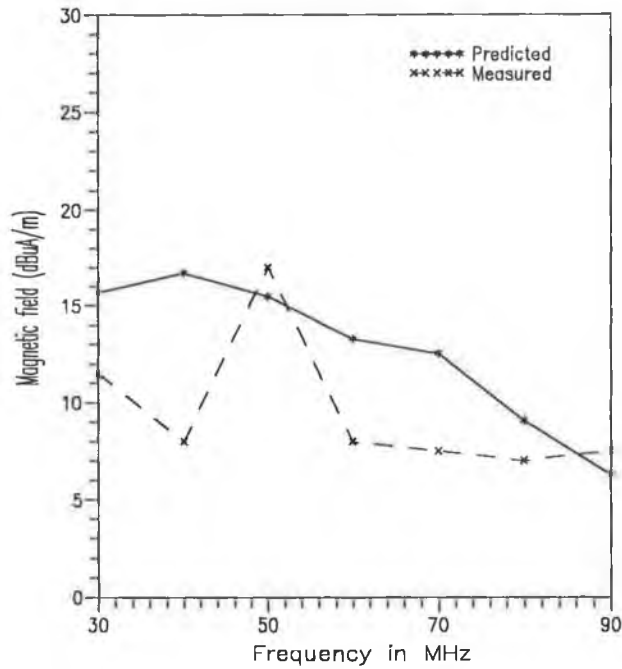


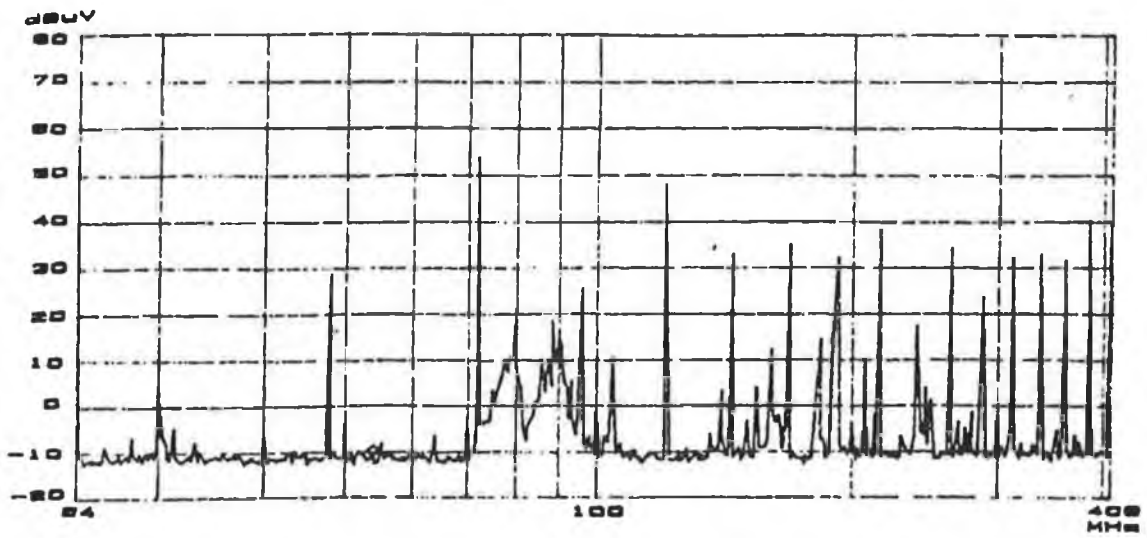
Fig. 7.20 Comparison between the predicted and the measured magnetic fields at a distance of 0.05 m.

the probe performance factor given by the manufacturer for a plane wave was used in determining the corrected field strength from spectrum analyser output. The measured field very near the test PCB (5 cm in this case) may not be a plane wave. However in most cases the measured values are lower than the predicted values.

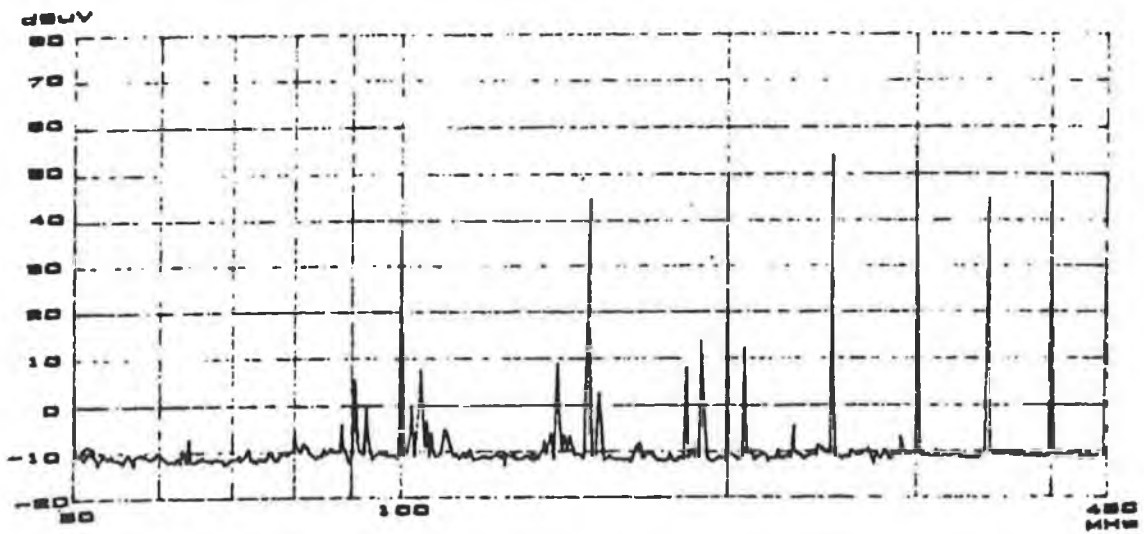
7.3.3.4 Comparison between TLM predicted and measured electric field

A simple PCB shown in Fig. 4.3 was considered for the test. The radiated electric field from the PCB was measured at $r = 0.05$ m, $\theta = 90^\circ$ and $\phi = 0^\circ$. The X-Y plotter output of the recorded field strength is shown in Fig. 7.21. The corrected field strength at the point of observation can be obtained using Eqn. 7.1.

The measured electric field was compared with that obtained from the extended TLM computation. A plot of the measured electric fields and the predicted fields as a function of frequency corresponding to odd harmonics of a pulse generated by a crystal oscillator is shown in Fig. 6.22. The plot shows a very good agreement between the extended TLM prediction and the measured value.



(a)



(b)

Fig. 7.21 Radiated electric field from circuit as shown in Fig. 4.3 at a distance of 0.05 m (a) 24 MHz crystal is used; (b) 50 MHz crystal is used.

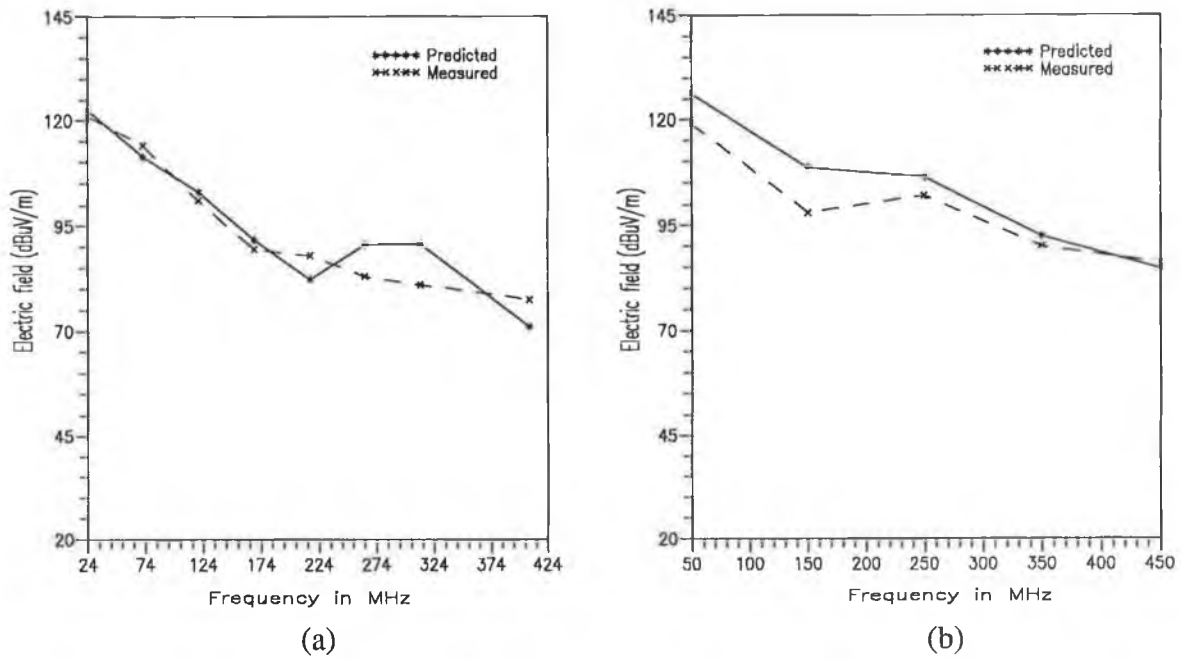


Fig. 7.22 Comparison between the extended TLM predicted electric field and the measured electric field (a) for 24 MHz crystal; (b) for 50 MHz crystal.

7.3.3.5 Determination of s/w ratio

Six samples of PCBs, each having two parallel tracks were made with different s/w ratios at constant w ($w = 0.48$ mm) for the test. The ratios were chosen arbitrarily as 1.1, 1.22, 1.5, 1.8, 3.5, and 5.0. One end of the two parallel tracks was terminated by a resistive load of 100Ω . The other end was connected to a RF signal generator through a 50Ω co-axial cable of length 0.75 m. A schematic diagram of the measurement set-up is shown in Fig. 7.23.

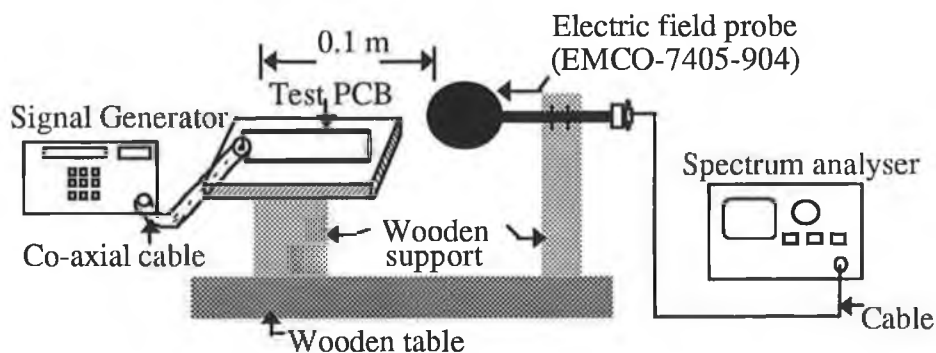


Fig. 7.23 A schematic diagram of the system used to measure radiated field in determining the optimum s/w ratio.

The generator was set to generate a signal of amplitude of 1 V at all frequencies. The test was performed at frequencies of 100 MHz, 150 MHz, and 200 MHz. The radiated electric field was measured at $r = 0.1$ m, $\theta = 90^\circ$ and $\phi = 0^\circ$. A best fit plot of the measured electric field as a function of s/w ratio is shown in Fig. 7.24. The plot shows that the optimum s/w ratio which could produce minimum radiation is about 1.5 to 1.8. This value is very close to the theoretical value (see section 6.4) of the s/w ratio.

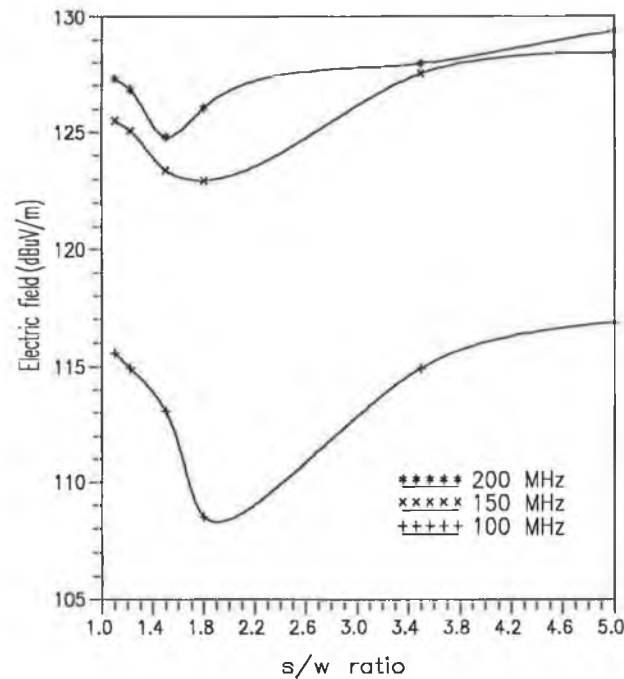


Fig. 7.24 A best fit plot of the radiated electric field as a function of s/w ratio.

7.3.3.6 Verification of shielding effect

Circuit #2 was chosen as a test circuit to verify the shielding techniques (described in section 5.5.2) in reducing the PCB radiation. The PCB was divided into eighteen rectangular sub-sections of equal size. At a particular section a shielding block was placed on both sides of the PCB. Section position was determined theoretically (described in section 5.5.2). Such a block was constructed by pasting thin aluminium tape on each side of an open ended rectangular box made of a paper. The size of the block depends on the section dimensions (i.e. length and width). The block and its position in the PCB are shown in Figs 7.25 (a) and 7.25 (b) respectively. The shielding effectiveness of the block is given in Appendix F3.

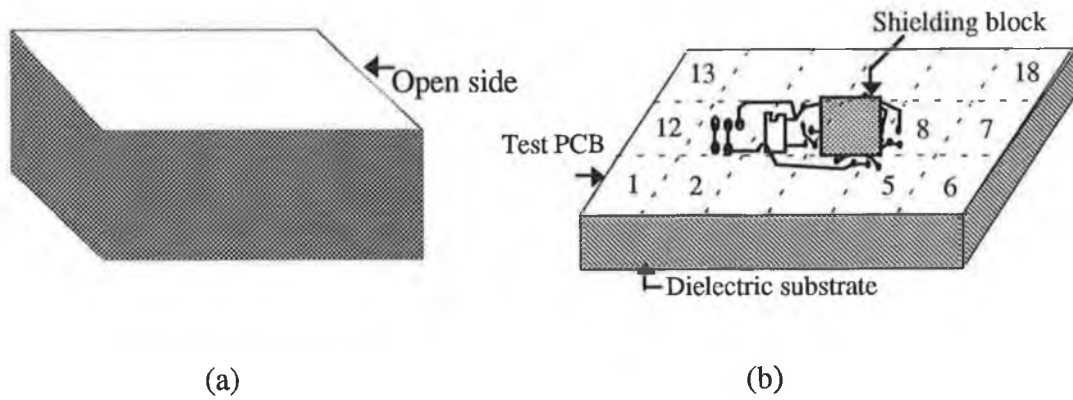


Fig. 7.25 Placement of a shielding block in a PCB (a) a box shaped shielding block having one side open; (b) position of the shielding block on top side of the PCB.

The radiated electric field was measured at $r = 0.05$ m, $\theta = 90^\circ$ and $\phi = 0^\circ$. A plot of the measured electric fields with and without the shielding block is shown in Fig. 7.26. The plot shows that in all cases the electric field with the shielding is less than that of without shielding. The maximum difference between the electric fields with and without shielding is about 6 dB.

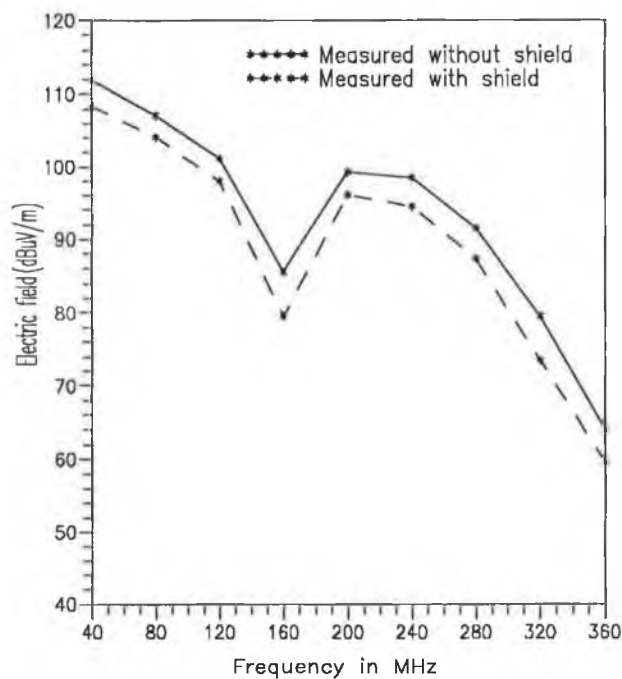


Fig. 7.26 A comparison between the measured electric fields with and without shielding.

7.4 EMISSION MEASUREMENT IN A SHIELDED ROOM

Measurement of the EM radiation from a PCB was performed at 1 m distance in the shielded room of the EMC laboratory at FORBAIRT¹ (formerly EOLAS), Dublin. The room is 2.35 m long, 2.35 m wide and 2.25 m high. The room dimensions and the measurement set-up in the shielded room are shown in Fig. 6.27.

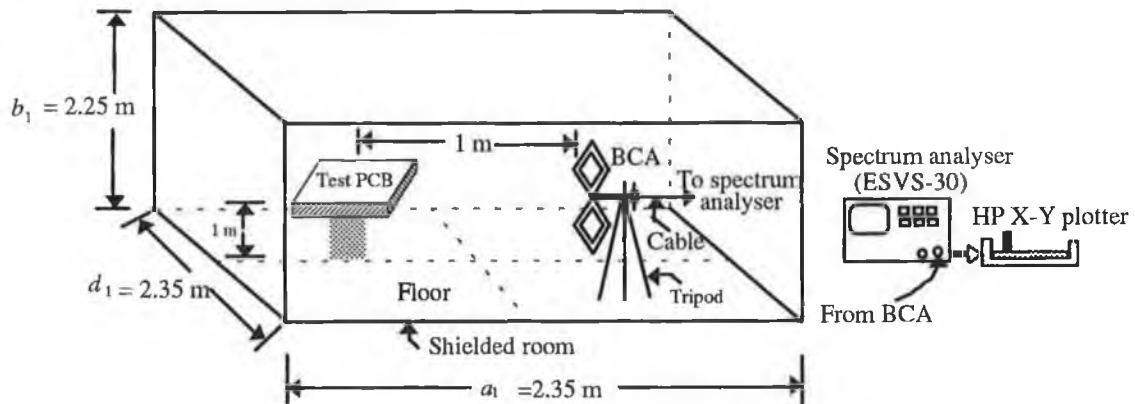


Fig. 7.27 A schematic of measurement set-up in a shielded room. Dimensions shown in the diagram are not in scale.

Generally a shielded room is intended to prevent external EM signal from contaminating the emission measurement. However the room resonance and multiple reflections from the room walls could result in measurement error as stated in section 2.7.2.2. The resonant frequencies of the room can be calculated from the room dimensions [107] using Eqn. 7.3.

$$f_{mnp} = \frac{1}{2\sqrt{\mu\epsilon}} \sqrt{\left(\frac{m}{a_1}\right)^2 + \left(\frac{n}{b_1}\right)^2 + \left(\frac{p}{d_1}\right)^2} \quad (7.3)$$

Where a_1 , b_1 and d_1 are the room dimensions, and m , n and p are positive integers.

¹The Irish Science and Technology Agency.

The resonance frequency of the shielded room is given in Table TF1 of Appendix F. The frequency response of the room was measured by exciting the room with a biconical antenna (a source) which was fed by a tracking generator over the swept frequency range of 30 to 200 MHz. The room response was recorded through another BCA (a receiving antenna). The frequency response of the empty room is shown in Fig. 7.28. The plot exhibits a number of resonances in the room. In some cases the calculated resonant frequencies differ from the measured frequencies. This difference may be due to the field perturbation by the antennas, coupling between the antennas and room walls, metallic tripod for masting the antenna, and imperfections in the screened room (e.g. internal walls are not smooth but have metal supports at intervals which will perturb the fields).

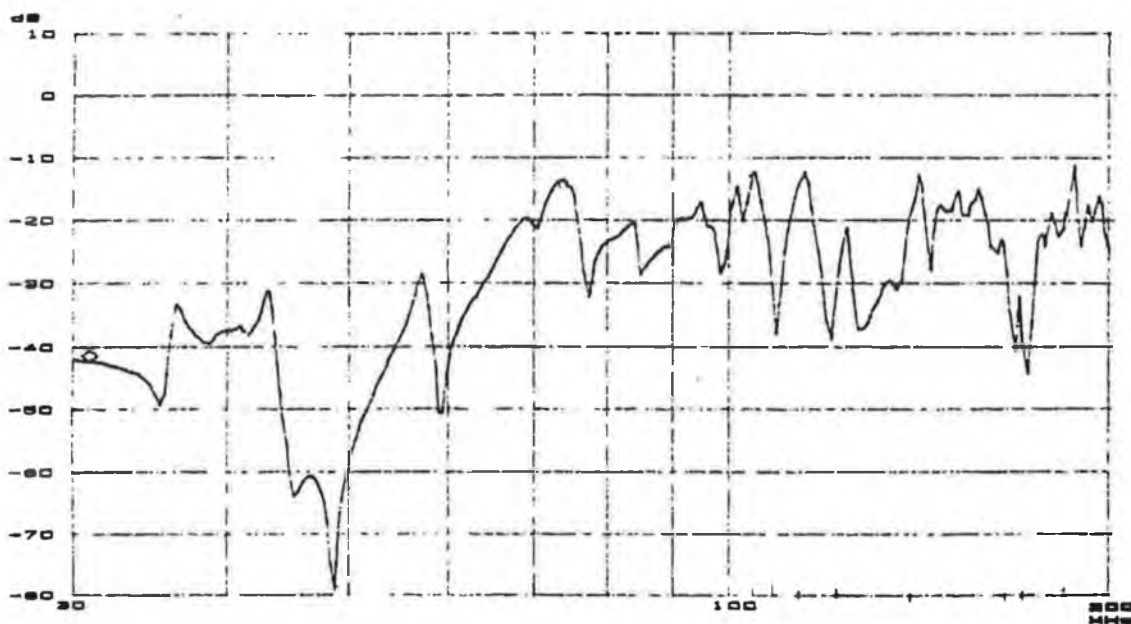


Fig. 7.28 Frequency response of the room.

This measurement error due to room resonance can be avoided by performing the measurement in an anechoic chamber. However the absorbing material of the anechoic chamber limits the emission measurement at low frequency as stated in section 2.7.2.6. Therefore an approach proposed by Dawson [59] for emission measurement in a shielded room at frequency below 200 MHz was attempted in this work. Dawson showed that the variation in the amplitude of the output voltage of the receiving antenna can be reduced from

± 40 dB to ± 10 dB by damping the room resonance. This can be done by reducing the Q of the resonance.

The Q of the resonance in a room is defined [59] as

$$Q = 2\pi \frac{U}{W_i} \quad (7.4)$$

Where, U is the average power stored in the room and W_i is the power dissipated in the room.

The Q can be reduced by increasing the power dissipation in the room. The power dissipation in the room can be increased by placing an EM field absorber at the position of field maximum (electric field absorber at the position of maximum electric field or a magnetic field absorber at the position of maximum magnetic field).

7.4.1 DETERMINATION OF POSITION OF FIELD MAXIMA

A shielded room can be treated as a resonant cavity which is similar to a waveguide terminated with a perfect conductor at both ends. The wave induced into the cavity will be reflected backwards and forwards establishing a standing wave pattern. As a result the propagating mode of the wave will be either transverse electric (TE) with no electric field in the direction of propagation or transverse magnetic (TM) with no magnetic field in the direction of propagation. The field distribution within the cavity can be obtained from the solution of Maxwell's equation with the boundary conditions (i.e. (i) the tangential component of electric fields to the walls will be zero and (ii) normal components of the magnetic field will be zero).

The fields within the cavity depend on the type and orientation of the field source. In this work, the field source is a piece of electronic equipment which radiates EM fields in the three orthogonal directions and the type of the radiated field is unknown. Therefore it was assumed that TE (or TM) modes of waves propagate in the three orthogonal directions (x,y,z) as shown in Fig. 7.29. The resultant field components in the room for TE (or TM) wave can be obtained from the vector addition of the individual field components in each direction.

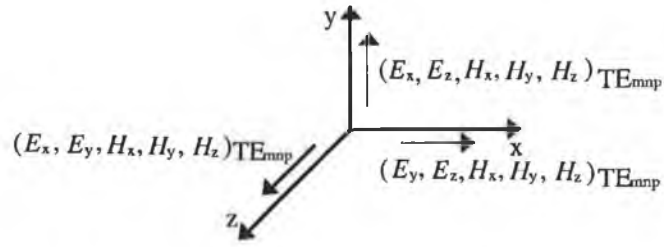


Fig. 7.29 The TE waves propagating in the three orthogonal directions and field components for each TE wave in each direction.

The expressions for the fields in the room for TE modes propagating in three orthogonal directions are given as (development of these expressions is given in Appendix F4):

$$E_x = j\omega\mu \sqrt{\frac{8}{a_1 b_1 d_1 \mu}} F_1' \cos\left(\frac{m\pi x}{a_1}\right) \sin\left(\frac{n\pi y}{b_1}\right) \sin\left(\frac{p\pi z}{d_1}\right) \quad (7.5)$$

$$E_y = j\omega\mu \sqrt{\frac{8}{a_1 b_1 d_1 \mu}} F_2' \sin\left(\frac{m\pi x}{a_1}\right) \cos\left(\frac{n\pi y}{b_1}\right) \sin\left(\frac{p\pi z}{d_1}\right) \quad (7.6)$$

$$E_z = j\omega\mu \sqrt{\frac{8}{a_1 b_1 d_1 \mu}} F_3' \sin\left(\frac{m\pi x}{a_1}\right) \sin\left(\frac{n\pi y}{b_1}\right) \cos\left(\frac{p\pi z}{d_1}\right) \quad (7.7)$$

$$H_x = \sqrt{\frac{8}{a_1 b_1 d_1 \mu}} F_4' \sin\left(\frac{m\pi x}{a_1}\right) \cos\left(\frac{n\pi y}{b_1}\right) \cos\left(\frac{p\pi z}{d_1}\right) \quad (7.8)$$

$$H_y = \sqrt{\frac{8}{a_1 b_1 d_1 \mu}} F_5' \cos\left(\frac{m\pi x}{a_1}\right) \sin\left(\frac{n\pi y}{b_1}\right) \cos\left(\frac{p\pi z}{d_1}\right) \quad (7.9)$$

$$H_z = \sqrt{\frac{8}{a_1 b_1 d_1 \mu}} F_6' \cos\left(\frac{m\pi x}{a_1}\right) \cos\left(\frac{n\pi y}{b_1}\right) \sin\left(\frac{p\pi z}{d_1}\right) \quad (7.10)$$

where F_1' , F_2' , F_3' , F_4' , F_5' and F_6' are functions of m , n , p and room dimensions and are given in Appendix F4.

Similarly the fields in the cavity for TM wave propagating in three orthogonal directions can be expressed as follows

$$E_x = \sqrt{\frac{8}{a_1 b_1 d_1 \epsilon}} G_1 \cos\left(\frac{m\pi x}{a_1}\right) \sin\left(\frac{n\pi y}{b_1}\right) \sin\left(\frac{p\pi z}{d_1}\right) \quad (7.11)$$

$$E_y = \sqrt{\frac{8}{a_1 b_1 d_1 \epsilon}} G_2 \sin\left(\frac{m\pi x}{a_1}\right) \cos\left(\frac{n\pi y}{b_1}\right) \sin\left(\frac{p\pi z}{d_1}\right) \quad (7.12)$$

$$E_z = \sqrt{\frac{8}{a_1 b_1 d_1 \epsilon}} G_3 \sin\left(\frac{m\pi x}{a_1}\right) \sin\left(\frac{n\pi y}{b_1}\right) \cos\left(\frac{p\pi z}{d_1}\right) \quad (7.13)$$

$$H_x = j\omega\epsilon \sqrt{\frac{8}{a_1 b_1 d_1 \epsilon}} G_4 \sin\left(\frac{m\pi x}{a_1}\right) \cos\left(\frac{n\pi y}{b_1}\right) \cos\left(\frac{p\pi z}{d_1}\right) \quad (7.14)$$

$$H_y = j\omega\epsilon \sqrt{\frac{8}{a_1 b_1 d_1 \epsilon}} G_5 \cos\left(\frac{m\pi x}{a_1}\right) \sin\left(\frac{n\pi y}{b_1}\right) \cos\left(\frac{p\pi z}{d_1}\right) \quad (7.15)$$

$$H_z = j\omega\epsilon \sqrt{\frac{8}{a_1 b_1 d_1 \epsilon}} G_6 \cos\left(\frac{m\pi x}{a_1}\right) \cos\left(\frac{n\pi y}{b_1}\right) \sin\left(\frac{p\pi z}{d_1}\right) \quad (7.16)$$

where G_1, G_2, G_3, G_4, G_5 and G_6 are functions of m, n, p and room dimensions and are given in Appendix F5.

The positions of the electric and magnetic field maxima for an empty room can be determined from the above expressions (Eqns. 7.5 to 7.16). The expressions clearly exhibit that the analytic determination of the position of field maxima is not possible. Therefore a numerical technique has been used. The Downhill Simplex method (refer to Appendix F6) for finding the minimum or maximum of a function of more than one independent variable was employed to find the field maximum point in the room. The computer programme listing of this method is given in Appendix F7.

The positions of the electric field maximum on the floor of the room for the first 32 (TE and TM) modes are shown in Fig. 7.30. The position of the magnetic field maximum for the first 32 (TE and TM) modes, on the walls are shown in Fig. 7.31.

A commercially available multilayer absorber (carbon loaded foam sheet) ECCOSORB® AN 79 was used to absorb energy from the electric field. The performance of this absorber is given in Appendix F8.

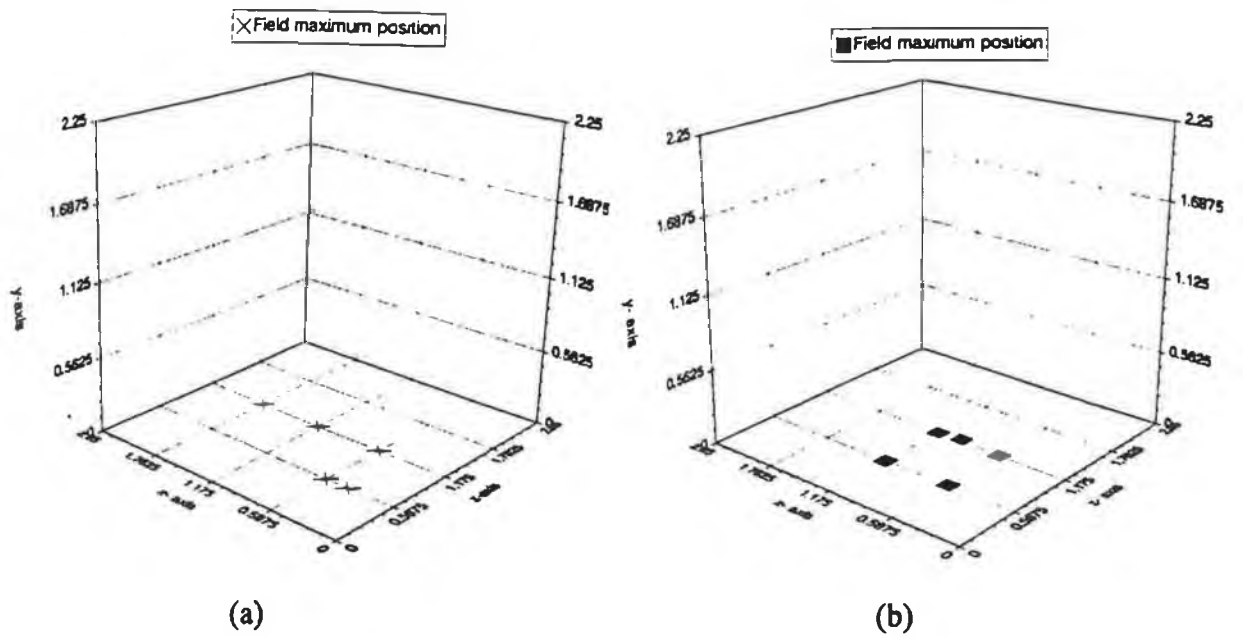


Fig. 7.30 Position of E-field maxima on the floor for the first 32: (a) TE modes; (b) TM modes.

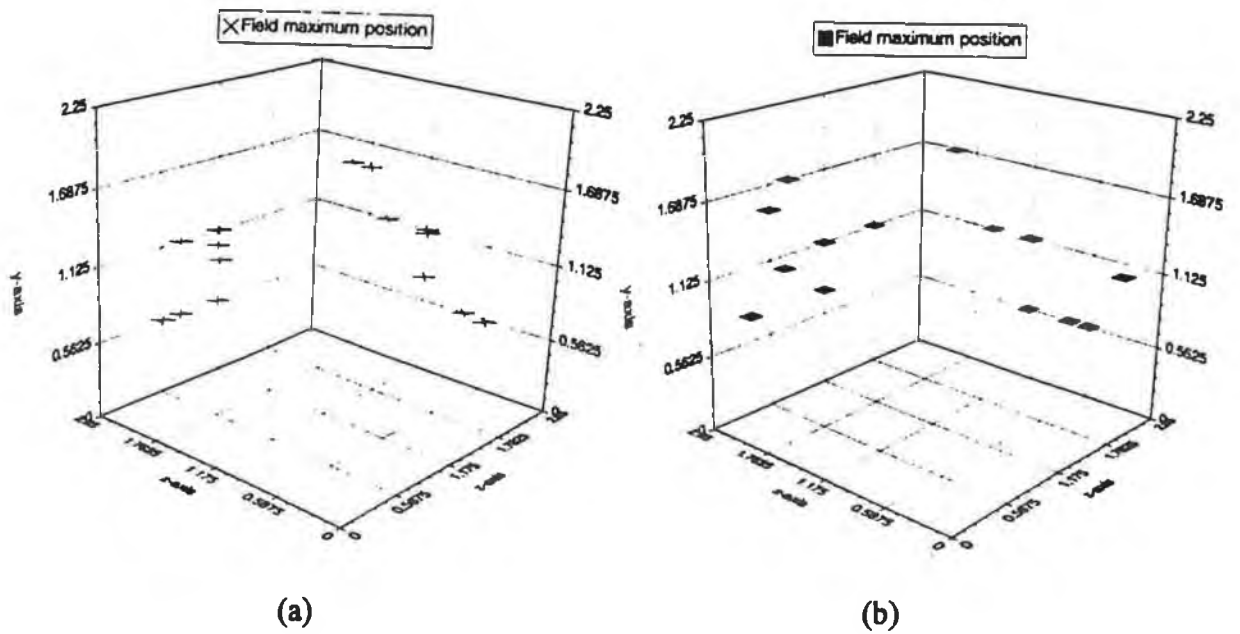


Fig. 6.31 Position of H-field maxima on the wall for the first 32: (a) TE modes; (b) TM modes.

Ferrite tiles (BOAM® BE-15) were used to absorb the energy from the magnetic field. The absorption characteristics of the ferrite tile over the frequency range 30 to 1000 MHz is given in Appendix F9.

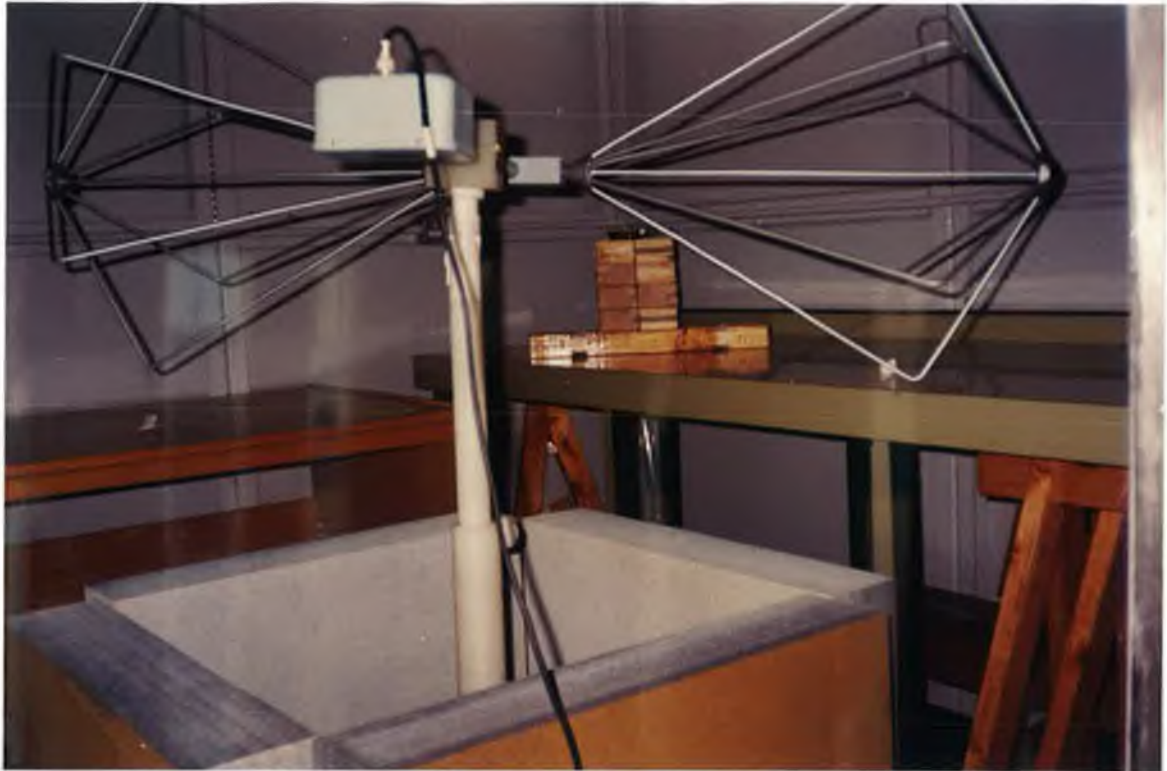
7.4.2 MEASUREMENT OF RADIATED ELECTRIC FIELD IN A LOADED ROOM

Radiated electric fields from PCBs were measured by a horizontally polarised dipole antenna. Two sets of measurement were taken. In the first measurement, the room was loaded with the electric field absorber (ECCOSORB® AN 79) which was placed on the floor. In the second case the room was loaded with the ferrite tile which was placed on the walls. The photographs of the measurement set-up are shown in Fig. 7.32.

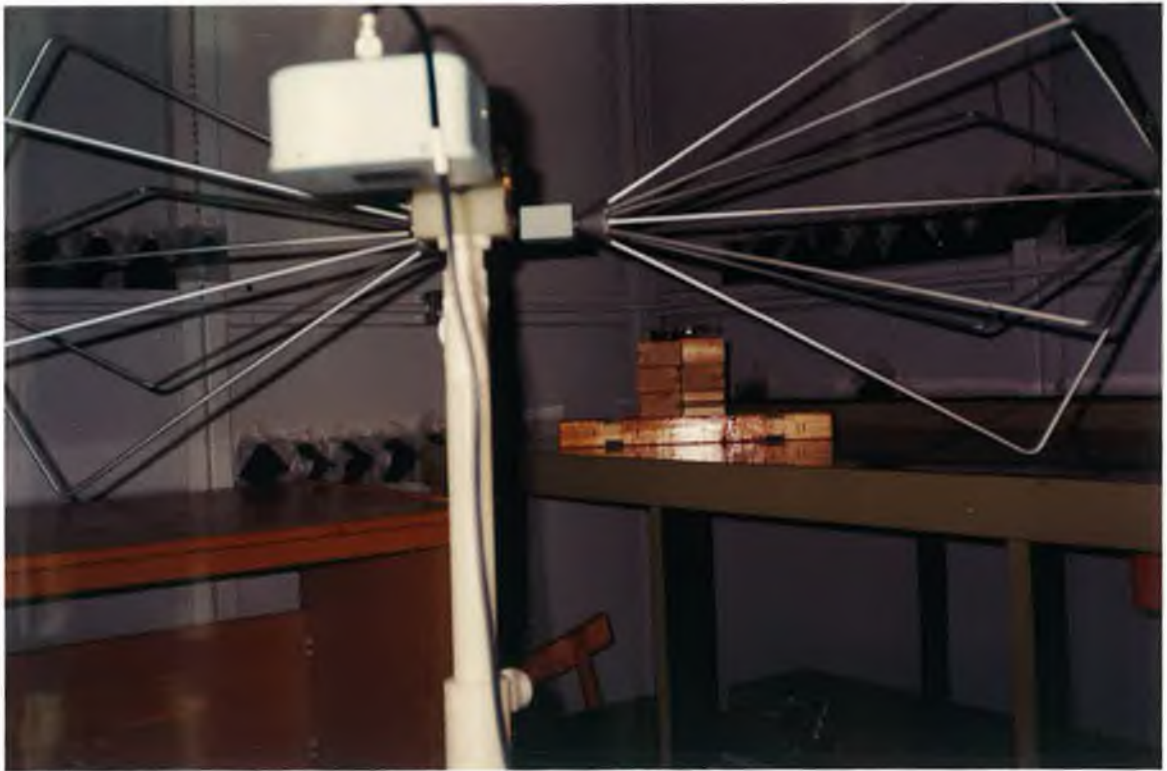
7.4.2.1 Room with electric field absorber

The electric field maxima on the floor shows that a box shape block of absorber can cover most of the field maximum points. Four absorber sheets (ECCOSORB® AN 79) were used to construct such a box. The sheet was 0.610 m long, 0.610 m width and 0.110 m deep. Thus the box can cover nearly one sixteenth of the room floor area, with one corner in the centre of the room and the sides of the box parallel to the walls of the room.

The radiated electric fields from sample PCBs (config. #3 of circuit #1, circuit #2 and circuit #3) were measured through a horizontally polarised BCA at frequencies below 200 MHz. Two sets of measurements were made. In the first case the radiated electric fields were measured without any loading in the room and in the second case the room was loaded with the electric field absorber as described at the beginning of this subsection. Figs. 7.33 and 7.34 show the X-Y plotter output where the radiated electric field (excluding the antenna factor and cable loss) is plotted as function of frequency corresponding to the harmonics of the pulse generated by a 24 MHz crystal oscillator. The radiated electric field from config. #3 of circuit #1 was measured at frequencies above 200 MHz using the horizontally polarised LPA. The X-Y plotter output is shown in Fig. 7.35.

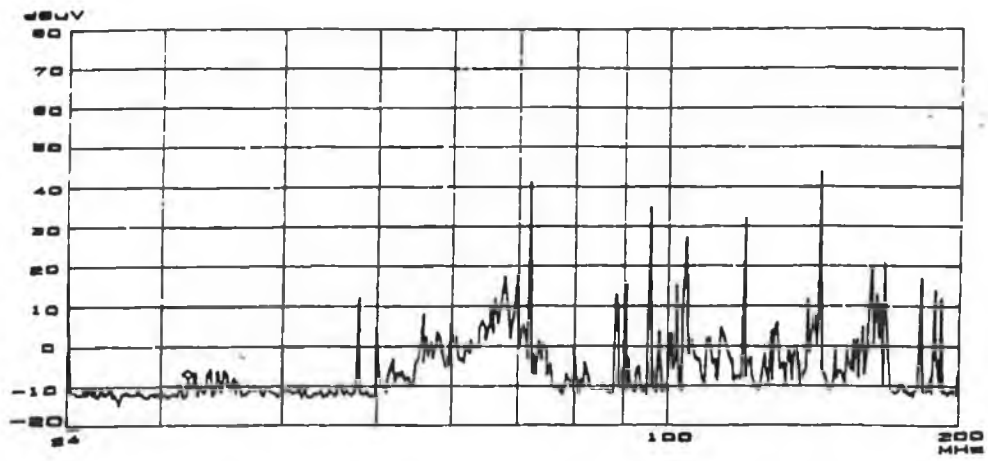


(a)

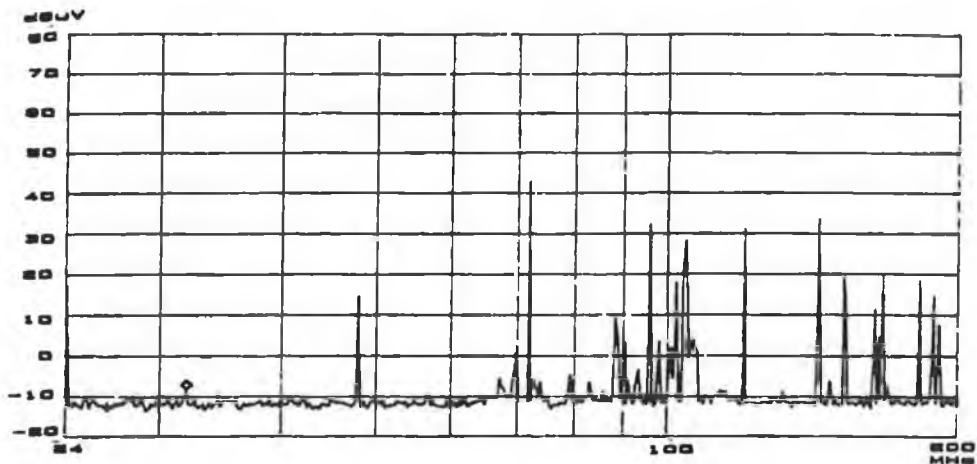


(b)

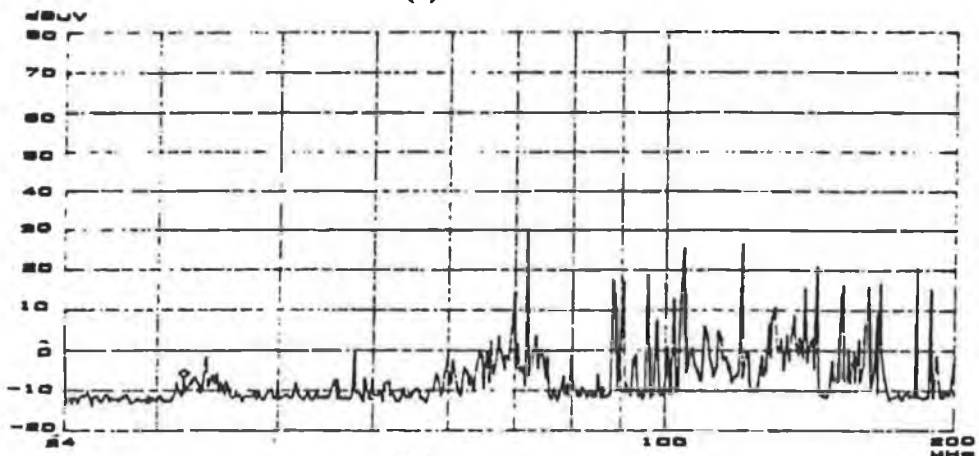
Fig. 7.32 Photographs of the measurement set-up in a shielded room loaded with (a) ECCOSORB®AN 79; (b) BOAM® BE 15.



(a)

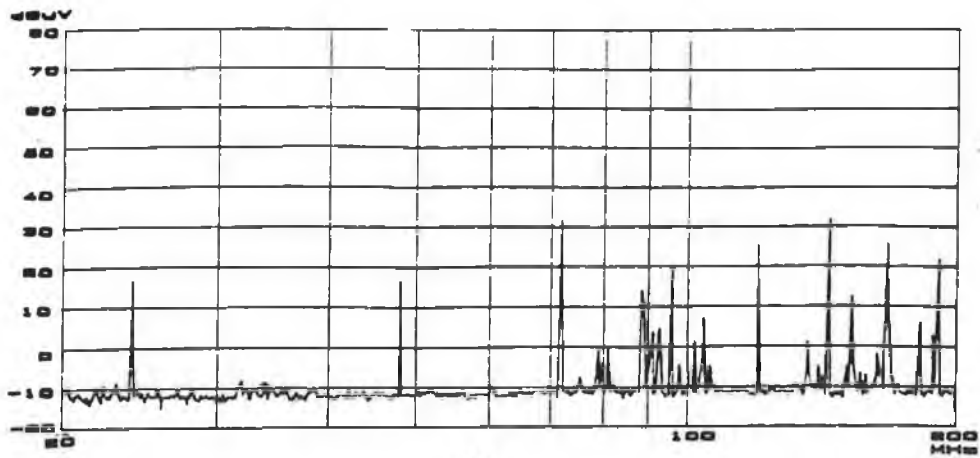


(b)

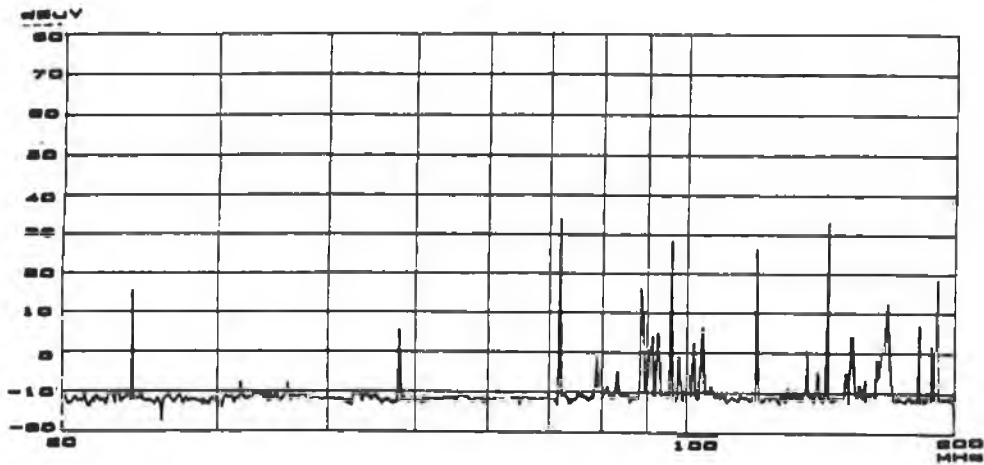


(c)

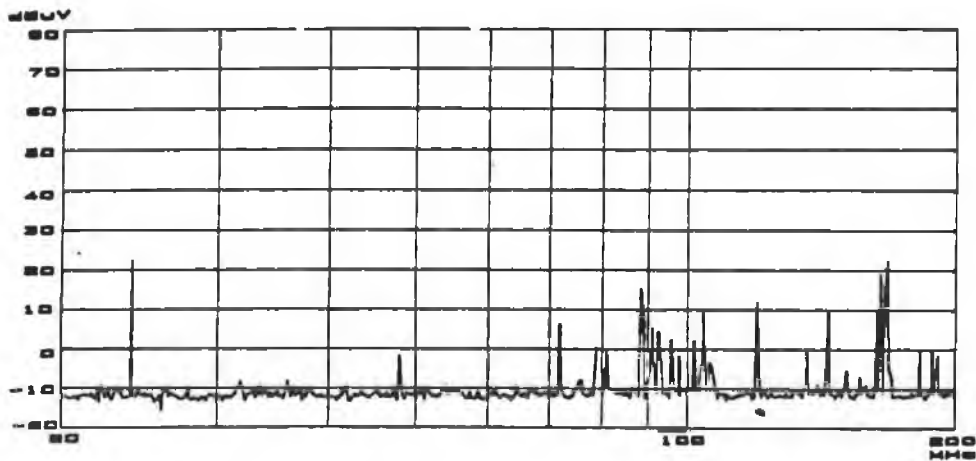
Fig. 7.33 Recorded electric field strength through BCA from the test circuit at 1 m distance in a shielded room without any absorber (a) circuit #1; (b) circuit #2; (c) circuit #3.



(a)



(b)



(c)

Fig. 7.34 Recorded electric field strength from the test circuit through BCA at 1 m distance in a shielded room with ECCOSORB®AN 79 (a) circuit #1; (b) circuit #2; (c) circuit #3.

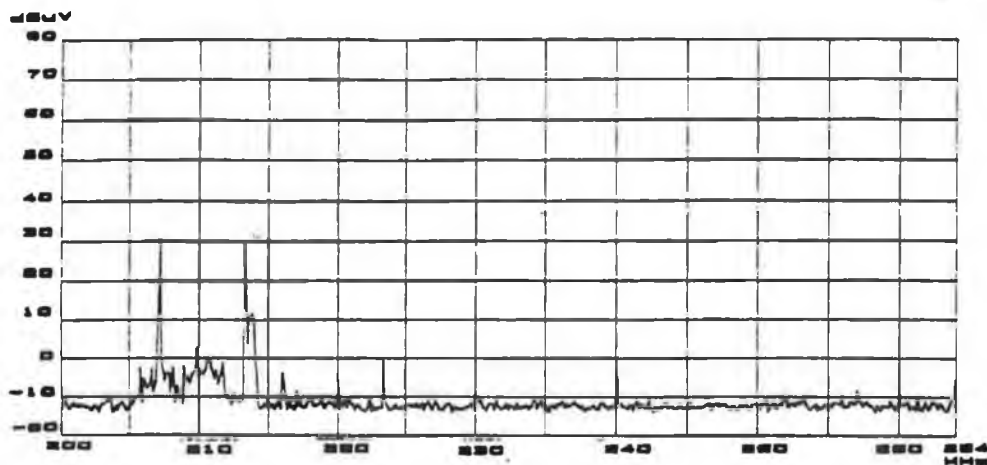
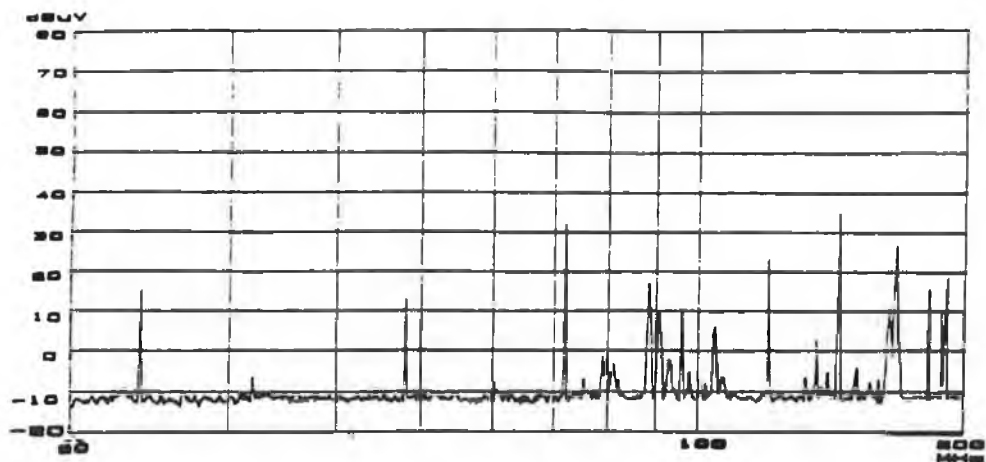


Fig. 7.35 Recorded electric field from circuit #1 through LPA at 1 m distance in a shielded room without any absorber.

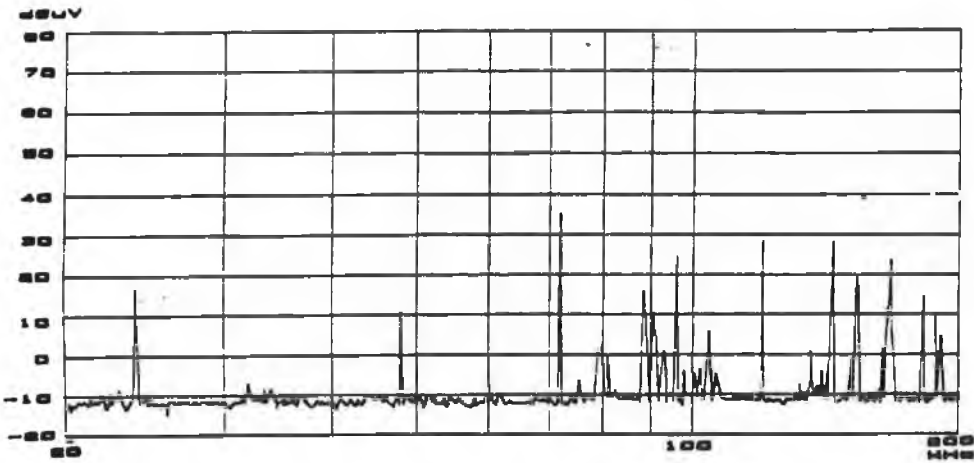
7.4.2.2 Room loaded with ferrite tile

The ECCOSORB® AN 79 is bulky and must be placed in the position of electric field maxima which indicates that the absorber is in the middle of the room. This creates problems when setting a test set-up especially in such a small room. On the other hand the position of the maximum magnetic field in the room are parallel and adjacent to the room walls. This means that magnetic field absorbers can be placed on the walls where these do not get in the way. The field perturbation due to the absorber will also be less as the reflective surface is close to the walls. Thus the position at which the initial waves are reflected is not moved significantly [59]. The tile was placed on the wall by masking tape shown in Fig. 7.32 (b).

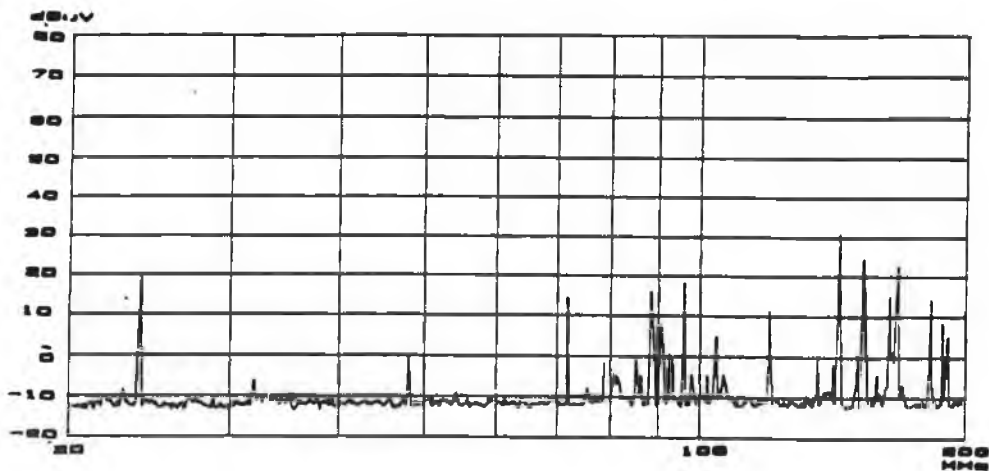
The radiated electric field measurement similar to the one mentioned in the previous subsection was performed through a horizontally polarised BCA. The recorded field strength is shown in Fig. 7.36. The measurement was also repeated for circuit #1 and circuit #3. In this case a crystal oscillator of 10 MHz was used as a source of the test circuits. The recorded field strength as a function of frequency is shown in Fig. 7.37.



(a)

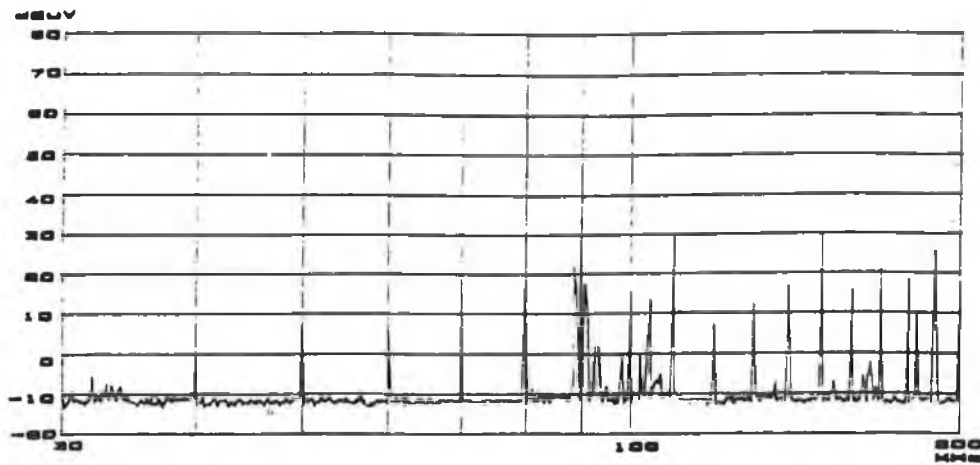


(b)

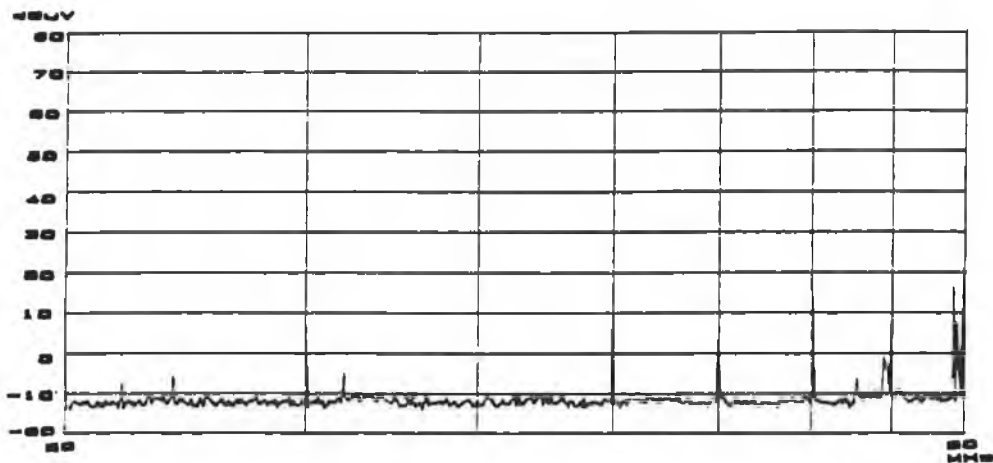


(c)

Fig. 7.36 The recorded radiated electric field from the test circuit through BCA at 1 m distance in a shielded room loaded with the BOAM® BE 15 (a) circuit #1; (b) circuit #2; (c) circuit #3.



(a)



(b)

Fig. 7.37 The recorded radiated electric field from the test circuit at 1 m distance in a shielded room loaded with the BOAM®BE 15 (a) circuit #1; (b) circuit #3. A 10 MHz crystal was used as a source of the test circuit.

7.4.2.3 Comparison between the measured and predicted field

The corrected field strength at the point of observation is obtained using Eqn. 7.1. The antenna factor (i.e. PF) at a specified frequency for the BCA and LPA can be found from Figs. F2-1 and F2-2 respectively in Appendix F. The cable loss was found from the recorded output of the tracking generator over the swept frequency range of 50 to 200 MHz as shown in Fig. 6.38. The amplitude of the signal which was generated by a tracking generator was normalised to 0 dB. Therefore the cable loss is found to be 1 dB from Fig. 7.38. Below 50 MHz, the cable loss was found to be very negligible (nearly 0 dB, not shown in Fig. 7.38).

The plots of the predicted electric fields and the measured fields are shown in Figs. 7.39 (in the case of 24 MHz crystal) and 7.40 (in the case of 10 MHz). The difference

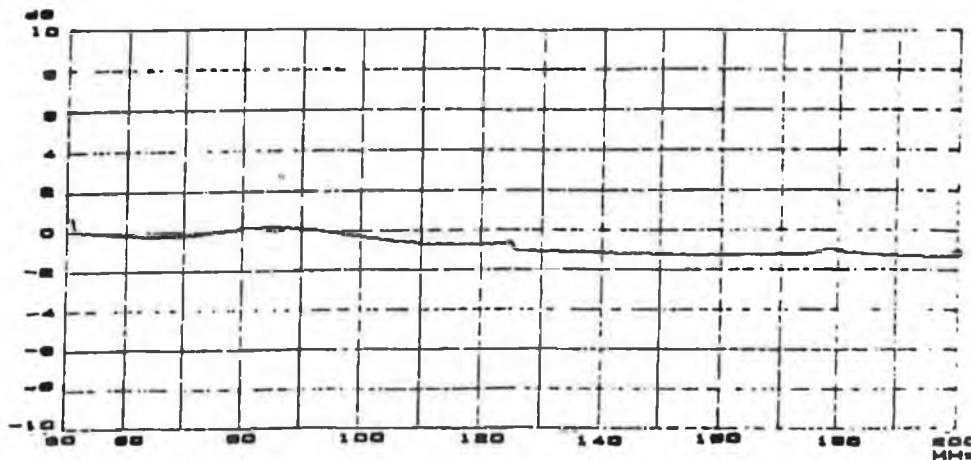
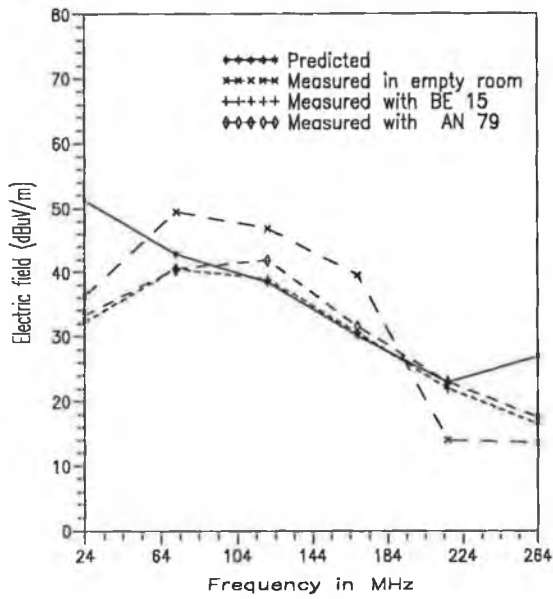


Fig. 7.38 A tracking generator output. Amplitude of the signal was normalised to 0 dB.

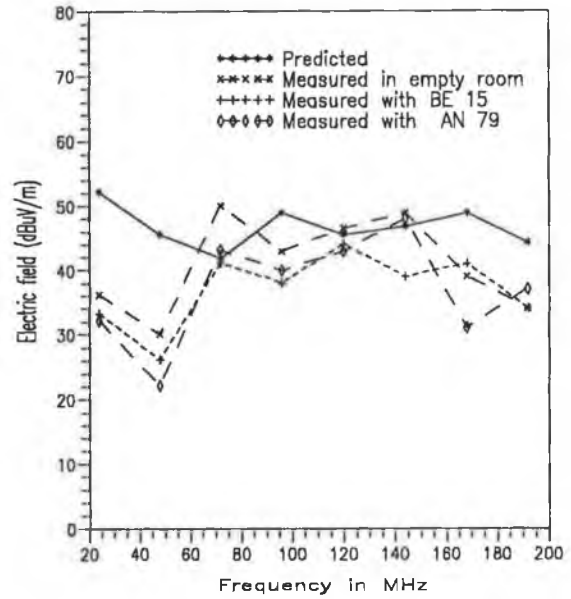
between the predicted field and measured field is significantly high (as high as ± 20 dB) at frequencies below 50 MHz. However, in most cases, above 50 MHz, the difference reduces to ± 10 dB when the measurement is carried out with the absorber in the shielded room. These differences may be due to any reflected wave (from room walls and ceiling) arriving at the antenna. The location of the test set-up in the room, the size and shape of the room and frequency of the signal may cause differences because the phase of the reflected wave arriving at the antenna relative to the phase of the direct wave at the antenna would be influenced by these factors [57].

It is evident from the plots that there is a good agreement between the predicted field and the measured field when the room is loaded with the magnetic field absorber (ferrite tile BE-15). This may be due to the performance of the ferrite tile which works well in the frequency range of 60 to 300 MHz and does not perturb the field significantly.

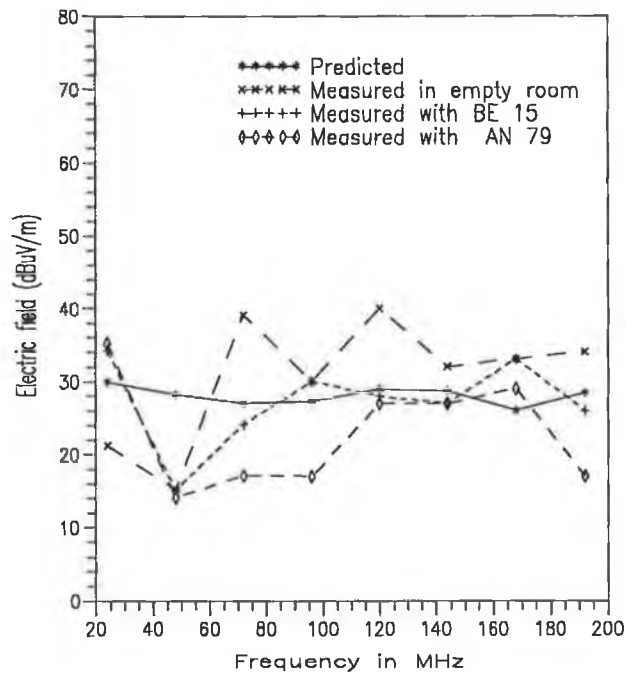
The plots show that in some cases the effect of the absorber is not significant. This may be due to the inaccurate position of the absorber in the room because the antenna will scatter the field incident on it and hence change the position of the field maxima.



(a)



(b)



(c)

Fig. 7.39 Comparison between the CAD predicted and measured electric fields in a shielded room (a) circuit #1; (b) circuit #2; (c) circuit #3. The 24 MHz crystal was used as a source for the test circuit.

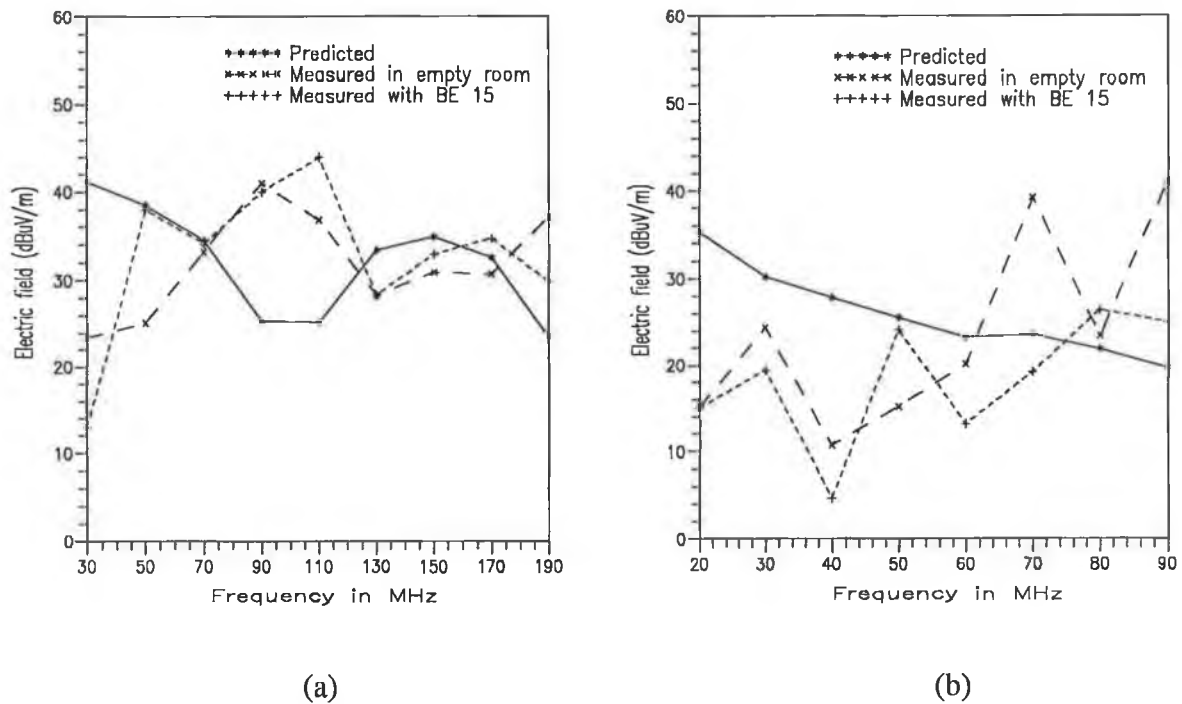


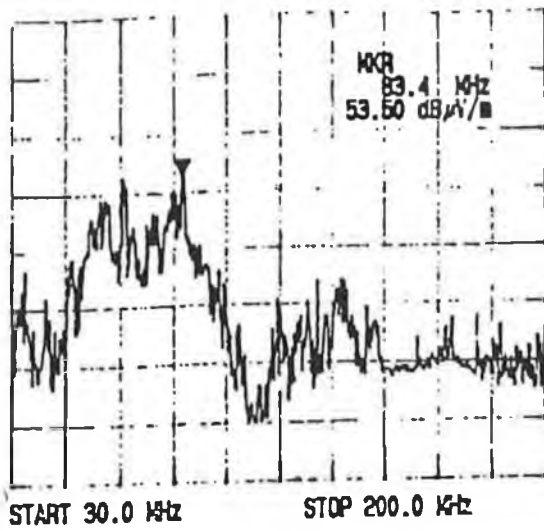
Fig. 7.40 Comparison between the CAD predicted and measured electric fields in a shielded room (a) circuit #1; (b) circuit #3. The 10 MHz crystal was used as a source for the test circuit.

7.5 EMISSION MEASUREMENT IN AN ANECHOIC CHAMBER

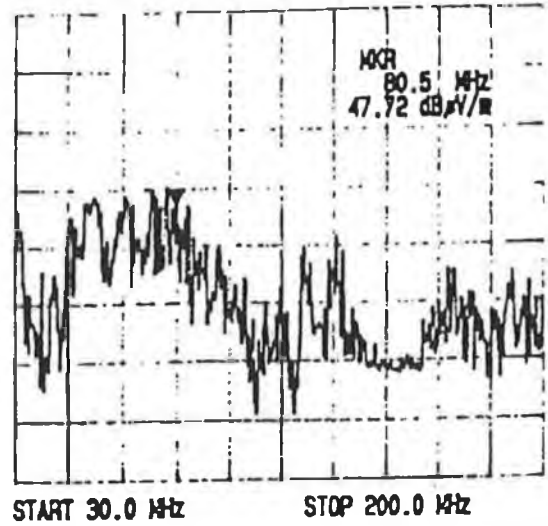
The measurement of radiated electric field from a PCB was performed at 3 m distance in an anechoic chamber of Power Electronics Ireland at the University of Limerick. The chamber was designed to operate at frequencies near 1 GHz and above. The chamber is 5 m wide, 3 m high and 7 m long. It is completely lined with the absorbing materials ECCOSORB® AN 27, including the floor (excluding the narrow wooden platform for operator's movement and placement of instruments inside the chamber).

There is an access door at one corner of the chamber which is made RF tight with beryllium copper finger springs at the edges. The inner side of the door is also lined with the same absorbing materials.

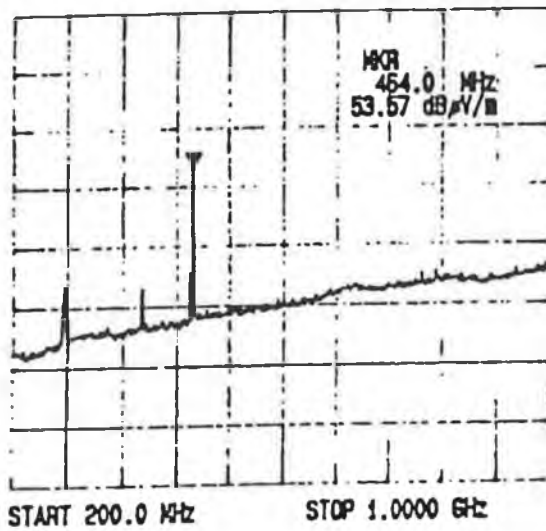
The reflectivity level of the chamber varied from 49% (at 100 MHz) down to 2% (at 1 GHz) and in the microwave range of frequencies it works as an almost completely absorbing and no echo) chamber.



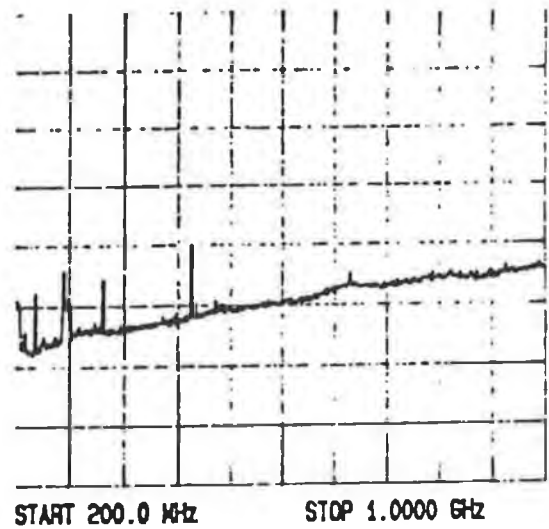
(a)



(b)



(c)



(b)

Fig. 7.41 Ambient noise level inside the chamber (a) with BCA for horizontal polarization; (b) with BCA for vertical polarization; (c) with LPA for horizontal polarization; (d) with LPA for vertical polarization.

In this work, the emission measurement was performed in the chamber at frequencies above 100 MHz.

The ambient noise level of the chamber is recorded through a BCA and a LPA over the swept frequency ranges of 30-200 MHz and 200- 1000 MHz respectively. The recorded ambient noise level is shown in Fig. 7.41. The noise level is negligible (ranging from 22 to 35 dB μ V/m) except at the lower frequency range of 50-100 MHz and at 460 MHz. At these specified frequencies it is significantly high (as high as 53.6 dB μ V/m). This noise level was found to be due to the motor which rotates the turn table and the motor drive electronics in the chamber.

7.5.1 MEASUREMENT SET-UP AND PROCEDURE

The basic instruments required for emission measurement have already been mentioned in the earlier sections. A schematic diagram of the measurement set-up at a 3 m distance in an anechoic chamber is shown in Fig. 7.42.

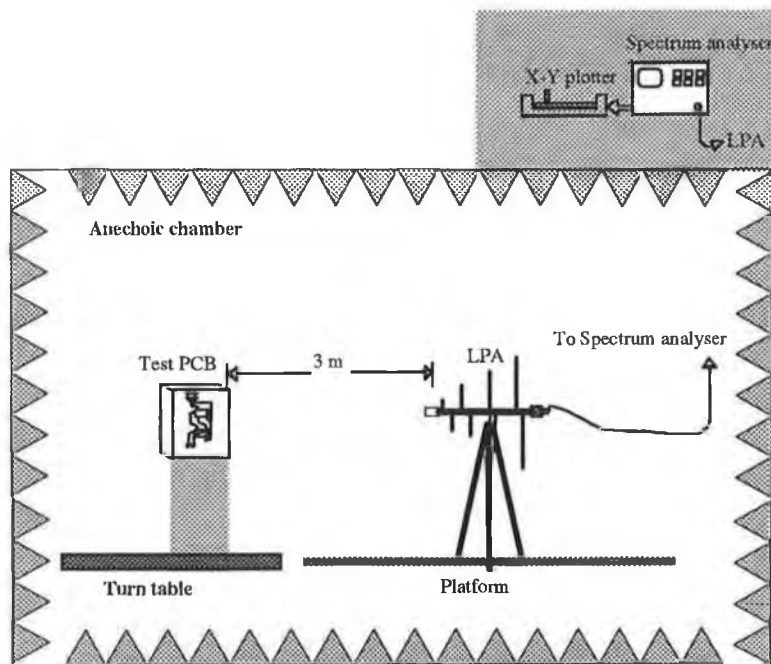


Fig. 7.42 Schematic diagram of the test arrangement for emission measurement in an anechoic chamber.

Two sets of measurements were taken. In the first case the test PCB (config. #3 of circuit #1) and the receiving antenna (BCA or LPA) are placed horizontally (horizontal polarisation of the antenna) at the same level. In the second case both the PCB and antenna are placed vertically (vertical polarisation of the antenna). A photograph of the measurement set up is shown in Fig. 7.43.

In both cases the maximum radiated field was measured. The reading of the spectrum analyser connected to the antenna was recorded on the X-Y plotter.

7.5.2. TEST RESULTS AND COMPARISON

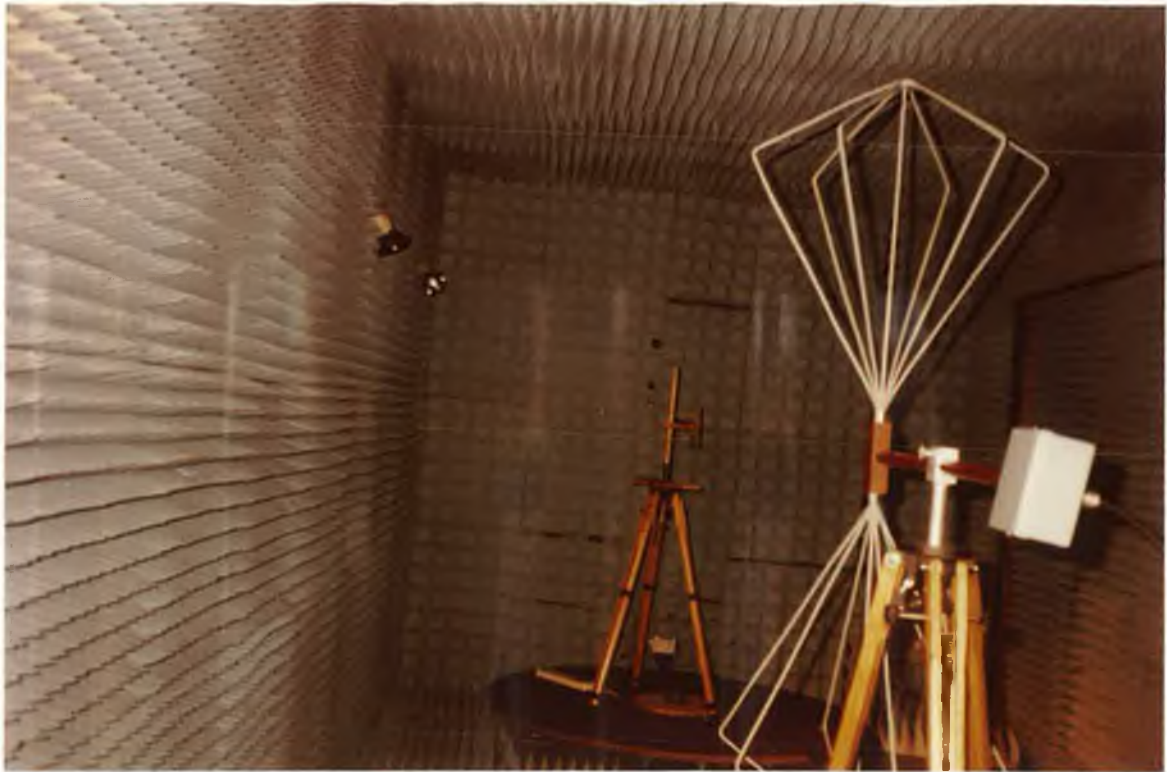
The plots of the recorded field strength (including the chamber noise) as a function of frequency are shown in Figs. 7.44 (for the horizontal polarisation) and 7.45 (for the vertical polarisation).

Using the antenna factor given by the manufacturer of the antenna, and the cable loss, the spectrum analyser was offset to provide the field strength at the point of observation. Therefore the actual measured radiated field could be obtained by subtracting the chamber noise (as given in Fig. 7.41) from the reading of the spectrum analyser.

The measured fields have been compared with the composite CAD predicted fields. A plot of the measured and the CAD predicted electric fields as a function of frequency (above 100 MHz) corresponding to the odd harmonics of the pulse generated by a crystal oscillator (two choices of crystal 24 MHz and 40 MHz) is shown in Figs. 7.46 and 7.47 for horizontal polarisation and vertical polarisation of the test antenna respectively.

In case of horizontal polarisation of the test antenna, the plot shows that the measured field does not differ significantly from the predicted field except at a few frequencies where the predicted values are found to be within ± 7 dB of the measured values.

In case of vertical polarisation of the test antenna the differences between the measured and the predicted field are greater (but still within ± 10 dB except at a few frequencies). This may be due to low performance of the chamber at low frequencies, (refer to section 7.5).

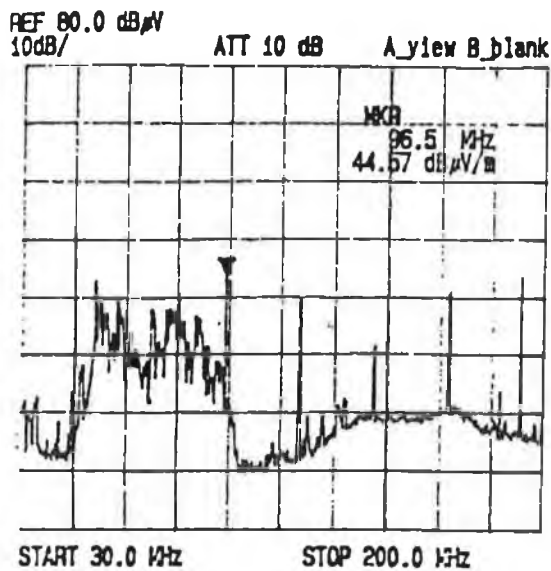


(a)

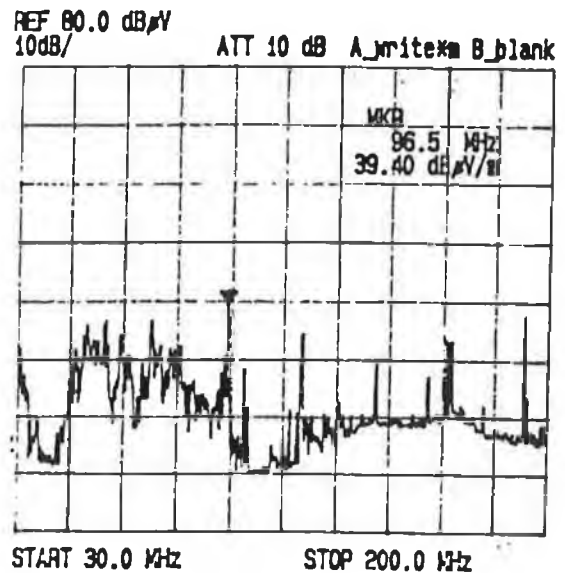


(b)

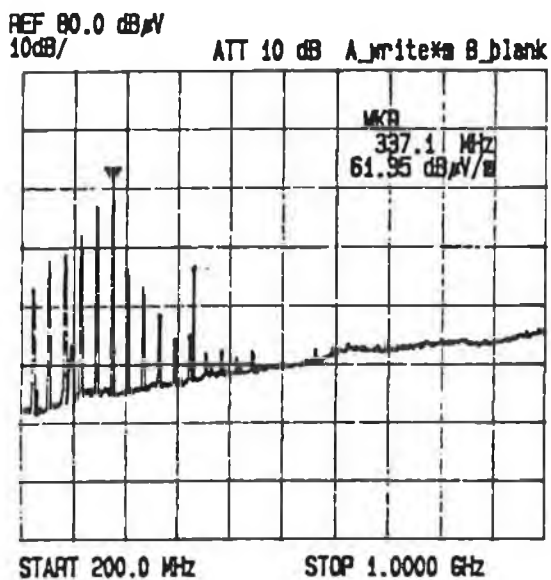
Fig. 7.43 Photographs of the measurement set-up in an anechoic chamber (a) with BCA; (b) with LPA.



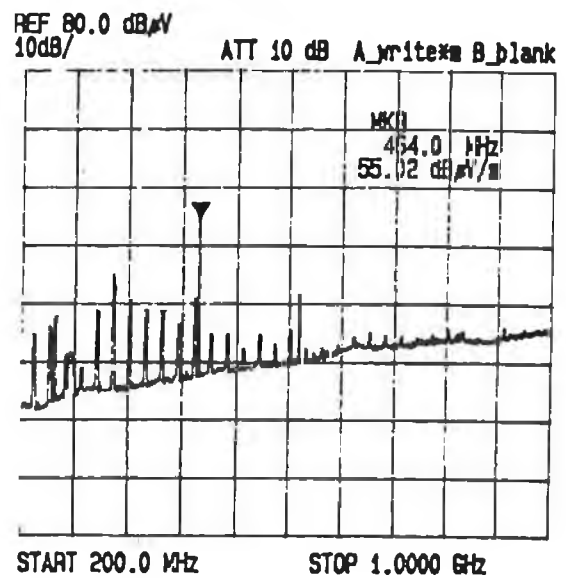
(a)



(b)

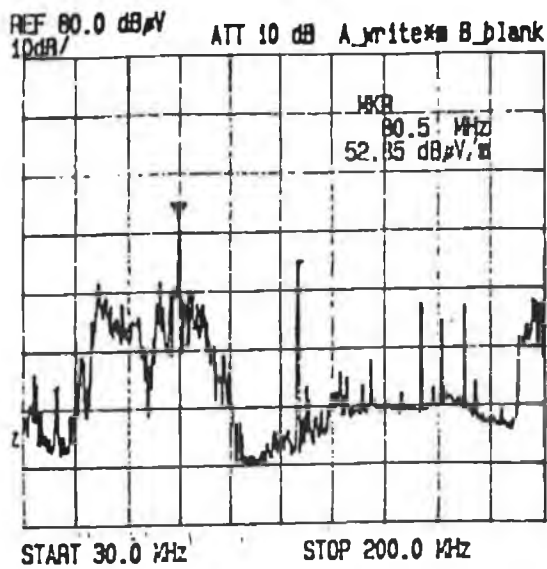


(c)

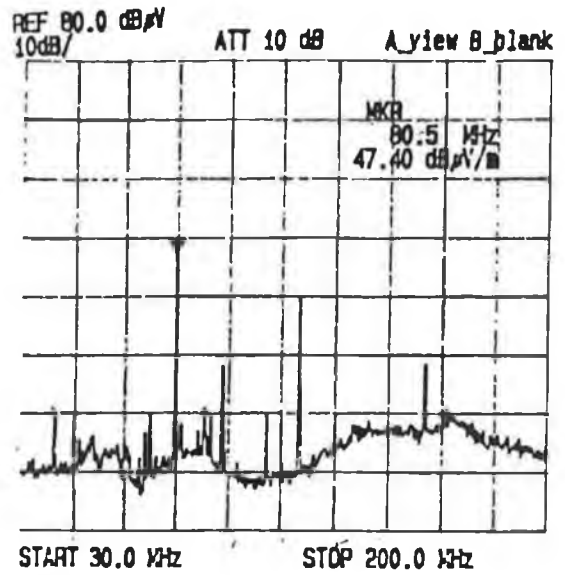


(b)

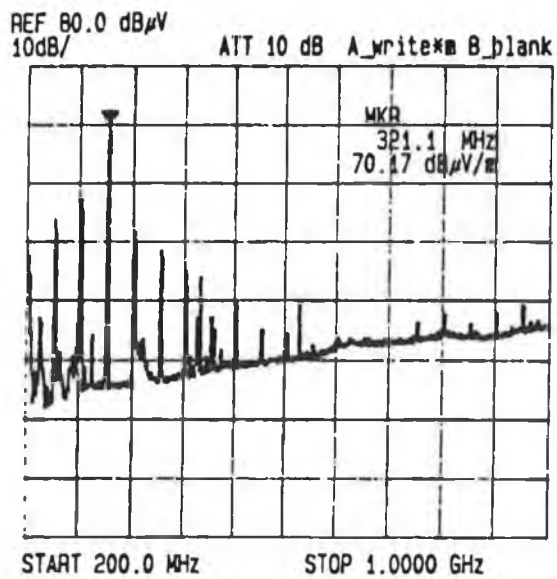
Fig. 7.44 Recorded field strength from config. #3 of circuit 1 (a) with BCA for horizontal polarization; (b) with BCA for vertical polarization; (c) with LPA for horizontal polarization; (d) with LPA for vertical polarization. The 24 MHz crystal was used as a source for the test circuit.



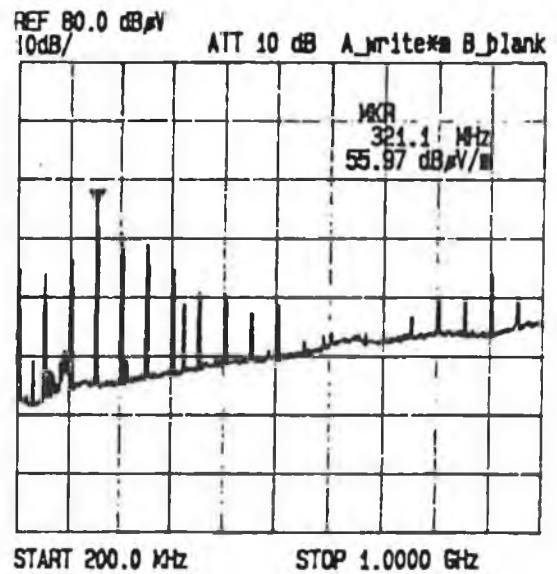
(a)



(b)

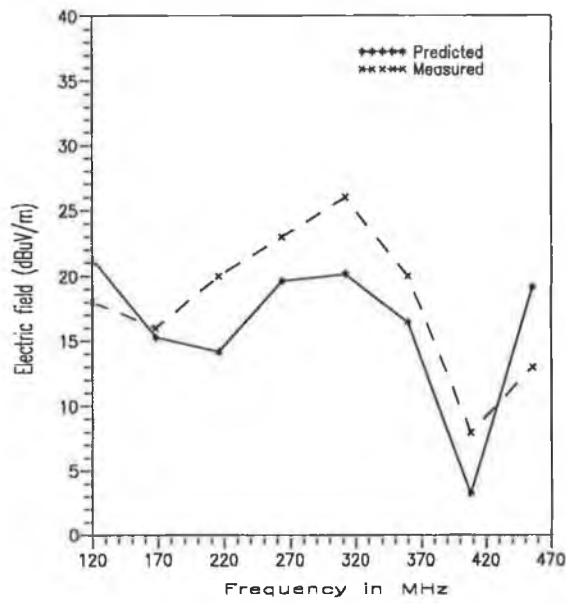


(c)

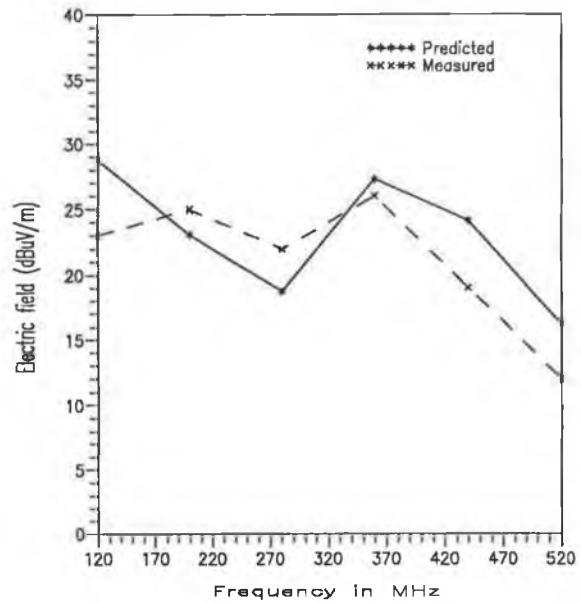


(b)

Fig. 7.45 Recorded field strength from config. #3 of circuit 1 (a) with BCA for horizontal polarisation; (b) with BCA for vertical polarization; (c) with LPA for horizontal polarization; (d) with LPA for vertical polarization. The 40 MHz crystal was used as a source for the test circuit.

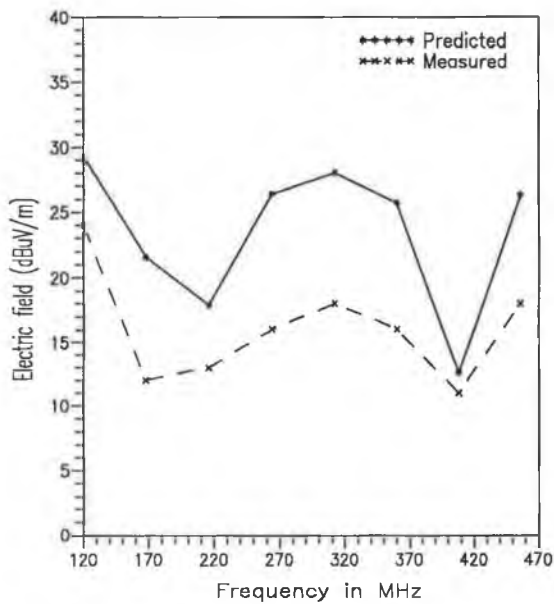


(a)

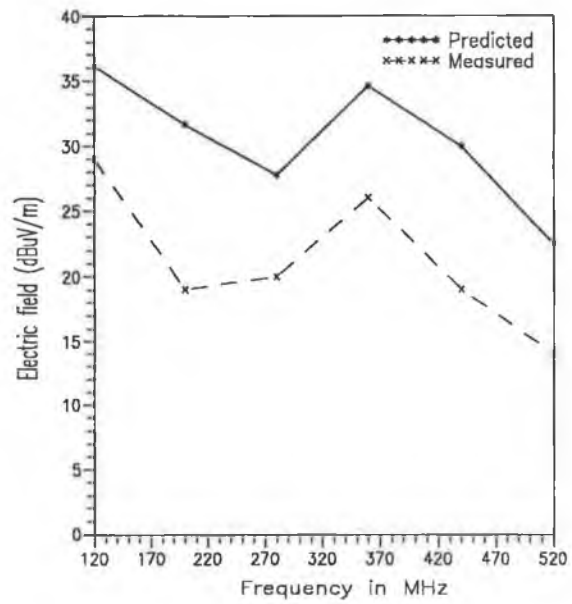


(b)

Fig. 7.46 The comparison between the predicted electric field and the measured field for horizontal polarization of test antenna (a) with 24 MHz crystal; (b) with 40 MHz crystal as a source for the test circuit.



(a)



(b)

Fig. 7.47 The comparison between the predicted electric field and the measured field for vertical polarization of test antenna (a) with 24 MHz crystal; (b) with 40 MHz crystal as source for the test circuit.

7.6 CONCLUDING REMARKS

The radiated EM fields from the sample PCBs were measured to validate the predicted EM fields. Radiated field measurements were performed using near field probes at a distance of both 0.1 m and 0.05 m from the test circuits. A good agreement was found between the measured and the predicted value. The effect of the provision of shielding in an appropriate section of the PCB was also observed as reducing the PCB radiation.

For the sake of interest, the radiated EM field from a simple circuit shown in Fig. 4.3, obtained from the extended TLM computation was compared with the measured value. A good agreement was found between the measured and TLM computed values. The optimum layout (s/w) was determined experimentally by measuring the near field radiation from a set of PCBs having different s/w ratios. It was found that the EM radiation from a PCB having parallel tracks (e.g. parallel signal and its return track) could be low so long $1.5 \leq s/w \leq 1.8$ remains valid. This was observed to be very close to the predicted value.

Measurement of the EM field at a 1 m distance was performed in a shielded room at a frequency below 200 MHz. To reduce the room resonance, the absorber was placed at the positions of field maxima (determined theoretically). The measured electric fields from sample PCBs were compared with predicted values. Comparison shows that in most cases the composite CAD predicted radiation is higher than the measured value. This indicates a reliable prediction of PCB radiation using the composite CAD package.

The radiated electric field from config. #3 of circuit #1 was measured at a 3 m distance in an anechoic chamber above 100 MHz. The maximum difference between the predicted and measured value is found to be ± 10 dB and in most cases the predicted field is above the measured value.

Chapter 8

CONCLUSIONS AND REMARKS

- ❑ CONCLUSIONS
- ❑ DIRECTIONS FOR FURTHER RESEARCH

8.1 CONCLUSIONS

The main objective of this research was the development of a composite CAD package for predicting and reducing the EM radiation from a PCB at the design stage of an electronic circuit. Combining an EM computation tool with circuit design packages (CDPs) was the starting point for such a CAD package. In this work, the NEC programme which was originally developed for EM analysis of a wire structure in free space or above a ground (perfect or imperfect) was used as an EM computation tool. This concluding section outlines the modification of this programme towards the development of composite CAD package.

The use of NEC for such an application was validated theoretically using a TLM computation. The extension of current TLM method (described in section 2.4.1.3) was a part of this research work. This discussion gives an insight about the new features of the TLM.

Finally, this concluding section discusses the salient features of the developed composite CAD package. The discussion is then followed by remarks on the level of success achieved through the application of this package for predicting and reducing the PCB radiation at design stage.

8.1.1 EM COMPUTATION TOOL (NEC-2)

In this work, the original NEC-2 programme was modified for near field computation by discarding some subroutines which are not required for the present application. Since the NEC-2 programme cannot be applied directly to predict EM radiation from a PCB, the PCB was considered as a loaded wire structure just above (but not contacting) an imperfect ground. The dielectric substrate of a PCB is known to have a minimal effect in far field radiation [25, 36, 38, 40] and therefore this effect was neglected in predicting the PCB radiation for far field regions.

An algorithm was developed to implement the geometrical modelling rules of NEC programme. In this work the minimum segment length was chosen to be 0.0003λ because it was observed that the double precision version of NEC (i.e. NEC2D) can support this fine segmentation [132]. In addition to the geometrical modelling rules, this algorithm also checks the segmentation scheme of the wire structure (i.e. simulated PCB track). It was observed that a uniform segmentation scheme or a scheme having equal length of source and its adjacent

segment gives more accurate results than that obtained using a non uniform segmentation of a wire structure (refer to Figs. 3.8 and 3.10).

NEC-2 has no facilities for EM analysis of a wire structure below or penetrating the ground surface. Thus in cases of predicting the EM radiation from a double or a multilayer PCB using NEC-2, far field approximation is necessary for neglecting the effect of dielectric on the radiated field. On the other hand without this approximation prediction of radiation could be performed using NEC-3 which has a capability to model a wire structure above, below or penetrating the ground surface [160]. But NEC-3 is restricted to use by DoD, USA and specific approval is necessary for its use.

8.1.2 THEORETICAL VALIDATION

It was necessary that some degree of theoretical validation of the use of NEC-2 for predicting the PCB radiation be obtained. For this reason the extended TLM was employed as a second technique to predict PCB radiation (section 2.6). The extended TLM is difficult to apply to a complex PCB due to circuit discontinuities (i.e. bends, vias) and its development for such an application was also beyond the scope of this work as it involves a rigorous analysis to replace the discontinuities by equivalent circuit parameters (i.e. inductance and capacitance) [24]. Therefore only a simple PCB having two parallel tracks was chosen as an example. For this simple geometry, the NEC-2 predicted radiation and that from TLM computation were in good agreement (see Figs. 4.7, 4.8, 4.9, 4.10, 4.11). From this it was assumed that the same agreement would be found for a complex PCB.

8.1.3 THE EXTENDED TLM

In the extended TLM, exact expressions were developed to determine the EM radiation from parallel PCB tracks running between two devices. Since the exact expressions for the PUL parameters and characteristic impedance of the transmission line (i.e. two parallel tracks) were used, the extended TLM can be applied for any track separation. As the effect of displacement current, which is confined between the two parallel tracks is considered, this model provides a more accurate result in computing the radiated field. The extended TLM predicted radiation from a sample PCB (designed for this simple geometry) was validated experimentally and results were in good agreement (see Fig. 7.22).

The effect of displacement current at near field radiation is highlighted. It was found that in the near field region, this current produces a larger radiation than that produced due to functional currents (see Figs. 4.12 and 4.13).

8.1.4 COMPOSITE CAD PACKAGE

The composite CAD package was developed by combining the modified NEC-2 programme with the other CDPs. The CDPs provide the electrical and geometrical data of a PCB. By transferring these data to NEC-2, the radiation from a proposed PCB is obtained and then compared with the pre-defined limit. In cases where the predicted radiation exceeds the limit (as stated in section 1.2.2) the designer could reduce or minimise radiation in the soft design process with the aid of various reducing techniques (described in section 5.5.1 and 5.5.2).

It should be noted here that the runtime of the composite CAD package cannot be determined as it is dependent on the complexity of the circuit to be designed. Other factors which also affect the runtime are: designer efficiency and machine speed.

8.1.5 DATA EXTRACTION

An algorithm was developed to extract the geometrical and load data of a PCB from the CDPs and was implemented using a Fortran programme. Using this algorithm it is possible to identify the track which is carrying the clock signal. A single or double sided PCB can be accommodated in this work and it could be extended for a multilayer PCB.

Generally, every algorithm may have some limitations. This algorithm restricts the size of the PCB. The developed algorithm can handle a PCB of about 25.4 cm length and 25.4 cm width. This size could be extended by modifying a part of the algorithm which is used to get the geometrical data from the BM output file. The developed Fortran programme limits the number of tracks and components in a PCB. This limitation is due to the large memory requirement for storing the data. For the current work, the maximum numbers of tracks and components in a PCB are given in Table TG1 of Appendix G1. However these numbers could be extended by simply changing the dimension statements of the Fortran programme.

An algorithm was developed and implemented using a Fortran programme for the extraction of electrical data from the output file of PSPICE. In this work this programme is

limited to 99 nodes in a PCB. However this number can be extended by changing the dimension statement of the Fortran programme.

An algorithm was developed to prepare an input file for PSPICE. The developed programme is user interactive and can accommodate a circuit having a maximum of 99 nodes and a maximum of 99 of each discrete component (e.g. transistor, diode, resistor, capacitor and inductor). These limitations are due to the memory requirements for storing data. However the programme can be extended to any number of nodes and components by simply changing the dimension statements of the routine.

8.1.6 REDUCING EM RADIATION

An algorithm to incorporate some techniques for reducing the PCB radiation into the composite CAD package was described. It has been shown that placing a shield at an appropriate position in a PCB, can reduce the EM radiation. This was experimentally justified (see Figs. 6.14 and 7.26).

8.1.7 APPLICATION AND EXPERIMENTAL VALIDATION OF COMPOSITE CAD PACKAGE

The EM radiation from different electronic circuits was predicted using the composite CAD package and then measured. In designing the PCB for circuit #1, different layouts of the PCB were chosen. As the model parameters of the logic device (74LS04) were unknown, the circuit analysis using PSPICE was not possible for circuit #1. In this case the logic chip was replaced by its input or output impedance. The amplitude of the individual harmonics of a digital or a clock signal (a trapezoidal shape pulse) was computed using Eqn. D7-1. The analysis for the other two circuits (an logic inverter and a combinational switching network) which were constructed using discrete components was performed using PSPICE.

The radiated EM fields from the sample PCBs were measured at a distance of 0.1 m from the test circuits. The measurement was also taken at a distance of 0.05 m. In both cases the experimental results exhibit very close agreement with those predicted (see Figs. 7.8, 7.9, 7.10, 7.12, 7.14, 7.16, 7.18 and 7.20) except in few cases where the difference between the predicted and the measured value is found to be about ± 6 dB. This difference may be due to the coupling effects between the circuit being measured and the probe with its associated cabling. The probe itself may reradiate the received field and so alter the field it is measuring.

However it was found that in most cases the measured field is below the predicted value which indicates a reliable prediction using the composite CAD package.

To validate the CAD predicted radiation at 1 m distance, the measurement of EM radiation from the sample PCBs was carried out in a shielded room. The room resonance was reduced by placing an absorber at the position of maximum field. The position of maximum field was determined numerically from the developed expressions for the field components in an empty room. The effect of the presence of absorber in the measurement of EM radiation in a shielded room has been described. It was found that in most cases the experimental results are within a few dB (about ± 10 dB) of the predicted value at a frequency above 50 MHz (see Figs 7.40 and 7.41). In addition to other reasons as stated in section 7.4.2.3, this difference may be due to the fact that free space antenna factor given by the manufacturer was used in determining the corrected field strength from spectrum analyser output (see Eqn. 7.1). However the actual antenna factor may change due to coupling between the room walls and the test antenna.

The radiated electric field at a 3 m distance from config. #3 of circuit #1 was carried out in an anechoic chamber at a frequency above 100 MHz. Experimental results were also within a few dB of the predicted value and in most cases below the predicted value.

It can be concluded that the developed composite CAD package is a reliable and an accurate tool for predicting the EM radiation from a PCB.

8.1.7.1 Reliability of the composite CAD predicted results

The reliability analysis of the composite CAD predicted EM radiation was carried out in terms of variations between the prediction and the test results. In computing the variations for 0.1 m distance, 10 data points were considered at frequencies corresponding to the harmonics generated by a crystal oscillator (two choices of crystals are 24 MHz and 40 MHz) for five different PCBs. These variations were grouped at different levels irrespective of frequency and are shown in Fig. 8.1. It is evident from the Fig. 8.1 (a) that the variations are within 0-6 dB for 75% of the predicted values and are less than 10 dB for almost 95% of the predicted values. Fig. 8.1 (b) shows that about 60% of the predicted values are higher than the measured values. Fig. 8.1 (c) shows that about 64% of the over predicted values differ from the measured values by about 6 dB and 95% of the predicted values differ by less than 10 dB. It can also be seen from Fig. 8.1 (d) that about 81% of the under predicted values differ from

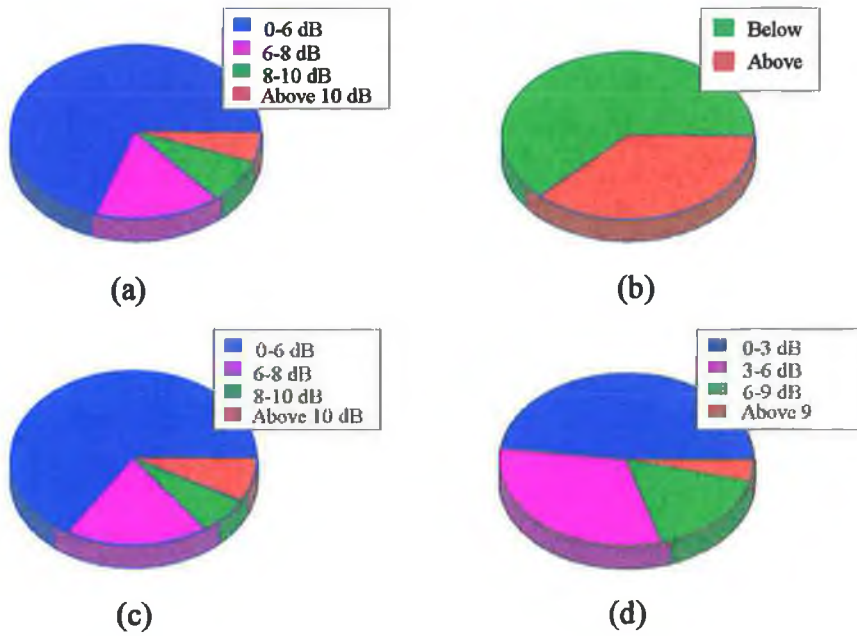


Fig. 8.1 Pictorial representation of the difference between the predicted and measured values at 0.1 m distance: (a) difference; (b) measured value above or below the predicted value; (c) measured value below the predicted value; (d) measured value above the predicted value.

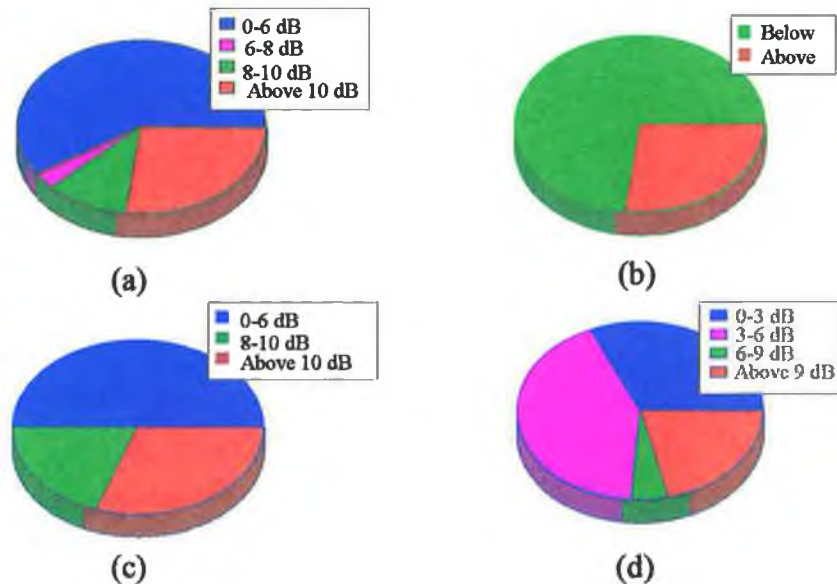


Fig. 8.2 Pictorial representation of the difference between the predicted and measured value at 1 m distance in a shielded room: (a) difference; (b) measured value above or below the predicted value; (c) measured value below the predicted value; (d) measured value above the predicted value.

the measured values by about 6 dB and about 97% of such predicted values differ from the test results by less than 9 dB.

The variations of the predicted radiation from the measured radiation for 1 m distance and 3 m distance are also shown in Figs. 8.2 and 8.3 respectively. In these cases, 8 data points at frequencies corresponding to the harmonics generated by a 24 MHz crystal were chosen for each PCB (three samples of PCBs for 1 m distance). Figs. 8.2 (a) and 8.3 (a) show that about 95% of the predictions vary from the test results by about 10 dB. It is also evident from Figs. 8.2 (d) and 8.3 (d) that about 95% of the under predicted radiation differs from the test results by about 6 dB.

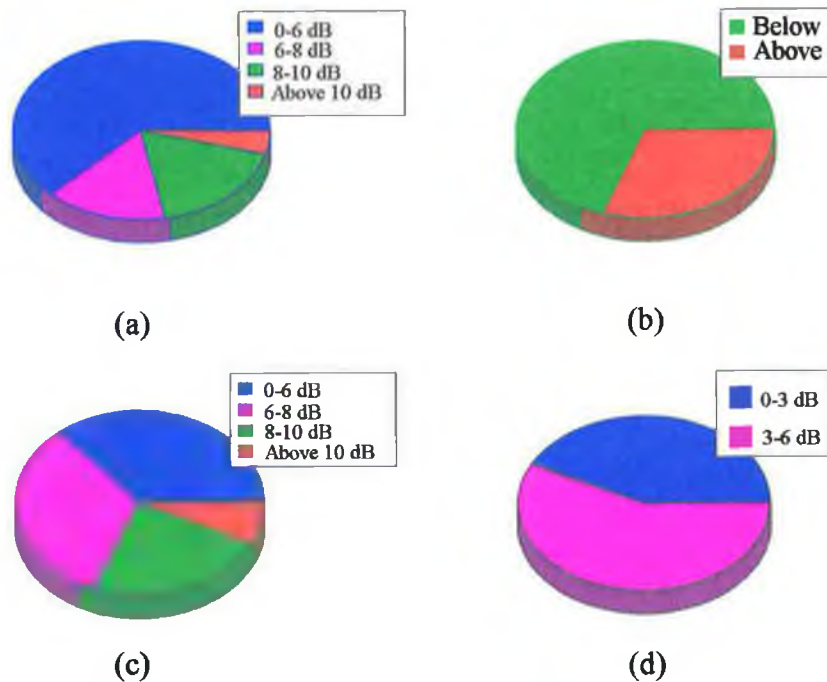
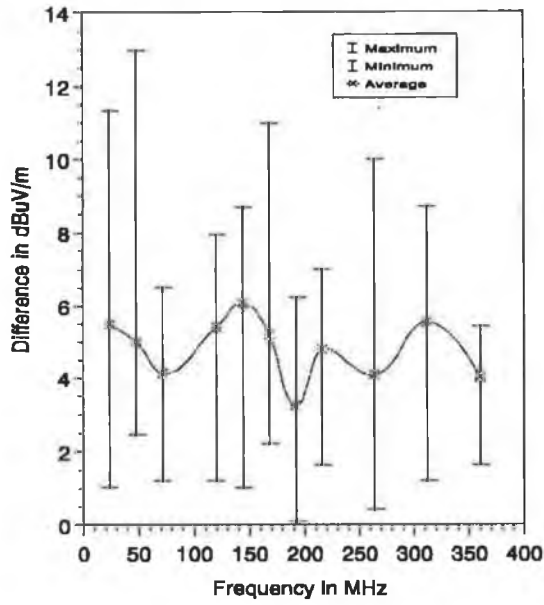
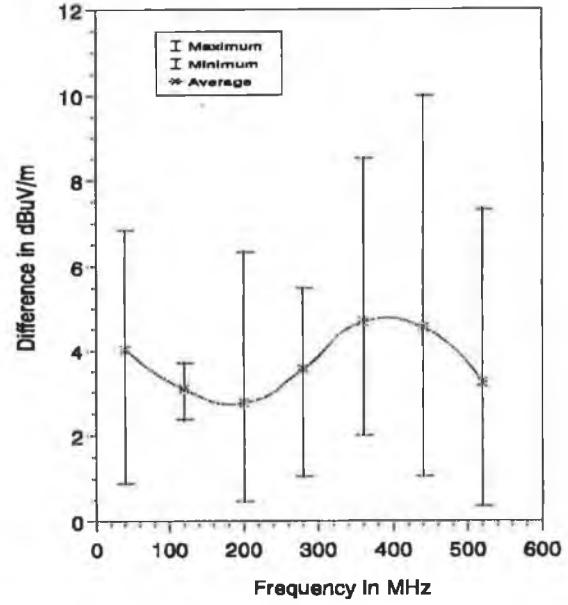


Fig. 8.3 Pictorial representation of the difference between the predicted and measured value at 3 m distance in an anechoic chamber: (a) difference; (b) measured value above or below the predicted value; (c) measured value below the predicted value; (d) measured value above the predicted value.

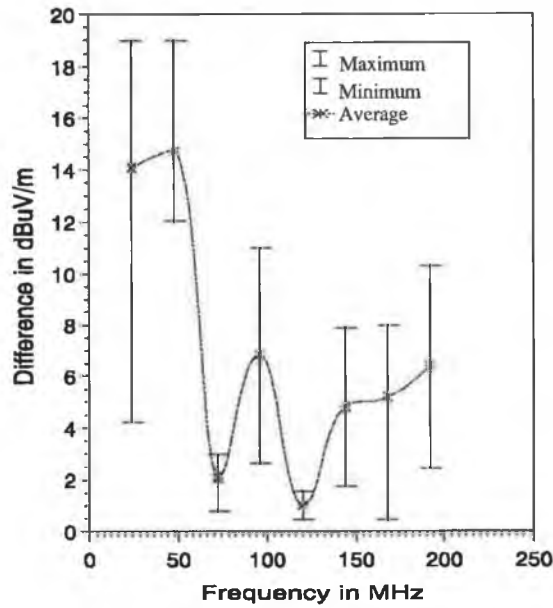
The difference between the predicted and measured radiation as a function of frequency corresponding to harmonics generated by a crystal oscillator is shown in Fig. 8.4. The error bars corresponding to each frequency as shown in Fig. 8.4 represent the minimum and maximum difference between the predicted and measured value. The dotted curve shown in Fig. 8.4 shows the average difference as a function of frequency.



(a)



(b)



(c)

Fig. 8.4 Difference between the predicted and measured value as function of frequency. Radiated EM fields were measured: (a) at 0.1 m distance, with 24 MHz crystal oscillator ; (b) at 0.1 m distance with 40 MHz crystal oscillator; (c) at 1 m distance in a shielded room, with 24 MHz crystal.

The average difference at each frequency is found to be about less than 6 dB except at frequencies below 48 MHz in the case of 1 m distance measurement in a shielded room. The probable reasons for this exception have already been described in section 7.4. In case of 0.1 m distance measurement, five data points were chosen to find the minimum, maximum and the average differences between the predicted and measured values at each frequency. Three data points were chosen for 1 m distance measurement.

8.2 DIRECTIONS FOR FURTHER RESEARCH

This section addresses the following research areas: application of the composite CAD package, extension of the developed composite CAD package, application of the extended TLM to compute the EM radiation from a PCB having more than two parallel tracks and the calibration of a shielded room to correlate the emission measurement in a shielded room to the open area test site measurement.

8.2.1 RESEARCH ON APPLICATION OF THE COMPOSITE CAD PACKAGE

Electronic equipment has to meet the susceptibility limit, in addition to the emission limit, set by the regulating bodies. Therefore, predicting and controlling the susceptibility of a PCB is equally important to predicting and minimising the EM radiation from a PCB at the design stage. Employing the composite CAD package for such an application could constitute an interesting research project.

In this work NEC-2 is used as an EM computation tool where a PCB is modelled as a loaded wire structure. The current induced on the wire structure, due to the incidence of an external electromagnetic wave on it, can indicate the level of susceptibility of the circuit. Fortunately, in addition to the voltage source, NEC-2 can also take an incident plane wave as an excitation of the wire structure. Therefore one can predict the induced current on a PCB due to the external EM field at the design stage. The predicted value should then be verified with the experimental results.

8.2.2 RESEARCH ON EXTENSION OF COMPOSITE CAD PACKAGE

Sophisticated electronic equipment may have both analogue and digital circuits. A digital simulator is necessary for simulating the digital part of such equipment. Therefore adding a digital simulator to the developed composite CAD package would appear to be essential for

EMC verification of such equipment. Since NEC-2 performs the EM analysis in the frequency domain, the digital signal which is in the time domain, has to be transformed into the frequency domain signal. This can be done by the well known FFT (fast fourier transform) technique. In this context, the proposed extension of the composite CAD package is shown in Fig. 8.5.

Following the same philosophy as described in this work, other CDPs which are commercially available can also be employed towards the development of such a composite CAD package. In such cases it might be necessary to modify the data extraction algorithms which depend on the format of the output files generated by the CDPs.

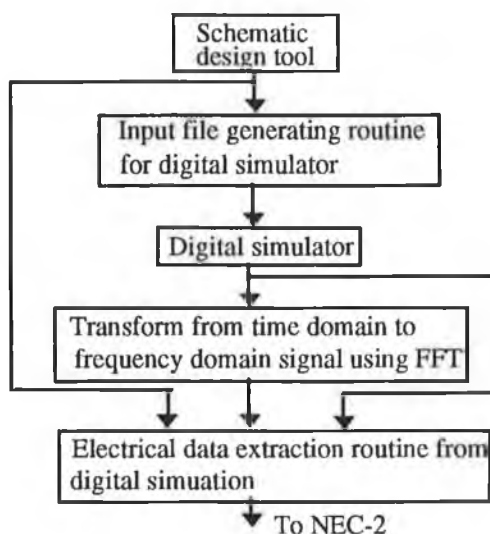


Fig. 8.5 A schematic block diagram for the proposed extension of the composite CAD package.

8.2.3 RESEARCH ON THE EXTENDED TLM

In this work, an extended TLM was presented for computing the EM radiation from a pair of tracks running between two devices on a PCB. Further work could be undertaken for a PCB containing a number of tracks, connecting to a number of devices. This work would be straightforward but laborious as it involves the computation of the PUL parameter's matrices (i.e. inductance and capacitance matrices) for PCB tracks. These can be computed by the various methods described in the literature [25, 90, 127]. Using the PUL parameter matrices, the current and voltage distributions along the track can be calculated from the transmission line equations. The displacement current can be calculated from the capacitance matrix and

the voltage distributions along the track. The radiated EM fields due to these currents can then be determined in a similar way to that described in chapter 4 of this thesis.

The current TLM is limited to parallel tracks in a PCB. Therefore further investigation could be carried out for a PCB where the tracks are not parallel.

8.1.4 RESEARCH ON EMISSION MEASUREMENT IN A SHIELDED ROOM

In this work, the method used for measurement of radiated emission from a PCB, in a shielded room, does not yield good results at a frequency below 50 MHz. An accurate result could be obtained if the measurement is carried out in an open area test site. In some cases open area measurement is not cost effective as described in chapter 2. Therefore the calibration of a shielded room to relate the field measurement in it to that in an open area test site appears to be an interesting research project. A schematic block diagram which outlines this research is shown in Fig. 8.6.

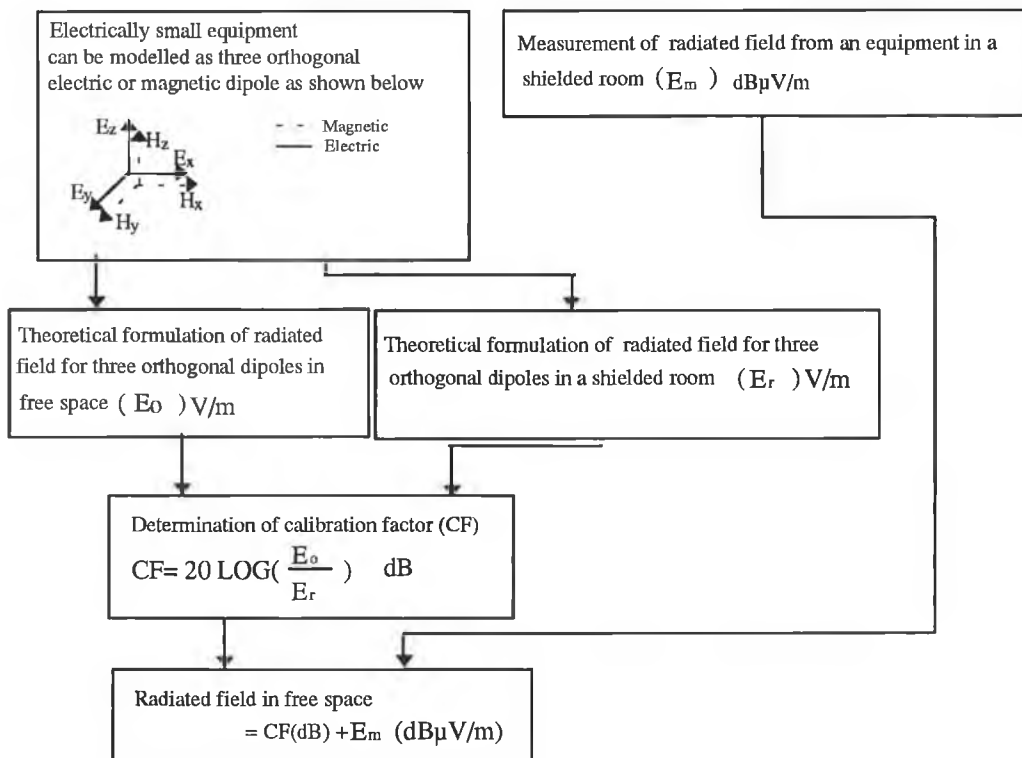


Fig. 8.6 A schematic of the proposed research for emission measurement in a shielded room at frequency below the fundamental resonant frequency.

Electrically small equipment can be modelled as three orthogonal electric or magnetic dipoles as shown in Fig. 8.6 [68]. Any arbitrary field distribution due to each dipole inside a shielded room (a cavity resonator) can be expressed as a linear combination of the cavity eigen functions (i.e. normal modes) [57, 133]. The expression for the resultant field distribution can be obtained from the vector addition of the individual fields. Similarly the expression for the field distribution due to these dipoles in free space can be derived from the antenna theory. The calibration factor can be obtained from the ratio of the EM field in a shielded room to that in free space.

APPENDICES

A1: RADIATED EMISSION LIMIT FOR CLASS B DIGITAL DEVICES

The radiated emission limit set by regulating bodies such as FCC and CISPR for Class "B" digital devices at 3 m measurement distance is furnished in table TA1.

Table TA1: FCC and CISPR radiated emission limit for Class "B" digital devices [97].

FCC		CISPR	
Frequency (MHz)	Radiated emission (dB μ V/m)	Frequency (MHz)	Radiated emission (dB μ V/m)
30 - 88	40.00	30 - 230	40.46
88 - 216	43.50	230 -1000	47.46
216 - 960	46.00		
> 960	54.00		

It should be noted here that the CISPR emission limit are converted to a 3 m measurement distance from their specified measurement distance of 10 m by adding 10.46 dB to the given limit.

B1: RADIATED EMISSION LIMIT FOR CLASS A DIGITAL DEVICES

The radiated emission limit set by regulating bodies such as FCC and CISPR for Class "A" digital devices at 10 m measurement distance is furnished in table TB1.

Table TB1: FCC and CISPR radiated emission limit for class "A" digital device [97].

FCC		CISPR	
Frequency (MHz)	Radiated emission (dB μ V/m)	Frequency (MHz)	Radiated emission (dB μ V/m)
30 - 88	39.00	30 - 230	40.46
88 - 216	43.50	230 -1000	47.46
216 - 960	46.00		
> 960	49.50		

It should be noted here that the CISPR emission limit are converted to a 10 m measurement distance from their specified measurement distance of 30 m by adding 10.46 dB to the given limit.

Table TB2: Characteristics of logics families [29]:

Logic families	Typical output voltage swing (V)	Rise & fall time (ns)	BW $1/\pi t_r$ (ns)	Max. V_{cr} voltage drop (V)	Input capacitance (pF)	DC noise margin (mV)
ECL 10K	0.8	2/2	160	0.2	3	125
ECL 100K	0.8	0.75	420	0.2	5	100
TTL	3.4	10.0	32	0.5	5	400
LP-TTL	3.5	20/10	21	----	5	400
LS-TTL	3.4	10/6	40	0.25	6	300
CMOS	5.0	90/100	3	----	5	1V
HS-CMOS	5.0	10	32	2.0	5	1V

C1: MOMENT METHOD SOLUTION FOR INTEGRODIFFERENTIAL EQUATION

For convenience let us write Eqn. 3.2 in the form :

$$-\bar{E}'(\bar{r}) = \int_l I(s')K(s, s')ds' \quad (C1-1)$$

where,

$$K(s, s') = \frac{-j\eta}{4\pi k} \left(k^2 \hat{s} \cdot \hat{s}' - \frac{\partial^2}{\partial s \partial s'} \right) g(\bar{r}, \bar{r}') \quad (C1-2)$$

Let φ_n be the basis functions (e.g. Eqn. 3.4) on which the unknown current $I(s')$ is expanded.

$$I(s') = \sum_n I_n \varphi_n(s') \quad (C1-3)$$

Substituting Eqn. C1-3 into Eqn. C1-1,

$$-\bar{E}'(\bar{r}) = \sum_n I_n \left[\int_l \varphi_n(s')K(s, s')ds' \right] \quad (C1-4)$$

The term within the square bracket of the left hand side (LHS) of the Eqn. C1-4, is the electric field \bar{E}_r radiated by a wire of length l through which a current $i_n = \varphi_n(s')$ flows. If the functions φ_n are defined on an elementary segment Δ_n of the wire, the integrals are zero outside this segment and \bar{E}_r is the electric field radiated by the segment of a wire of length Δ_n through which the current i_n flows.

Let $\{W_m\}$ be a set of testing (or weighting) functions defined on elementary segments Δ_m . Putting $i_m = W_m(s)$, the scalar product of the both sides of the Eqn. C1-4 by $\{W_m\}$ gives [150]:

$$\int_{\Delta_m} \vec{i}_m \cdot \bar{E}'(\bar{r}) ds = \sum_n I_n \int_{\Delta_m} \bar{E}_r \vec{i}_m ds = \sum_n I_n Z_{mn} \quad (C1-5)$$

where,

$$Z_{mn} = \int_{\Delta_m} \vec{E}_r \cdot \vec{i}_m ds \quad (C1-6)$$

If the weighting function is a delta function (see section 3.2.2) the LHS of Eqn. C1-5 is written as

$$\int_{\Delta_m} \vec{i}_m \cdot \vec{E}^i(\vec{r}) ds = \vec{E}^i(s_m) \cdot \Delta_m \quad (C1-7)$$

Eqn. C1-7 represents the voltage induced in the m th segment of a wire of length Δ_m by the incident field \vec{E}^i and is referred to as V_m [150]. The $[V_m]$ is consequently the excitation matrix. When the wire structure being considered is an antenna excited by a voltage source U_m located in the m th segment of length Δ_m . The term $\vec{E}^i(s_m)$ is replaced by U_m/Δ_m and the excitation matrix is given by

$$[V_m] = \begin{bmatrix} 0 \\ \cdot \\ \cdot \\ U_m \\ \cdot \\ \cdot \\ 0 \end{bmatrix} \quad (C1-8)$$

Eqn. C1-8 shows that all the matrix elements are zero except the m th element which is equal to the voltage of the source.

Eqn. C1-5 then takes the following form which is used to obtain the unknown current distribution along the wire.

$$[V_m] = [I_n][Z_{mn}] \quad (C1-9)$$

C2: FORMULA TO COMPUTE THE NEAR FIELD COMPONENTS IN THE CYLINDRICAL CO-ORDINATE SYSTEM

The fields are evaluated with the source segment on the axis of a local cylindrical co-ordinate system as shown in Fig. C2-1.

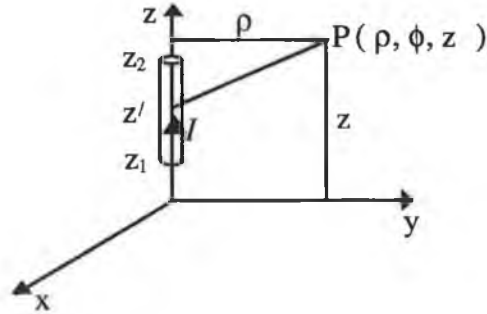


Fig. C2-1 Geometry of the source segment for thin wire kernel. Adapted from [111].

The ρ and z components of the electric fields due to sine and cosine component of current (I) are expressed by the following equations as given in [111],

$$\text{For } I = I_0 \begin{pmatrix} \sin(kz') \\ \cos(kz') \end{pmatrix}$$

$$E_\rho(\rho, z) = \frac{-I_0}{\lambda} \frac{j\eta}{2k^2\rho} G_0 \left\{ k(z-z') \begin{pmatrix} \cos(kz') \\ -\sin(kz') \end{pmatrix} + \left[1 - (z-z')^2 (1 + jkr_0) \frac{1}{r_0^2} \right] \begin{pmatrix} \sin(kz') \\ \cos(kz') \end{pmatrix} \right\} \Bigg|_{z_1}^{z_2} \quad (\text{C2-1})$$

$$E_z(\rho, z) = \frac{I_0}{\lambda} \frac{j\eta}{2k^2} G_0 \left\{ k \begin{pmatrix} \cos(kz') \\ -\sin(kz') \end{pmatrix} - \left[(z-z')(1 + jkr_0) \frac{1}{r_0^2} \right] \begin{pmatrix} \sin(kz') \\ \cos(kz') \end{pmatrix} \right\} \Bigg|_{z_1}^{z_2} \quad (\text{C2-2})$$

For a constant current of strength I_0 the ρ and z components of the fields can be obtained from the following expressions [111],

$$E_\rho(\rho, z) = -\frac{I_0}{\lambda} \frac{j\eta\rho}{2k^2} \left[(1 + jkr_0) \frac{G_0}{r_0^2} \right]_{z_1}^{z_2} \quad (\text{C2-3})$$

$$E_z(\rho, z) = -\frac{I_0}{\lambda} \frac{j\eta}{2k^2} \left\{ \left[(1 + jkr_0)(z - z') \frac{G_0}{r_0^2} \right]_{z_1}^{z_2} + k^2 \int_{z_1}^{z_2} G_0 dz' \right\} \quad (\text{C2-4})$$

where, $G_0 = \frac{e^{-jkr}}{kr}$ and $r_0 = \sqrt{\rho^2 + (z - z')^2}$

The resultant ρ or z component of the field can be obtained from the vector addition of the individual fields (i.e. field due to cosine, sine and constant term of the current).

C3: COMPUTER PROGRAMME LISTING FOR SUBROUTINE SPECTRA

The function of this subroutine is to compute the amplitude of the n th harmonic of the pulse generated by a crystal oscillator. The inputs of this subroutine are pulse amplitude, width, period and pulse rise or fall time.

COMPUTER PROGRAMME LISTING

```
Subroutine spectra(Ans,PFR)
dimension atst(2)
complex Ans,Vs
integer atst,ain
real n,PFR
data atst/2hbf,2haf/
PI=3.1415927
open(unit=23,status='unknown',file='pulse.out')
c atst and ain represent the integer flag to indicate the computation
c of the amplitude of the nth harmonic below or above the fundamental

write(*,*) 'ain'
read(*,2) ain
2 format(a2)

c Vr = Pulse amplitude
c nh = The value of n
c tau = The pulse width
c tr = Pulse rise time = Pulse fall time
c T = Pulse period

c Get data from user
write(*,*) ' Vr,nh,tau,tr,T'
read(*,*) Vr,nh,tau,tr,T
Vs=cplx(Vr,0.0)

c f = Fundamental frequency in MHz

f=(1/T)*1.0e-6
if(ain .eq. atst(2)) then
n=1.0*nh

c Ans = Amplitude of the nth harmonic
c PFR = Frequency of the nth harmonic

Ans=2*Vs*(tau/T)*(sin(n*PI*tau/T)/(n*PI*tau/T))*(sin(n*PI*tr/T)/(n
1*PI*tr/T))
PFR=n*f
Write(23,7) Ans, PFR
end if
```

```
if (ain .eq. atst(1)) then
  n=1./nh
  Ans=2*Vs*(tau/T)*(sin(n*PI*tau/T)/(n*PI*tau/T))*(sin(n*PI*tr/T)/(n
  1*PI*tr/T))
  PFR=n*f
  Write(23,7)Ans, PFR
end if
7 Format(2E12.5,E12.5)
return
end
```


C4: FUNCTION OF EACH SUBROUTINE IN MODIFIED NEC PROGRAMME

The modified NEC programme calls 34 subroutines for near field computation. The subroutine linkage chart is illustrated in Fig. 3.3. The function of each subroutine as given in [111] is described below in alphabetical order.

- BLCKOT - To control the writing and reading of matrix blocks on files for the out-of-core matrix solution. The routine also checks for the end-of-file condition during reading.
- CABC - To compute the coefficients in the current function on each segment, given the basis function amplitudes.
- COMPS - To compare the predicted radiated field with the radiated emission limit set by the regulating bodies and then set the integer flag to indicate whether the minimising the radiated emission is required or not.
- CMSET - To control the filling of the interaction matrix.
- CMWW - To call the subroutines to compute the electric field at segment centers due to current on other segments and to store matrix elements in array locations.
- EFLD - To compute the near electric field due to constant, sine and cosine current distribution on a segment in free space or over ground.
- EKSC - To compute the electric field due to current filaments with $\sin(kz)$, $\cos(kz)$ and constant distributions
- ENF - To check the end of file.
- ETMNS - To fill the array representing the right-hand side of the matrix equation with the negative of the electric field tangent to the segments and with the tangential magnetic field on the surfaces.
- FACTRS - To call the appropriate subroutines for the LU (lower and upper) decomposition of a matrix.
- FBLOCK - To set parameters for storage of the interaction matrix.
- GF - To supply the values of the integrated function (e^{ikr}/kr) to the numerical integration routine INTX.
- GH - To compute the function that is numerically integrated for the near magnetic field of a segment.
- GX - To evaluate the terms for the field contribution due to segment ends in the thin wire kernel.

HFKE	- To compute the near H field of a uniform current filament by numerical integration.
HSFLD	- To compute the near magnetic field due to constant, sine, and cosine current distributions on a segment in free space or over ground.
INTRP	- To evaluate the Sommerfeld integral contributions to the field of a source over ground by interpolation in pre computed tables.
INTX	- To numerically compute the integral of the function (e^{ikr}/kr) .
LOAD	- To compute the impedances at a given frequency for the loading specified by LD cards.
NEFLD	- To compute the near electric field due to currents induced on a structure.
NETWK	- To solve the structure currents for a given excitation.
NFPAT	- To compute the near E or H over a range of points.
NHFLD	- To compute the near magnetic field due to currents induced on a structure.
ROM2	- To numerically integrate over the current distribution on a segment to obtain the field due to Sommerfeld integral.
SBF	- To evaluate the current expansion function associated with a given segment, returning only that portion on a particular segment.
SOLGF	- To solve for the basis function amplitudes in the Numerical Green Function (NGF) procedure.
SOLVE	- To solve the system $LUx = B$, where L is a lower triangular matrix with ones on the diagonal, U is an upper triangular matrix, and B is the right hand side (RHS) vector.
SOLVES	- To solve the solution of the matrix equation, including transforming and reordering the solution vector.
TEST	- To compute the relative difference of two numerical integration results for the Romberg variable-interval-width integration routine.
TRIO	- To evaluate each of the parts of current expansion functions on a single segment due to each of the segments connected to the given segments.
ZINT	- To compute the internal impedance of a circular wire with finite conductivity.

C5: IMPLEMENTATION OF GEOMETRICAL MODELLING RULES

An algorithm to check the geometrical modelling rules for NEC-2 is described in the main text. The algorithm is implemented using a Fortran programme. This routine is used as a subroutine of the modified NEC-2 programme. The computer programme listing of this subroutine is given below.

```

C*****
C This subroutine is used to check the geometrical rules, implement the segmentation schemes. It is also
C used to divide the wire into a number of segments.
C*****

      SUBROUTINE WSN(PFR,NTN,NSS)
      DIMENSION NSS(50),LWS(50),XWW1(50),XWW2(50),YWW1(50)
1     ,YWW2(50),ZWW1(50),ZWW2(50), RADD(50), ATST(1)

      INTEGER NTN,NSS,PSP,ATST, BIN,TNO

      C LWS=LENGTH OF WIRE OR WIRE SEGMENT
      C TNO=TRACK NUMBER

      REAL LWS,PFR,LAMBDA,LIMIT1,LIMIT2,XWW1,XWW2,YWW1,YWW2,ZWW1,ZWW2
1     ,LIMIT3, RADD, LK,DDELTA,RDR
      DATA ATST/EN'/
      OPEN (UNIT=60, STATUS='UNKNOWN', FILE='EXND.DAT')
      REWIND 2
      READ(2,301)PSP
301  FORMAT(I2)
      WRITE(*,*) NTN
      DO 200 I=1,NTN
      READ(2,201) XWW1(I),XWW2(I),YWW1(I),YWW2(I),ZWW1(I),ZWW2(I),
1     RADD(I)
201  FORMAT(5X,7(1x,F10.6))
200  CONTINUE
      WRITE(*,*)(XWW1(I),I=1,NTN),(XWW2(I),I=1,NTN)

      C COMPUTE WAVELENGTH
      C PFR=FREQUENCY OF THE NTH HARMONICS OF THE PULSE

      WRITE(*,*) PFR
      LAMBDA=300.0/PFR
      LIMIT1=.05*LAMBDA
      LIMIT2=.07*LAMBDA
      LIMIT3=.125*LAMBDA

      C COMPUTE THE WIRE AND SEGMENT LENGTH AS WELL AS NO OF SEGMENTS

      WRITE(*,*) 'DEFINE K TO SET SEGMENT LENGTH'
      READ(*,*) LK
      DO 102 I=1,NTN
      LWS(I)=SQRT((XWW2(I)-XWW1(I))**2+(YWW2(I)-YWW1(I))**2+
1     (ZWW2(I)-ZWW1(I))**2)

      C CHECK THE GEOMETRICAL MODELLING RULES

104  IF(LWS(I) .LT. (0.00001*LAMBDA)) GO TO 103

      IF (LK .GT. 0.2 .OR. LK .LT. 0.0003) GO TO 104
106  DDELTA=LK*LAMBDA
      RDR=DDELTA/RADD(I)
      IF(RDR .GE. 8) GO TO 105
      LK=RADD(I)/LAMBDA+LK
      GO TO 106
105  CONTINUE
      IF(PFR .LT. 200.0) THEN
      DNS=LWS(I)/LIMIT1
      WRITE(*,*) DNS
      NSS(I)=DNS+1
      ELSE
      IF(PFR .GT. 200 .AND. PFR .LE. 300) THEN
      DNS=LWS(I)/LIMIT2

```

```

NSS(1)=DNS+1
ELSE
DNS=LWS(1)/LIMIT3
NSS(1)=DNS+1
END IF
END IF

C CHECK THE SOURCE SEGEMENT

REWIND 60
603 READ(60,601)BIN
601 FORMAT(A2)
IF(BIN .EQ. ATST(1)) GO TO 102
BACKSPACE 60
READ(60,602)TNO
602 FORMAT(3X,I2)
IF(TNO .NE. 1) GO TO 603
IF(NSS(1) .LE. 3) THEN
IF(LWS(1) .LT. (0.15*LAMBDA)) THEN
WRITE(*,*) 'EQUAL SEGMENTATION IS NOT POSSIBLE'
ELSE
NSS(1)=3
END IF
END IF
102 CONTINUE

WRITE(*,*) (NSS(I), I=1,NTN)
GO TO 110
103 WRITE(*,*) 'WIRE LENGTH IS LESS THAN MINIMUM SEGEMENT LENGTH'
STOP
110 RETURN
END

```

D1: DISTANCE BETWEEN SOURCE AND OBSERVATION POINT

The geometry involved to compute the vector potential due to functional currents is shown in Fig. 4.6. The distance between the source (x -directed and y -directed sources) and observation point is given as

$$R_{x1} = \sqrt{(x - x')^2 + \left(y + \frac{l}{2}\right)^2 + z^2} \quad (D1-1)$$

$$R_{x2} = \sqrt{(x - x')^2 + \left(y - \frac{l}{2}\right)^2 + z^2} \quad (D1-2)$$

$$R_{y1} = \sqrt{\left(x + \frac{s}{2}\right)^2 + (y - y')^2 + z^2} \quad (D1-3)$$

$$R_{y2} = \sqrt{\left(x - \frac{s}{2}\right)^2 + (y - y')^2 + z^2} \quad (D1-4)$$

D2: EXACT EXPRESSIONS FOR COMPONENTS OF ELECTRIC FIELD DUE TO FUNCTIONAL CURRENTS (I_x , I_y and $I(y')$)

The expressions for electric field components in the rectangular co-ordinate system due to functional currents are given in Eqns 4.30, 4.31 and 4.32. The spatial derivatives of the vector potentials as shown in the above mentioned equations have been evaluated analytically and are given below:

Evaluation of the spatial derivatives

$\partial^2 A_x / \partial x^2$ can be written as,

$$\frac{\partial^2 A_x}{\partial x^2} = \left(\frac{\partial}{\partial x'}\right) \left(\frac{\partial x'}{\partial x}\right) \left(\frac{\partial A_x}{\partial x}\right) \quad (D2-1)$$

By substituting the expression for A_x (Eqn. 4.25), Eqn. D2-1 becomes,

$$\frac{\partial^2 A_x}{\partial x^2} = \frac{\mu}{4\pi} (x-x') \left\{ \frac{I_g (1+j\beta R_{x1}) e^{-j\beta R_{x1}}}{R_{x1}^3} - \frac{I_l (1+j\beta R_{x2}) e^{-j\beta R_{x2}}}{R_{x2}^3} \right\} \Bigg|_{\frac{s}{2}}^{-\frac{s}{2}} \quad (\text{D2-2})$$

Similarly,

$$\begin{aligned} \frac{\partial^2 A_x}{\partial y \partial x} &= \left(\frac{\partial}{\partial y} \right) \left(\frac{\partial}{\partial x'} \frac{\partial x'}{\partial x} A_x \right) \\ &= \frac{\mu}{4\pi} \left\{ I_g \frac{\left(y + \frac{l}{2} \right) (1+j\beta R_{x1}) e^{-j\beta R_{x1}}}{R_{x1}^3} - I_l \frac{\left(y - \frac{l}{2} \right) (1+j\beta R_{x2}) e^{-j\beta R_{x2}}}{R_{x2}^3} \right\} \Bigg|_{\frac{s}{2}}^{-\frac{s}{2}} \end{aligned} \quad (\text{D2-3})$$

$$\begin{aligned} \frac{\partial^2 A_x}{\partial z \partial x} &= \left(\frac{\partial}{\partial z} \right) \left(\frac{\partial}{\partial x'} \frac{\partial x'}{\partial x} A_x \right) \\ &= \frac{\mu}{4\pi} z \left\{ I_g \frac{(1+j\beta R_{x1}) e^{-j\beta R_{x1}}}{R_{x1}^3} - I_l \frac{(1+j\beta R_{x2}) e^{-j\beta R_{x2}}}{R_{x2}^3} \right\} \Bigg|_{\frac{s}{2}}^{-\frac{s}{2}} \end{aligned} \quad (\text{D2-4})$$

$\partial^2 A_y / \partial y^2$ can be written as,

$$\frac{\partial^2 A_y}{\partial y^2} = \left(\frac{\partial}{\partial y'} \right) \left(\frac{\partial y'}{\partial y} \right) \left(\frac{\partial A_y}{\partial y} \right) \quad (\text{D2-5})$$

By substituting the expression for A_y (Eqn. 4.26), Eqn. D2-5 becomes,

$$\frac{\partial^2 A_y}{\partial y^2} = \frac{\mu}{4\pi} (y-y') I(y') \left\{ \frac{(1+j\beta R_{y1}) e^{-j\beta R_{y1}}}{R_{y1}^3} - \frac{(1+j\beta R_{y2}) e^{-j\beta R_{y2}}}{R_{y2}^3} \right\} \Bigg|_{-\frac{l}{2}}^{\frac{l}{2}} \quad (\text{D2-6})$$

Similarly,

$$\begin{aligned} \frac{\partial^2 A_y}{\partial x \partial y} &= \left(\frac{\partial}{\partial x} \right) \left(\frac{\partial}{\partial y'} \frac{\partial y'}{\partial y} A_y \right) \\ &= \frac{\mu}{4\pi} I(y') \left\{ \frac{\left(x + \frac{s}{2} \right) (1 + j\beta R_{y1}) e^{-j\beta R_{y1}}}{R_{y1}^3} - \frac{\left(x - \frac{s}{2} \right) (1 + j\beta R_{y2}) e^{-j\beta R_{y2}}}{R_{y2}^3} \right\} \Bigg|_{-\frac{l}{2}}^{\frac{l}{2}} \end{aligned} \quad (D2-7)$$

$$\begin{aligned} \frac{\partial^2 A_y}{\partial z \partial y} &= \left(\frac{\partial}{\partial z} \right) \left(\frac{\partial}{\partial y'} \frac{\partial y'}{\partial y} A_y \right) \\ &= \frac{\mu}{4\pi} I(y') z \left\{ \frac{(1 + j\beta R_{y1}) e^{-j\beta R_{y1}}}{R_{y1}^3} - \frac{(1 + j\beta R_{y2}) e^{-j\beta R_{y2}}}{R_{y2}^3} \right\} \Bigg|_{-\frac{l}{2}}^{\frac{l}{2}} \end{aligned} \quad (D2-8)$$

Expressions for the electric field components

The exact expressions for the electric field components due to functional currents can be then obtained by substituting the spatial derivatives of the vector potentials into Eqns. 4.30-4.32 and are given as

$$\begin{aligned} E_x &= -j\omega A_x - \frac{j}{4\pi\omega\epsilon} \left\{ (x-x') \left\{ \frac{I_g (1 + j\beta R_{x1}) e^{-j\beta R_{x1}}}{R_{x1}^3} - \frac{I_l (1 + j\beta R_{x2}) e^{-j\beta R_{x2}}}{R_{x2}^3} \right\} \right\} \Bigg|_{-\frac{s}{2}}^{\frac{s}{2}} \\ &\quad + I(y') \left\{ \frac{(x+0.5s)(1 + j\beta R_{y1}) e^{-j\beta R_{y1}}}{R_{y1}^3} - \frac{(x+0.5s)(1 + j\beta R_{y2}) e^{-j\beta R_{y2}}}{R_{y2}^3} \right\} \Bigg|_{-\frac{l}{2}}^{\frac{l}{2}} \end{aligned} \quad (D2-9)$$

$$\begin{aligned} E_y &= -j\omega A_y - \frac{j}{4\pi\omega\epsilon} \left\{ (y-y') I(y') \left\{ \frac{(1 + j\beta R_{y1}) e^{-j\beta R_{y1}}}{R_{y1}^3} - \frac{(1 + j\beta R_{y2}) e^{-j\beta R_{y2}}}{R_{y2}^3} \right\} \right\} \Bigg|_{-\frac{l}{2}}^{\frac{l}{2}} \\ &\quad - \left\{ I_g \frac{(y+0.5l)(1 + j\beta R_{x1}) e^{-j\beta R_{x1}}}{R_{x1}^3} - I_l \frac{(y+0.5l)(1 + j\beta R_{x2}) e^{-j\beta R_{x2}}}{R_{x2}^3} \right\} \Bigg|_{-\frac{s}{2}}^{\frac{s}{2}} \end{aligned} \quad (D2-10)$$

$$E_z = \frac{-j}{4\pi\omega\epsilon} z \left\{ \left[I_g \frac{(1+j\beta R_{x1})e^{-j\beta R_{x1}}}{R_{x1}^3} - I_l \frac{(1+j\beta R_{x2})e^{-j\beta R_{x2}}}{R_{x2}^3} \right] \right\}^{\frac{l}{2}} \Bigg|_{-\frac{l}{2}}^{\frac{l}{2}} + I(y') \left\{ \frac{(1+j\beta R_{y1})e^{-j\beta R_{y1}}}{R_{y1}^3} - \frac{(1+j\beta R_{y2})e^{-j\beta R_{y2}}}{R_{y2}^3} \right\}^{\frac{l}{2}} \Bigg|_{-\frac{l}{2}}^{\frac{l}{2}} \quad (D2-11)$$

D3: EXACT EXPRESSION FOR MAGNETIC FIELD COMPONENTS DUE TO FUNCTIONAL CURRENTS

The components of magnetic field due to the functional currents can be obtained from the Eqns. 4.34, 4.35 and 4.36. To obtain the exact expression for the magnetic field the spatial derivative of the vector potentials of the above mentioned equations were evaluated analytically in a similar way as described in appendix D2. The expressions for the magnetic field components are as follows:

$$H_x = \frac{1}{4\pi} \int_{-\frac{l}{2}}^{\frac{l}{2}} z I(y') \left\{ \frac{(1+j\beta R_{y1})e^{-j\beta R_{y1}}}{R_{y1}^3} - \frac{(1+j\beta R_{y2})e^{-j\beta R_{y2}}}{R_{y2}^3} \right\} dy' \quad (D3-1)$$

$$H_y = \frac{1}{4\pi} \int_{-\frac{l}{2}}^{\frac{l}{2}} z \left\{ I_g \frac{(1+j\beta R_{x1})e^{-j\beta R_{x1}}}{R_{x1}^3} - I_l \frac{(1+j\beta R_{x2})e^{-j\beta R_{x2}}}{R_{x2}^3} \right\} dx' \quad (D3-2)$$

$$H_x = \frac{1}{4\pi} \int_{-\frac{l}{2}}^{\frac{l}{2}} I(y') \left\{ \frac{(x-0.5s)(1+j\beta R_{y2})e^{-j\beta R_{y2}}}{R_{y2}^3} - \frac{(x+0.5s)(1+j\beta R_{y1})e^{-j\beta R_{y1}}}{R_{y1}^3} \right\} dy' + \frac{1}{4\pi} \int_{-\frac{s}{2}}^{\frac{s}{2}} \left\{ I_g \frac{(y+0.5l)(1+j\beta R_{x1})e^{-j\beta R_{x1}}}{R_{x1}^3} - I_l \frac{(y+0.5l)(1+j\beta R_{x2})e^{-j\beta R_{x2}}}{R_{x2}^3} \right\} dx' \quad (D3-3)$$

D4: GEOMETRY INVOLVED IN THE COMPUTATION OF VECTOR POTENTIAL DUE TO DISPLACEMENT CURRENT (I_d)

The geometry of the two parallel tracks used for computation of the vector potential due to displacement current is shown in Fig. D4-1. The primed co-ordinate with subscript (d) denotes the source co-ordinate due to displacement current.

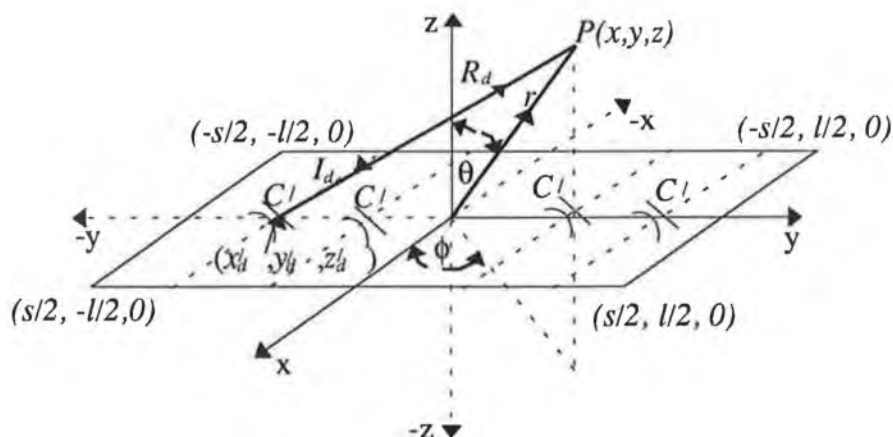


Fig. D4-1 Geometry of the field point to compute the vector potential due to displacement current.

The distance (R_d) between the source due to displacement current and the observation point P is

$$R_d = \sqrt{(x - x'_d)^2 + (y - y'_d)^2 + (z - z'_d)^2} \quad (\text{D4-1})$$

where x'_d , y'_d and z'_d are the co-ordinates of the x -directed line source due to displacement current in the rectangular co-ordinate system.

D5: FIELD COMPONENTS DUE TO DISPLACEMENT CURRENT

The displacement current which is virtually capacitance current [18] is confined between the two parallel tracks as shown in Fig. D4-1. To compute the radiated fields due to displacement current the track is divided into a number of small segments of length Δy as shown in Fig. 4.7. The components of radiated field (electric and magnetic) from each segment due to displacement current can be obtained from Eqns. 4.39, 4.40, 4.41, 4.42 and 4.43. The spatial derivatives of the vector potential due to displacement current can be evaluated in a similar way as described in Appendix D2.

The expressions for the field components become as:

$$E_{xd} = -j\omega A_{xd} - \frac{jsI_d}{4\pi\omega\epsilon} \frac{e^{-j\beta R_d}}{R_d} \left[\frac{(x-x'_d)^2(1+j\beta R_d)(j\beta)}{R_d^3} + \frac{(x-x'_d)^2(3+j2\beta R_d)}{R_d^4} - \frac{(1+j\beta R_d)}{R_d^2} \right] \quad (D5-1)$$

$$E_{yd} = -\frac{jsI_d(x-x'_d)(y-y'_d)}{4\pi\omega\epsilon} \frac{e^{-j\beta R_d}}{R_d} \left[\frac{(1+j\beta R_d)}{R_d^3} + \frac{(3+2j\beta R_d)}{R_d^4} \right] \quad (D5-2)$$

$$E_{zd} = -\frac{jsI_d(x-x'_d)(z-z'_d)}{4\pi\omega\epsilon} \frac{e^{-j\beta R_d}}{R_d} \left[\frac{(1+j\beta R_d)}{R_d^3} + \frac{(3+2j\beta R_d)}{R_d^4} \right] \quad (D5-3)$$

$$H_{xd} = 0 \quad (D5-4)$$

$$H_{yd} = \frac{sI_d}{4\pi} \left[\frac{(z-z'_d)(1+j\beta R_d)}{R_d^3} \right] e^{-j\beta R_d} \quad (D5-5)$$

$$H_{zd} = \frac{sI_d}{4\pi} \left[\frac{(y-y'_d)(1+j\beta R_d)}{R_d^3} \right] e^{-j\beta R_d} \quad (D5-6)$$

The expressions for I_d and A_{xd} are given in Eqns. 4.17 and 4.37 respectively.

D7: CLOCK OR DATA SIGNAL

A clock or data signal of trapezoidal shaped pulse is illustrated in Fig D7-1. The key parameters (pulse rise and fall times, duty cycle) to the HF content of the pulse shaped waveform are described in section 1.5. It is assumed the pulse as depicted in Fig. D7-1 has equal rise and fall times ($t_r = t_f$). The amplitude of the n th harmonic component of this pulse is given by Paul [97]

$$V_{ns} = 2 V_s \frac{\tau}{T} \frac{\sin(f\pi\tau)}{f\pi\tau} \frac{\sin(f\pi t_r)}{f\pi t_r} \quad \text{for } f \neq 0 \quad (\text{D7-1})$$

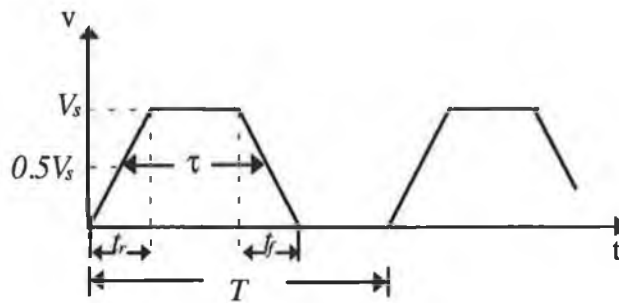


Fig. D7-1. A periodic trapezoidal pulse train representing the data or clock signal.
where,

- n = harmonic number
- f = frequency of the n th harmonic of clock signal = n/T
- T = pulse period
- V_s = pulse amplitude
- V_{ns} = amplitude of the n th harmonic
- τ = pulse width which is the time measured between the pulse rising and falling edges at the mid amplitude level (i.e. $0.5V_s$).
- t_r = pulse rise or fall time

Table TD1: Specifications of crystal oscillators [125, 126].

Frequency in MHz	Supply voltage in Volts	Pulse rise time in ns	Pulse fall time in ns	Pulse period in ns	Pulse duty cycle
6	5±0.5	10	10	166.667	40 to 60 %
10	5±0.5	10	10	100.000	40 to 60 %
24	5±0.5	5	5	41.667	40 to 60 %
40	5±0.5	5	5	25.000	40 to 60 %
50	5±0.5	5	5	20.000	40 to 60 %

D8: COMPUTER PROGRAMME LISTING TO COMPUTE RADIATED FIELD DUE TO FUNCTIONAL CURRENTS

The formulation to compute the radiated field using the extended TLM is described in the main text. A computer programme listing is given here. All relevant subroutines are also listed here.

```

C *****
C Computation of radiated field due to functional currents using the extended TLM
C *****

      DIMENSION ATST(2)
      COMPLEX Z0,ZL,ZIN,ZS,ANS,VS,MULT,IG,IL,I1,I2,VG
1     ,HX,HY,HZ,EX,EY,EZ,SET,SEP,SER
      REAL L,MU,LS,MUR,OMEGA,LL
      INTEGER AIN,ATST
C     XP,YP,ZP = CO-ORDINATE OF SOURCE POINTS
      DATA ATST /1HR,1HS/
      PI=3.141592654
      MULT=CMPLX(0.0,1.0)
      IFLAG=0
      OPEN(UNIT=1,STATUS='OLD',FILE='TLMPCB1.DAT')
      OPEN(UNIT=2,STATUS='OLD',FILE='PULSE1.DAT')
      OPEN(UNIT=6,STATUS='OLD',FILE='FLDPC1.DAT')
      OPEN(UNIT=7,STATUS='OLD',FILE='DEVICE1.DAT')
      OPEN(UNIT=3,STATUS='UNKNOWN',FILE='TLMEFLD.OUT')
      OPEN(UNIT=4,STATUS='UNKNOWN',FILE='TLMPCB.OUT')
      OPEN(UNIT=5,STATUS='UNKNOWN',FILE='HFLD.OUT')
      OPEN(UNIT=8,STATUS='UNKNOWN',FILE='EF2.DAT')
      OPEN(UNIT=9,STATUS='UNKNOWN',FILE='HF2.DAT')
      OPEN(UNIT=10,STATUS='UNKNOWN',FILE='DIFFLM.OUT')

C     READ LAYOUT DATA OF A PCB
C     HT=THICKNESS OF THE DIELECTRIC SHEET

      READ(1,*) L,HH,W,EPR1,MUR,MU,HT,EPR0
      READ(1,*) XP,YP
      WRITE(3,*) XP,YP
      WRITE(*,*) 'NWS,NS'
      READ(*,*) NWS,NS
      DELY=2*L/NS

C     GET THE SOURCE AND LOAD IMPEDANCE

      READ(7,*) RS,CS,R1,C,LL,LS

C     X,Y,Z = CO-ORDINATE OF THE FIELD OBSERVATION POINT
C     IX,IY,IZ=NUMBER OF OBSERVATION POINTS IN THE X,Y AND Z CO-ORDINATE RESPECTIVELY
C     DIX,DIY,DIZ= INCREMENT OF X,Y AND Z CO-ORDINATE RESPECTIVELY.
C     COMPUTE THE CHARACTERISTIC IMPEDANCE AND PUL PARAMETERS

      CALL ZEPCB(HT,HH,W,EPR1,EPR2,RZ0,CPP)
      EPR=EPR2
      Z0=CMPLX(RZ0,0.0)
      WRITE(4,8) Z0
8     FORMAT(/CHARACTERISTIC IMPEDANCE Z0 =',2X,2F10.5)

C     GET EXCITATION DATA

      READ(2,*) VR,TAU,T,TR
312  FORMAT(F8.3,E9.3,E10.3,E7.3)
      VS=CMPLX(VR,0.0)
80   WRITE(*,*) 'NTH HARMONIC'
      READ(*,*) NN
      CALL PULSE(ANS,VS,TAU,NN,T,TR,FR)
      WRITE(4,245) NN,FR
245  FORMAT(/10X,'NN=' ,I3,5X,'FREQUENCY=' ,F10.5)
      WRITE(4,146) ANS
146  FORMAT(/5X,'ANS=' ,2E12.6)

```

```

      BETA0=((2.*PI*FR)/300.)*SQRT(EPR*MUR)
      OMEGA=2*PI*FR*1.0E6

C   COMPUTE SOURCE AND LOAD IMPEDANCE

      CALL TPARA(R1,C,RS,CS,LL,LS,BETA0,Z0,ZS,ZIN,ZL,FR,L)
      CALL CURRENT(IG,IL,I1,I2,BETA0,Z0,ZL,ZIN,ZS,ANS,VG,DELY,NS,L)

C   CALCULATE ELECTRIC FIELD COMPONENT

      WRITE(3,137)
137  FORMAT(///15X,'ELECTRIC FIELD CALCULATION')
      WRITE(3,145) NN,FR
145  FORMAT(/10X,'NN = ',I3,5X,'FREQUENCY = ',F10.5)
      WRITE(3,138)
138  FORMAT(///'X',5X,'Y',5X,'Z',10X,'E')
      WRITE(3,139)
139  FORMAT(/24X,'MAG',6X,'ANGLE')
      BETA=BETA0/(SQRT(EPR*MUR))

      WRITE(*,*) 'TYPES OF CO-ORDINATE'
      READ(*,700) AIN
700  FORMAT(A1)

C   ENTER THE OBSERVATION POINTS
      WRITE(*,*) 'XOB(R),YOB(TH),ZOB(PH),IXOB,IYOB,IZOB,DIXOB,DIYOB,DIZO
1   B'
      READ(*,*) XOB,YOB,ZOB,IXOB,IYOB,IZOB,DIXOB,DIYOB,DIZOB

C   SAVE THE INITIAL VALUE OF FIELD POINTS
      XI=XOB
      YI=YOB
      ZI=ZOB
      DO 62 II = 1,IXOB
        XOB=XI+(II-1)*DIXOB
      DO 60 KK = 1,IYOB
        YOB=YI+(KK-1)*DIYOB
      DO 61 JJ = 1,IZOB
        ZOB=ZI+(JJ-1)*DIZOB
      IF (AIN .EQ. ATST(1)) THEN
        X=XOB
        Y=YOB
        Z=ZOB
        R=SQRT(X*X+Y*Y+Z*Z)
        F(Z .EQ. 0) THEN
          THETA=PI/2
        ELSE
          THETA=ATAN(SQRT(X*X+Y*Y)/Z)
        END IF
        IF(X .EQ. 0.0) THEN
          PHI=PI/2.0
        ELSE
          PHI=ATAN(Y/X)
        END IF
        ELSE
          R=XOB
          THETA=YOB*PI/180
          PHI=ZOB*PI/180
          X=R*SIN(THETA)*COS(PHI)
          Y=R*SIN(THETA)*SIN(PHI)
          Z=R*COS(THETA)
        END IF
      CALL ELECF(EX,EY,EZ,ANS,Z0,ZL,ZS,ZIN,L,X,Y,Z,XP,YP,BETA,EPR0
1   ,OMEGA,BETA0,HH,EPR,IG,IL)
      WRITE(10,1000) EX,EY,EZ
1000  FORMAT(1X,5(1X,E12.3))
      E=SQRT((CABS(EX))**2+(CABS(EY))**2+(CABS(EZ))**2)
      EDB= 20*LOG10(E*1.0E6)
      WRITE(3,136) X,Y,Z,E
136  FORMAT(/F5.2,2X,F6.2,2X,F6.2,2X,E10.5)
      WRITE(3,*) EDB

C   COMPUTE THE MAGNETIC FIELD

      CALL HFIELD(HX,HY,HZ,ANS,Z0,ZL,ZS,L,X,Y,Z,XP,YP,BETA
1   ,OMEGA,BETA0,HH,IG,IL)
      H=SQRT((CABS(HX))**2+(CABS(HY))**2+(CABS(HZ))**2)
      HDB= 20*LOG10(H*1.0E6)
      WRITE(5,*) H, HDB,FR,X'

```

```

        WRITE(5,*) H,IIDB,FR,X
        WRITE(9,*) RTHETA,IIDB
61      CONTINUE
60      CONTINUE
62      CONTINUE
        X=XI
        Y=YI
        Z=ZI

C      IFLAG IS AN INTEGER FLAG TO REQUEST THE USER FOR NEXT COMPUTATION

        WRITE(*,*) IFLAG'
        READ(*,*) IFLAG
        IF(IFLAG.EQ.0) GO TO 37
        FR=0.0
        ANS=CMPLX(0.0,0.0)
        GO TO 80
37      STOP
        END

```

Subroutine 1

C This subroutine computes the source , load impedance and input impedance at a desired frequency

```

SUBROUTINE TPARA(R1,C,RS,CS,LL,LS,BETA0,Z0,ZS,ZIN,ZL,FR,L)
COMPLEX ZIN,ZL,ZS,Z0,MULT,ZLS,ZSS
REAL L,LL,LS
PI=3.141592654
MULT=CMPLX(0.0,1.0)
OMEGA=2*PI*FR*1.0E+6
DZL=1+(OMEGA*R1*C)**2
XZL=R1/DZL
YZL=(-1)*R1*R1*OMEGA*C/DZL
ZLS=CMPLX(XZL,YZL)
ZL=MULT*OMEGA*LL+ZLS
ZIN=Z0*(ZL*COS(BETA0*L*2)+MULT*Z0*SIN(BETA0*L*2))/(Z0*COS(BETA0*L
1 *2)+MULT*ZL*SIN(BETA0*L*2))
DZS=1+(OMEGA*RS*CS)**2
XZS=RS/DZS
YZS=(-1)*RS*RS*OMEGA*CS/DZS
ZSS=CMPLX(XZS,YZS)
ZS=MULT*OMEGA*LL+ZSS
WRITE(4,9) ZS,ZL,ZIN
9  FORMAT(\2X,'ZS=',2X,2E12.5,2X,'ZL=',2X,2E12.5,2X,'ZIN=',2X
1 ,2E12.5)
RETURN
END

```

Subroutine 2

C The subroutine 2 computes the functional currents as described in chapter 4

```

SUBROUTINE CURRENT (IG,IL,I1,I2,BETA0,Z0,ZL,ZIN,ZS,ANS,VG,DELY,NS
1 ,L)
COMPLEX IG,IL,I1,I2,ZIN,ZL,ZS,MULT,ANS,D,VG,Z0
REAL L
MULT=CMPLX(0.0,1.0)
IG=ANS/(ZS+ZIN)
D=Z0*COS(BETA0*L*2)+MULT*ZL*SIN(BETA0*L*2)
IL=(IG*Z0)/D
WRITE(3,10) IG,IL
10  FORMAT (/2X,IG=',2X,2E12.5,2X,IL=',2X,2E12.5)
VG=ANS*ZIN/(ZS+ZIN)
WRITE(4,102)
102  FORMAT(/5X,'Y' 30X,'CURRENT(I1)')
WRITE(4,103)
103  FORMAT(/18X,'REAL',20X,'TMAG',17X,'MAGNITUDE')
DO 90 I=1,NS
Y=DELY*I-DELY/2.0
I1=IG*COS(BETA0*Y)-(MULT*VG*SIN(BETA0*Y))/Z0
XI1=REAL(I1)
YI1=IMAG(I1)
ABSI1=SQRT(XI1*XI1+YI1*YI1)
I2=(-1)*I1
XI2=REAL(I2)
YI2=IMAG(I2)
ABSI2=SQRT(XI2*XI2+YI2*YI2)
WRITE(4,104) Y,XI1,YI1,ABSI1

```

```

104 FORMAT(/2X,F7.5, 6X,E12.6,10X,E12.6,10X,E12.6)
90 CONTINUE
RETURN
END

```

Subroutine 3

C This subroutine is to calculate amplitude of the nth harmonic of a trapezoid pulse

```

SUBROUTINE PULSE(ANS,VS,TAU,NN,T,TR,FR)
DIMENSION ATST(2)
COMPLEX ANS,VS
INTEGER ATST,AIN
REAL NF
DATA ATST/2HBF,2HAF/
WRITE(*,*) 'AIN'
READ(*,20) AIN
20 FORMAT(A2)
PI=3.141592654
IF(AIN.EQ. ATST(2)) THEN
NF=1.0*NN
END IF
IF(AIN.EQ. ATST(1)) THEN
NF=1.0/NN
END IF
ANS1=(SIN(NF*PI*TAU/T))/(NF*PI*TAU/T)
ANS2=(SIN(NF*PI*TR/T))/(NF*PI*TR/T)
ANS=2*VS*(TAU/T)*ANS1*ANS2
AANS=ABS(ANS)

```

C FR =FREQUENCY IN MHZ

```

FR=NF*(1/T)*1.0E-6
RETURN
END

```

Subroutine 4

C This subroutine is to calculate the characteristic impedance and effective dielectric constant

```

SUBROUTINE ZEPCB (HT,HH,W,EPR1,EPR2,RZ0,CPP)
REAL KP,KPM
PI=3.1415926
KP=2*HH/(2*HH+4*W)
WRITE(*,*) 'LAYER'
READ(*,*) LAYER
IF(LAYER.NE. 2) GO TO 8000
EPR2=EPR1
RZ0=377*1.414*(LOG(4*HT/W)+(1/8)*(W/H)**2-(1/2)*(EPR2-1)/(EPR2+1)
1 *(0.452+0.242/EPR2))/(PI*SQRT(EPR2+1))
GO TO 8001
8000 EPR2=(EPR1+1)/2*(TANH(0.775*LOG(HT/(2*W))+1.75)+(KP*2*W/HT)
1 *(.04-0.7*KP+.01*(1-1*EPR1)*(.25+KP)))
WRITE(*,*) HH,W
IF((HH/W).GT. 10.0) GO TO 8002
KPM= SQRT(1-KP**2)
IF(KP.GE. 0.0 .AND. KP.LE. .707) THEN
RZ0=(377.0*PI)/(SQRT(EPR2)*LOG(2*(1+SQRT(KPM))/(1-SQRT(KPM))))
CPP=8.854E-12*EPR2*LOG(2*(1+SQRT(KPM))/(1-SQRT(KPM)))/PI
END IF
IF (KP .GE. .707 .AND. KP .LE. 1.0) THEN
RZ0=(377.0/(SQRT(EPR2)*PI))*LOG(2*(1+SQRT(KP))/(1-SQRT(KP)))
CPP=8.854E-12*EPR2*PI/LOG(2*(1+SQRT(KP))/(1-SQRT(KP)))
END IF
GO TO 8001
8002 RZ0=120/SQRT(EPR1)*LOG((HH/W)+SQRT((HH/W)**2-1))
CPP=8.854E-12*EPR2*PI/LOG(2*(1+SQRT(KP))/(1-SQRT(KP)))
8001 RETURN
END

```

BEGINNING OF FUNCTION SUBROUTINES

Subroutine 5

```

COMPLEX FUNCTION F1 (X,Y,XP,Z,L,IG,IL,BETA)
COMPLEX IG,IL,MULT

```



```

      REAL L
      MULT=CMPLX(0,1.0)
      F1=IG*EXP((-1)*BETA*MULT*SQRT((X-XP)**2+(Y+L)**2+Z**2))/
1   SQRT((X-XP)**2+(Y+L)**2+Z**2)-IL*EXP((-1)*BETA*MULT*SQRT((X-XP
2   )**2+(Y-L)**2+Z**2))/SQRT((X-XP)**2+(Y-L)**2+Z**2)
      RETURN
      END

```

Subroutine 6

```

      COMPLEX FUNCTION F2(X,Y,Z,YP,D,ANS,Z0,ZL,BETA,
1   L,H,BETA0)
      COMPLEX ANS,Z0,ZL,D,MULT
      REAL L
      MULT=CMPLX(0.0,1.0)
      F2=(EXP((-1)*BETA*MULT*SQRT((X+H)**2+(Y-YP)**2+Z**2))/
1   SQRT((X+H)**2+(Y-YP)**2+Z**2)-EXP((-1)*BETA*MULT*SQRT((X-H
2   )**2+(Y-YP)**2+Z**2))/SQRT((X-H)**2+(Y-YP)**2+Z**2))*
3   (ANS/D)*(Z0*COS(BETA0*(2*L-YP))+MULT*ZL*SIN(BETA0*(2*L-YP)))
      RETURN
      END

```

Subroutine 7

```

      COMPLEX FUNCTION F3(X,Y,Z,XP,L,BETA,IG,IL)
      REAL L
      COMPLEX IG,IL,MULT
      MULT=CMPLX(0.0,1.0)
      WRITE(*,*) X,XP,Y,L
      F3=IG*(X-XP)*(1+MULT*BETA*SQRT((X-XP)**2+(Y+L)**2+Z**2))*(EXP(
1   (-1)*BETA*SQRT((X-XP)**2+(Y+L)**2+Z**2)*MULT))/
2   (SQRT((X-XP)**2+(Y+L)**2+Z**2)**3)-IL*(X-XP)*
3   (1+MULT*BETA*SQRT((X-XP)**2+(Y-L)**2+Z**2))*(EXP((-1)*BETA*
4   SQRT((X-XP)**2+(Y-L)**2+Z**2)*MULT))/
5   (SQRT((X-XP)**2+(Y-L)**2+Z**2)**3)
      RETURN
      END

```

Subroutine 8

```

      COMPLEX FUNCTION F4(X,Y,Z,YP,Z0,ZL,BETA,L,H,ANS,D,BETA0)
      COMPLEX Z0,ZL,D,ANS,MULT
      REAL L
      MULT=CMPLX(0.0,1.0)
      F4=((X+H)*(1+MULT*BETA*SQRT((X+H)**2+(Y-YP)**2+Z**2))*EXP((-1)*
1   BETA*MULT*SQRT((X+H)**2+(Y-YP)**2+Z**2)))/((SQRT((X+H)**2+(Y-YP)
2   **2+Z**2)**3)-(X-H)*(1+MULT*BETA*SQRT((X-H)**2+(Y-YP)**2+Z**2))*
3   EXP((-1)*BETA*MULT*SQRT((X-H)**2+(Y-YP)**2+Z**2)))/((SQRT((X-H)
4   **2+(Y-YP)**2+Z**2)**3)*(ANS/D)*(Z0*COS(BETA0*(2*L-YP))+MULT*ZL
5   *SIN(BETA0*(2*L-YP)))
      RETURN
      END

```

Subroutine 9

```

      COMPLEX FUNCTION F5(X,XP,Y,L,Z,IG,IL,II,BETA)
      COMPLEX IG,IL,MULT
      REAL L
      MULT=CMPLX(0.0,1.0)
      F5=IG*(Y+L)*(1+MULT*BETA*SQRT((X-XP)**2+(Y+L)**2+Z**2))*EXP((-1
1   )*MULT*BETA*SQRT((X-XP)**2+(Y+L)**2+Z**2))/(SQRT((X-XP)**2+(Y+L)
2   **2+Z**2)**3)-IL*(Y-L)*(1+MULT*BETA*SQRT((X-XP)**2+(Y-L)**2+Z**2)
3   )*EXP((-1)*MULT*BETA*SQRT((X-XP)**2+(Y-L)**2+Z**2))/(SQRT((X-X
4   P)**2+(Y+L)**2+Z**2)**3)
      RETURN
      END

```

Subroutine 10

```

      COMPLEX FUNCTION F6(X,Y,Z,YP,L,Z0,ZL,ANS,D,BETA,H,BETA0)
      COMPLEX Z0,ZL,ANS,D,MULT
      REAL L
      MULT=CMPLX(0.0,1.0)
      F6=(Y-YP)*(ANS/D)*(Z0*COS(BETA0*(2*L-YP))+MULT*ZL*SIN(BETA0*(2*L
1   -YP)))/((1+MULT*BETA*SQRT((X+H)**2+(Y-YP)**2+Z**2))*EXP((-1)*
2   MULT*BETA*SQRT((X+H)**2+(Y-YP)**2+Z**2))/(SQRT((X+H)**2+(Y-YP)**
3   2+Z**2)**3)-(1+MULT*BETA*SQRT((X-H)**2+(Y-YP)**2+Z**2))*EXP((-1

```

```

4 )*MULT*BETA*SQRT((X-H)**2+(Y-YP)**2+Z**2))/(SQRT((X-H)**2+(Y-YP)
5 **2+Z**2)**3))
RETURN
END

```

Subroutine 11

```

COMPLEX FUNCTION F7 (X,Y,Z,YP,L,Z0,ZL,ANS,D,BETA,H,BETA0)
COMPLEX Z0,ZL,ANS,D,MULT
REAL L
MULT=CMPLX(0.0,1.0)
F7=(Z)*(ANS/D)*(Z0*COS(BETA0*(2*L-YP))+MULT*ZL*SIN(BETA0*(2*L
1 -YP)))*(1+MULT*BETA*SQRT((X+H)**2+(Y-YP)**2+Z**2))*EXP((-1)*
2 MULT*BETA*SQRT((X+H)**2+(Y-YP)**2+Z**2))/(SQRT((X+H)**2+(Y-YP)**
3 2+Z**2)**3)-(1+MULT*BETA*SQRT((X-H)**2+(Y-YP)**2+Z**2))*EXP((-1
4 )*MULT*BETA*SQRT((X-H)**2+(Y-YP)**2+Z**2))/(SQRT((X-H)**2+(Y-YP)
5 **2+Z**2)**3))
RETURN
END

```

Subroutine 12

```

COMPLEX FUNCTION F8 (X,XP,Y,L,Z,IG,IL,H,BETA)
COMPLEX IG,IL,MULT
REAL L
MULT=CMPLX(0.0,1.0)
F8=IG*Z*(1+MULT*BETA*SQRT((X-XP)**2+(Y+L)**2+Z**2))*EXP((-1)
2 *MULT*BETA*SQRT((X-XP)**2+(Y+L)**2+Z**2))/(SQRT((X-XP)**2+(Y+L)
3 **2+Z**2)**3)-IL*Z*(1+MULT*BETA*SQRT((X-XP)**2+(Y-L)**2+Z**2))
4 *EXP((-1)*MULT*BETA*SQRT((X-XP)**2+(Y-L)**2+Z**2))/(SQRT((X-XP
5 )**2+(Y+L)**2+Z**2)**3)
RETURN
END

```

Subroutine 13

```

COMPLEX FUNCTION F11 (X,Y,Z,XP,YP,IG,BETA,H,L)
COMPLEX IG,MULT
REAL L
MULT=CMPLX(0.0,1.0)
F11=IG*(1+MULT*BETA*SQRT((X-XP)**2+(Y+L)**2+Z**2))*EXP((-1)*
1 MULT*BETA*SQRT((X-XP)**2+(Y+L)**2+Z**2))/(SQRT((X-XP)**2+(Y+L)**
2 2+Z**2)**3)
RETURN
END

```

Subroutine 14

```

COMPLEX FUNCTION F12(X,Y,Z,XP,YP,IL,BETA,H,L)
COMPLEX IL,MULT
REAL L
MULT=CMPLX(0.0,1.0)
F12=IL*(1+MULT*BETA*SQRT((X-XP)**2+(Y-L)**2+Z**2))*EXP((-1)*
1 MULT*BETA*SQRT((X-XP)**2+(Y-L)**2+Z**2))/(SQRT((X-XP)**2+(Y-L)
2 **2+Z**2)**3)
RETURN
END

```

Subroutine 15

```

COMPLEX FUNCTION F9(X,Y,Z,XP,YP,ANS,D,Z0,ZL,BETA,BETA0,L,H)
COMPLEX ANS,D,Z0,ZL,MULT
REAL L
MULT=CMPLX(0.0,1.0)
F9=(ANS/D)*(Z0*COS(BETA0*(2*L-YP))+MULT*ZL*SIN(BETA0*(2*L-YP)))
1 *(1+MULT*BETA*SQRT((X+H)**2+(Y-YP)**2+Z**2))*EXP((-1)*MULT*
2 BETA*SQRT((X+H)**2+(Y-YP)**2+Z**2))/(SQRT((X+H)**2+(Y-YP)**2+Z
3 **2)**3)
RETURN
END

```

Subroutine 16

```

COMPLEX FUNCTION F10(X,Y,Z,XP,YP,ANS,D,Z0,ZL,BETA,BETA0,L,H)
COMPLEX ANS,D,Z0,ZL,MULT
REAL L

```

```

MULT=CMPLX(0.0,1.0)
F10=(ANS/D)*(Z0*COS(BETA0*(2*L-YP))+MULT*ZL*SIN(BETA0*(2*L-YP)))
1 *(1+MULT*BETA*SQRT((X-H)**2+(Y-YP)**2+Z**2))*EXP((-1)*MULT*
2 BETA*SQRT((X-H)**2+(Y-YP)**2+Z**2))/(SQRT((X-H)**2+(Y-YP)**2+
3 Z**2)**3)
RETURN
END

```

END of function subroutines

Subroutine 17

C This Subroutine is to determine the electric field

```

SUBROUTINE BLECF(EX,EY,EZ,ANS,Z0,ZL,ZS,ZIN,L,X,Y,Z,XP,YP,BETA,EPR0
1 ,OMEGA,BETA0,HH,EPR,IG,IL)
EXTERNAL F3,F4,F5,F6,F7,F8
COMPLEX ANS,Z0,ZL,ZS,ZIN,MULT,IG,IL, EX,EY,EZ,D,F1V,F3V,F4V,F2V,
1 F5V,F6V,F7V,F8V
REAL L,MU
C=3.0E8
EPR0=8.854E-12
PI=3.14159
MULT=CMPLX(0.0,1.0)
MU=12.56E-7
H=HH
D=Z0*(ZS+ZL)*COS(BETA0*2*L)+MULT*(Z0*Z0+ZS*ZL)*SIN(BETA0*2*L)
RX1=SQRT(X**2+Y**2+Z**2)
R=C/OMEGA

C FIND EX
CALL EF1V(X,Y,XP,ZL,IG,IL,BETA,H,F1V)
CALL EF3V(F3,X,Y,Z,XP,L,BETA,IG,IL,H,F3V)
CALL EF4V(F4,X,Y,Z,YP,Z0,ZL,BETA,L,H,ANS,D,BETA0,F4V)
EX=-MULT*OMEGA*1/(4*PI)*MU*F1V-(MULT/(OMEGA*EPR0*4*PI))*
1 (F3V+F4V)

C FIND EY
CALL EF2V(X,Y,Z,YP,D,ANS,Z0,ZL,BETA,L,H,BETA0,F2V)
CALL EF5V(F5,X,XP,Y,L,Z,IG,IL,H,BETA,F5V)
CALL EF6V(F6,X,Y,Z,YP,L,Z0,ZL,ANS,D,BETA,H,BETA0,F6V)
EY=-MULT*OMEGA*1/(4*PI)*MU*F2V-(MULT/(OMEGA*EPR0*4*PI))
1 *(F5V+F6V)

C FIND EZ
EZ=CMPLX(0.0,0.0)
CALL EF8V(F8,X,XP,Y,L,Z,IG,IL,H,BETA,F8V)
CALL EF7V(F7,X,Y,Z,YP,L,Z0,ZL,ANS,D,BETA,H,BETA0,F7V)
EZ=-MULT/(OMEGA*EPR0)*(1/(4*PI)*F8V+F7V/(4*PI))
RETURN
END

```

Subroutine 18

```

SUBROUTINE EF1V(X,Y,XP,ZL,IG,IL,BETA,H,F1V)
EXTERNAL F1
COMPLEX IG,IL,SF1V,F1V
REAL L,L1
UL=-H
L1=H
IW=XP
CALL SIMP(F1,X,Y,XP,Z,L,IG,IL,BETA,H,SF1V,IW,UL,L1)
SF1V=F1V
RETURN
END

```

Subroutine 19

```

SUBROUTINE EF3V(F3,X,Y,Z,XP,L,BETA,IG,IL,H,F3V)
COMPLEX IG,IL,F3,F3V1,F3V2,F3V
REAL L
PXP=XP
XP=H
F3V1=F3(X,Y,Z,XP,L,BETA,IG,IL)
XP=-H

```

```

F3V2=F3(X,Y,Z,XP,L,BETA,IG,IL)
F3V=F3V2-F3V1
XP=XP
RETURN
END

```

Subroutine 20

```

SUBROUTINE EF4V (F4,X,Y,Z,YP,Z0,ZL,BETA,L,H,ANS,D,BETA0,F4V)
COMPLEX Z0,ZL,ANS,D,F4V1,F4V2,F4V,F4
REAL L
PYP=YP
YP=L
F4V1=F4(X,Y,Z,YP,Z0,ZL,BETA,L,H,ANS,D,BETA0)
YP=-L
F4V2=F4(X,Y,Z,YP,Z0,ZL,BETA,L,H,ANS,D,BETA0)
F4V=F4V1-F4V2
YP=PYP
RETURN
END

```

Subroutine 21

```

SUBROUTINE EF2V (X,Y,Z,YP,D,ANS,Z0,ZL,BETA,L,H,BETA0,F2V)
EXTERNAL F2
REAL L
COMPLEX D,ANS,Z0,ZL,F2V,S
UL=L
L1=-L
IW=YP
CALL SIMP1 (F2,X,Y,Z,YP,D,ANS,Z0,ZL,BETA,L,H,BETA0,S,UL,L1,IW)
F2V=S
RETURN
END

```

Subroutine 22

```

SUBROUTINE EF5V(F5,X,XP,Y,L,Z,IG,IL,H,BETA,F5V)
COMPLEX IG,IL,F5V,F5V1,F5V2,F5
REAL L
XP5P=XP
XP=H
F5V1=F5(X,XP,Y,L,Z,IG,IL,H,BETA)
XP=-H
F5V2=F5(X,XP,Y,L,Z,IG,IL,H,BETA)
F5V=F5V2-F5V1
XP=XP5P
RETURN
END

```

Subroutine 23

```

SUBROUTINE EF6V (F6,X,Y,Z,YP,L,Z0,ZL,ANS,D,BETA,H,BETA0,F6V)
COMPLEX Z0,ZL,ANS,D,F6V,F6V1,F6V2,F6
REAL L
PIYP=YP
YP=L
F6V1=F6(X,Y,Z,YP,L,Z0,ZL,ANS,D,BETA,H,BETA0)
YP=-L
F6V2=F6(X,Y,Z,YP,L,Z0,ZL,ANS,D,BETA,H,BETA0)
F6V=F6V1-F6V2
YP=PIYP
RETURN
END

```

Subroutine 24

```

SUBROUTINE EF8V (F8,X,XP,Y,L,Z,IG,IL,H,BETA,F8V)
COMPLEX IG,IL,F8V,F8,F8V1,F8V2
REAL L
XP8P=XP
XP=H
F8V1=F8(X,XP,Y,L,Z,IG,IL,H,BETA)
XP=-H

```

```

F8V2=F8(X,XP,Y,L,Z,IG,IL,H,BETA)
F8V=F8V2-F8V1
XP=XP8P
RETURN
END

```

Subroutine 25

```

SUBROUTINE EF7V (F7,X,Y,Z,YP,L,Z0,ZL,ANS,D,BETA,H,BETA0,F7V)
COMPLEX Z0,ZL,ANS,D ,F7V1,F7V2,F7V,F7
REAL L
P2YP=YP
YP=L
F7V1=F7(X,Y,Z,YP,L,Z0,ZL,ANS,D,BETA,H,BETA0)
YP=-L
F7V2=F7(X,Y,Z,YP,L,Z0,ZL,ANS,D,BETA,H,BETA0)
F7V=F7V1-F7V2
YP=P2YP
RETURN
END

```

Subroutine 26

C This Subroutine is used to compute the magnetic field

```

SUBROUTINE HFIELD(HX,HY,IZ,ANS,Z0,ZL,ZS,L,X,Y,Z,XP,YP,BETA
1 ,OMEGA,BETA0,HH,IG,IL)
EXTERNAL F9,F10,F11,F12
COMPLEX HX,HY,HZ,ANS,Z0,ZL,ZS,IG,IL,D,F9V,F10V,F11V,F12V
REAL L,MU
PI=3.14159
MU=12.56E-7
H=HH
D=Z0*(ZS+ZL)*COS(BETA0*2*L)+MULT*(Z0*Z0+ZS*ZL)*SIN(BETA0*2*L)
UL=L
L1=L
IW=YP
CALL SIMP1 (F9,F10,X,Y,Z,XP,YP,Z0,ZL,ANS,D,BETA,BETA0,H,L,F9V,F10V, UL,L1,IW)
HX=(Z/(4.*PI))*(F9V-F10V)
UL=H
L1=H
IW=XP
CALL SIMP1 (F11,F12,X,Y,Z,XP,YP,IG,IL,BETA,BETA0,H,L,F11V,F12V,UL,L1,IW)
HY=(Z/(4.*PI))*(F12V-F11V)
HZ=((X-H)*F10V-(X+H)*F9V+(Y+L)*F11V-(Y-L)*F12V)/(4.*PI)
WRITE(*,*) HX,HY,HZ
RETURN
END

```

Subroutine 26

C THIS SUBROUTINE IS USED FOR INTEGRATION BY SIMPSON'S RULE

```

SUBROUTINE SIMP(F,X,Y,Z,YP,D,ANS,Z0,ZL,BETA,L,H,BETA0,S,UL,L1,IW)
COMPLEX Z0,ZL,SUMS11,SUMS22,SUMS1,SUMS2,F,VA1,VA2,ANS,D,S
REAL YP,DELH,L
INTEGER M
A=L1
B=UL
PPYP=IW
WRITE(5,*) 'A,B'
DELH=(B-A)/64.
WRITE(*,*) 'DELH,M'
WRITE(*,*) A,B,DELH
SUMS11=CMPLX(0.0,0.0)
SUMS22=CMPLX(0.0,0.0)
DO 50 I=1,32
YYP=A+(2*I-1)*DELH
SUMS11=SUMS11+F(X,Y,Z,YP,D,ANS,Z0,ZL,BETA,L,H,BETA0)
50 CONTINUE
SUMS1=4.*SUMS11
DO 51 I= 1,31
YYP=A+2*I*DELH
SUMS22=SUMS22+F(X,Y,Z,YP,D,ANS,Z0,ZL,BETA,L,H,BETA0)
51 CONTINUE

```

```

SUMS2=2.*SUMS22
YYP=A
VA1=F(X,Y,Z,YY,D,ANS,ZO,ZL,BETA,L,H,BETA0)
YYP=B
VA2=F(X,Y,Z,YY,D,ANS,ZO,ZL,BETA,L,H,BETA0)
S=DELH*(VA1+SUMS1+SUMS2+VA2)/3.0
IW=PPYP
WRITE(*,*)S
RETURN
END

```

Subroutine 27

```

SUBROUTINE SIMP1 (FUNC1,FUNC2,X,Y,Z,XP,YP,IG,IL,BETA,BETA0,H,L,S1V
1 ,S2V, UL, L1,IW)
COMPLEX IG,IL,SFUMS11,SFUMS22,SFUMS1,SFUMS2,VFA1,VFA2,F11V
1 ,SFSUMS11,SFSUMS22,SFSUMS1,SFSUMS2,VSFA1,VSFA2,F12V,FUNC1, FUNC2
REAL XP,DELH2,L,AA,BB
INTEGER N
AA=UL
BB=L1
PPXP1=IW
DELH2=(BB-AA)/64.
WRITE(*,*) AA,BB,DELH2
N=32
SFUMS11=CMPLX(0.0,0.0)
SFUMS22=CMPLX(0.0,0.0)
SFSUMS11=CMPLX(0.0,0.0)
SFSUMS22=CMPLX(0.0,0.0)
DO 50 I=1,32
XXP=AA+(2*I-1)*DELH2
SFUMS11=SFUMS11+FUNC1(X,Y,Z,XXP,YP,IG,BETA,H,L)
SFSUM11=SFSUMS11+FUNC2(X,Y,Z,XXP,YP,IL,BETA,H,L)
50 CONTINUE
SFUMS1=4.*SFUMS11
SFSUMS1=4.*SFSUMS11
DO 51 I= 1,31
XXP=AA+2*I*DELH2
SFUMS22=SFUMS22+FUNC1(X,Y,Z,XXP,YP,IG,BETA,H,L)
SFSUMS22=SFSUMS22+FUNC2(X,Y,Z,XXP,YP,IL,BETA,H,L)
51 CONTINUE
SFUMS2=2.*SFUMS22
SFSUMS2=2.*SFSUMS22
XXP=AA
VFA1=FUNC1(X,Y,Z,XXP,YP,IG,BETA,H,L)
VSFA1=FUNC2(X,Y,Z,XXP,YP,IL,BETA,H,L)
XXP=BB
VFA2=FUNC1(X,Y,Z,XP,YP,IG,BETA,H,L)
VSFA2=FUNC2(X,Y,Z,XP,YP,IL,BETA,H,L)
S1V=DELH2*(VFA1+SFUMS1+SFUMS2+VFA2)/3.0
S2V=DELH2*(VSFA1+SFSUMS1+SFSUMS2+VSFA2)/3.0
IW=PPXP1
RETURN
END

```

D9: RADIATED ELECTRIC FIELDS DUE TO DISPLACEMENT CURRENT

The formulation to compute the radiated electric field due to displacement current is described in chapter 4. A computer programme listing is given here. A few subroutines are also listed here. The other subroutines have been given in appendix D8.

```

C*****
C Computation of radiated electric field due to displacement current
C*****

      DIMENSION ATST(2)
      COMMON /LOAD2/ R1,C,RS,CS,LI,LS,Z0,ZS,ZIN,ZL,CP
      COMMON /PCB/ L,W,HH,HT,EPR1
      COMMON /EXCT3/ FR,OMEGA,BETA0,BETA.VS
      COMMON /PULSE1/ ANS,VG,TR,TF,T,TAU
      COMMON /CURR/ IG,IL,I1,I2,ID
      COMMON /WIRE1/ DELY,NS,NW
      COMMON /FLDC/ X,Y,Z
      COMMON /RFIELD/ EXD,EYD,EZD,EPR
      COMMON /SOURCE/ XDP,YDP,ZDP,JI
      DIMENSION XDP(40),YDP(40),ZDP(40),ID(40)
      COMPLEX Z0,ZL,ZIN,ZS,ANS,VS,MULT,IG,IL,I1,I2,VG,EXD,EYD,EZD,ID
      ,EX,EY,EZ
1     REAL L,MU,LS,MUR,OMEGA,LI
      INTEGER AIN,ATST
      DATA ATST /1HR,1HS/
      PI=3.141592654
      MULT=CMPLX(0.0,1.0)
      IFLAG=0
      OPEN(UNIT=1,STATUS='OLD',FILE='TLMPCB1.DAT')
      OPEN(UNIT=2,STATUS='OLD',FILE='PULSE1.DAT')
      OPEN(UNIT=6,STATUS='OLD',FILE='FLDPC1.DAT')
      OPEN(UNIT=7,STATUS='OLD',FILE='DEVICE1.DAT')
      OPEN (UNIT=3, STATUS='UNKNOWN',FILE='DISTLM.OUT')
      OPEN (UNIT=4, STATUS='UNKNOWN', FILE='DISTLMP.OUT')
      OPEN (UNIT=5, STATUS='UNKNOWN',FILE='DHFLD.OUT')
      OPEN (UNIT=8,STATUS='UNKNOWN',FILE='DEF2.DAT')
      OPEN (UNIT=9,STATUS='UNKNOWN',FILE='DHF2.DAT')

C     READ LAYOUT DATA OF A PCB
C     HT=THICKNESS OF THE DIELECTRIC SHEET

80    READ(1,*) L,HH,W,EPR1,MUR,MU,HT,EPR0
      READ(1,*) XP,YP
      WRITE(*,*) 'NWS,NS'
      READ (*,*) NWS,NS
      CALL SCR
      DELY=2*L/NS
      READ(7,*) RS,CS,R1,C,LI,LS

C     X,Y,Z = CO-ORDINATE OF THE FIELD OBSERVATION POINT
C     IX,IY,IZ=NO OF OBSERVATION POINTS IN THE X,Y AND Z CO-ORDINATE RESPECTIVELY.
C     DIX,DIY,DIZ= INCREMENT OF X,Y AND Z CO-ORDINATE RESPECTIVELY.

      CALL ZEPCB(EPR2,RZ0,CPP)
      EPR=EPR2
      CP=CPP
      Z0=CMPLX(RZ0,0.0)
      WRITE(*,8) Z0
8     FORMAT(/CHARACTERISTIC IMPEDANCE Z0 =,2X,2F10.5)

C     READ EXCITATION DATA

      READ(2,*) VR,TAU,T,TR
      VS=CMPLX(VR,0.0)
      WRITE (*,*) 'NTH HARMONIC'
      READ (*,*) NN
      CALL PULSE(NN)
      BETA0=((2.*PI*FR)/300.)*SQRT(EPR*MUR)

```

```

OMEGA=2*PI*FR*1.0E+6
CALL TPARA
CALL DCURRENT

C BEGINNING OF ROUTINE TO CALCULATE ELECTRIC FIELD COMPONENT

WRITE(3,137)
137 FORMAT(///15X,'ELECTRIC FIELD CALCULATION')
WRITE(3,145) NN, FR
145 FORMAT(10X,'NN =',I3,5X,'FREQUENCY=',F10.5)
WRITE(3,138)
138 FORMAT(///X',5X,'Y',5X,'Z',10X,'E')
WRITE(3,139)
139 FORMAT(24X,'MAG',6X,'ANGLE')
BETA=BETA0/(SQRT(EPR*MUR))

WRITE(*,*) 'TYPES OF CO-ORDINATE SYSTEM '
READ(*,700) AIN
700 FORMAT(A1)
WRITE(*,*) 'XOB,YOB,ZOB,IXOB,IYOB,IZOB,DIXOB,DIYOB,DIZOB'
READ(*,*) XOB,YOB,ZOB,IXOB,IYOB,IZOB,DIXOB,DIYOB,DIZOB

C SAVE THE INITIAL VALUE OF FIELD POINTS

XI=XOB
YI=YOB
ZI=ZOB
DO 62 II = 1,IXOB
XOB=XI+(II-1)*DIXOB
DO 60 KK = 1,IYOB
YOB=YI+(KK-1)*DIYOB
DO 61 JJ = 1,IZOB
ZOB=ZI+(JJ-1)*DIZOB
IF (AIN .EQ. ATST(1)) THEN
X=XOB
Y=YOB
Z=ZOB
R=SQRT(X*X+Y*Y+Z*Z)
IF(Z .EQ. 0) THEN
THETA=PI/2
ELSE
THETA=ATAN(SQRT(X*X+Y*Y)/Z)
END IF
IF(X .EQ. 0.0) THEN
PHI=PI/2.0
ELSE
PHI=ATAN(Y/X)
END IF
ELSE
R=XOB
THETA=YOB*PI/180
PHI=ZOB*PI/180
X=R*SIN(THETA)*COS(PHI)
Y=R*SIN(THETA)*SIN(PHI)
Z=R*SIN(THETA)
END IF
EX=CMLPX(0.0,0.0)
EY=CMLPY(0.0,0.0)
EZ=CMLPZ(0.0,0.0)
DO 200 J=1,NS-1
J=J
CALL DELECTF
EX=EX+EXD
EY=EY+EYD
EZ=EZ+EZD
200 CONTINUE

E=SQRT((CABS(EX))**2+(CABS(EY))**2+(CABS(EZ))**2)
EDB=20*LOG10(E*1.0E+6)
WRITE(*,*) EDB
WRITE(3,136) X,Y,Z, E
136 FORMAT(F5.2,2X,F6.2,2X,F6.2,2X,E10.5)
WRITE(4,400) EX,EY,EZ
400 FORMAT(1X,6(1X,E12.3))
WRITE(3,*) EDB
RTHETA=THETA*180./PI
WRITE(8,*) RTHETA,EDB
61 CONTINUE
60 CONTINUE

```



```

62  CONTINUE
    WRITE(*,*) 'FLAG'
    READ(*,*) IFLAG
    IF(IFLAG .EQ. 0) GO TO 37
    REWIND 1
    REWIND 2
    REWIND 6
    REWIND 7
    GO TO 80
37  STOP
    END

```

Subroutine 1

C This routine is used to compute the displacement current

```

SUBROUTINE DCURRENT
COMMON /LOAD2/ R1,C,RS,CS,LI,LS,Z0,ZS,ZIN,ZL,CP
COMMON /PCB/ L,W,HH,HT,EPR1
COMMON /EXCI3/ FR,OMEGA,BETA0,BETA,VS
COMMON /PULSE1/ ANS,VG,TR,TF,T,TAU
COMMON /CURR/ IG,IL,I1,I2,ID
COMMON /WIRE1/ DELY,NS,NW
DIMENSION ID(40)
COMPLEX ZIN,ZL,ZS,Z0,MULT,ID,VS
COMPLEX IG,IL,I1,I2,ANS,DD,VG,DC
REAL L,LI,LS,OMEGA
MULT=CPLX(0.0,1.0)
DC=Z0*(ZL+ZS)*COS(BETA0*L*2)+MULT*(Z0*Z0+ZS*ZL)*SIN(BETA0*2*L)
VG=ANS*ZIN/(ZS+ZIN)
WRITE(*,103)
103  FORMAT(/18X,'REAL',20X,'IMAG',17X,'MAGNITUDE')
    WRITE(*,*) 'CP',DELY,CP
    DO 90 II=1,NS
    Y=DELY*II-DELY/2.0
    YD=DELY*II
    IF(II .EQ. NS) GO TO 90

c    ID = Displacement current

    ID(II)= MULT*OMEGA*CP*DELY*.5*ANS*Z0*(ZL*COS(BETA0*(2*L-YD))+MULT*Z0*
1    SIN(BETA0*(2*L-YD)))/DC
    WRITE(*,*) YD,ID(II)
90  CONTINUE
    RETURN
    END

```

BEGINNING OF FUNCTION SUBROUTINE

Subroutine 2

```

COMPLEX FUNCTION FD1 (RD)
COMMON /PCB/ L,W,HH,HT,EPR1
COMMON /EXCI3/ FR,OMEGA,BETA0,BETA,VS
COMMON /CURR/ IG,IL,I1,I2,ID
COMMON /SOURCE/ XDP,YDP,ZDP,JI
COMMON /FLDC/ X,Y,Z
DIMENSION ID(40),XDP(40),YDP(40),ZDP(40)
COMPLEX ID,IG,IL,I1,I2,MULT,VS
REAL L,OMEGA
MULT=CPLX(0.0,1.0)
PI=3.14159
FD1=ID(JI)*2*HH*EXP((-1)*MULT*BETA*RD)/(4*PI*RD)
WRITE(5,*) 'FD1',FD1,RD,BETA
RETURN
END

```

Subroutine 3

```

COMPLEX FUNCTION FD2(RD)
COMMON /PCB/ L,W,HH,HT,EPR1
COMMON /EXCI3/ FR,OMEGA,BETA0,BETA,VS
COMMON /CURR/ IG,IL,I1,I2,ID
COMMON /SOURCE/ XDP,YDP,ZDP,JI
COMMON /FLDC/ X,Y,Z

```

```

DIMENSION ID(40),XDP(40),YDP(40),ZDP(40)
COMPLEX ID,IG,IL,I1,I2,MULT,VS
REAL L,OMEGA
MULT=CMPLX(0.0,1.0)
PI=3.14159
FD2=(X-XDP(JI))**2*(1+MULT*BETA*RD)*(MULT*BETA)/(RD**3)+(X-XDP(JI)
1) **2*(3+MULT*2*BETA*RD)/(RD**4)-(1+MULT*BETA*RD)/RD**2
WRITE(5,*) FD2,FD2,RD,BETA
RETURN
END

```

Subroutine 4

```

COMPLEX FUNCTION FD3(RD)
COMMON /PCB/L,W,HH,HT,EPR1
COMMON /EXCI3/FR,OMEGA,BETA0,BETA,VS
COMMON /CURR/IG,IL,I1,I2,ID
COMMON /SOURCE/ XDP,YDP,ZDP,JI
COMMON /FLDC/ X,Y,Z
DIMENSION ID(40),XDP(40),YDP(40),ZDP(40)
COMPLEX ID,IG,IL,I1,I2,MULT,VS
REAL L,OMEGA
MULT=CMPLX(0.0,1.0)
PI=3.14159
FD3=(1+MULT*BETA*RD)/(RD**3)+(3+MULT*2*BETA*RD)/(RD**4)
WRITE(5,*)FD3,FD3,RD,BETA
RETURN
END

```

END OF FUNCTION SUBROUTINE

Subroutine 5

C This routine is used to find the source co-ordinate i.e. co-ordinate of displacement current element

```

SUBROUTINE SCR
COMMON /PCB/L,W,HH,HT,EPR1
COMMON /SOURCE/ XDP,YDP,ZDP,JI
COMMON /WIRE1/ DELY,NS,NW
DIMENSION XDP(40),YDP(40),ZDP(40)
REAL L
Y1=L
Y2=L
X1=HH
X2=-HH
YDP(1)=Y1+(Y2-Y1)/(NS)
DO 100 I=1,NS
XDP(I)=X1+(X2-X1)/2
ZDP(I)=0.0
100 CONTINUE
DO 101 J=1,NS-2
YDP(J+1)=YDP(1)+(Y2-Y1)*J/NS
101 CONTINUE
WRITE(*,*) (YDP(J),J=1,NS)
RETURN
END

```

Subroutine 6

C This subroutine is for computing the radiated electric field due to displacement current

```

SUBROUTINE DELECF
COMMON /LOAD2/ R1,C,RS,CS,LI,LS,Z0,ZS,ZIN,ZL,C1
COMMON /PCB/L,W,HH,HT,EPR1
COMMON /EXCI3/FR,OMEGA,BETA0,BETA,VS
COMMON /PULSE1/ ANS,VG,TR,TF,T,TAU
COMMON /CURR/IG,IL,I1,I2,ID
COMMON /SOURCE/ XDP,YDP,ZDP,JI
COMMON /FLDC/ X,Y,Z
COMMON /RFIELD/ EXD,EYD,EZD,EPR
DIMENSION XDP(40),YDP(40),ZDP(40),ID(40)
EXTERNAL FD1,FD2,FD3
COMPLEX ANS,Z0,ZL,ZS,ZIN,MULT,IG,IL,ID,EXD,EYD,EZD,I1,I2,VG,VS,
1 FD1,FD2,FD3
REAL L,MU,OMEGA
CV=3.0E+08
EPR0=8.854E-12

```

```
PI=3.14159
MULT=CMPLX(0.0,1.0)
MU=12.56E-7
H=H#1
```

```
C COMPUTE EX COMPONENT
```

```
RD=SQRT((X-XDP(JI))**2+(Y-YDP(JI))**2+(Z-ZDP(JI))**2)
XSAV=RD
EXD=-MULT*OMEGA*MU*FD1(XSAV)-MULT*FD1(XSAV)*FD2(XSAV)/(OMEGA*
1 8.854E-12)
```

```
C COMPUTE EY COMPONENT
```

```
EYD=-MULT*(X-XDP(JI))*(Y-YDP(JI))*FD1(XSAV)*FD3(XSAV)/(OMEGA*
1 8.854E-12)
```

```
C COMPUTE EZ COMPONENT
```

```
EZD=-MULT*(X-XDP(JI))*(Z-ZDP(JI))*FD1(XSAV)*FD3(XSAV)/(OMEGA*
1 8.854E-12)
RETURN
END
```

E1: BATCH ROUTINE

The function of this routine is to link all the circuit design packages and the EM computation tool. A listing of this routine is given below. All commands are MSDOS¹ command.

Listing of batch routine

```

ECHO OFF
REM *****
REM * WRITTEN BY P.K.SAHA
REM * THIS FILE EXECUTE ALL THE
REM * PROGRAMS TO PREDICT AND MINIMISE THE EM RADIATION
REM * FROM A PCB
REM *****
If exist COMPS.DAT erase COMPS.DAT
cls
time
:LOOP2
ECHO DESIGN THE CIRCUIT SCHEMATIC

call draft %1.cir /c

ECHO PREPARE THE NETLIST
call netlist %1.cir comv.dat tango/s
call netlist %1.cir spice.net spice/s /c

:LOOP1

ECHO DESIGN THE PCB LAYOUT, GENERATE A POSTSCRIPT FILE AND COMPONENT LIST

call Bm

ECHO EXTRACT THE GEOMETRICAL AND LOAD DATA

call d:\fortran\bin\VLDE
ECHO PREPARE AN INPUT FILE FOR PSPICE
edit SPICE.NET
call c:\cad\SIFNU

ECHO PERFORMME THE CIRCUIT SIMULATION

CALL c:\cad\NPSPICE.BAT

```

¹Microsoft Disk Operating System

ECHO EXTRACT THE ELECTRICAL DATA

call D:\FORTRAN\BIN\VEDR

ECHO COMPUTE EM RADIATION FROM A PCB, COMPARE PREDICTED FIELD WITH THE ECHO STANDARD, REQUESTS FOR SHIELDING, SET FLAG TO MODIFY THE DESIGN

call c:\cad\somnec

call d:\fortran\bin\vecPC

ECHO MINIMISE THE EM RADIATION WHERE NECESSARY

If exist COMPS.DAT goto LOOP

exit

:LOOP

If exist MPCB.DAT erase MPCB.DAT

If exist DCIR.DAT erase DCIR.DAT

Call c:\cad\RMFF.EXE

If exist MPCB.DAT goto LOOP1

If exist DCIR.DAT goto LOOP2

cls

exit

ECHO OFF

E2: COMPUTER PROGRAMME LISTING OF IFGR

The function of this routine is to prepare an input file for PSPICE. The algorithm is described in the main text (section 5.3.2.1). The computer programme listing is given below.

Computer programme listing

```
C *****
C      THIS ROUTINE IS USED TO CREATE A INPUT FILE
C      FROM NETLIST , NODE DATA AND OUTPUT OPTIONS FOR
C      ANALOG CIRCUIT SIMULATOR PACKAGE LIKE PSPICE.
C *****
C      DIMENSION ATST(20),MODT(10),DMOD(10),NODE(10),SPIN1(2),SPIN2(2)
C      INTEGER ATST,AIN,SN,SVAL,PIN1,PIN2,PIN3,SFREQ,RVAL,MODT
C      1 _DMOD,TYPE,BFV,V1,V2,DCV,TSTEP,TSTOP,FREQ,
C      2 SPIN1,SPIN2,UN,CMP,RB,RC,TR1,VA
C      REAL TF1,CJC,CJE,CCS,BR,TD,TR,TF,PW,PER

C      NS=NO OF INPUT SIGNAL
C      SVAL= SIGNAL VALUE
C      S=SOURCE IS SINUSIOD
C      P=SOURCE IS PULSE
C      CMP=CHANGE THE DEFAULT MODEL PARAMETER

C      OPEN(UNIT=1,STATUS='OLD',FILE='D:\ORCAD\SPICE.NET')
C      OPEN(UNIT=3,STATUS='UNKNOWN',FILE='SPICE.CIR')
C      OPEN(UNIT=2,STATUS='OLD',FILE='BJT.MOD')
C      OPEN(UNIT=4,STATUS='OLD',FILE='TXND.DAT')
C      DATA ATST/1HV,1HR,1HC,1HL,1HQ,1HU,1HD,2HCC,2HBE,1H 3HZEN,1HS,
C      1 1HP,2HFO,2HTR,2HAC,2H ,1HJ,1HM,2HEN/
```

```

WRITE(3,1000)
1000 FORMAT('TEST.CIR')
C   READ DATA FROM FILE CREATED BY ORCAD

100 READ(1,10) AIN
10  FORMAT(A1)
   IF(AIN.EQ.ATST(10)) GO TO 101
   IF(AIN.EQ.ATST(1)) GO TO 40
   IF(AIN.EQ.ATST(2)) GO TO 42
   IF(AIN.EQ.ATST(5)) GO TO 43
   IF(AIN.EQ.ATST(3)) GO TO 44
   IF(AIN.EQ.ATST(4)) GO TO 45
   IF(AIN.EQ.ATST(7)) GO TO 46
   IF(AIN.EQ.ATST(6)) GO TO 300
   GO TO 100

C   BEGINING OF ROUTINE TO REPLACE A CRYSTAL OSSCILATOR BY A
C   TRAPEZODIAL PULSE INPUT TO THE CIRCUIT

300 BACKSPACE 1
   READ(1,5001) PIN1,PIN2
5001 FORMAT(6X,I2,3X,I2)
   WRITE(*,*) 'ENTER PULSE FUNCTION(V1,V2,TD,TR,TF,PW,PER)'
   READ(*,*) V1,V2,TD,TR,TF,PW,PER
   WRITE(*,*) 'UNIT OF TIME IN NS, US, MS'
   READ(*,5002) UN
5002 FORMAT(A1)
   WRITE(3,580) PIN2,PIN1,V1,V2,TD,UN,TR,UN,TF,UN,PW,UN,PER,UN
580  FORMAT('VIN1',1X,I2,1X,I2,1X,'PULSE',12,1X,I2,1X,F7.3,A1,1X,F7.3
1    ',A1,1X,F7.3,A1,1X,F7.3,A1,1X,F7.3,A1')
   GO TO 100

C   END OF REPLACEMENT

40  BACKSPACE 1
   READ(1,11) AIN
11  FORMAT(1X,A2)
   IF(AIN.EQ.ATST(8)) GO TO 41
   IF(AIN.EQ.ATST(9)) GO TO 41
   BACKSPACE 1
   NS=NS+1
   READ(1,12) SN,PIN1,PIN2,TYPE
12  FORMAT(3X,I1,3X,I2,3X,I2,1X,A1)
   SPIN1(NS)=PIN1
   SPIN2(NS)=PIN2
   IF(TYPE.EQ.ATST(12)) THEN
   WRITE(*,*) 'ENTER AMPLITUDE AND FREQUENCY OF SINUSOID INPUT
1 AND UNIT'
   READ(*,*) SVAL,SFREQ
   READ(*,302) UN
302  FORMAT(A3)
   WRITE(3,30) SN,PIN1,PIN2,SVAL,SFREQ,UN
30  FORMAT('VIN1',3X,I2,3X,I2,1X,I2,'V',1X,I3,A3)
   ELSE IF(TYPE.EQ.ATST(13)) THEN
   WRITE(*,*) 'ENTER PULSE FUNCTION(V1,V2,TD,TR,TF,PW,PER)'
   READ(*,*) V1,V2,TD,TR,TF,PW,PER
   WRITE(*,*) 'UNIT OF TIME IN NS, US, MS'
   READ(*,301) UN
301  FORMAT(A1)
   WRITE(3,80) SN,PIN1,PIN2,V1,V2,TD,UN,TR,UN,TF,UN,PW,UN,PER,UN
80  FORMAT('VIN1',1X,I2,1X,I2,1X,'PULSE',12,1X,I2,1X,F7.3,A1,1X,F7.3
1    ',A1,1X,F7.3,A1,1X,F7.3,A1,1X,F7.3,A1')
   ELSE
   WRITE(*,*) 'ENTER THE DC VALUE'
   READ(*,*) DCV
   WRITE(3,81) SN,PIN1,PIN2,DCV
81  FORMAT('VIN1',3X,I2,3X,I2,1X,I2,'DC')
   END IF
   GO TO 100
41  BACKSPACE 1
   READ(1,13) SN,PIN1,PIN2
13  FORMAT(1X,A2,4X,I2,1X,I1)
   WRITE(*,*) 'DC VOLTAGE TO TRANSISTORS'
   READ(*,*) PVAL
   WRITE(3,31) SN,PIN1,PIN2,PVAL
31  FORMAT('V',A2,4X,I2,1X,I1,1X,F5.1)
   GO TO 100
42  BACKSPACE 1
   READ(1,14) SN,PIN1,PIN2,RVAL

```

```

14 FORMAT(1X,I2,3X,I2,3X,I2,1X,I4)
   IF(SN .LT. 10) THEN
   WRITE(3,32)SN,PIN1 ,PIN2,R VAL
32 FORMAT('R'I1,3X,I2,3X,I2,1X,I4)
   ELSE
   WRITE(3,62)SN,PIN1 ,PIN2,R VAL
62 FORMAT('R'I2,3X,I2,3X,I2,1X,I4)
   END IF
   GO TO 100
43 BACKSPACE 1
   READ(1,15)SN,PIN1 ,PIN2,PIN3
15 FORMAT(1X,I2,3X,I2,3X,I2,3X,I2)
   BACKSPACE 1
   READ(1,19)MODT(SN)
19 FORMAT(19X,A3)
   NT=NT+1
   IF(SN .LT. 10) THEN
   WRITE(3,33)SN,PIN1 ,PIN2,PIN3,MODT(SN)
33 FORMAT('Q'I1,1X,I2,1X,I2,1X,I2,1X,A3)
   ELSE
   WRITE(3,63)SN,PIN1 ,PIN2,PIN3,MODT(SN)
63 FORMAT('Q'I2,1X,I2,1X,I2,1X,I2,1X,A3)
   END IF
   GO TO 100
44 BACKSPACE 1
   READ(1,16) SN,PIN1 ,PIN2,C VAL
16 FORMAT(1X,I2,3X,I2,3X,I2,1X,I3)
   WRITE(3,34) SN,PIN1 ,PIN2,C VAL
34 FORMAT('C',I2,3X,I2,3X,I2,3X,I2,1X,I3)
   GO TO 100
45 BACKSPACE 1
   READ(1,17) SN,PIN1 ,PIN2,L VAL
17 FORMAT(1X,I2,3X,I2,3X,I2,1X,I3)
   WRITE(3,35) SN,PIN1 ,PIN2,C VAL
35 FORMAT('C',I2,3X,I2,3X,I2,3X,I2,1X,I3)
   GO TO 100
46 BACKSPACE 1
   READ(1,18) SN,PIN1 ,PIN2
18 FORMAT(1X,I2,3X,I2,3X,I2)
   ND=ND+1
   BACKSPACE 1
   READ(1,23) DMOD(SN)
23 FORMAT(14X,A3)
   IF(SN .LT. 10) THEN
   WRITE(3,36)SN,PIN1 ,PIN2,DMOD(SN)
36 FORMAT('D',I1,3X,I2,3X,I2,1X,A3)
   ELSE
   WRITE(3,66)SN,PIN1 ,PIN2,DMOD(SN)
66 FORMAT('D',I2,3X,I2,3X,I2,1X,A3)
   END IF
   GO TO 100
101 WRITE(*,*)'ENTER THE MODEL PARAMETER '

C CHECK FOR TRANSISTORS

   NTM=0
   IF(NT .EQ. 0) GO TO 102
107 NTM=NTM+1

C ENTER THE MODEL PARAMETER FOR BJT
C BFV=VALUE OF IDEAL MAXIMUM FORWARD BETA

   IF (NTM .EQ. 1) GO TO 104
   DO 50 I =1,NTM-1
   IF(MODT(I) .EQ. MODT(NTM)) FLAG=1
50 CONTINUE
   IF (FLAG .EQ. 1) GO TO 105
104 WRITE(*,*) 'ENTER THE TYPE OF TRANSISTORS I.E. BJT, FET OR MOS'
   READ(*,303) TYPE
303 FORMAT(A1)
   IF(TYPE .EQ. ATST(18)) THEN
   WRITE(*,*) 'TYPE OF THE JFET'
   READ(*,21)TYPE
21 FORMAT(A3)
   WRITE(3,51)MODT(NTM),TYPE
51 FORMAT('MODEL'1X,A3,1X,A3)
   ELSE IF(TYPE .EQ. ATST(19)) THEN
   WRITE(*,*) 'THE TYPE OF MOSFET'
   READ(*,304) TYPE

```

```

304 FORMAT(A4)
WRITE(3,305)MODT(NTM),TYPE
305 FORMAT('MODEL'1X,A3,1X,A4)
ELSE
WRITE(*,*) 'THE TYPE OF BJT'
READ(*,306) TYPE
306 FORMAT(A3)
WRITE(*,*) 'DO YOU WANT TO CHANGE THE DEFAULT MODEL PARAMETER SET
1 CMP=1 IF YES '
READ(*,*) CMP
IF(CMP.NE. 1) GO TO 501
READ(2,601) BFV,BR,RB,RC,TF1,TR1,CJE,CJC,CCS,VA
601 FORMAT(I3,F3.1,I2,I2,F3.1,I2,F3.1,F3.1,F3.1,I2)
WRITE(3,507)MODT(NTM),TYPE,BFV,BR,RB,RC,TF1,TR1
507 FORMAT('MODEL'1X,A3,1X,A3,'(BF='I3,1X,'BR='F3.1,1X,'RB='I2,1X,
1 RC='I2,1X,'TF='F3.1,'N' 1X,'TR='I2,'N')
WRITE(3,508)CJE,CJC,CCS,VA
508 FORMAT('+'1X,'CJE='F3.1,'P'1X,'CJC='F3.1,'P'1X,'CCS='F3.1,'P'
1 1X,'VA='I2,')
GO TO 509
501 WRITE(*,*) 'BFV'
READ(*,*) BFV
WRITE(3,510)MODT(NTM),TYPE,BFV
510 FORMAT('MODEL'1X,A3,1X,A3,'(BF='I3 ')')
509 CONTINUE
END IF
105 FLAG=0
IF(NTM.GE. NT) GO TO 102
GO TO 107

C ENTER THE DIODE MODEL PARAMETER

102 NDM=0
IF(ND.EQ. 0) GO TO 109
116 NDM=NDM+1
IF (NDM.EQ. 1) GO TO 114
DO 70 I=1,NDM-1
IF(DMOD(I).EQ. DMOD(NDM)) FLAG=1
70 CONTINUE
IF (FLAG.EQ. 1) GO TO 115
114 WRITE(*,*) 'ENTER THE TYPE OF DIODE'
READ(*,22) TYPE
22 FORMAT(A3)
IF(TYPE.EQ. ATST(11)) THEN
WRITE(*,*) 'REVERSE BREAKDOWN VOLTAGE AND CURRENT OF DIODE '
READ(*,*)BV,IBV
WRITE(3,71)DMOD(NDM),BV,IBV
71 FORMAT('MODEL'1X,A3,1X,'D','(BV='F3.1,'IBV='I2 'M)')
ELSE
WRITE(3,72)DMOD(NDM)
72 FORMAT('MODEL'1X,A3,1X,'D')
END IF
115 FLAG=0
IF(NDM.GE. ND) GO TO 109
GO TO 116
109 WRITE(*,*) 'ENTER THE TYPE OF CIRCUIT ANALYSIS'
READ(*,82)TYPE
82 FORMAT(A2)
IF(TYPE.EQ. ATST(15)) GO TO 90
IF(TYPE.EQ. ATST(16)) GO TO 91
IF(TYPE.EQ. ATST(14)) GO TO 92
IF(TYPE.EQ. ATST(17)) GO TO 93
WRITE(*,*) 'NO ANALYSIS'
STOP
90 TFLAG=1
WRITE(*,*)'ENTER THE DATA FOR TRANSIENT ANALYSIS(UNIT IN
1 N,U,M, TSTEP,TSTOP)'
READ(*,310) UN
310 FORMAT(A1)
READ(*,*)TSTEP,TSTOP
WRITE(3,83)TSTEP,UN,TSTOP,UN
83 FORMAT('TRAN'1X,I2,A1,1X,I4,A1)
GO TO 109
92 IF(TFLAG.NE. 1) GO TO 94
WRITE(*,*) 'ENTER THE DATA FOR FOURIER ANALYSIS(FREQUENCY,NODE)'
READ(*,*)FREQ
WRITE(*,*) 'ENTER THE UNIT OF FREQUENCY'
READ(*,308)UN
308 FORMAT(A3)

```



```

4004 READ(4,4001)AIN
4001 FORMAT(A2)
      IF(AIN.EQ.ATST(20)) GO TO 94
      BACKSPACE 4
      READ(4,4002)NOD
4002 FORMAT(I2)
      WRITE(3,96) FREQ,UN,NOD
96   FORMAT('FOUR'1X,I3,A3,1X,'V(',I2,')')
      GO TO 4004
94   GO TO 109
91   WRITE(*,*) 'ENTER THE DATA FOR AC ANALYSIS(NP,FSTART,FSTOP)'
      NA=NA+1
      READ(*,*)NP,FSTART,FSTOP
      WRITE(*,*) 'ENTER THE UNIT OF FREQUENCY'
      READ(*,309)UN
309  FORMAT(A3)
      WRITE(3,99)NP,FSTART,UN,FSTOP,UN
99   FORMAT('AC'1X,LIN'1X,I2,1X,I2,A3,1X,I3,A3)
      GO TO 109
93   WRITE(*,*) 'ENTER THE OUTPUT OPTIONS FOR ANALYSIS'
      READ(*,200)TYPE
200  FORMAT(A2)
      IF(TYPE.EQ.ATST(15)) GO TO 201
      IF(TYPE.EQ.ATST(17)) GO TO 204
      IF(TYPE.EQ.ATST(14)) GO TO 401
201  CONTINUE
      DO 210 I=1,NF
      IF(I.EQ.1)THEN
      WRITE(3,202) SPIN1(NS),SPIN2(NS)
202  FORMAT('PRINT'1X,TRAN'1X,'V(',I2,',',I2,')')
      ELSE
      WRITE(3,203)NODE(I)
203  FORMAT('PRINT'1X,TRAN'1X,'V(',I2,')')
      END IF
210  CONTINUE
      GO TO 93
401  REWIND 4
410  READ(4,4010) AIN
4010 FORMAT(A2)
      IF(AIN.EQ.ATST(20)) GO TO 204
      BACKSPACE 4
      READ(4,4011) NOD
4011 FORMAT(I2)
      WRITE(3,402) NOD
402  FORMAT('PRINT'1X,FOUR'1X,'V(',I2,')')
      GO TO 410
      GO TO 93
204  WRITE(3,205)
205  FORMAT('END')
      END

```

E3: COMPUTER PROGRAMME LISTING FOR EXTRACTION OF GEOMETRICAL AND LOAD DATA

A schematic of the 16 pin DIL socket is shown in Fig E3-1.

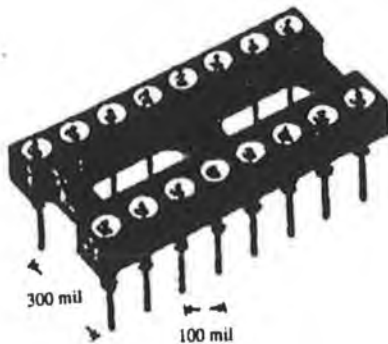


Fig. E3-1 Schematic of 16 pin DIL.

COMPUTER PROGRAMME LISTING

The algorithm to extract the geometrical and load data of a PCB is described in the main text. The developed algorithm has been implemented using a Fortran programme LDER. The computer programme listing for the LDER is given below. All the subroutines called by this routine are also listed here.

Main programme LDER

```
C *****
C ROUTINE TO EXTRACT LAYOUT DATA OF A PCB FROM OUTFILE (POSTSCRIPT) OF LAYOUT TOOL (BM 2.3)
C *****

      DIMENSION C(100,5),X(100,2),Y(100,2),W(100),XX(100,2),YY(100,2)
1     ,PCX(10,16),PCY(10,16),PX(10,16),PY(10,16),ATST(10),PADX(50)
2     ,PADY(50),PADXX(50),PADYY(50),GWX(100,2),GWY(100,2),GWZ(100,2)
3     ,RW(100),NP(20),PERV(20),PELV(20),PECV(20),U(20),TW(100),GW(100)
4     ,RLC(20),PADD(50),TCX(10,3),TCY(10,3),DX(4,2),DY(4,2),VX(2,2)
5     ,VY(2,2),TNEC(20),NODE(20),Z(100,2),LDX1(2,10),LDX2(2,10),LDY1
6     (2,10),LDY2(2,10),RPADX(50),RPADY(50),RGW(100),TTNEC(20)

      INTEGER C,PIN1,ATST,PCX,PCY,EF,PADXX,PADYY,CH1,U,TNS,TWN3,GW,
1     PERV,ND2,PADD,TCX,TCY,DX,DY,VX,VY,PADX,PADY,TNEC,AIN,S0,RPADX
2     ,RPADY,TTNEC,RGW
      REAL LDX1,LDX2,LDY1,LDY2
      DATA ATST/1HR,4Hshow,1Hh,1HL,1HC,1HR,2HEN,1HD,4H%%Tr,4H%%Eo /

C N=no of Track segment
C X(N,1)= X-CO-ORDINATE OF END 1 OF NTH TRACK SEGMENT = C(N,1)
C X(N,2)= X-CO-ORDINATE OF END 2 OF NTH TRACK SEGMENT = C(N,3)
C Y(N,1)= Y-CO-ORDINATE OF END 1 OF NTH TRACK SEGMENT = C(N,2)
C Y(N,2)= Y-CO-ORDINATE OF END 2 OF NTH TRACK SEGMENT = C(N,4)
C W(N)= WIDTH OF THE NTH TRACK SEGMENT=C(N,5)
C NS=NO OF ICS ON THE PCB
C NP(NS)=NO OF PINS OF NSth IC
C PX(NS,NP)= X-CO-ORDINATE OF NPth PIN OF NSth IC
C PY(NS,NP)= Y-CO-ORDINATE OF NPth PIN OF NSth IC
C PIN1=FLAG TO FIND THE IC ON THE PCB
C EF=FLAG FOR END OF OUTPUTFILE OF A LAYOUT TOOL(BM)
C NPD=NO OF PAD
C PADX(NPD)= X-CO-ORDINATE OF NPDth PAD
C PADY(NPD)= Y-CO-ORDINATE OF NPDth PAD
C RX(NR,J)= X-CO-ORDINATE OF Jth END OF NRth RESISTANCE
C RY(NR,J)= Y-CO-ORDINATE OF Jth END OF NRth RESISTANCE
C LX(NL,J)= X-CO-ORDINATE OF Jth END OF NLth INDUCTANCE
C LY(NL,J)= Y-CO-ORDINATE OF Jth END OF NLth INDUCTANCE
C CX(NC,J)= X-CO-ORDINATE OF Jth END OF Ncth CAPACITANCE
C CY(NC,J)= Y-CO-ORDINATE OF Jth END OF Ncth CAPACITANCE

      OPEN (UNIT=1,STATUS='OLD',FILE='LAYOUT.DAT')
      OPEN (UNIT=3,STATUS='UNKNOWN',FILE='LOAD.DAT')
      OPEN (UNIT=50,STATUS='OLD',FILE='LAYOUT1.DAT')
      OPEN(UNIT=6,STATUS='UNKNOWN',FILE='GEMDN.DAT')
      OPEN(UNIT=70,STATUS='UNKNOWN',FILE='EXND.DAT')
      OPEN(UNIT=4,STATUS='UNKNOWN',FILE='EXND1.DAT')

C SKIPS FIRST 36 LINES OF THE OUTPUT FILE(POSTSCRIPT) OF LAYOUT TOOL(BM)

      NF=0
      NS=0
      DO 800 I=1,20
        NP(I)=0
800    CONTINUE
        IC=1
        NPD=0
        WRITE(*,*) 'THE LAYER NO'
        READ(*,*) LAYER
8001   CONTINUE
        IF(LAYER.EQ. 1) THEN
          READ(1,2)
2     FORMAT(38(/))
```

```

READ(1,6000) (C(1,J),J=1,5)
6000 FORMAT(14,6X,14,6X,14,6X,14,6X,BN,13)
WRITE(*,*) (C(1,J),J=1,5)

C CHECK FOR TERMINATION OF SEGMENTATION DATA

ELSE IF(LAYER .EQ. 2) THEN
READ(50,522)
522 FORMAT(38(/))
READ(50,56000) (C(1,J),J=1,5)
56000 FORMAT(14,6X,14,6X,14,6X,14,6X,BN,13)
END IF
N=2
IF(LAYER .EQ. 1) THEN
60 READ(1,20) CH1
20 FORMAT(28X,A1)

C CHECK FOR STARTING OF PASSIVE COMPONENT(R,L,C ETC)

IF(CH1 .EQ. ATST(3)) GO TO 555
WRITE(*,1000) CH1
1000 FORMAT(1X,A1)

C CHECK FOR STARTING OF SYMBOLS(ICs)

BACKSPACE 1
BACKSPACE 1
READ(1,21) CH1
21 FORMAT(36X,A1)
IF(CH1 .EQ. ATST(1)) GO TO 556
BACKSPACE 1
READ(1,3) C(N,3)
3 FORMAT(20X,BN,13)
T=C(N,3)/1000.0
IF(T .LT. .1) GO TO 50
BACKSPACE 1
WRITE(*,*) 'PROGRAM IS RUNNING'
READ(1,4) (C(N,J),J=1,5)
4 FORMAT(14,6X,14,6X,14,6X,14,6X,BN,13)
WRITE(*,6) (C(N,J),J=1,5)
6 FORMAT(14,2X,14,2X,14,2X,14,2X,13)
N=N+1
IF(N .GE. 500) GO TO 500
GO TO 60

C BEGINNING OF ROUTINE TO FIND PIN (DIP14,16,18 ...) CO-ORDINATE OF ICs
ON THE PCB

50 CONTINUE
556 BACKSPACE 1
BACKSPACE 1

100 READ(1,700) EF
700 FORMAT(/A4)
IF(EF .EQ. ATST(2)) GO TO 702
BACKSPACE 1
READ(1,80) PIN1
80 FORMAT( 36X,A1)
WRITE(*,103) PIN1
103 FORMAT(1X,A1)
IF(PIN1 .NE. ATST(1)) GO TO 90
NS=NS+1
IC=NS
NP(IC)=1
BACKSPACE 1
READ(1,82) PCX(NS,NP(IC)),PCY(NS,NP(IC))
82 FORMAT(14,6X,14)
I=NS
J=NP(IC)
WRITE(*,*) I,J, PCX(I,J),PCY(I,J)
PX(I,J)=PCX(I,J)
PY(I,J)=PCY(I,J)
WRITE(*,*) 'SYMBOL',NS
GO TO 100
BACKSPACE 1
IC=NS
NP(IC)=NP(IC)+1
READ(1,83) PCX(NS,NP(IC)),PCY(NS,NP(IC))
83 FORMAT(14,6X,14)

```

```

DIFPX=PCX(NS,NP(IC))-PCX(NS,NP(IC)-1)
DIFPY=PCY(NS,NP(IC))-PCY(NS,NP(IC)-1)
IF(DIFPX .EQ. 0 .OR. DIFPY .EQ. 0) THEN
I=NS
J=NP(IC)
PX(I,J)=PCX(I,J)
PY(I,J)=PCY(I,J)
WRITE(*,*) I,J, PX(I,J),PY(I,J)
GO TO 100
END IF
NP(IC)=NP(IC)-1
GO TO 703
702 NP(IC)=NP(IC)
WRITE(4,*) (NP(IC),IC=1,NS)
GO TO 304
703 WRITE(*,*) (NP(IC),IC=1,NS)

C END OF ROUTINE TO FIND PIN CO-ORDINATE

C BEGINNING OF ROUTINE TO FIND THE PAD POSITION

GO TO 557
555 BACKSPACE 1
557 BACKSPACE 1
BACKSPACE 1

301 READ(1,23) EF
23 FORMAT(/A4)
WRITE(*,679) EF
679 FORMAT(1X,A4)
IF(EF .EQ. ATST(2)) GO TO 304
IF(EF .EQ. ATST(9)) GO TO 300
IF(EF .EQ. ATST(10)) GO TO 300
BACKSPACE 1
READ(1,200) PIN1
200 FORMAT(36X,A1)
WRITE(*,678) PIN1
678 FORMAT(1X,A1)
IF(PIN1 .EQ. ATST(1)) GO TO 556
BACKSPACE 1
NPDD=NPDD+1

READ(1,201) PADXX(NPDD),PADYY(NPDD)
201 FORMAT(14,6X,I4)
READ(1,901) PADD(NPDD)
901 FORMAT(20X,I2)
BACKSPACE 1
GO TO 301
304 IF(NPDD .EQ. 0 .OR. DIFPX .EQ. 0) GO TO 300
NPDD=NPDD+1
BACKSPACE 1
BACKSPACE 1
READ(1,203) PADXX(NPDD),PADYY(NPDD)
203 FORMAT(14,6X,I4)

300 WRITE(*,*) 'END OF FILE'
IF (NPDD .EQ. 0) GO TO 701
WRITE(*,*) 'NEW OPTION'
701 CONTINUE

C END OF EXTRACTION OF LAYOUT DATA FOR LAYER 1
C SAVE THE SEGMENT CO-ORDINATE
C COMPUTE THE END CO-ORDINATE OF THE NTH TRACK SEGMENT
C ORIGIN (0,0) IS BOTTOM LEFT CORNER OF THE BOARD
C UNIT IN METER

M=N-1
DO 70 I=1,M
X(I,1)=C(I,1)
X(I,2)=C(I,3)
Y(I,1)=C(I,2)
Y(I,2)=C(I,4)
W(I)=C(I,5)
Z(I,1)=1.0E-6
Z(I,2)=1.0E-6
70 CONTINUE

C END OF ROUTINE TO READ THE END CO-ORDINATES OF TRACK'S SEGMENTS FOR LAYER 1

```

```

DO 72 I=1,M
WRITE(*,*) W(I)
72 CONTINUE

C   END OF ROUTINE TO READ THE WIDTH OF TRACK'S SEGMENTS FOR LAYER 1

DO 400 I=1,M
DO 401 J=1,2
XX(I,J)=X(I,J)
YY(I,J)=Y(I,J)
WRITE(*,*) XX(I,J),YY(I,J)
401 CONTINUE
400 CONTINUE
N=M

C   BEGINNING OF ROUTINE TO FIND THE TRACK CONNECTED TO THE COMPONENT AND

C   NT=THE TRACK NO WHICH IS CONNECTED TO THE Pth PIN OF NSth IC
C   P=PIN NO OF THE NSth IC
C   IC=TAG NO OF IC

C   BEGINING OF ROUTINE FOR LAYER 2

ELSE IF(LAYER .EQ. 2) THEN
260 READ(50,520) CH1
520 FORMAT(28X,A1)

C   CHECK FOR STARTING OF PASSIVE COMPONENT(R,L,C ETC)

IF(CH1 .EQ. ATST(3)) GO TO 2555
WRITE(*,21000) CH1
21000 FORMAT(1X,A1)

C   CHECK FOR STARTING OF SYMBOLS(ICs)

BACKSPACE 50
BACKSPACE 50
READ(50,521) CH1
521 FORMAT(36X,A1)
IF(CH1 .EQ. ATST(1)) GO TO 2556
BACKSPACE 50
READ(50,53) C(N,3)
53 FORMAT(20X,BN,I3)
T=C(N,3)/1000.0
IF(T .LT. .1) GO TO 22500
BACKSPACE 50
WRITE(*,*) 'PROGRAM IS RUNNING'
READ(50,54) (C(N,J),J=1,5)
54 FORMAT(14,6X,I4,6X,I4,6X,I4,6X,I4,6X,BN,I3)
WRITE(*,26) (C(N,J),J=1,5)
26 FORMAT(14,2X,I4,2X,I4,2X,I4,2X,I3)
N=N+1
IF(N .GE. 500) GO TO 500
GO TO 260

22500 CONTINUE
2556 BACKSPACE 50
BACKSPACE 50

2100 READ(50,5700) EF
5700 FORMAT(A4)
IF(EF .EQ. ATST(2)) GO TO 2702

BACKSPACE 50
READ(50,580) PIN1
580 FORMAT(36X,A1)
WRITE(*,2103) PIN1
2103 FORMAT(1X,A1)
IF(PIN1 .NE. ATST(1)) GO TO 290
NS=NS+1
IC=NS
NP(IC)=1
BACKSPACE 50
READ(50,582) PCX(NS,NP(IC)),PCY(NS,NP(IC))
582 FORMAT(14,6X,I4)
I=NS
J=NP(IC)
WRITE(*,*) I,J, PCX(I,J),PCY(I,J)

```

```

        PX(I,J)=PCX(I,J)
        PY(I,J)=PCY(I,J)
        WRITE(*,*) 'SYMBOL',NS
        GO TO 2100
290  BACKSPACE 50
        IC=NS
        NP(IC)=NP(IC)+1
        READ(50,583) PCX(NS,NP(IC)),PCY(NS,NP(IC))
583  FORMAT(14,6X,14)

        DIFPX=PCX(NS,NP(IC))-PCX(NS,NP(IC)-1)
        DIFPY=PCY(NS,NP(IC))-PCY(NS,NP(IC)-1)
        IF(DIFPX .EQ. 0 .OR. DIFPY .EQ. 0) THEN
            I=NS
            J=NP(IC)
            PX(I,J)=PCX(I,J)
            PY(I,J)=PCY(I,J)
            WRITE(*,*) I,J, PX(I,J),PY(I,J)
            GO TO 2100
        END IF
        NP(IC)=NP(IC)-1
        GO TO 2703
2702 NP(IC)=NP(IC)
        WRITE(*,*) (NP(IC),IC=1,NS)
        GO TO 2304
2703 WRITE(*,*) (NP(IC),IC=1,NS)

C     END OF ROUTINE TO FIND PIN CO-ORDINATE OF IC FOR LAYER 2

C     BEGINNING OF ROUTINE TO FIND THE PAD POSITION FOR LAYER 2

        GO TO 2557
2555 BACKSPACE 50
2557 BACKSPACE 50
        BACKSPACE 50

2301 READ(50,523) EF
523  FORMAT(A4)
        IF(EF .EQ. ATST(2)) GO TO 2304
        BACKSPACE 50
        READ(50,5200) PIN1
5200 FORMAT(36X,A1)
        IF(PIN1 .EQ. ATST(1)) GO TO 2556
        BACKSPACE 50
        NPDD=NPDD+1
        READ(50,5201) PADXX(NPDD),PADYY(NPDD)
5201 FORMAT(14,6X,14)
        READ(50,5901) PADD(NPDD)
5901 FORMAT(20X,I2)
        BACKSPACE 50
        WRITE(*,*) NPDD,PADD(NPDD)
        GO TO 2301
2304 IF(NPDD .EQ. 0 .OR. DIFPX .EQ. 0) GO TO 2300
        NPDD=NPDD+1
        BACKSPACE 50
        BACKSPACE 50
        READ(50,5203) PADXX(NPDD),PADYY(NPDD)
5203 FORMAT(14,6X,14)

2300 WRITE(*,*) 'END OF FILE'
        IF (NPDD .EQ. 0) GO TO 2701
        WRITE(*,*) 'NEW OPTION'
2701 CONTINUE

C     END OF EXTRACTION OF LAYOUT DATA FOR LAYER 2

C     SAVE THE SEGMENT CO-ORDINATE FOR LAYER 2

C     COMPUTE THE END CO-ORDINATE OF THE NTH TRACK SEGMENT
C     ORIGIN (0,0) IS BOTTOM LEFT CORNER OF THE BOARD
C     UNIT IN METER
        M=N-1
        DO 270 I=1,M
            X(I,1)=C(I,1)
            X(I,2)=C(I,3)
            Y(I,1)=C(I,2)
            Y(I,2)=C(I,4)
            W(I)= C(I,5)

```

```

      Z(I,1)=-1.445E-3
      Z(I,2)=-1.445E-3
270  CONTINUE

C END OF ROUTINE TO READ THE END CO-ORDINATES OF TRACK'S SEGMENTS

      DO 22400 I=1,M
      DO 22401 J=1,2
      XX(I,J)=X(I,J)
      YY(I,J)=Y(I,J)
      WRITE(*,*) XX(I,J),YY(I,J)
22401 CONTINUE
22400 CONTINUE
      N=M
      END IF

C BEGINNING OF ROUTINE TO IDENTIFY THE COMPONENT

      CALL TDSP1(PADXX,PADYY,PADD,TCX,TCY,DX,DY,NT,ND,NPDD,PADX,PADY,VX,
1      VY,NPD,RPADX,RPADY)

C BEGINNING OF ROUTINE TO FIND THE NET DATA FROM PCB

      CALL COMV1(PERV,PELV,PECV,U,NRR,NLL,NCC,NII,NTS,NVCC,NGND)

C BEGINNING OF ROUTINE TO FIND THE TRACK WHICH IS CARRYING THE CLOCK OR RF SIGNAL AND ALSO TO FIND THE
C LOADED TRACK

      CALL STC1(XX,YY,PX,PY,M,NS,NP,W,TNS,TWN3,NPD,PADX,PADY,PERV,PELV
1      ,PECV,LW,TCX,TCY,NT,VX,VY,DX,DY,RPADX,RPADY)

C FIND THE NODE AND THE CO-ORDINATE OF THE TRACK
      WRITE(24,2409)
2409 FORMAT('EN')
      REWIND 24
2406 READ(24,2400)AIN
2400 FORMAT(A2)
      IF(AIN.EQ.ATST(7)) GO TO 2401
      BACKSPACE 24
      ND=ND+1
      READ(24,2402)TNEC(ND),NODE(ND)
2402 FORMAT(I2,1X,I2)
      IF(ND.EQ.1) GO TO 2403
      DO 2404 I=1,ND-1
      IF(NODE(ND).EQ.NODE(I)) THEN
      NFLAG=1
      END IF
2404 CONTINUE
      IF(NFLAG.EQ.1) GO TO 2405

2403 WRITE(70,2408) NODE(ND),TNEC(ND)
2408 FORMAT(I2,1X,I2)
2405 NFLAG=0
      GO TO 2406
2401 WRITE(70,2420)
2420 FORMAT('EN')
      REWIND 20
      REWIND 23

C FORMATING AND PREPARING INPUT FILES FOR GEOMETRICAL AND LOAD DATA FOR NEC PROGRAM
C T=THICKNESS OF THE TRACK
C FOR ONE OUNCE COPPER CLADDING , T=1.38 MILs
C FOR TWO OUNCE COPPER CLADDING , T=2.76 MILs

      S0=0
      T=.035E-3
      NF=TNS+TWN3
      WRITE(6,2000)NF
2000 FORMAT(I2)
      DO 450 I=1,TNS
      READ(20,451) GW(I),GWX(I,1),GWX(I,2),GWY(I,1),GWY(I,2)
451 FORMAT(I2,2X,F10.5,F10.5,2X,F10.5,F10.5)
      II=GW(I)

      TW(I)=W(II)*0.0254/1000.0

C COMPUTE THE RADIUS OF SIMULATED PCB TRACK ( ROUND WIRE)

```

```

RW(I)=.335*TW(I)*(8+T/TW(I))

C CONVERT THE TRACK CO-ORDINATE IN METERS

DO 452 J=1,2
GWX(I,J)=GWX(I,J)*.0254/1000
GWY(I,J)=GWY(I,J)*.0254/1000
GWZ(I,J)=Z(I,J)

452 CONTINUE
IJ=I
IF(GWX(I,1).EQ. GWX(I,2).AND. GWY(I,1).EQ. GWY(I,2)) THEN
S0=S0+1
ELSE
IJ=IJ-S0

C SAVE THE ORIGINAL TAG NUMBER OF THE SIMULATED TRACK

RGW(I)=IJ
WRITE(6,453) IJ,(GWX(I,J),J=1,2),(GWY(I,J),J=1,2),(GWZ(I,J),J=1,2)
1 ,RW(I)
453 FORMAT('G',I2,2X,7(1X,F10.6))
END IF
450 CONTINUE

DO 460 I=1,TWN3
READ(23,461) GW(I),GWX(I,1),GWX(I,2),GWY(I,1),GWY(I,2)
461 FORMAT(I2,2X,F10.5,F10.5,2X,F10.5,F10.5)
II=GW(I)
TW(I)=W(II)*0.0254/1000.0
RW(I)=.335*TW(I)*(8+T/TW(I))
DO 462 J=1,2
GWX(I,J)=GWX(I,J)*.0254/1000
GWY(I,J)=GWY(I,J)*.0254/1000
GWZ(I,J)=Z(II,J)
462 CONTINUE
JJ=TNS+I
IF(GWX(I,1).EQ. GWX(I,2).AND. GWY(I,1).EQ. GWY(I,2))THEN
S0=S0+1
ELSE
JJ=JJ-S0
WRITE(6,454) JJ,(GWX(I,J),J=1,2),(GWY(I,J),J=1,2),(GWZ(I,J),J=1,2)
1 ,RW(I)
454 FORMAT('G',I2,2X,7(1X,F10.6))
END IF
460 CONTINUE

C FORMATING THE LOAD TRACK FOR NEC

REWIND 28
DO 610 I=1,LW
GW(I)=TNS+TWN3+I
J=GW(I)
READ(28,601) ND2,GWX(J,1),GWX(J,2),GWY(J,1),GWY(J,2),RLC(I)
601 FORMAT(A1,2X,F10.5,2X,F10.5,2X,F10.5,2X,F10.5,2X,F10.6)
TW(J)=W(I)*0.0254/1000.0
IF(TW(J).EQ. 0) GO TO 611
RW(J)=.335*TW(J)*(8+T/TW(J))
GWZ(J,1)=Z(J,1)
GWZ(J,2)=Z(J,2)
GWX(J,1)=GWX(J,1)*0.0254/1000.0
GWX(J,2)=GWX(J,2)*0.0254/1000.0
GWY(J,2)=GWY(J,2)*0.0254/1000.0
GWY(J,1)=GWY(J,1)*0.0254/1000.0
LDX1(LAYER,D)=GWX(J,1)
LDX2(LAYER,D)=GWX(J,2)
LDY1(LAYER,D)=GWY(J,1)
LDY2(LAYER,D)=GWY(J,2)
IF(LAYER.EQ. 1) GO TO 8002
GWZ(J,1)=0.001445
GWZ(J,2)=0.001445
DLIFFX1=LDX1(1,I)-LDX1(2,I)
DLIFFX2=LDX2(1,I)-LDX2(2,I)
DLIFFY1=LDY1(1,I)-LDY1(2,I)
DLIFFY2=LDY2(1,I)-LDY2(2,I)
IF(DLIFFX1.EQ. 0.AND. DLIFFX2.EQ. 0.AND. DLIFFY1.EQ. 0
1 .AND. DLIFFY2.EQ. 0) GO TO 610
8002 JL=J-S0
WRITE(6,605) JL,GWX(J,1),GWX(J,2),GWY(J,1),GWY(J,2),GWZ(J,1),GWZ

```



```

1 (J,2),RW(I)
605 FORMAT('G',I2,2X,7(1X,F10.6))
IF(ND2 .EQ. ATST(6)) GO TO 602
IF(ND2 .EQ. ATST(4)) GO TO 603
IF(ND2 .EQ. ATST(5)) GO TO 604
GO TO 600
602 LD TYP=0
WRITE(3,612) LD TYP,J,RLC(I)
612 FORMAT('L',I2,I3,10X,E12.7)
GO TO 610
603 LD TYP=0
WRITE(3,613) LD TYP,J,RLC(I)
613 FORMAT('L',I2,I3,22X,E12.7)
GO TO 610
604 LD TYP=0
WRITE(3,614) LD TYP,J,RLC(I)
614 FORMAT('L',I2,I3,34X,E12.7)
GO TO 610
611 S0=S0+1
610 CONTINUE
WRITE(3,615)
615 FORMAT(//)

C ROUTINE TO FIND THE TRACK WHICH HAS EXCITATION
IT=0
REWIND 70
911 READ(70,900) AIN
900 FORMAT(A2)
IF(AIN .EQ. ATST(7)) GO TO 920
BACKSPACE 70
IT=IT+1
READ(70,901) NOD,TTNEC(IT)
9011 FORMAT(I2,1X,I2)
REWIND 20
DO 921 I=1,TNS
READ(20,925) GW(I)
925 FORMAT(I2)
IF(TTNEC(IT) .EQ. GW(I)) THEN
WRITE(*,*) TTNEC(IT), GW(I)
TTNEC(IT)=RGW(I)
WRITE(4,912) NOD, TTNEC(IT)
912 FORMAT(I2,1X,I2)
GO TO 911
END IF
921 CONTINUE
920 WRITE(4,922)
922 FORMAT('EN')

C CHECK FOR SINGLE SIDED OR DOUBLESIDED PCB

WRITE(*,*) 'PCB IS SINGLE OR DOUBLE SIDED'

8000 READ(*,8000) AIN
FORMAT(A1)
IF(AIN .NE. ATST(8)) GO TO 600
LAYER=2
M=0
N=0
NF=NF+TNS+TWN3+LW
TNS=0
TWN3=0
NPD=0
NS=0
NP=0
NVCC=0
NGND=0
REWIND 10
REWIND 14
REWIND 20
REWIND 24
REWIND 23
REWIND 21
REWIND 22
REWIND 26
REWIND 27
REWIND 28
LW=0
NR=0
GO TO 8001

```

```

500 WRITE(*,*) 'NO OF TRACKS SEGMENT MORE THAN 500'
600 WRITE(6,999)
999 FORMAT(/)
STOP
END

```

SUBROUTINES

Subroutine 1

```

C *****
C THIS SUBROUTINE IS CALLED BY LDER TO IDENTIFY THE COMPONENTS SUCH AS RESISTOR,
C INDUCTOR, CAPACITOR, DIODE, TRANSISTOR AND SIGNAL GENERATOR
C *****
SUBROUTINE TDSP(PADXX,PADYY,PADD,TCX,TCY,DX,DY,NT,ND,NPDD,PADX,
1 PADY,VX,VY,NFD)

DIMENSION PADXX(50),PADYY(50),TCX(10,3),TCY(10,3),DX(4,2),DY(4,2),
1 VX(2,2),VY(2,2),PADD(50),PADX(20),PADY(20),PADX1(10),PADY1(10)

INTEGER PADXX,PADYY,TCX,TCY,DX,DY,VX,VY,PADD,PADX,PADY

C NT=NO OF TRANSISTOR
C ND=NO OF DIODE
C NV=NO OF SIGNAL
C DEFAULT PAD INNER DIAMETER FOR FIXING TRANSISTOR IS 27 THOU
C DEFAULT PAD INNER DIAMETER FOR FIXING DIODE IS 27
C DEFAULT AXIAL LENGTH FOR DIODE IS 300 THOU
C DEFAULT PAD INNER DIAMETER FOR COMPONENTS(C,L,R) IS 31 THOU
C DEFAULT AXIAL LENGTH FOR COMPONENTS IS 400 THOU
C DEFAULT PAD INNER DIAMETER AND AXIAL LENGTH FOR SIGNAL IS 31 AND
C 500 THOU

NT=0
NV=0
ND=0
NF=1
NNPD=0
100 I=NF
IF(PADD(I) .EQ. 27) THEN
IF(ABS(PADXX(I)-PADXX(I+1)).EQ. 300 .OR. ABS(PADYY(I)-PADYY(I+1))
1 .EQ. 300) GO TO 101
IF(ABS(PADXX(I)-PADXX(I+1)).NE. 200) GO TO 108
NT=NT+1
TCX(NT,1)=PADXX(I)
TCX(NT,3)=PADXX(I+2)
TCX(NT,2)=PADXX(I+1)
TCY(NT,1)=PADYY(I)
TCY(NT,3)=PADYY(I+2)
TCY(NT,2)=PADYY(I+1)
NF=NF+3
WRITE(*,*)(TCX(NT,J),J=1,3),(TCY(NT,J),J=1,3)
GO TO 102
101 ND=ND+1
DX(ND,1)=PADXX(I)
DX(ND,2)=PADXX(I+1)
DY(ND,1)=PADYY(I)
DY(ND,2)=PADYY(I+1)
NF=NF+2
WRITE(*,*)(DX(ND,J),J=1,2),(DY(ND,J),J=1,2)
102 CONTINUE
ELSE IF(PADD(I) .EQ. 31) THEN
IF(ABS(PADXX(I)-PADXX(I+1)) .EQ. 400 .OR. ABS(PADYY(I)-PADYY(I+1))
1 .EQ. 400) GO TO 104
NV=NV+1
VX(NV,1)=PADXX(I)
VX(NV,2)=PADXX(I+1)
VY(NV,1)=PADYY(I)
VY(NV,2)=PADYY(I+1)
NF=NF+2
WRITE(*,*)(VX(NV,J),J=1,2),(VY(NV,J),J=1,2)
GO TO 105
104 NPDD=NNPD+1
PADX(NPDD)=PADXX(I)
PADY(NPDD)=PADYY(I)
PADX(NPDD+1)=PADXX(I+1)

```

```

PADY(NPD+1)=PADYY(I+1)
NNPD=NPV+1
WRITE(*,*) NPD, NNPD,PADX(NPD),PADX(NPD+1),PADY(NPD),PADY(NPD+1)
NF=NF+2
105 CONTINUE
ELSE IF(PADD(I) .EQ. 23) THEN
NF=NF+1
END IF
GO TO 110
108 NPV=NPV+1
PADX1(NPV)=PADXX(I)
PADY1(NPV)=PADYY(I)
NF=NF+1
110 ITER=ITER+1
IF(ITER .GE. NPDD) GO TO 106
GO TO 100
106 NPV=NNPD+NPV
DO 111 I=1, NPV
PADX(I+NNPD)=PADX1(I)
PADY(I+NNPD)=PADY1(I)
111 CONTINUE
DO 112 I=1, NPD
WRITE(*,*) I,PADX(I), PADY(I)
112 CONTINUE
WRITE(50,*) 'END OF TDSP'
RETURN
END

```

Subroutine 2

```

C *****
C THIS ROUTINE IS USED TO FIND THE TYPE AND VALUE OF PASSIVE ELEMENTS,
C THE TYPE OF ACTIVE ELEMENT, AND NET DATA
C *****

SUBROUTINE COMV (PERV,PELV,PECV,U,NRR,NLI,NCC,NII,NTS,NVCC,NGND)
DIMENSION PERV(20),PECV(20),PELV(20),BN(13),U(20),Q(10),VIN(10)
1 ,D(10),BECN(5)
INTEGER BF,BN,BE,AIN,BND,PERV,LIC,U,ND1 ,PIN,NI)2,BEC,BECN,QT,PINQ,
1 VN,DN

DATA BECN/2HCO,2HEM,2HBA,2HAN,2HCA/
DATA BF/1H/
DATA BE/0/
DATA BND/1H/
DATA BN/1HC,1HL,1HR,1HU,1HS,1HF,1HC,1HN,1HV,1HG,1H),1HQ,1HD/

C NR=NO OF RESISTANCE
C NL=NO OF INDUCTANCE
C NC=NO OF CAPACITANCE
C NIC=NO OF IC
C NQ=NO OF TRANSISTORS
C ND=NO OF DIODE
C NVIN=NO OF INPUT SIGNAL

NR=0
NL=0
NICT=0
NICC=0
NC=0
NODE=0
NVC=0
NGN=0
NCC=0
NRR=0
NLL=0
NQ=0
ND=0
NVIN=0
QT=0
VN=0
DN=0

C BF=BEGINNING OF NET DATA
C BE=END OF NET FILE
C BND=BEGINING OF COMPONENT

```

```

OPEN(UNIT=10, STATUS='OLD', FILE='COMV.DAT')
OPEN(UNIT=14, STATUS='UNKNOWN', FILE='NET.DAT')
1 READ(10,30)AIN
30 FORMAT(BZ,A1)
IF(AIN.EQ.0) THEN
WRITE(*,15) AIN
15 FORMAT(1X,I1)
END IF
WRITE(*,16) AIN
16 FORMAT(1X,A1)
IF(AIN.EQ.BF) GO TO 60
IF(AIN.EQ.BND) GO TO 70
IF(AIN.EQ.BE) GO TO 80
CONTINUE
GO TO 80

C BEGINNING OF ROUTINE TO FIND THE COMPONENTS AND ITS VALUE

60 READ(10,31) AIN
31 FORMAT(A1)
IF(AIN.EQ.BN(1)) GO TO 61
IF(AIN.EQ.BN(2)) GO TO 62
IF(AIN.EQ.BN(3)) GO TO 63
IF(AIN.EQ.BN(4)) GO TO 64
IF(AIN.EQ.BN(12)) GO TO 180
IF(AIN.EQ.BN(9)) GO TO 181
IF(AIN.EQ.BN(13)) GO TO 182
GO TO 1
12 READ(10,33)
33 FORMAT(4(/))
GO TO 1

C READ THE VALUE OF CAPACITANCE

61 NCC=NCC+1
READ(10,32) PECV(NCC)
32 FORMAT(F10.6)
GO TO 12

C READ THE VALUE OF INDUCTANCE

62 NLL=NLL+1
READ(10,34) PELV(NLL)
34 FORMAT(F10.6)
GO TO 12

C READ THE VALUE OF RESISTANCE

63 BACKSPACE 10
READ(10,630) NRN
630 FORMAT(1X,I2)
IF (NRN.LT. 10) THEN
BACKSPACE 10
READ(10,631) NRN
631 FORMAT(2X,I1)
END IF
NRR=NRR+1
READ(10,35) PERV(NRN)
35 FORMAT(I4)
GO TO 12

C LIC= FLAG TO FIND THE TTL OR CMOS LOGIC IC

64 READ(10,36) LIC
36 FORMAT(I2)
IF(LIC.EQ.74.OR.LIC.EQ.54) GO TO 65
NICC=NICC+1
TYPE=1.0
READ(10,37) U(NICC)
37 FORMAT(BN,I5)
BACKSPACE 10
GO TO 12
65 NICT=NICT+1
TYPE=2.0
READ(10,38) LIC
38 FORMAT(2X,A1)
WRITE(*,8) LIC
8 FORMAT(1X,A1)
IF(LIC.EQ.BN(5).OR.LIC.EQ.BN(6).OR.LIC.EQ.BN(7))GO TO 66

```

```

BACKSPACE 10
READ(10,39) U(NICT)
39  FORMAT(4X,BN,14)
BACKSPACE 10
GO TO 12
66  BACKSPACE 10
READ(10,40) U(NICT)
40  FORMAT(3X,BN,14)
BACKSPACE 10
GO TO 12

C    ROUTINE TO FIND THE NO OF TRANSISTORS

180  NQ=NQ+1
READ(10,135) Q(NQ)
135  FORMAT(A2,1X,I3)
GO TO 12

C    TO FIND THE INPUT SIGNAL

181  NVIN=NVIN+1
READ(10,136) VIN(NQ)
136  FORMAT(BN,A5)
GO TO 12

C    TO FIND THE DIODE

182  ND=ND+1
READ(10,137) D(ND)
137  FORMAT(BN,A5)
GO TO 12

C    READ BEGINING OF NET DATA

70  READ(10,41) ND1
41  FORMAT(A1)
IF(ND1 .EQ. BN(8)) GO TO 200
IF(ND1 .EQ. BN(9)) GO TO 201
IF(ND1 .EQ. BN(10)) GO TO 202
GO TO 1

C    'BEGINING OF NODE DATA'

200  NODE=NODE+1
207  READ(10,42) ND2
42  FORMAT(A1)
IF(ND2 .NE. BN(11)) GO TO 302
GO TO 1
302  BACKSPACE 10

C    READ BEGINING OF NODE DATA
READ(10,43) ND2
43  FORMAT(A1)

C    CHECK FOR NODE CONSISTING OF IC,C,L,R,ANY INPUT SIGNAL,Q,D

IF(ND2 .EQ. BN(4)) GO TO 203
IF(ND2 .EQ. BN(3)) GO TO 204
IF(ND2 .EQ. BN(2)) GO TO 205
IF(ND2 .EQ. BN(1)) GO TO 206
IF(ND2 .EQ. BN(12)) GO TO 307
IF(ND2 .EQ. BN(9)) GO TO 308
IF(ND2 .EQ. BN(13)) GO TO 309
GO TO 207
203  BACKSPACE 10
READ(10,44) IC,PIN
44  FORMAT(1X,I2,1X,I2)
WRITE(14,140) ND1,ND2,NODE,IC,PIN
140  FORMAT(A1,1X,A1,1X,I2,1X,I2,1X,I2)
GO TO 207

C    ROUTINE TO FIND THE TRANSISTOR CONNECTED TO THE NET

307  BACKSPACE 10
READ(10,310) QT,BEC
310  FORMAT(1X,I2,1X,A2)

C    PINQ=3, COLLECTOR, PINQ=2, BASE, PINQ=1, EMITTER

```

```

IF(BEC .EQ. BECN(1)) THEN
PINQ=3
ELSE IF(BEC .EQ. BECN(2)) THEN
PINQ=1
ELSE IF(BEC .EQ. BECN(3)) THEN
PINQ=2
ELSE
WRITE(*,*) 'TRANSISTOR PIN CONNECTION ERROR'
END IF
WRITE(14,311) ND1,ND2,NODE,QT,PINQ
311  FORMAT(A1,1X,A1,1X,I2,1X,I2,1X,I2)
GO TO 207

C   ROUTINE TO FIND THE NET FOR INPUT SIGNAL

308  BACKSPACE 10
    READ(10,312) VN,J
312  FORMAT(3X,I1,1X,BN,I2)
    WRITE(14,313) ND1,ND2,NODE,VN,J
313  FORMAT(A1,1X,A1,1X,I2,1X,I2,1X,I2)
GO TO 207

309  BACKSPACE 10
    READ(10,314) DN,BEC
314  FORMAT(1X,I2,1X,A2)
    IF(BEC .EQ. BECN(4)) THEN
    J=1
    ELSE IF(BEC .EQ. BECN(5)) THEN
    J=2
    ELSE
    END IF
    WRITE(14,315) ND1,ND2,NODE,DN,J
315  FORMAT(A1,1X,A1,1X,I2,1X,I2,1X,I2)
GO TO 207

204  BACKSPACE 10
    READ(10,45) NR,J
45   FORMAT(1X,I2,1X,I1)
    WRITE(14,141) ND1,ND2,NODE,NR,J
141  FORMAT(A1,1X,A1,1X,I2,1X,I2,1X,I2)
GO TO 207

205  BACKSPACE 10
    READ(10,46) NL,J
46   FORMAT(1X,I2,1X,I1)
    WRITE(14,142) ND1,ND2,NODE,NL,J
142  FORMAT(A1,1X,A1,1X,I2,1X,I2,1X,I2)
GO TO 207

206  BACKSPACE 10
    READ(10,47) NC,J
47   FORMAT(1X,I2,1X,BN,I1)
    WRITE(14,143) ND1,ND2,NODE,NC,J
143  FORMAT(A1,1X,A1,1X,I2,1X,I2,1X,I2)
GO TO 207

201  NVC=NVC+1
208  READ(10,48) ND2
48   FORMAT(A1)
    IF(ND2 .NE. BN(11)) GO TO 303
GO TO 1

303  BACKSPACE 10

C   READ BEGINNING OF VCC DATA

    READ(10,49) ND2
49   FORMAT(A1)

C   CHECK FOR NODE CONSISTING OF IC,C,L,R,ANY VCC

    IF(ND2 .EQ. BN(4)) GO TO 209
    IF(ND2 .EQ. BN(3)) GO TO 210
    IF(ND2 .EQ. BN(2)) GO TO 211
    IF(ND2 .EQ. BN(1)) GO TO 212
    IF(ND2 .EQ. BN(12)) GO TO 407
    IF(ND2 .EQ. BN(9)) GO TO 408
    IF(ND2 .EQ. BN(13)) GO TO 409
GO TO 208

209  BACKSPACE 10
    READ(10,50) IC,PIN
50   FORMAT(1X,I2,1X,I2)
    WRITE(14,144) ND1,ND2,NVC,IC,PIN
144  FORMAT(A1,1X,A1,1X,I2,1X,I2,1X,I2)

```

```

      GOTO 208
407  BACKSPACE 10
      READ(10,410) QT,BEC
410  FORMAT(1X,I2,1X,A2)

C    PINQ=3, COLLECTOR, PINQ=2, BASE, PINQ=1, EMITTER

      IF(BEC .EQ. BECN(1)) THEN
        PINQ=3
      ELSE IF(BEC .EQ. BECN(2)) THEN
        PINQ=1
      ELSE IF(BEC .EQ. BECN(3)) THEN
        PINQ=2
      ELSE
        END IF
      WRITE(14,411) ND1,ND2,NODE,QT,PINQ
411  FORMAT(A1,1X,A1,1X,I2,1X,I2,1X,I2)
      GOTO 208

408  BACKSPACE 10
      READ(10,412) VN,J
412  FORMAT(3X,I1,1X,BN,I2)
      WRITE(14,313) ND1,ND2,NODE,VN,J
413  FORMAT(A1,1X,A1,1X,I2,1X,I2,1X,I2)
      GOTO 208

409  BACKSPACE 10
      READ(10,414) DN,BEC
414  FORMAT(1X,I2,1X,A2)
      IF(BEC .EQ. BECN(4)) THEN
        J=1
      ELSE IF(BEC .EQ. BECN(5)) THEN
        J=2
      ELSE
        END IF
      WRITE(14,415) ND1,ND2,NODE,DN,J
415  FORMAT(A1,1X,A1,1X,I2,1X,I2,1X,I2)
      GOTO 208

210  BACKSPACE 10
      READ(10,51) NR,J
      51  FORMAT(1X,I2,1X,BN,I1)
      WRITE(14,145) ND1,ND2,NVC,NR,J
145  FORMAT(A1,1X,A1,1X,I2,1X,I2,1X,I2)
      GOTO 208

211  BACKSPACE 10
      READ(10,52) NI,J
      52  FORMAT(1X,I2,1X,BN,I1)
      WRITE(14,146) ND1,ND2,NVC,NI,J
146  FORMAT(A1,1X,A1,1X,I2,1X,I2,1X,I2)
      GOTO 208

212  BACKSPACE 10
      READ(10,53) NC,J
      53  FORMAT(1X,I2,1X,BN,I1)
      WRITE(14,147) ND1,ND2,NVC,NC,J
147  FORMAT(A1,1X,A1,1X,I2,1X,I2,1X,I2)
      GOTO 208

202  NGN=NGN+1
213  READ(10,54) ND2
      54  FORMAT(A1)
      IF(ND2 .NE. BN(11)) GO TO 305
      GOTO 80
305  BACKSPACE 10

C    READ BEGINING OF GND DATA

      READ(10,55) ND2
      55  FORMAT(A1)

C    CHECK FOR NODE CONSISTING OF IC,C,L,R,Q,D,ANY INPUT SIGNAL AND GND

      IF(ND2 .EQ. BN(4)) GO TO 214
      IF(ND2 .EQ. BN(3)) GO TO 215
      IF(ND2 .EQ. BN(2)) GO TO 216
      IF(ND2 .EQ. BN(1)) GO TO 217
      IF(ND2 .EQ. BN(12)) GO TO 507
      IF(ND2 .EQ. BN(9)) GO TO 508
      IF(ND2 .EQ. BN(13)) GO TO 509
      GOTO 213
214  BACKSPACE 10

```

```

      READ(10,56) IC,PIN
56  FORMAT(1X,I2,1X,I2)
      WRITE(14,148) ND1,ND2,NGN,IC,PIN
148  FORMAT(A1,1X,A1,1X,I2,1X,I2,1X,I2)
      GO TO 213
215  BACKSPACE 10
      READ(10,57) NRJ
57  FORMAT(1X,I2,1X,BN,I1)
      WRITE(14,158) ND1,ND2,NGN,NRJ
158  FORMAT(A1,1X,A1,1X,I2,1X,I2,1X,I2)
      GO TO 213
507  BACKSPACE 10
      READ(10,510) QT,BEC
510  FORMAT(1X,I2,1X,A2)
      IF(BEC .EQ. BECN(1)) THEN
          PINQ=3
      ELSE IF(BEC .EQ. BECN(2)) THEN
          PINQ=1
      ELSE IF(BEC .EQ. BECN(3)) THEN
          PINQ=2
      ELSE
          END IF
      WRITE(14,511) ND1,ND2,NGN,QT,PINQ
511  FORMAT(A1,1X,A1,1X,I2,1X,I2,1X,I2)
      GO TO 213
508  BACKSPACE 10
      READ(10,512) VNJ
512  FORMAT(3X,I1,1X,BN,I2)
      WRITE(14,513) ND1,ND2,NGN,VNJ
513  FORMAT(A1,1X,A1,1X,I2,1X,I2,1X,I2)
      GO TO 213
509  BACKSPACE 10
      READ(10,514) DN,BEC
514  FORMAT(1X,I2,1X,A2)
      IF(BEC .EQ. BECN(4)) THEN
          J=1
      ELSE IF(BEC .EQ. BECN(5)) THEN
          J=2
      ELSE
          END IF
      WRITE(14,515) ND1,ND2,NGN,DNJ
515  FORMAT(A1,1X,A1,1X,I2,1X,I2,1X,I2)
      GO TO 213
216  BACKSPACE 10
      READ(10,58) NLJ
58  FORMAT(1X,I2,1X,BN,I1)
      WRITE(14,149) ND1,ND2,NGN,NLJ
149  FORMAT(A1,1X,A1,1X,I2,1X,I2,1X,I2)
      GO TO 213
217  BACKSPACE 10
      READ(10,59) NCJ
59  FORMAT(1X,I2,1X,BN,I1)
      WRITE(14,150) ND1,ND2,NGN,NCJ
150  FORMAT(A1,1X,A1,1X,I2,1X,I2,1X,I2)
      GO TO 213
80  CONTINUE
      DO 100 I=1,NCC
          WRITE(*,111) I,PECV(I)
111  FORMAT(1X,I3,F10.6)
100  CONTINUE
          DO 101 I=1,NLL
              WRITE(*,112) I,PELV(I)
112  FORMAT(1X,I3,F10.6)
101  CONTINUE
              DO 102 I=1,NRR
                  WRITE(*,113) I,PERV(I)
113  FORMAT(1X,I3,2X,I4)
102  CONTINUE
                  NII=NICC+NICT
                  DO 103 I=1,NII
                      IF(TYPE .EQ. 1.0) THEN
                          WRITE(*,114) NICC,U(I)
114  FORMAT(1X,I3,1X,I4)
                      END IF
                      IF(TYPE .EQ. 2.0) THEN
                          WRITE(*,115) I,U(I)
115  FORMAT(1X,I3,1X,54/74'42)
                      ENDDF
103  CONTINUE

```



```

        WRITE(14,151)
151  FORMAT(//)
90   RETURN
      END

```

Subroutine 3

```

C*****
C   This subroutine (STC) is used to find the signal and the ground tracks.
C   The routine also identifies the track which has loading.
C*****

      SUBROUTINE STC (XX,YY,PX,PY,M,NS,NP,W,TNS,TWN3,NPD,PADX,PADY
1  ,PERV,PELV,PECV,LW,TCX,TCY,NT,VX,VY,DX,DY,RPADX,RPADY)
      DIMENSION XX(100,2),YY(100,2),PX(10,16),PY(10,16)
1  ,NP(10),NPP(10),ATST(10),TPCX(15,15),TPCY(15,15),GW(100)
2  ,TPGX(15,15),TPGY(15,15),TPVX(10,10),TPVY(10,10),W(100),
3  ,GWX(100,2),GWY(100,2),GWZ(100,2),RW(100),SGX(15,15),SGY(15,15)
4  ,PADX(50),PADY(50),PERV(20),PECV(20),PELV(20),NQQ(10),TCX(10,3)
5  ,TCY(10,3),VX(2,2),VY(2,2),DX(4,2),DY(4,2),NVV(2),NDD(4),
6  ,RPADX(50),RPADY(50)
      INTEGER AIN1,AIN2,ITMP1,ITMP2,ITMP3,ATST,GW,TNS,TNS2,TWN3,PERV,
1  ,TCX,TCY,VX,VY,DX,DY,PADX,PADY,TPGX,TPGY,RPADX,RPADY
      DATA ATST/1HN,1HV,1HG,1HC,1HL,1HR,1HU,1H,1HD,1HQ/

C   TPDIFFX=DIFFERENCE BETWEEN THE X-CO-ORDINATE OF THE TRACK AND PIN OF IC
C   TPDIFFY=DIFFERENCE BETWEEN THE Y-CO-ORDINATE OF THE TRACK AND PIN OF IC
C   TPCX=X-CO-ORDINATE OF ANY TRACK SEGMENT END CARRYING THE CLOCK SIGNAL
C   TPCY=Y-CO-ORDINATE OF ANY TRACK SEGMENT END CARRYING THE CLOCK SIGNAL
C   TPGX=X-CO-ORDINATE OF ANY TRACK SEGMENT END CONNECTED TO GROUND
C   TPGY=Y-CO-ORDINATE OF ANY TRACK SEGMENT END CONNECTED TO GROUND
C   NC=NO OF TRACK SEGMENT CARRYING THE CLOCK SIGNAL
C   NG=NO TRACK SEGMENT CONNECTED TO GROUND
C   GWX,GWY,GWZ=X,Y,Z CO-ORDINATE OF THE TRACK (WIRE)
C   RW=EQUIVALENT RADIUS OF THE RECTANGULAR TRACK
C   INITIALIZE THE TRACK END ,IC, AND PIN
C   TOLERANCE EPSILON IS GIVEN IN MIL

      NTS=0
      NTG=0
      NTV=0
      NSS=0
      EPSILON=4.0
      REWIND 14
      DO 200 I=1,NT
      DO 201 J=1,3
      WRITE(*,*) I,J,TCX(I,J),TCY(I,J)
201  CONTINUE
200  CONTINUE
104  READ(14,140) AIN1,AIN2,ITMP1,ITMP2,ITMP3
140  FORMAT(A1,1X,A1,1X,I2,1X,I2,1X,I2)
      IF(AIN1 .EQ. ATST(1)) GO TO 100
      IF(AIN1 .EQ. ATST(2)) GO TO 101
      IF(AIN1 .EQ. ATST(3)) GO TO 102
      IF(AIN1 .EQ. ATST(4)) RETURN
      CALL RSG(XX,YY,M,TNS)
      CALL RSG1(XX,YY,M,TNS2,TWN3)

C   FIND THE TRACK WHICH HAS LOAD

      CALL PESG3(RPADX,RPADY,LW,PERV,PECV,PELV)
      RETURN

C   ROUTINE TO CHECK THE IC PIN CONNECTED TO THE NODE
100  IF(AIN2 .EQ. ATST(7)) THEN
      NS=ITMP2
      NODE=ITMP1
      NP(NS)=ITMP3
      NTS=NTS+1
      TPCX(NTS,NODE)=PX(NS,NP(NS))
      TPCY(NTS,NODE)=PY(NS,NP(NS))
      NTW=NTS
      NOD=NODE
      SGX(NTW,NOD)=TPCX(NTS,NODE)
      SGY(NTW,NODE)=TPCY(NTS,NODE)

```

```

C FIND THE TRACK WHICH IS CONNECTED TO SIGNAL NODE

CALL TEWG (SGX,SGY,XX,YY,M,NTW,NOD,W,GWX,GWY,GWZ,RW,GW,NNS,TNS)
WRITE(*,*) NTS,NODE,TPCX(NTS,NODE),TPCY(NTS,NODE)

C ROUTINE TO CHECK THE TRANSISTOR PIN CONNECTED TO THE NODE

ELSE IF(AIN2 .EQ. ATST(10)) THEN

C NTT=TAG NO OF THE TRANSISTOR

NTT=ITMP2
NODE=ITMP1
NQQ(NTT)=ITMP3
NTS=NTS+1
TPCX(NTS,NODE)=TCX(NTT,NQQ(NTT))
TPCY(NTS,NODE)=TCY(NTT,NQQ(NTT))
NTW=NTS
NOD=NODE
SGX(NTW,NOD)=TPCX(NTS,NODE)
SGY(NTW,NOD)=TPCY(NTS,NODE)
WRITE(*,*) NTS,NODE,TPCX(NTS,NODE),TPCY(NTS,NODE)
CALL TEWG(SGX,SGY,XX,YY,M,NTW,NOD,W,GWX,GWY,GWZ,RW,GW,NNS,TNS)
ELSE IF(AIN2 .EQ. ATST(2)) THEN
NV=ITMP2
NODE=ITMP1
NVV(NV)=ITMP3
NTS=NTS+1
TPCX(NTS,NODE)=VX(NV,NVV(NV))
TPCY(NTS,NODE)=VY(NV,NVV(NV))
NTW=NTS
NOD=NODE
SGX(NTW,NOD)=TPCX(NTS,NODE)
SGY(NTW,NOD)=TPCY(NTS,NODE)
WRITE(*,*) NTS,NODE,TPCX(NTS,NODE),TPCY(NTS,NODE)
CALL TEWG(SGX,SGY,XX,YY,M,NTW,NOD,W,GWX,GWY,GWZ,RW,GW,NNS,TNS)
ELSE IF(AIN2 .EQ. ATST(9)) THEN
ND=ITMP2
NODE=ITMP1
NDD(ND)=ITMP3
NTS=NTS+1
TPCX(NTS,NODE)=DX(NV,NDD(ND))
TPCY(NTS,NODE)=DY(NV,NDD(ND))
NTW=NTS
NOD=NODE
SGX(NTW,NOD)=TPCX(NTS,NODE)
SGY(NTW,NOD)=TPCY(NTS,NODE)
WRITE(*,*) NTS,NODE,TPCX(NTS,NODE),TPCY(NTS,NODE)
CALL TEWG(SGX,SGY,XX,YY,M,NTW,NOD,W,GWX,GWY,GWZ,RW,GW,NNS,TNS)
ELSE
WRITE(*,*) NO IC AND Q'
END IF
GO TO 104

C END OF SIGNAL NODE DATA

C BEGINNING OF ROUTINE TO FIND THE TRACK WHICH IS CONNECTED TO GROUND NODE

102 IF(AIN2 .EQ. ATST(7)) THEN
NTG=NTG+1
NS=ITMP2
NGN=ITMP1
NP(NS)=ITMP3
TPGX(NTG,NGN)=PX(NS,NP(NS))
TPGY(NTG,NGN)=PY(NS,NP(NS))
NTW=NTG
NOD=NGN
SGX(NTW,NOD)=TPGX(NTG,NGN)
SGY(NTW,NOD)=TPGY(NTG,NGN)
CALL TEWG1 (SGX,SGY,XX,YY,M,NTW,NOD,W,GWX,GWY,GWZ,RW,GW,NSS,TNS2)
WRITE(*,*)NTG,NGN,TPGX(NTG,NGN),TPGY(NTG,NGN)
ELSE IF (AIN2 .EQ. ATST(10)) THEN
NTT=ITMP2
NGN=ITMP1
NQQ(NTT)=ITMP3
NTG=NTG+1
TPGX(NTG,NGN)=TCX(NTT,NQQ(NTT))
TPGY(NTG,NGN)=TCY(NTT,NQQ(NTT))
NTW=NTG

```

```

NOD=NGN
SGX(NTW,NOD)=TPGX(NTG,NGN)
SGY(NTW,NOD)=TPGY(NTG,NGN)
CALL TEWG1 (SGX,SGY,XX,YY,M,NTW,NOD,W,GWX,GWY,GWZ,RW,GW,NNS,TNS2)
ELSE IF (AIN2 .EQ. ATST(9)) THEN
NI=ITMP2
NGN=ITMP1
NDD(ND)=ITMP3
NTG=NTG+1
TPGX(NTG,NGN)=DX(ND,NDD(ND))
TPGY(NTG,NGN)=DY(ND,NDD(ND))
NTW=NTG
NOD=NGN
SGX(NTW,NOD)=TPGX(NTG,NGN)
SGY(NTW,NOD)=TPGY(NTG,NGN)
CALL TEWG1 (SGX,SGY,XX,YY,M,NTW,NOD,W,GWX,GWY,GWZ,RW,GW,NNS,TNS2)
ELSE IF (AIN2 .EQ. ATST(2)) THEN
NV=ITMP2
NGN=ITMP1
NVV(NV)=ITMP3
NTG=NTG+1
TPGX(NTG,NGN)=VX(NV,NVV(NV))
TPGY(NTG,NGN)=VY(NV,NVV(NV))
NTW=NTG
NOD=NGN
SGX(NTW,NOD)=TPGX(NTG,NGN)
SGY(NTW,NOD)=TPGY(NTG,NGN)
WRITE(*,*) NTG,NOD,TPGX(NTS,NOD),TPGY(NTS,NOD)
CALL TEWG1 (SGX,SGY,XX,YY,M,NTW,NOD,W,GWX,GWY,GWZ,RW,GW,NNS,TNS2)
END IF
GO TO 104
101 NTV=NTV+1
NS=ITMP2
NVC=ITMP1
NP(NS)=ITMP3
IF(AIN2 .EQ. ATST(7)) THEN
TPVX(NTV,NVC)=PX(NS,NP(NS))
TPVY(NTV,NVC)=PY(NS,NP(NS))
ELSE IF (AIN2 .EQ. ATST(9)) THEN
TPVX(NTV,NVC)=DX(NS,NP(NS))
TPVY(NTV,NVC)=DY(NS,NP(NS))
ELSE IF (AIN2 .EQ. ATST(10)) THEN
TPVX(NTV,NVC)=TCX(NS,NP(NS))
TPVY(NTV,NVC)=TCY(NS,NP(NS))
ELSE
END IF
GO TO 104
END

```

Subroutine 4

```

C *****
C This subroutine is used to find the track which is directly connected to a signal node
C *****

```

```

SUBROUTINE TEWG(SGX,SGY,XX,YY,M,NTW,NOD,W,GWX,GWY,GWZ,RW,GW,
1 NSS,TNS)
DIMENSION SGX(15,15),SGY(15,15), XX(100,2),YY(100,2)
1 ,GWX(100,2),GWY(100,2),GWZ(100,2),RW(100),GW(100)
INTEGER FDUP,TNS,GW,FLAG
OPEN(UNIT=20,STATUS='UNKNOWN',FILE='TEWG.OUT')
OPEN(UNIT=24,STATUS='UNKNOWN',FILE='NODE.OUT')

C NW= WIRE NUMBER
C NS=TOTAL NUMBER OF SEGMENTS

105 K=1
DO 100 I=K,M
IF(I .EQ. NW) GO TO 100
DO 101 J=1,2
DIFFSX=SGX(NTW,NOD)-XX(I,J)
DIFFSY=SGY(NTW,NOD)-YY(I,J)
IF(ABS(DIFFSX) .LE. 4 .AND. ABS(DIFFSY) .LE. 4) THEN
NSS=NSS+1
NW=I
GWX(NSS,1)=XX(I,J)

```

```

      GWY(NSS,1)=YY(I,J)
      IF(J .EQ. 2)THEN
        GWX(NSS,2)=XX(I,1)
        GWY(NSS,2)=YY(I,1)
      ELSE
        GWX(NSS,2)=XX(I,2)
        GWY(NSS,2)=YY(I,2)
      END IF
      GW(NSS)=NW
      IF(NSS .EQ. 1) GO TO 106
      DO 104 JJ=1,NSS-1
      IF(GW(NSS) .EQ. GW(JJ)) THEN
        FDUP=1
      END IF
104  CONTINUE
      IF (FDUP .EQ. 1) GO TO 107
106  TNS=TNS+1
      GW(TNS)=GW(NSS)
      WRITE(20,201) GW(TNS),(GWX(NSS,II),II=1,2),
1    (GWY(NSS,II),II=1,2)
201  FORMAT(I2,2X,2F10.5,2X,2F10.5)
      WRITE(24,220) GW(TNS),NOD
220  FORMAT(I2,1X,I2)
107  SGX(NTW,NOD)=GWX(NSS,2)
      SGY(NTW,NOD)=GWY(NSS,2)
      GO TO 105
      END IF
101  CONTINUE
100  CONTINUE
      FDUP=0
      RETURN
      END

```

Subroutine 5

```

*****
C   This subroutine is used to find the track which is directly connected to a ground node
*****

      SUBROUTINE TEWG1 (SGX,SGY,XX,YY,M,NTW,NOD,W,GWX,GWY,GWZ,RW,GW,
1    NSS,TNS2)
      DIMENSION SGX(15,15),SGY(15,15), XX(100,2),YY(100,2)
1    ,GWX(100,2),GWY(100,2),GWZ(100,2),RW(100),GW(100)
      INTEGER FDUP,TNS2,GW_FLAG
      OPEN(UNIT=23,STATUS='UNKNOWN',FILE='TEWG2.OUT')

C   NW= WIRE NUMBER
C   NS=TOTAL NO OF SEGMENT

105  K=1
      DO 100 I=K,M
      IF(I .EQ. NW) GO TO 100
      DO 101 J=1,2
      DIFFGX=SGX(NTW,NOD)-XX(I,J)
      DIFFGY=SGY(NTW,NOD)-YY(I,J)
      IF(ABS(DIFFGX) .LE. 4 .AND. ABS(DIFFGY) .LE. 4) THEN
        NSS=NSS+1
        NW=I
        GWX(NSS,1)=XX(I,J)
        GWY(NSS,1)=YY(I,J)
        IF(J .EQ. 2)THEN
          GWX(NSS,2)=XX(I,1)
          GWY(NSS,2)=YY(I,1)
        ELSE
          GWX(NSS,2)=XX(I,2)
          GWY(NSS,2)=YY(I,2)
        END IF
        GW(NSS)=NW
        IF(NSS .EQ. 1) GO TO 106
        DO 104 JJ=1,NSS-1
        IF(GW(NSS) .EQ. GW(JJ)) THEN
          FDUP=1
        END IF
104  CONTINUE
      IF (FDUP .EQ. 1) GO TO 107

```

```

106 TNS2=TNS2+1
    GW(TNS2)=GW(NSS)
    WRITE(23,201) GW(TNS2),(GWX(NSS,II),II=1,2),
1   (GWY(NSS,II),II=1,2)
201 FORMAT(12,2X,2F10.5,2X,2F10.5)
107 SGX(NTW,NOD)=GWX(NSS,2)
    SGY(NTW,NOD)=GWY(NSS,2)
    GO TO 105
    END IF
101 CONTINUE
100 CONTINUE
    FDUP=0
    RETURN
    END

```

Subroutine 6

```

C*****
C   This subroutine finds the remaining signal tracks.
C*****

```

```

    SUBROUTINE RSG (XX,YY,M,TNS)
    DIMENSION XX(100,2),YY(100,2),GWX(100,2),GWY(100,2)
1   ,GX(100,2),GY(100,2),G(100),GW(100)
    INTEGER GDUP,TWN,GW,TNSS,G,TNS
    TNSS=TNS
    OPEN(UNIT=21,STATUS='UNKNOWN',FILE='RSG.OUT')
    OPEN(UNIT=22,STATUS='UNKNOWN',FILE='RSG1.OUT')
    ITER=0
    ITMAX=M-TNS
    TWN=TNS
    IT=1
    REWIND 20
500 WRITE(22,*) 'CHECK 1, TNS'
    WRITE(22,*) TNS,M
    DO 120 I=IT,TNS
    READ(20,301) GW(I),GWX(I,1),GWX(I,2),GWY(I,1),GWY(I,2)
301 FORMAT(12,2X,F10.5,F10.5,2X,F10.5,F10.5)
120 CONTINUE
    DO 100 I=IT,TNS

```

C BEGINNING OF THE TRACKS ON THE PCB

```

    DO 102 II=1,M
    LL=1
304 IF(II .EQ. GW(LL)) GO TO 102
    LL=LL+1
    IF(LL .GT. TNS) GO TO 303
    GO TO 304

```

C CHECK WITH THE FIRST END OF THE TRACK

```

303 CONTINUE
    DO 101 J=1,2
    DO 103 JJ=1,2
    DIFFSGX=GWX(I,J)-XX(II,JJ)
    DIFFSGY=GWY(I,J)-YY(II,JJ)
    IF(ABS(DIFFSGX) .LE. 4 .AND. ABS(DIFFSGY) .LE. 4) THEN
    TWN=TWN+1
    NW=II
    GX(TWN,1)=XX(II,JJ)
    GY(TWN,1)=YY(II,JJ)
    IF(JJ .EQ. 2) THEN
    GX(TWN,2)=XX(II,1)
    GY(TWN,2)=YY(II,1)
    ELSE
    GX(TWN,2)=XX(II,2)
    GY(TWN,2)=YY(II,2)
    END IF
    GW(TWN)=NW
    DO 108 K=1,TWN-1
    IF(GW(TWN) .EQ. GW(K)) THEN
    GDUP=1
    END IF
108 CONTINUE
    IF(GDUP .EQ. 1) GO TO 110

```

```

      TNSS=TNSS+1
      WRITE(20,201) GW(TWN),(GX(TWN,KK),KK=1,2),(GY(TWN,KK),KK=1,2)
201  FORMAT(I2,2X,2F10.5,2X,2F10.5)
      WRITE(21,201) GW(TWN),(GX(TWN,KK),KK=1,2),(GY(TWN,KK),KK=1,2)
221  FORMAT(I2,2X,2F10.5,2X,2F10.5)
      END IF
103  CONTINUE
101  CONTINUE
102  CONTINUE
110  GDUP=0
100  CONTINUE
      IT=TNS
      NB=TWN-TNS+1
      IF(TWN .GE. M) RETURN
      DO 501 I=1,NB
      BACKSPACE 20
501  CONTINUE
      TNS=TWN
      ITER=ITER+1
      IF(ITER .GE. ITMAX) RETURN
      GDUP=0
      GO TO 500
      TNS=TNSS
      RETURN
      END

```

Subroutine 7

```

C*****
C  This subroutine identifies the track which has loading and also finds the type and value of the load
C*****

```

```

      SUBROUTINE PESG (RPADX,RPADY,LW,PERV,PECV,PELV)
      DIMENSION GWX(100,2),GWY(100,2),RPADX(50),RPADY(50),ATST(5)
1     ,PERV(20),PECV(20),PELV(20)
      INTEGER GW,ND1,ND2,AIN,TNC,L,C,ATST,RPADX,RPADY,PERV,PECV,PELV
      DATA ATST/1HR,1HL,1HC,1H ,2HPA/
      OPEN(UNIT=27, STATUS='OLD', FILE='COM.REP')
      OPEN(UNIT=28, STATUS='UNKNOWN', FILE='LOAD1.OUT')
      II=1
      READ(27,101)
101  FORMAT(///)
106  READ(27,100) AIN
100  FORMAT(4X,A2)
      WRITE(*,110)AIN
110  FORMAT(4X, A2)
      IF(AIN .EQ. ATST(5)) GO TO 103
      WRITE(*,*) 'PROGRAM IS OK'
      BACKSPACE 27
      READ(27,120)ND2
120  FORMAT(6X,BN,I2)
      WRITE(*,200)ND2
200  FORMAT(I2)
      IF(ND2 .EQ. 0) GO TO 103
      BACKSPACE 27
      READ(27,104) ND2
104  FORMAT(11X, A1)
      WRITE(*,214)ND2
214  FORMAT(1X,A1)
      IF(ND2 .EQ. ATST(1)) GO TO 105
      GO TO 106
105  BACKSPACE 27
      READ(27,107) TNC
107  FORMAT(12X,BN,I2)
      LW=LW+1
      RL=PERV(TNC)
      WRITE(*,*)II, RPADX(II), RPADX(II+1), RPADY(II), RPADY(II+1)
      GWX(LW,1)=RPADX(II)
      GWX(LW,2)=RPADX(II+1)
      GWY(LW,1)=RPADY(II)
      GWY(LW,2)=RPADY(II+1)
      WRITE(28,211) ND2, GWX(LW,1),GWX(LW,2),GWY(LW,1),GWY

```

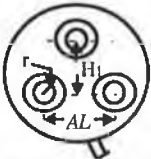
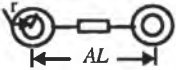
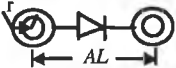
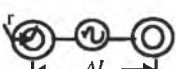
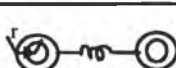
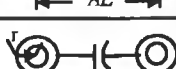

```

1 (LW,2),RL
211 FORMAT(A1,2X,F10.5,2X,F10.5,2X,F10.5,2X,F10.5,2X,F10.5)
    II=II+2
    GO TO 106

103 WRITE(28,601)
601 FORMAT(//)
    RETURN
    END

```

TABLE TE1: Default dimensions for discrete components, pad and via in a PCB.

Components, Pad via, signal generator	Symbol	Symbol name	Dimensions
Transistor		T ₀₅	Inner pad diameter (<i>IPD</i>) = 2r 2r = 0.685 mm, H ₁ = 2.54 mm, AL = 5.08 mm
Resistor		Axial 0.4	<i>IPD</i> = 0.787 mm, AL = 1.016 cm
Diode		Axial 0.3	<i>IPD</i> = 0.787 mm, AL = 7.62 mm
Signal generator		Axial 0.5	<i>IPD</i> = 0.787 mm, AL = 1.27 cm
Inductor		Axial 0.25	<i>IPD</i> = 0.787 mm, AL = 6.35 mm
Capacitor		Axial 0.24	<i>IPD</i> = 0.686 mm, AL = 6.0 mm
Placed pad		None	0.005 < <i>IPD</i> < 1.34 cm Outer pad diameter (<i>OPD</i>), 0.016 < <i>OPD</i> < 1.35 cm
Placed via	As placed pad	None	0.005 < <i>IPD</i> < 0.704 cm 0.016 < <i>OPD</i> < 0.714 cm

E4: LINE FORMAT OF THE FILE CREATED BY SUBROUTINE COMV FOR LDER

The line format of the netfile created by subroutine COMV is shown in Fig. E4-1.

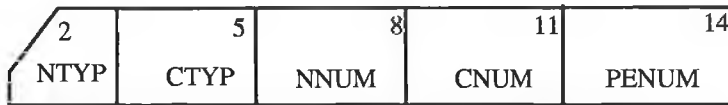


Fig. E4-1 Line format of an output file created by subroutine "COMV".

Parameters:

Characters:

NTYP - Determines the type of node which is used as

N - Signal node

G - Ground Node

V - Power node

CTYP - Determines the types of components

U - Integrated circuit (IC)

Q - Transistor

D - Diode

SG - Signal generator

R - Resistor

L - Inductor

C - Capacitor

Integers

NNUM - Indicates the node number

CNUM - Indicates the component number

PENUM - Indicates the pin or end number of a component which is connected to a node.

E5: COMPUTER PROGRAMME LISTING FOR EXTRACTION OF ELECTRICAL DATA

The routine EDER extracts the electrical data from the output file of a circuit simulation package PSPICE and then prepares an input file for NEC-2. The algorithm is described in chapter 5. The computer programme listing of this routine is given below.

Computer programme listing

```

C *****
C THIS ROUTINE IS TO EXTRACT THE ELECTRICAL DATA FROM
C A CIRCUIT SIMULATION PACKAGE(PSPICE/SPICE)
C *****
      DIMENSION ATST(14),VFN(20,20),VAC(20,20),FR(20),PN(20)
      INTEGER AIN, ATST,TB,TE,FF,FSTEP,TNOD,TEX,ITN,PN

C TYPE OF EXCITATION TEX=0 i.e. VOLTAGE SOURCE
C TOTAL NO OF NODES TNOD

      DATA ATST /1HN,'T','I',2HMO,2HEN,2HAC,2HTR,2HFO,2HPR,
1 3HCON,1HG, 2HIN/
      OPEN(UNIT=1, STATUS='OLD', FILE='COMV.DAT')
      OPEN(UNIT=2, STATUS='OLD', FILE='SPICE.OUT')
      OPEN(UNIT=3, STATUS='UNKNOWN', FILE='EXCL.OUT')
      OPEN(UNIT=4, STATUS='UNKNOWN', FILE='EXND.DAT')
      OPEN(UNIT=5, STATUS='OLD', FILE='SPICE.CIR')
      OPEN(UNIT=6, STATUS='UNKNOWN', FILE='EDR.OUT')
      OPEN(UNIT=7, STATUS='UNKNOWN', FILE='FR.DAT')
      NODE=0
      ITN=0
      IT=0
      NP=1
      TNOD=0
      WRITE(*,*) 'TYPE OF EXCITATION'
      READ(*,*) TEX
506 READ(5,501) AIN
501 FORMAT(1X,A2)
      IF(AIN .EQ. ATST(7)) GO TO 502
      BACKSPACE 5
      READ(5,503) AIN
503 FORMAT(3X, A2)
      IF (AIN .EQ. ATST(14)) THEN
      BACKSPACE 5
      IT=IT+1
      READ(5,504) PN(IT)
504 FORMAT(14X,I2)
      END IF
      GO TO 506
502 REWIND 5
14 READ(1,10) AIN
10 FORMAT(A1)
      IF(AIN .EQ. ATST(2)) GO TO 11
      IF(AIN .EQ. ATST(3)) GO TO 12
      IF(AIN .EQ. ATST(4)) GO TO 13
      GO TO 14
11 READ(1,15)
15 FORMAT(6(/))
      GO TO 14
12 READ(1,16) AIN
16 FORMAT(A1)
      IF(AIN .EQ. ATST(1)) GO TO 17
      IF(AIN .EQ. ATST(5)) GO TO 14
      IF(AIN .EQ. ATST(13)) GO TO 13
      GO TO 14
17 NODE=NODE+1
      GO TO 12
13 CONTINUE

C END OF ROUTINE TO FIND THE NUMBER OF NODES FROM NETLIST CREATED BY SCHEMATIC DESIGN TOOL
C TO FIND THE TEMPORARY FILE FOR FREQUENCY

```

```

204 READ(5,200)AIN
200 FORMAT(1X,A2)
   IF(AIN.EQ. ATST(7)) GO TO 201
   IF(AIN.EQ. ATST(8)) GO TO 202
   IF(AIN.EQ. ATST(10)) GO TO 203
   GO TO 204
203 BACKSPACE 5

C   GET FUNDAMENTAL FREQUENCY OF THE PULSE

   READ(5,205) FF
205 FORMAT(6X,I3)
   DO 206 I=1,9
   FR(I)=1*FF*1.0E6
206 CONTINUE
   GO TO 204
202 BACKSPACE 5

C   FSTART = START FREQUENCY OF AC ANALYSIS
C   FSTOP = STOP FREQUENCY OF AC ANALYSIS

   READ(5,207) FSTART,FSTOP
207 FORMAT(11X,I2,4X,I3)
   MF=FSTOP/FSTART
   DO 208 I=1,MF
   FR(I)=1*FSTART*1.0E6
208 CONTINUE
   GO TO 204

C   BEGINNING OF ROUTINE TO EXTRACT ELECTRICAL DATA
C   FIND THE NO OF PAGES TO BE SKIPPED i.e. NUMBER OF MODEL PARAMETER

201 CONTINUE
   READ(2,18)
18  FORMAT(/)
21  READ(2,19) AIN
19  FORMAT(14X,A3)
   IF(AIN.EQ. ATST(12)) GO TO 43
   BACKSPACE 2
   READ(2,52) AIN
52  FORMAT(10X,A2)
   WRITE(*,53) AIN
53  FORMAT(1X,A2)
   IF(AIN.EQ. ATST(8)) GO TO 44
   BACKSPACE 2
   READ(2,42) AIN
42  FORMAT(1X,A2)
   IF(AIN.EQ. ATST(10)) GO TO 23
   GO TO 21
23  FSTEP=9
   ITN=ITN+1
   NFC=PN(ITN)
   READ(2,33)
33  FORMAT(4(/))
   WRITE(*,32) AIN
32  FORMAT(1X,A2)
   TNOD=TNOD+1
   DO 40 I=1,9
   READ(2,34) F,VFN(NFC,I)
34  FORMAT(/9X,D12.3,1X,D12.3)
105 READ(4,100) AIN
100 FORMAT(A2)
   IF(AIN.EQ. ATST(7)) GO TO 101
   BACKSPACE 4
   READ(4,102) NODE
102 FORMAT(I2)
   IF(NODE.NE. NFC) GO TO 105
   BACKSPACE 4
   READ(4,103) NTRACK
103 FORMAT(3X,I2)
   WRITE(3,301) NFC, F,NTRACK, VFN(NFC,I)
301 FORMAT(I2,1X,E10.3,1X,I2,1X,E10.3)
101 REWIND 4
   BACKSPACE 2
40  CONTINUE
   GO TO 21
44  FSTEP=MF
   READ(2,46) NAC

```

```

46  FORMAT(////18X,11//)
    WRITE(*,51) AIN
51  FORMAT(1X,A2)
    DO 50 I=1,14
    READ(2,47) F,VAC(NAC,I)
47  FORMAT(E11.3,3X,E11.3)
106 READ(4,107) AIN
107 FORMAT(A2)
    IF(AIN .EQ. ATST(7)) GO TO 108
    BACKSPACE 4
    READ(4,109) NODE
109 FORMAT(I2)
    IF(NODE .NE. NFC) GO TO 106
    BACKSPACE 4
    READ(4,110) NTRACK
110 FORMAT(3X,I2)

    WRITE(3,302) NAC,F,NTRACK,VAC(NAC,I)
302 FORMAT(I2,1X,E10.3,1X,I2,1X,E10.3)
108 REWIND 4
50  CONTINUE
    GO TO 21
43  WRITE(*,*) 'PROGRAM IS OK'
    WRITE(6,600) TNOD
6000 FORMAT(I2)

C   ROUTINE FOR CREATING A FILE WHICH CONTAINS THE EXCITATION DATA

    WRITE(7,700)(FR(I),I=1,9)
700 FORMAT('FR',1X,E10.3)
    WRITE(7,701)
701 FORMAT('EN')
    WRITE(3,300)
300 FORMAT('EN')
    REWIND 3
    DO 303 I=1,9
306 READ(3,304) AIN
304 FORMAT(A2)
    IF(AIN .EQ. ATST(7)) GO TO 310
    BACKSPACE 3
    READ(3,305) F
305 FORMAT(3X,E10.3)
    WRITE(*,*) F,FR(I)
    IF(F .NE. FR(I)) GO TO 306
    BACKSPACE 3
    READ(3,307) NODE, F,NTRACK,VOR
307 FORMAT(I2,1X,E10.3,1X,I2,1X,E10.3)

C   SEGMENT NUMBER OF NTH TRACK IS CREATED BY NEC SO THAT FIELD TO BE BLANK
C   IMAGINARY PART OF EXCITATION = VOI=0.0
    VOI=0.0
    WRITE(6,600) TEX,NTRACK,VOR,VOI
600 FORMAT('EX'1X,I2,2X,I3,4X,'0' 3X,'00' 1X,E10.3,1X,E10.3)
    GO TO 306
310 CONTINUE
    REWIND 3
303 CONTINUE
    WRITE(6,601)
601 FORMAT('EN')
    STOP
    END

```

E6 : CORNER CO-ORDINATES OF A SHIELDED SECTION IN A PCB

The co-ordinates of the rectangular shielded section as shown in Fig. E6-1 can be obtained from the following expressions

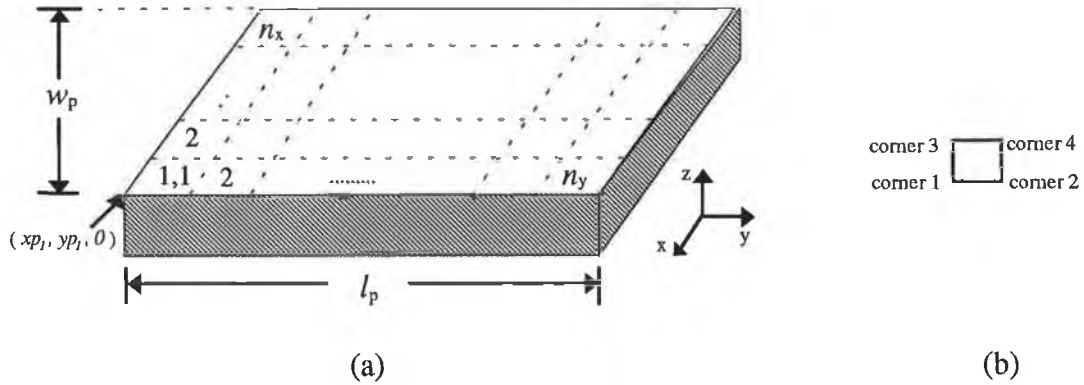


Fig. E6-1 A sample PCB (a) size of the PCB and division of the PCB in the x and y directions; (b) corner of the shielded sections.

$$xs_1(i, j) = xs_2(i, j) = xp_1 + (i - 1) \frac{w_p}{n_x} \quad (\text{E6-1})$$

$$xs_3(i, j) = xs_4(i, j) = xs_1(i, j) + \frac{w_p}{n_x} \quad (\text{E6-2})$$

$$ys_1(i, j) = ys_3(i, j) = yp_1 + (j - 1) \frac{l_p}{n_y} \quad (\text{E6-3})$$

$$ys_2(i, j) = ys_4(i, j) = ys_1(i, j) + \frac{l_p}{n_y} \quad (\text{E6-4})$$

where, $i = 1, 2, \dots, n_x$, $j = 1, 2, \dots, n_y$, xs and ys are the x-y co-ordinates of the shielded sections and subscripts denote the corner number of the shielded section, (xp_1, yp_1) is the x-y co-ordinate of the first corner of the PCB, n_x is the number of divisions along the width (w_p) of the PCB and n_y is the number of divisions along the length (l_p) of the PCB. In this work the origin of the PCB layout (see Fig. 7.2) was assumed as the first corner of the PCB.

E7: COMPUTER PROGRAMME LISTING FOR SUBROUTINE "SHIELD"

The function of this subroutine is to find the co-ordinates of a shielded section in a PCB and exclude the shielded portion from the radiating structure (i.e. PCB). A computer programme listing is given below.

Computer programme listing

```
C *****
C THIS ROUTINE IS USED TO PROVIDE SHIELDING ON SOME PART
C OF THE CIRCUIT TO REDUCE RADIATION AS MUCH AS POSSIBLE.
C *****
SUBROUTINE SHIELDD

C XS1,XS2,YS1,YS2= CORNER CO-ORDINATE OF NSPth SHIELDED PART
C ISS=NO OF SEGMENT WHICH IS SHIELDED
C NSP=TAG NO OF SHIELDED PART

  DIMENSION XS1(50),XS2(50),YS1(50),YS2(50),ISS(50,50),
1 INSS(50)
  REAL SHXC,SHYC,SHZC,XS1,XS2,YS1,YS2
  INTEGER SHFLAG,ISS,INSS,NPS,NPSS
  COMMON /DATA/ LD,N1,N2,N,NP,M1,M2,M,MP,X(50),Y(50),Z(50),SI(50),
1 BI(50),ALP(50),BET(50),ICON1(100),ICON2(100),ITAG(100),ICONX
2 (250),WLAM,IPSYM
  COMMON /SHELDDP/ SHXC(50),SHYC(50),SHZC(50),XS1,XS2,YS1,YS2
  COMMON /SHIELD/ SHFLAG,NSPT,ISS,INSS,NPS,NPSS

C DEFINE THE SIZE OF PCB

  DO 300 I=1,N
  WRITE(*,*) SHXC(I),SHYC(I)
300 CONTINUE
  WRITE(*,*) 'DEFINE THE SIZE OF PCB(XPB1,XPB2,YPB1,YPB2)'
  READ(*,*) XPB1,XPB2,YPB1,YPB2

C DEVIDE THE PCB INTO A NUMBER OF RECTANGULAR PARTS

  WRITE(*,*) 'THE NO OF DIVISION IN X AND Y DIRECTION'
  READ(*,*) NX,NY
C NSPT=TOTAL NO OF DIVIDED PARTS OF PCB
  NSPT=NX*NY

C FIND THE CO-ORDINATE OF SHIELDED PART

  DX=(XPB2-XPB1)/NX
  DY=(YPB2-YPB1)/NY
  XXS1=XPB1
  YYS1=YPB1
  INSP=0
  DO 100 I=1,NY
  DO 101 J=1,NX
  INSP=INSP+1
  YS1(INSP)=YYS1+(I-1)*DY
  YS2(INSP)=YS1(INSP)+DY
  XS1(INSP)=XXS1+(J-1)*DX
  XS2(INSP)=XS1(INSP)+DX

C NSP(INSP)=INSP

101 CONTINUE
100 CONTINUE
  DO 200 I=1,INSP
  WRITE(*,*) XS1(I),XS2(I),YS1(I),YS2(I)
200 CONTINUE
C FIND THE SEGMENT WHICH LIES ON THE NSPth SHIELD PART

  WRITE(*,*) N
  DO 201 I=1,INSP
  INSS(I)=0
  DO 202 J=1,N
  IF(SHXC(J).EQ.0.0.AND.SHYC(J).EQ.0) GO TO 202
```

```

      IF(SHXC(J) .GE. XS1(I) .AND. SHXC(J) .LE. XS2(I) .AND. SHYC(J)
1    .GE. YS1(I) .AND. SHYC(J) .LE. YS2(I)) THEN
      INSS(I)=INSS(I)+1
      ISS(INSS(I),J)=J
      END IF
202 CONTINUE
      WRITE(50,*) I,INSS(I), (ISS(J,I),JJ=1,INSS(I))
201 CONTINUE
      RETURN
      END

```

E8: COMPUTER PROGRAMME LISTING FOR SUBROUTINE "ASSC"

The function of this subroutine is to arrange the predicted radiated fields in an ascending order for identifying the shielding part in a PCB which can minimise EM radiation from the PCB. A computer programme listing is given below.

Computer programme listing

```

C *****
SUBROUTINE ASSC
DIMENSION XS1(20),YS1(20),XS2(20),YS2(20),
1 SHE1DB(20),B(20),C(20),D(20),A(20),F(20)
REAL XS1,XS2,YS1,YS2,A,B,C,D,F,SHE1DB,SHXC,SHYC,SHZC,EMIN
INTEGER NSPT,NSPTT
COMMON /SHIELD/ SHXC(50),SHYC(50),SHZC(50),XS1,XS2,YS1,YS2
COMMON /RADS/ SHE1DB,EMIN,X1MIP,X2MIP,Y1MIP,Y2MIP,NSPTT
WRITE(*,*) NSPTT
DO 80 I=1,NSPTT
WRITE (*,81) XS1(I),XS2(I),YS1(I),YS2(I),SHE1DB(I)
81 FORMAT(E12.6,2X,E12.6,2X,E12.6,2X,E12.6,2X,E12.6)
80 CONTINUE
NSPT=NSPTT
WRITE(50,*) 'NSPT'
WRITE(50,*) NSPT
NN=NSPT-1
DO 50 I=1,NN
DO 60 J=1,-1,-1
A(J)=SHE1DB(J)
B(J)=XS1(J)
C(J)=XS2(J)
D(J)=YS1(J)
F(J)=YS2(J)
IF(SHE1DB(J+1) .GE. SHE1DB(J)) THEN
SHE1DB(J)=SHE1DB(J+1)
SHE1DB(J+1)=A(J)
XS1(J)=XS1(J+1)
XS1(J+1)=B(J)
XS2(J)=XS2(J+1)
XS2(J+1)=C(J)
YS1(J)=YS1(J+1)
YS1(J+1)=D(J)
YS2(J)=YS2(J+1)
YS2(J+1)=F(J)
END IF
60 CONTINUE
50 CONTINUE
DO 70 I=NSPT,1,-1
WRITE(50,*) XS1(I),XS2(I),YS1(I),YS2(I),SHE1DB(I)
70 CONTINUE
X1MIP=XS1(1)
X2MIP=XS2(1)
Y1MIP=YS1(1)
Y2MIP=YS2(1)
EMAX=SHE1DB(1)
X1MIP=XS1(NSPT)
X2MIP=XS2(NSPT)
Y1MIP=YS1(NSPT)
Y2MIP=YS2(NSPT)
EMIN=SHE1DB(NSPT)

```

```
WRITE(50,*) 'THE MAXIMUM RADIATION AND POSITION OF SHIELD'  
WRITE(50,800) X1MP,X2MP,Y1MP,Y2MP,EMAX  
800 FORMAT(6(1X,E12.6))  
WRITE(50,*) 'THE MINIMUM RADIATION AND POSITION OF SHIELD'  
WRITE(50,810) X1MIP,X2MIP,Y1MIP,Y2MIP,EMIN  
810 FORMAT(6(1X,E12.6))  
RETURN  
END
```

E9 : DETERMINATION OF OPTIMUM LAYOUT (s/w)

The minimisation of the magnitude of the radiated fields with respect to s/w is described in the main text. The expressions for the electric field components are given in Eqns. 5.31 and 5.32. The expressions for $F_1, F_2, F_3, F_4, \alpha_1$ and α_2 are given as follows

$$F_1(Z_0) = \frac{V_s \sqrt{F_{11}^2 + F_{12}^2}}{R_{x1} \sqrt{F_{13}^2 + F_{14}^2}} \quad (\text{E9-1})$$

$$F_2(Z_0) = \frac{V_s Z_0}{R_{x2} \sqrt{F_{13}^2 + F_{14}^2}} \quad (\text{E9-2})$$

$$F_3(Z_0) = \sqrt{[R_L \sin\{\beta(l-y')\}]^2 + [X_L \sin\{\beta(l-y')\} - Z_0 \cos\{\beta(l-y')\}]^2} \quad (\text{E9-3})$$

$$F_4(Z_0) = \sqrt{F_{13}^2 + F_{14}^2} \quad (\text{E9-4})$$

$$\alpha_1(Z_0) = \tan^{-1} \left(\frac{\alpha_{11} - \alpha_{12}}{1 + \alpha_{11} \alpha_{12}} \right) \quad (\text{E9-5})$$

$$\alpha_2(Z_0) = -\tan^{-1} \left(\frac{\alpha_{13} + \alpha_{12}}{1 - \alpha_{13} \alpha_{12}} \right) \quad (\text{E9-6})$$

where,

$$F_{11} = Z_0 (R_s + R_L) \cos(\beta R_{x1}) - X_L \sin(\beta l) \cos(\beta R_{x1}) + R_L \sin(\beta l) \sin(\beta R_{x1})$$

$$F_{12} = X_L \sin(\beta l) \sin(\beta R_{x1}) + R_L \sin(\beta l) \cos(\beta R_{x1}) - Z_0 \cos(\beta l) \sin(\beta R_{x1})$$

$$F_{13} = Z_0 (R_s + R_L) \cos(\beta l) - (R_L X_s + X_L X_s) \sin(\beta l)$$

$$F_{14} = (Z_0^2 + R_s R_L - X_L X_s) \sin(\beta l)$$

$$\alpha_{11} = \frac{X_L \sin(\beta l) \sin(\beta R_{x1}) + R_L \sin(\beta l) \cos(\beta R_{x1}) - Z_0 \cos(\beta l) \sin(\beta R_{x1})}{Z_0 \cos(\beta l) \cos(\beta R_{x1}) - X_L \sin(\beta l) \cos(\beta R_{x1}) + R_L \sin(\beta l) \sin(\beta R_{x1})}$$

$$\alpha_{12} = \frac{(X_s + X_L) \cos(\beta l) + (Z_0^2 + R_s R_L - X_L X_s) \sin(\beta l)}{Z_0 (R_s + R_L) \cos(\beta l) - (R_L X_s + X_L R_s) \sin(\beta l)}$$

$$\alpha_{13} = \tan(\beta R_{x2})$$

where the expression for R_{x1} and R_{x2} are given in Eqns. D1-1 and D1-2 respectively.

E10: COMPUTER PROGRAMME LISTING TO FIND THE OPTIMUM LAYOUT

The computer programme that determines the optimum layout (s/w) and the magnitude of the radiated field for different s/w ratio is listed here. All the subroutines are also listed.

Computer programme listing

```
C *****
C THIS ROUTINE IS USED TO FIND THE OPTIMUM LAYOUT TO
C GET MINIMUM RADIATION FROM A PCB.
C *****
COMMON /DATA/ RS,XS,RL,XL,ZS,ZL,BETA,L,EPR,H,S
COMMON /DISTN/ XX,YY,ZZ,XXP,YYP,ZZP
REAL L
OPEN(UNIT=3, STATUS='UNKNOWN', FILE='OPTLAY.OUT')
OPEN(UNIT=4, STATUS='UNKNOWN', FILE='OPTLAY1.OUT')
OPEN(UNIT=1, STATUS='OLD', FILE='OPTLAY.DAT')

PI=3.14159

C GET THE DATA FOR ANALYSIS

WRITE(*,*) 'XX,YY,ZZ,XXP,YYP,ZZP'
READ(*,*) XX,YY,ZZ,XXP,YYP,ZZP
WRITE(*,*) 'L,H,EPR,HT'
READ(*,*) L,H,EPR,HT
WRITE(*,*) 'FR,VS'
READ(*,*) FR,VS
WRITE(*,*) 'RS,XS,RL,XL'
READ(*,*) RS,XS,RL,XL
ZS=RS
ZL=RL
BETA=(2.*PI)*FR/300.0
CALL OPTLAY
STOP
END
```

SUBROUTINES

SUBROUTINE 1

```
SUBROUTINE OPTLAY
PARAMETER(TOL=1.0E-4,EQL=1.0E-3)
COMMON /DATA/ RS,XS,RL,XL,ZS,ZL,BETA,L,EPR,H,S
COMMON /DISTN/ XX,YY,ZZ,XXP,YYP,ZZP
DIMENSION AMIN(20)
EXTERNAL FUNC
REAL L
NMIN=0
PI=3.14159

C DEFINE THE S/W RATIO RANGE
C GET THE LOWER AND UPPER LIMIT OF S/W

DO 12 I=1,20
AX=1+.1*I
BX=AX+.1

CALL MNBRAK(AX,BX,CX,FA,FB,FC,FUNC)

B=BRENT(AX,BX,CX,FUNC,TOL,XMIN)
```

```

IF(NMIN .EQ. 0) THEN
  AMIN(1)=XMIN
  NMIN=1
ELSE
  IFLAG=0
DO 11 J=1,NMIN
  IF(ABS(XMIN-AMIN(J)) .LE. EQL*XMIN) IFLAG=1
11 CONTINUE
IF(IFLAG .EQ. 0) THEN
  NMIN=NMIN+1
  AMIN(NMIN)=XMIN
ENDIF
12 CONTINUE
WRITE(*,*) XMIN,B
RETURN
END

```

SUBROUTINE 2

```

FUNCTION BRENT(AX,BX,CX,F,TOL,XMIN)
PARAMETER(ITMAX=100,CGOLD=0.3819660,ZEPS=1.0E-5)
COMMON /DATA/ RS,XS,RL,XL,ZS,ZL,BETA,L,EPR,H,S
COMMON /DISTN/ XX,YY,ZZ,XXP,YYP,ZZP
REAL L
PI=3.14159
A=MIN(AX,CX)
B=MAX(AX,CX)
V=BX
W=V
X=V
E=0.0
FX=F(X)
FV=FV
FW=FX
DO 11 ITER=1,ITMAX
  XM=0.5*(A+B)
  TOL1=TOL*ABS(X)+ZEPS
  TOL2=2.0*TOL1
  IF(ABS(X-XM) .LE. (TOL2-0.5*(B-A))) GO TO 3
  IF(ABS(E) .GT. TOL1) THEN
    R=(X-W)*(ABS(FX)-ABS(FV))
    Q=(X-V)*(ABS(FX)-ABS(FW))
    P=(X-V)*Q-(X-W)*R
    Q=2.*(Q-R)
    IF(Q .GT. 0) P=-P
    Q=ABS(Q)
    ETEMP=E
    E=D
    IF(ABS(P) .GE. ABS(0.5*Q*ITEMP) .OR. P .LE. Q*(A-X) .OR.
1 P .GE. Q*(B-X)) GO TO 1
    D=P/Q
    U=X+D
    IF((U-A) .LT. TOL2 .OR. (B-U) .LT. TOL2) D=SIGN(TOL1,XM-X)
    GO TO 2
  END IF
1 IF(X .GE. XM) THEN
  E=A-X
ELSE
  E=B-X
ENDIF
D=CGOLD*E
2 IF(ABS(D) .GE. TOL1) THEN
  U=X+D
ELSE
  U=X+SIGN(TOL1,D)
ENDIF
FU=F(U)
IF(ABS(FU) .LE. ABS(FX)) THEN
  IF(U .GE. X) THEN
    A=X
  ELSE
    B=X
  END IF
  V=W
  FW=FU
  W=X

```

```

FW=FX
X=U
FX=FU
ELSE
IF(U .LT. X) THEN
A=U
ELSE
B=U
END IF
IF(ABS(FU) .LE. ABS(FW) .OR. W .EQ. X) THEN
V=W
FV=F*W
W=U
FW=F*U
ELSE IF(ABS(FU) .LE. ABS(FV) .OR. V .EQ. X .OR. V .EQ. W) THEN
V=U
FV=FU
END IF
END IF
11 CONTINUE
PAUSE 'BRENT EXCEED MAXIMUM ITERATION'
3 XMIN=X
BRENT=FX
RETURN
END

```

SUBROUTINE 3

```

SUBROUTINE MNBRAK(AX,BX,CX,FA,FB,FC,FUNC)
PARAMETER (GOLD=1.618034, GLIMIT=100, TINY=1.0E-10)
COMMON /DATA/ RS, XS, RL, XL, ZS, ZL, BETA, L, EPR, H, S
COMMON /DISTN/ XX, YY, ZZ, XXP, YYP, ZZP
REAL L
PI=3.14159
FA=FUNC(AX)
FB=FUNC(BX)
WRITE(4,*) AX,FA
IF(FB .GT. FA) THEN
DUM=AX
AX=BX
BX=DUM
DUM=FB
FB=FA
FA=DUM
END IF
CX=BX+GOLD*(BX-AX)
IF(CX .LE. 1.0) CX=1.01
WRITE(3,*)CX
WRITE(3,*) CX
FC=FUNC(CX)
1 IF(FB .GE. FC) THEN
WRITE(3,*) 'PARNAB'
R=(BX-AX)*(FB-FC)
Q=(BX-CX)*(FB-FA)
U=BX-((BX-CX)*Q-(BX-AX)*R)/(2.*SIGN(MAX(ABS(Q-R),TINY),(Q-R)))
IF(U .LE. 1.0) U=1.01
WRITE(3,*) U
ULIM=BX+GLIMIT*(CX-BX)
IF((BX-U)*(U-CX) .GT. 0) THEN
WRITE(3,*)U
FU=FUNC(U)
IF(FU .LT. FC) THEN
AX=BX
FA=FB
BX=U
FB=FU
GO TO 1
ELSE IF(FU .GT. FB) THEN
CX=U
FC=FU
GO TO 1
END IF
U=CX+GOLD*(CX-BX)
WRITE(*,*) U
FU=FUNC(U)
ELSE IF((CX-U)*(U-ULIM) .GT. 0) THEN
WRITE(3,*) U

```

```

FU=FUNC(U)
IF(FU .LT. FC) THEN
BX=CX
CX=U
U=CX+GOLD*(CX-BX)
IF(U .LE. 1.0) U=1.01
FB=FC
FC=FU
WRITE(3,*) U
FU=FUNC(U)
END IF
ELSE IF((U-ULIM)*(ULIM-CX) .GE. 0) THEN
U=ULIM
WRITE(3,*) U
FU=FUNC(U)
ELSE
U=CX+GOLD*(CX-BX)
WRITE(3,*) U
IF(U .LE. 1.0) U=1.01
FU=FUNC(U)
END IF
AX=BX
BX=CX
CX=U
FA=FB
FB=FC
FC=FU
GO TO 1
END IF
RETURN
END

```

SUBROUTINE 4

```

FUNCTION FUNC(X)
COMMON /DATA/ RS,XS,RL,XL,ZS,ZL,BETA,L,EPR,H,S
COMMON /DISTN/ XX,YY,ZZ,XXP,YYP,ZZP
REAL L
VS=1.0
XSAV=X
S=H*XSAV
WRITE(3,*) XSAV
CALL FUNV(XSAV,AT)
FUNC=AT
RETURN
END

```

SUBROUTINE 5

C THIS ROUTINE IS TO FIND THE FUNCTION VALUE

```

SUBROUTINE FUNV(ZX,AT)
REAL L
COMMON /DATA/ RS,XS,RL,XL,ZS,ZL,BETA,L,EPR,H,S
COMMON /DISTN/ XX,YY,ZZ,XXP,YYP,ZZP
COMMON /CHAR/ Z0
EXTERNAL FFF2,FFF1
VS=1.0
PI=22.0/7.0
Z0=120/SQRT(EPR)*FFF1(ZX)
S=H*ZX
OMGA= BETA*300.0*1.0E6
CALL XDVA(AX)
RAX=(S*AX)*(OMGA*12.56E-7)/(4*PI)
RAY=(VS*FFF2(ZX))*(OMGA*12.56E-7)/(4*PI)
AT=SQRT(RAX**2+RAY**2)
RETURN
END

```

SUBROUTINE 6

```

FUNCTION FFF1(ZX)
REAL K,KP
KP=SQRT(1-K*K)
PI=22.0/7.0
FFF1=LOG(ZX+SQRT(ZX*ZX-1))
RETURN

```

END

SUBROUTINE 7

```
FUNCTION FFF2(ZX)
COMMON /DATA/ RS,XS,RL,XL,ZS,ZL,BETA,L,EPR,H,S
COMMON /DISTN/ XX,YY,ZZ,XXP,YYP,ZZP
COMMON /CHAR/ Z0
REAL L
PI=22.0/7.0
CALL FUNVI(SS)
FFF2=SS
RETURN
END
```

SUBROUTINE 8

```
SUBROUTINE XDVA(AX)
COMMON /DATA/ RS,XS,RL,XL,ZS,ZL,BETA,L,EPR,H,S
COMMON /DISTN/ XX,YY,ZZ,XXP,YYP,ZZP
COMMON /CHAR/ Z0
REAL L
VS=1.0
RX1=SQRT((XX-XXP)**2+(YY+0.5*L)**2+ZZ**2)
RX2=SQRT((XX-XXP)**2+(YY-0.5*L)**2+ZZ**2)

RIGX=(VS/RX1)*SQRT((Z0*COS(BETA*L)*COS(BETA*RX1)+RL*SIN(BETA*L)
1 *SIN(BETA*RX1)-XL*SIN(BETA*L)*COS(BETA*RX1))**2+(XL*SIN(BETA*L)
2 *SIN(BETA*RX1)+RL*SIN(BETA*L)*COS(BETA*RX1)-Z0*COS(BETA*L)*SIN
3 (BETA*RX1))**2)/SQRT((Z0*(RS+RL)*COS(BETA*L)-(RL*XS+XL*XS)*SIN
4 (BETA*L))**2+((XS+XL)*COS(BETA*L)+(Z0*Z0+RS*RL-XL*XS)*SIN(BETA
5 *L))**2)

RILX=(VS/RX2)*Z0/SQRT((Z0*(RS+RL)*COS(BETA*L)-(RL*XS+XL*XS)*SIN
1 (BETA*L))**2+((XS+XL)*COS(BETA*L)+(Z0*Z0+RS*RL-XL*XS)*SIN(BETA
2 *L))**2)

A1=(RL*SIN(BETA*L)*COS(BETA*RX1)-Z0*COS(BETA*L)*SIN(BETA*RX1)+
1 XL*SIN(BETA*L)*SIN(BETA*RX1))/(Z0*COS(BETA*L)*COS(BETA*RX1)+RL*
2 SIN(BETA*L)*SIN(BETA*RX1)-XL*SIN(BETA*L)*COS(BETA*RX1))

A2=((RS*RL+Z0**2-XL*XS)*SIN(BETA*L)+(XS+XL)*COS(BETA*L))/
1 (Z0*(RS+RL)*COS(BETA*L)-(RL*XS+XL*RS)*SIN(BETA*L))

A3=TAN(BETA*RX2)

AA1=ATAN((A1-A2)/(1+A1*A2))
AA2=ATAN((A3+A2)/(1-A3*A2))

AX=SQRT((RIGX*COS(AA1)-RILX*COS((-1)*AA2))**2+(RIGX*SIN(AA1)-
1 RILX*SIN((-1)*AA2))**2)

RETURN
END
```

SUBROUTINE 9

C THIS ROUTINE IS USED TO FIND THE INTEGRATION OF A FUNCTION

```
SUBROUTINE FUNVI(SS)
EXTERNAL FUNC12
REAL L
COMMON /DATA/ RS,XS,RL,XL,ZS,ZL,BETA,L,EPR,H,S
COMMON /DISTN/ XX,YY,ZZ,XXP,YYP,ZZP
COMMON /CHAR/ Z0
NVAL=10
X1=-L/2
X2=L/2
DX=(X2-X1)/NVAL
DO 11 I=1,NVAL
X=X1+I*DX
CALL QGAUSS(FUNC12,X1,X,SS)
WRITE(*,*) X,SS
11 CONTINUE
RETURN
END
```

SUBROUTINE 10

```
FUNCTION FUNC12(X)
REAL L
COMMON /DATA/ RS,XS,RL,XL,ZS,ZL,BETA,L,EPR,II,S
COMMON /DISTN/ XX,YY,ZZ,XXP,YYP,ZZP
COMMON /CHAR/ Z0
WRITE(*,*) RL,RS,XX,BETA
FUNC12=F3(X)*SQRT((Z0*COS(BETA*(L-X)))**2+(XL*SIN(BETA*(L-X)))**2
1+(RL*SIN(BETA*(L-X)))**2)/SQRT((Z0*(RS+RL)*COS(BETA*L)-(RL*XS+RS
2*XL)*SIN(BETA*L))**2+(XS+XL)*COS(BETA*L)+(Z0*Z0+RS*RL-XL*XS)*
3 SIN(BETA*L)**2)
RETURN
END
```

SUBROUTINE 11

```
FUNCTION F3(X)
EXTERNAL F4,F5
REAL L
COMMON /DATA/ RS,XS,RL,XL,ZS,ZL,BETA,L,EPR,II,S
COMMON /DISTN/ XX,YY,ZZ,XXP,YYP,ZZP
RY1=F4(X)
RY2=F5(X)

F3=(1/(RY1*RY2))*SQRT(RY2*RY2+RY1*RY1-2*RY2*RY1*COS(BETA*
1 (RY1-RY2)))
WRITE(*,*) F3
RETURN
END
```

SUBROUTINE 12

```
FUNCTION F4(X)
REAL L
COMMON /DATA/ RS,XS,RL,XL,ZS,ZL,BETA,L,EPR,II,S
COMMON /DISTN/ XX,YY,ZZ,XXP,YYP,ZZP
F4=SQRT((XX+0.5*S)**2+(YY-X)**2+ZZ**2)
RETURN
END
```

SUBROUTINE 13

```
FUNCTION F5(X)
REAL L
COMMON /DATA/ RS,XS,RL,XL,ZS,ZL,BETA,L,EPR,II,S
COMMON /DISTN/ XX,YY,ZZ,XXP,YYP,ZZP

F5=SQRT((XX-0.5*S)**2+(YY-X)**2+ZZ**2)
RETURN
END
```

SUBROUTINE 14

```
SUBROUTINE QGAUSS(FUNC12,A,B,SS)
DIMENSION X(5),WW(5)
REAL L
COMMON /DATA/ RS,XS,RL,XL,ZS,ZL,BETA,L,EPR,II,S
COMMON /DISTN/ XX,YY,ZZ,XXP,YYP,ZZP
COMMON /CHAR/ Z0
DATA X/0.1488743389,0.4333953941,0.6794095682,0.850633666,
1 .9739065285/
DATA WW/0.2955242247,0.2692667193,0.2190863625,0.1494513491,
1 0.0666713443/
XM=0.5*(B+A)
XR=0.5*(B-A)
SS=0
DO 11 J=1,5
```

```
DX=XR*X(J)
SS=SS+WW(J)*(FUNC12(XM+DX)+FUNC12(XM-DX))
11 CONTINUE
SS=XR*SS
RETURN
END
```

Note: Part of the subroutines 2, 4 and 14 has been copied from chapter 10 of Numerical Recipes by Press et al. published by Cambridge University press, Cambridge 1986.

F1: PROBE PERFORMANCE FACTOR (*PF*)

The performance factors (*PF*) for the ball (EMCO 7405-904) and the loop probes (EMCO 7405-901) are shown in Figs. F1-1 and F1-2 respectively.

Fig. F1-1 Performance factor for the ball probe EMCO 7405-904.

Fig. F1-2 Performance factor for the loop probe EMCO 7405-901.

F1: PROBE PERFORMANCE FACTOR (PF)

The performance factors (*PF*) for the ball (EMCO 7405-904) and the loop probes (EMCO 7405-901) are shown in Figs. F1-1 and F1-2 respectively.

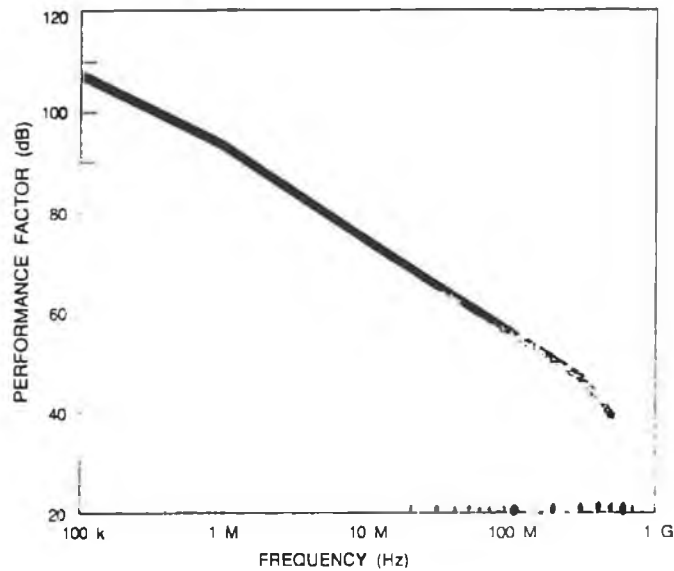


Fig. F1-1 Performance factor for the ball probe EMCO 7405-904.

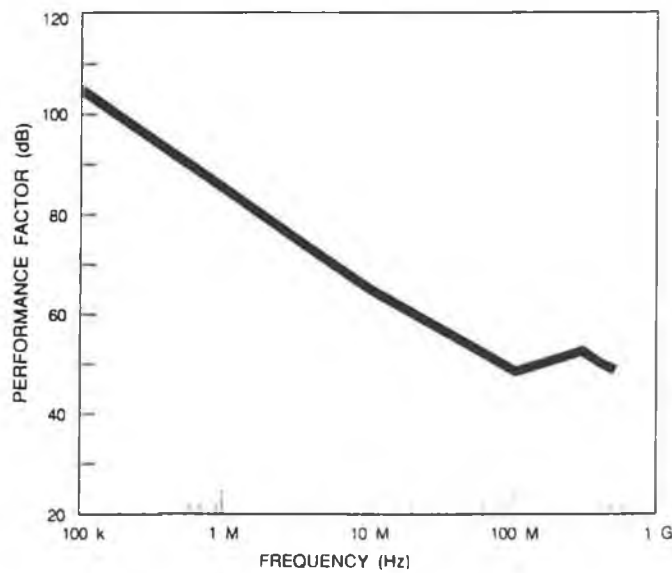


Fig. F1-2 Performance factor for the loop probe EMCO 7405-901.

F2: ANTENNA FACTORS (AF) FOR BCA AND LPA

The plots of antenna factors, for BCA (Electro-Metrics model number BIA 30) and LPA (Electro-Metrics LPA 30), as a function of frequency, at 1 m distance are shown in Figs. F2-1 and F2-2 respectively. The *AF*s which have been supplied by the manufacturer have been used for these plots.

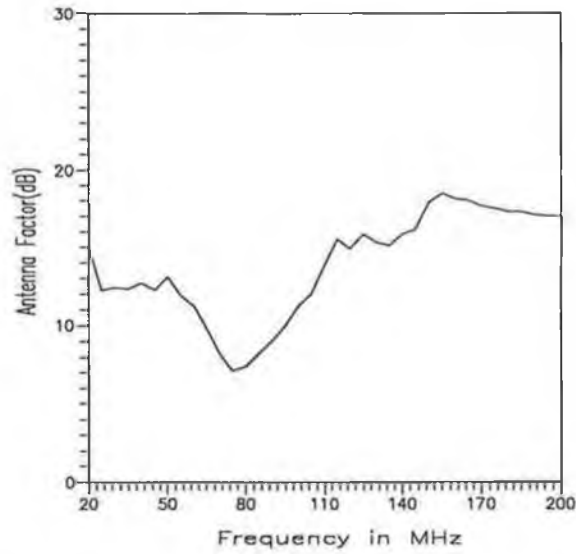


Fig. F2-1 Antenna factor for BCA at 1 m distance.

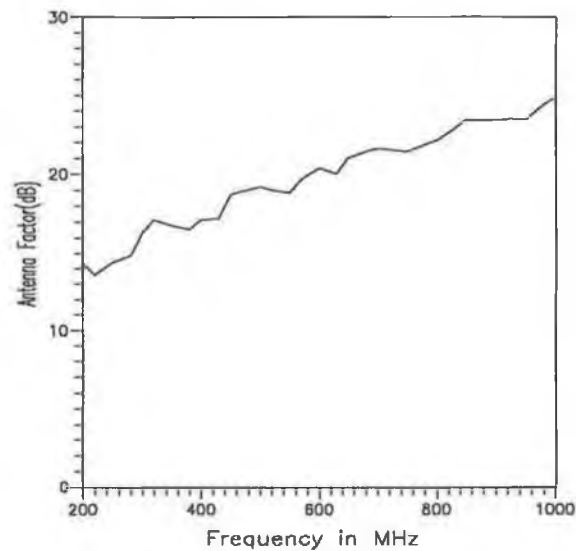


Fig. F2-2 Antenna factor for LPA at 1 m distance.

F3. SHIELDING EFFECTIVENESS OF SHIELDING BLOCK

The shielding effectiveness (SE) of a plane metallic sheet against normally incident plane wave has been developed theoretically by Schulz *et al.* [119]. The SE of a metal sheet is expressed as

$$SE = A + R + B \quad \text{dB} \quad (\text{F3-1})$$

where the absorption loss

$$A = 8.686\sqrt{\pi\mu f\sigma t} \quad \text{dB} \quad (\text{F3-2})$$

and the reflection loss

$$R = -20 \log_{10} \left| \frac{4k}{(1+k)^2} \right| \quad \text{dB} \quad (\text{F3-3})$$

and the correction term for successive reflections

$$B = 20 \log_{10} \left| 1 - \frac{(k-1)^2}{(k+1)^2} e^{-2\gamma t} \right| \text{dB} \quad (\text{F3-4})$$

In the above set of equations, f is the frequency, μ and σ are the permeability and the conductivity of the material, t is the thickness of the material and $k = Z_w / \eta$ (for plane wave, $Z_w = 377.0$), η is the intrinsic impedance of the sheet and γ is the propagation constant of an EM wave inside the material.

The shielding effectiveness of the aluminium tape of thickness 56 μm (used in this work) has been calculated from the Eqn. F3-1 using Mathcad® [121]. The SE value as a function of frequency is shown in Fig. F3-1.

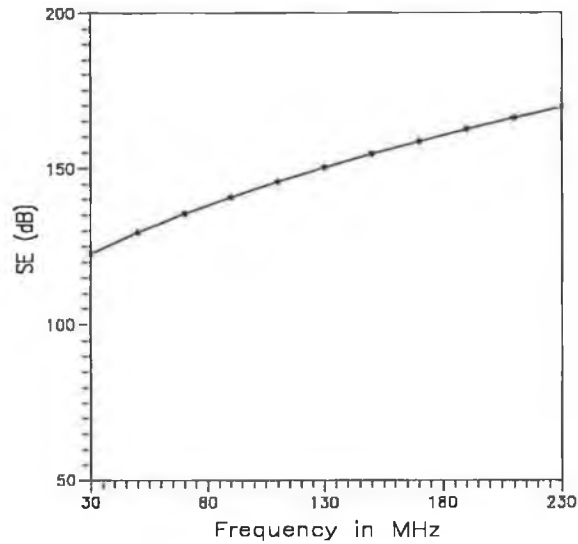


Fig. F3-1 The *SE* of a thin aluminium sheet of 56 μm thick as a function of frequency.

Table TF1: The frequency of the resonant modes in the screened room.

m	n	p	Frequency (MHz)	m	n	p	Frequency (MHz)
0	1	1	92.30	1	2	1	161.00
0	1	2	144.00	1	2	2	195.30
0	1	3	202.80	1	3	0	209.90
0	2	1	147.80	2	0	1	142.70
0	2	2	184.60	2	0	2	180.50
1	0	1	90.27	2	1	0	144.00
1	0	2	142.70	2	1	1	157.50
1	0	3	201.80	2	1	2	192.50
1	1	0	92.30	2	2	0	184.60
1	1	1	112.20	2	2	1	195.30
1	1	2	157.50	3	0	1	201.80
1	2	0	147.80	3	1	0	202.80

Table TF1 depicts the frequencies of the resonance calculated from Eqn. 7.3 for the dimensions of the room under consideration ($2.35 \times 2.35 \times 2.25$ m).

F4: DEVELOPMENT OF THE EXPRESSIONS FOR FIELDS IN AN EMPTY ROOM DUE TO TE WAVES

TE modes propagating in the z-direction

The positively and negatively travelling TE modes in the z-direction, in a rectangular cavity may be combined to yield the field expressions in the cavity. The expressions are given in [95], as

$$E_{xz} = \frac{j\omega\mu C}{k_c^2} \frac{n\pi}{b_1} \cos\left(\frac{m\pi x}{a_1}\right) \sin\left(\frac{n\pi y}{b_1}\right) \sin\left(\frac{p\pi z}{d_1}\right) \quad (\text{F4-1})$$

$$E_{yz} = -\frac{j\omega\mu C}{k_c^2} \frac{m\pi}{a_1} \sin\left(\frac{m\pi x}{a_1}\right) \cos\left(\frac{n\pi y}{b_1}\right) \sin\left(\frac{p\pi z}{d_1}\right) \quad (\text{F4-2})$$

$$H_{zx} = C \cos\left(\frac{m\pi x}{a_1}\right) \cos\left(\frac{n\pi y}{b_1}\right) \sin\left(\frac{p\pi z}{d_1}\right) \quad (\text{F4-3})$$

$$H_{yz} = -\frac{C}{k_c^2} \frac{p\pi}{d_1} \frac{m\pi}{a_1} \sin\left(\frac{m\pi x}{a_1}\right) \cos\left(\frac{n\pi y}{b_1}\right) \cos\left(\frac{p\pi z}{d_1}\right) \quad (\text{F4-4})$$

$$H_{xz} = -\frac{C}{k_c^2} \frac{p\pi}{d_1} \frac{n\pi}{b_1} \cos\left(\frac{m\pi x}{a_1}\right) \sin\left(\frac{n\pi y}{b_1}\right) \cos\left(\frac{p\pi z}{d_1}\right) \quad (\text{F4-5})$$

where, $k_c^2 = \left(\frac{m\pi}{a_1}\right)^2 + \left(\frac{n\pi}{b_1}\right)^2$ and C is constant.

The constant C can be obtained by normalizing the magnetic field by C . For TE modes, to normalize the magnetic field, the following condition has to be satisfied [57],

$$\mu \int_v |H_i|^2 dv = \mu \int_0^{d_1} \int_0^{b_1} \int_0^{a_1} \left[|H_{ixz}|^2 + |H_{iyz}|^2 + |H_{izz}|^2 \right] dx dy dz = 1 \quad (\text{F4-6})$$

where i is the mode index.

By substituting the expression for H_{xz} , H_{yz} , and H_{zx} from Eqns. F4-3, F4-4 and F4-5 respectively and by considering that

$$\int_0^a \sin^2\left(\frac{m\pi x}{a}\right) dx = \int_0^a \cos^2\left(\frac{m\pi x}{a}\right) dx = \frac{a}{2}$$

Eqn. F4-6 becomes as

$$\frac{C^2 \mu a_1 b_1 d_1}{8} \left[1 + \frac{1}{k_c^4} \left(\frac{p\pi}{d_1} \right)^2 \left\{ \left(\frac{m\pi}{a_1} \right)^2 + \left(\frac{n\pi}{b_1} \right)^2 \right\} \right] = 1 \quad (\text{F4-7})$$

Finally the constant C can be expressed as,

$$C = \sqrt{\frac{8}{a_1 b_1 d_1 \mu} \frac{\left(\frac{m}{a_1} \right)^2 + \left(\frac{n}{b_1} \right)^2}{\left(\frac{m}{a_1} \right)^2 + \left(\frac{n}{b_1} \right)^2 + \left(\frac{p}{d_1} \right)^2}} \quad (\text{F4-8})$$

TE modes propagating in the x-direction

For the TE modes propagating in the x-direction, the fields in the cavity can be expressed as,

$$E_{yx} = \frac{j\omega\mu C_1}{k_{c1}^2} \frac{p\pi}{d_1} \sin\left(\frac{m\pi x}{a_1}\right) \cos\left(\frac{n\pi y}{b_1}\right) \sin\left(\frac{p\pi z}{d_1}\right) \quad (\text{F4-9})$$

$$E_{zx} = -\frac{j\omega\mu C_1}{k_{c1}^2} \frac{n\pi}{b_1} \sin\left(\frac{m\pi x}{a_1}\right) \sin\left(\frac{n\pi y}{b_1}\right) \cos\left(\frac{p\pi z}{d_1}\right) \quad (\text{F4-10})$$

$$H_{xx} = C_1 \sin\left(\frac{m\pi x}{a_1}\right) \cos\left(\frac{n\pi y}{b_1}\right) \cos\left(\frac{p\pi z}{d_1}\right) \quad (\text{F4-11})$$

$$H_{yx} = -\frac{C_1}{k_{c1}^2} \frac{n\pi}{b_1} \frac{m\pi}{a_1} \cos\left(\frac{m\pi x}{a_1}\right) \sin\left(\frac{n\pi y}{b_1}\right) \cos\left(\frac{p\pi z}{d_1}\right) \quad (\text{F4-12})$$

$$H_{zx} = -\frac{C_1}{k_{c1}^2} \frac{p\pi}{d_1} \frac{m\pi}{a_1} \cos\left(\frac{m\pi x}{a_1}\right) \cos\left(\frac{n\pi y}{b_1}\right) \sin\left(\frac{p\pi z}{d_1}\right) \quad (\text{F4-13})$$

where, $k_{c1}^2 = \left(\frac{n\pi}{b_1} \right)^2 + \left(\frac{p\pi}{d_1} \right)^2$ and C_1 is constant which can be expressed as

$$C_1 = \sqrt{\frac{8 \left(\left(\frac{n}{b_1} \right)^2 + \left(\frac{p}{d_1} \right)^2 \right)}{a_1 b_1 d_1 \mu \left(\left(\frac{m}{a_1} \right)^2 + \left(\frac{n}{b_1} \right)^2 + \left(\frac{p}{d_1} \right)^2 \right)}} \quad (\text{F4-14})$$

TE waves propagating in the y direction

For the TE modes propagating in the y-direction, the fields in the cavity can be expressed as,

$$E_{xy} = -\frac{j\omega\mu C_2}{k_{c2}^2} \frac{p\pi}{d_1} \cos\left(\frac{m\pi x}{a_1}\right) \sin\left(\frac{n\pi y}{b_1}\right) \sin\left(\frac{p\pi z}{d_1}\right) \quad (\text{F4-15})$$

$$E_{zy} = \frac{j\omega\mu C_2}{k_{c2}^2} \frac{p\pi}{d_1} \cos\left(\frac{m\pi x}{a_1}\right) \sin\left(\frac{n\pi y}{b_1}\right) \sin\left(\frac{p\pi z}{d_1}\right) \quad (\text{F4-16})$$

$$H_{xy} = C_2 \cos\left(\frac{m\pi x}{a_1}\right) \sin\left(\frac{n\pi y}{b_1}\right) \cos\left(\frac{p\pi z}{d_1}\right) \quad (\text{F4-17})$$

$$H_{zy} = \frac{C_2}{k_{c2}^2} \frac{n\pi}{b_1} \frac{m\pi}{a_1} \sin\left(\frac{m\pi x}{a_1}\right) \cos\left(\frac{n\pi y}{b_1}\right) \cos\left(\frac{p\pi z}{d_1}\right) \quad (\text{F4-18})$$

$$H_{xy} = \frac{C_2}{k_{c2}^2} \frac{p\pi}{d_1} \frac{n\pi}{b_1} \cos\left(\frac{m\pi x}{a_1}\right) \cos\left(\frac{n\pi y}{b_1}\right) \sin\left(\frac{p\pi z}{d_1}\right) \quad (\text{F4-19})$$

where, $k_{c2}^2 = \left(\frac{m\pi}{a_1} \right)^2 + \left(\frac{p\pi}{d_1} \right)^2$ and C_2 is constant which can be expressed as

$$C_2 = \sqrt{\frac{8 \left(\left(\frac{m}{a_1} \right)^2 + \left(\frac{p}{d_1} \right)^2 \right)}{a_1 b_1 d_1 \mu \left(\left(\frac{m}{a_1} \right)^2 + \left(\frac{n}{b_1} \right)^2 + \left(\frac{p}{d_1} \right)^2 \right)}} \quad (\text{F4-20})$$

The resultant fields for TE modes propagating in the three orthogonal directions can be obtained from the vector addition of the individual field. The resultant field can be expressed as

$$\bar{E}_x = \bar{E}_{xy} + \bar{E}_{xz} \quad (\text{F4-21})$$

$$\bar{E}_y = \bar{E}_{yz} + \bar{E}_{yx} \quad (\text{F4-22})$$

$$\bar{E}_z = \bar{E}_{zx} + \bar{E}_{zy} \quad (\text{F4-23})$$

$$\bar{H}_x = \bar{H}_{xx} + \bar{H}_{xy} + \bar{H}_{xz} \quad (\text{F4-24})$$

$$\bar{H}_y = \bar{H}_{yx} + \bar{H}_{yy} + \bar{H}_{yz} \quad (\text{F4-25})$$

$$\bar{H}_z = \bar{H}_{zx} + \bar{H}_{zy} + \bar{H}_{zz} \quad (\text{F4-26})$$

The expressions for the resultant fields are given in Eqns. 7.5 to 7.10, where

$$F'_1 = \frac{1}{\sqrt{\left(\frac{m\pi}{a_1}\right)^2 + \left(\frac{n\pi}{b_1}\right)^2 + \left(\frac{p\pi}{d_1}\right)^2}} \left[\frac{\frac{n}{b_1}}{\sqrt{\left(\frac{m}{a_1}\right)^2 + \left(\frac{n}{b_1}\right)^2}} - \frac{\frac{p}{d_1}}{\sqrt{\left(\frac{m}{a_1}\right)^2 + \left(\frac{p}{d_1}\right)^2}} \right] \quad (\text{F4-27})$$

$$F'_2 = \frac{1}{\sqrt{\left(\frac{m\pi}{a_1}\right)^2 + \left(\frac{n\pi}{b_1}\right)^2 + \left(\frac{p\pi}{d_1}\right)^2}} \left[\frac{\frac{p}{d_1}}{\sqrt{\left(\frac{n}{b_1}\right)^2 + \left(\frac{p}{d_1}\right)^2}} - \frac{\frac{m}{a_1}}{\sqrt{\left(\frac{m}{a_1}\right)^2 + \left(\frac{n}{b_1}\right)^2}} \right] \quad (\text{F4-28})$$

$$F'_3 = \frac{1}{\sqrt{\left(\frac{m\pi}{a_1}\right)^2 + \left(\frac{n\pi}{b_1}\right)^2 + \left(\frac{p\pi}{d_1}\right)^2}} \left[\frac{\frac{m}{a_1}}{\sqrt{\left(\frac{m}{a_1}\right)^2 + \left(\frac{p}{d_1}\right)^2}} - \frac{\frac{n}{b_1}}{\sqrt{\left(\frac{n}{b_1}\right)^2 + \left(\frac{p}{d_1}\right)^2}} \right] \quad (\text{F4-29})$$

$$F'_4 = \frac{1}{\sqrt{\left(\frac{m}{a_1}\right)^2 + \left(\frac{n}{b_1}\right)^2 + \left(\frac{p}{d_1}\right)^2}} \left[\sqrt{\left(\frac{n}{b_1}\right)^2 + \left(\frac{p}{d_1}\right)^2} + \frac{\left(\frac{m}{a_1}\right)\left(\frac{n}{b_1}\right)}{\sqrt{\left(\frac{m}{a_1}\right)^2 + \left(\frac{p}{d_1}\right)^2}} + \frac{\left(\frac{p}{d_1}\right)\left(\frac{m}{a_1}\right)}{\sqrt{\left(\frac{m}{a_1}\right)^2 + \left(\frac{n}{b_1}\right)^2}} \right] \quad (\text{F4-30})$$

$$F'_5 = \frac{1}{\sqrt{\left(\frac{m}{a_1}\right)^2 + \left(\frac{n}{b_1}\right)^2 + \left(\frac{p}{d_1}\right)^2}} \left[\sqrt{\left(\frac{m}{a_1}\right)^2 + \left(\frac{p}{d_1}\right)^2} - \frac{\left(\frac{p}{d_1}\right)\left(\frac{n}{b_1}\right)}{\sqrt{\left(\frac{m}{a_1}\right)^2 + \left(\frac{n}{b_1}\right)^2}} - \frac{\left(\frac{n}{b_1}\right)\left(\frac{m}{a_1}\right)}{\sqrt{\left(\frac{p}{d_1}\right)^2 + \left(\frac{n}{b_1}\right)^2}} \right] \quad (\text{F4-31})$$

$$F'_6 = \frac{1}{\sqrt{\left(\frac{m}{a_1}\right)^2 + \left(\frac{n}{b_1}\right)^2 + \left(\frac{p}{d_1}\right)^2}} \left[\sqrt{\left(\frac{m}{a_1}\right)^2 + \left(\frac{n}{b_1}\right)^2} + \frac{\left(\frac{p}{d_1}\right)\left(\frac{n}{b_1}\right)}{\sqrt{\left(\frac{m}{a_1}\right)^2 + \left(\frac{p}{d_1}\right)^2}} - \frac{\left(\frac{p}{d_1}\right)\left(\frac{m}{a_1}\right)}{\sqrt{\left(\frac{p}{d_1}\right)^2 + \left(\frac{n}{b_1}\right)^2}} \right] \quad (\text{F4-32})$$

F5: DEVELOPMENT OF THE EXPRESSIONS FOR FIELDS IN AN EMPTY ROOM DUE TO TM WAVES

The field expressions due to TM waves propagating in the three orthogonal direction, can be obtained in a similar way as described in the previous section for the TE waves. These expressions are given in Eqns. 7.11 to 7.16, where

$$G_1 = \frac{1}{\sqrt{\left(\frac{m}{a_1}\right)^2 + \left(\frac{n}{b_1}\right)^2 + \left(\frac{p}{d_1}\right)^2}} \left[\sqrt{\left(\frac{n}{b_1}\right)^2 + \left(\frac{p}{d_1}\right)^2} - \frac{\left(\frac{m}{a_1}\right)\left(\frac{p}{d_1}\right)}{\sqrt{\left(\frac{m}{a_1}\right)^2 + \left(\frac{n}{b_1}\right)^2}} - \frac{\left(\frac{n}{b_1}\right)\left(\frac{m}{a_1}\right)}{\sqrt{\left(\frac{m}{a_1}\right)^2 + \left(\frac{p}{d_1}\right)^2}} \right] \quad (\text{F5-1})$$

$$G_2 = \frac{1}{\sqrt{\left(\frac{m}{a_1}\right)^2 + \left(\frac{n}{b_1}\right)^2 + \left(\frac{p}{d_1}\right)^2}} \left[\sqrt{\left(\frac{m}{a_1}\right)^2 + \left(\frac{p}{d_1}\right)^2} - \frac{\left(\frac{m}{a_1}\right)\left(\frac{n}{b_1}\right)}{\sqrt{\left(\frac{n}{b_1}\right)^2 + \left(\frac{p}{d_1}\right)^2}} - \frac{\left(\frac{n}{b_1}\right)\left(\frac{p}{d_1}\right)}{\sqrt{\left(\frac{m}{a_1}\right)^2 + \left(\frac{n}{b_1}\right)^2}} \right] \quad (\text{F5-2})$$

$$G_3 = \frac{1}{\sqrt{\left(\frac{m}{a_1}\right)^2 + \left(\frac{n}{b_1}\right)^2 + \left(\frac{p}{d_1}\right)^2}} \left[\sqrt{\left(\frac{m}{a_1}\right)^2 + \left(\frac{n}{b_1}\right)^2} - \frac{\left(\frac{m}{a_1}\right)\left(\frac{p}{d_1}\right)}{\sqrt{\left(\frac{n}{b_1}\right)^2 + \left(\frac{p}{d_1}\right)^2}} - \frac{\left(\frac{n}{b_1}\right)\left(\frac{p}{d_1}\right)}{\sqrt{\left(\frac{m}{a_1}\right)^2 + \left(\frac{p}{d_1}\right)^2}} \right] \quad (\text{F5-3})$$

$$G_4 = \frac{1}{\sqrt{\left(\frac{m\pi}{a_1}\right)^2 + \left(\frac{n\pi}{b_1}\right)^2 + \left(\frac{p\pi}{d_1}\right)^2}} \left[\frac{\frac{n}{b_1}}{\sqrt{\left(\frac{m}{a_1}\right)^2 + \left(\frac{n}{b_1}\right)^2}} - \frac{\frac{p}{d_1}}{\sqrt{\left(\frac{m}{a_1}\right)^2 + \left(\frac{p}{d_1}\right)^2}} \right] \quad (\text{F5-4})$$

$$G_5 = \frac{1}{\sqrt{\left(\frac{m\pi}{a_1}\right)^2 + \left(\frac{n\pi}{b_1}\right)^2 + \left(\frac{p\pi}{d_1}\right)^2}} \left[\frac{\frac{p}{d_1}}{\sqrt{\left(\frac{n}{b_1}\right)^2 + \left(\frac{p}{d_1}\right)^2}} - \frac{\frac{m}{a_1}}{\sqrt{\left(\frac{m}{a_1}\right)^2 + \left(\frac{n}{b_1}\right)^2}} \right] \quad (\text{F5-5})$$

$$G_6 = \frac{1}{\sqrt{\left(\frac{m\pi}{a_1}\right)^2 + \left(\frac{n\pi}{b_1}\right)^2 + \left(\frac{p\pi}{d_1}\right)^2}} \left[\frac{\frac{m}{a_1}}{\sqrt{\left(\frac{m}{a_1}\right)^2 + \left(\frac{p}{d_1}\right)^2}} - \frac{\frac{n}{b_1}}{\sqrt{\left(\frac{n}{b_1}\right)^2 + \left(\frac{p}{d_1}\right)^2}} \right] \quad (\text{F5-6})$$

F6: DOWNHILL SIMPLEX METHOD

The downhill simplex method [113] is an algorithm used for multi-dimensional minimisation of a function. Simplex is a geometrical figure consisting, in n dimensions, of $n + 1$ points (vertices) and all their interconnecting line segments, polygonal faces. In two dimensions, a simplex is a triangle. In three dimensions, it is a tetrahedron and so on.

The simplex method of minimisation must be started with $n + 1$ starting points (i.e. $n+1$ function values) for n variables, defining an initial simplex. The simplex method then goes through a series of iterative steps.

Firstly, the point of the simplex where function is largest is moved to the opposite face of the simplex (reflections) to a lower point (i.e. to a low function value). If it can find a lower function value, the method expands into another direction to take larger steps. If a lower point is found through reflections, the method tries for different ways such as reflection and expansion or reflection and contraction or a contraction along all dimensions of the simplex to

find a low point of the function. These steps are iterated until the function reaches the lowest value.

If the given function has several minima then the simplex method may converge to one of the local minima points. Therefore it is always advisable to start the minimisation procedure with different starting values.

A termination criterion can be difficult in multidimensional minimisation. Therefore, the user has to provide a termination criterion that is suited for the function.

F7: COMPUTER PROGRAMME TO FIND THE FIELD MAXIMA

The formulation to find the field maxima in a shielded enclosure is described in the main text (section 7.4.1). The computer programme is listed here. All subroutines are also included in this listing.

```

C *****
C ROUTINE TO FIND THE MAXIMA FIELD POINTS IN A SHIELDED ENCLOSURE AT FORBAIRT, DUBLIN.
C DOWNHILL SIMPLEX METHOD, A MULTIDIMENSIONAL MINIMISATION OF A FUNCTION
C HAS BEEN EMPLOYED HERE.
C *****

EXTERNAL FUNK
PARAMETER(NP=3,MP=4,FTOL=1.0E-6)

C A,B,D ARE THE DIMENSION OF THE ENCLOSURE
DIMENSION P(MP,MP),Y(MP),X(NP),P1(MP,NP)
INTEGER PX
REAL OMEGA
COMMON/DATA/A,B,D
PI=3.14159
WRITE(*,*) 'A,B,D,C,DD'
READ(*,*) A,B,D,C,DD
OPEN(UNIT=4, STATUS='UNKNOWN', FILE='ENFLM1.OUT')
OPEN(UNIT=6, STATUS='UNKNOWN', FILE='EFUNV.OUT')
OPEN(UNIT=3, STATUS='UNKNOWN', FILE='ENFLM.OUT')
WRITE(*,*) '((P1(I,J), J=1, NP), I=1, MP)'
READ(*,*) ((P1(I,J), J=1, NP), I=1, MP)

C MFLAG= INTEGER FLAG TO INDICATE THE TE OR TM MODES
C F= FREQUENCY
C IFLAG= AN INTEGER FLAG TO INDICATE THE E OR H FIELD

WRITE(*,*) F
READ(*,*) F
OMEGA=2*PI*F*1.0E6
DO 100 II=1,2
MFLAG=II-1
DO 101 JJ=1,2
IFLAG=JJ-1
WRITE(3,71)
71 FORMAT(///)
IF (MFLAG.EQ.0 .AND. IFLAG.EQ.0) THEN
WRITE(3,*) 'TE MODES AND MAXIMIZE THE E FIELD'
ELSE IF (MFLAG.EQ.0 .AND. IFLAG.EQ.1) THEN
WRITE(3,*) 'TE MODES AND MAXIMIZE THE H FIELD'
ELSE IF (MFLAG.EQ.1 .AND. IFLAG.EQ.0) THEN
WRITE(3,*) 'TM MODES AND MAXIMIZE THE E FIELD'
ELSE IF (MFLAG.EQ.1 .AND. IFLAG.EQ.1) THEN
WRITE(3,*) 'TM MODES AND MAXIMIZE THE H FIELD'
END IF

```

```

C M,N,PX =1,2,3 ....
DO 51 IM=1,4
M=IM-1
DO 52 JN=1,4
N=JN-1
DO 53 KPX=1,4
PX=KPX-1
IF (M .EQ. 0 .AND. N .EQ. 0 .AND. PX .EQ. 0) GO TO 53
CALL CONS(M,N,PX,OMEGA,C,DD,CZ,BX,DY,FX,FY,MFLAG)

C ROUTINE TO FIND THE FUNCTION VALUE
DO 500 I=1,101
X(1)=(I-1)*A/100
X(2)=0
X(3)=(I-1)*D/100
EFUNV=FUNK(X,M,N,PX,MFLAG,IFLAG,CZ,BX,DY,FX,FY)
WRITE(6,*) X(1),EFUNV
500 CONTINUE
DO 30 I=1,MP
DO 31 J=1,NP
P(I,J)=P1(I,J)
X(J)=P(I,J)
31 CONTINUE
Y(I)=FUNK(X,M,N,PX,MFLAG,IFLAG,CZ,BX,DY,FX,FY)
30 CONTINUE
IF (MFLAG .EQ. 0 .AND. IFLAG .EQ. 0) THEN
WRITE(3,60) F,M,N,PX
60 FORMAT(/2X,'FREQUENCY='1X,F7.2,'MHZ',5X,'TE',I1,I1,I1,2X,'E FIELD'
1 )
ELSE IF(MFLAG .EQ. 0 .AND. IFLAG .EQ. 1) THEN
WRITE(3,61) F,M,N,PX
61 FORMAT(/2X,'FREQUENCY='1X,F7.2,'MHZ',5X,'TE',I1,I1,I1,2X,'H FIELD'
1 )
ELSE IF(MFLAG .EQ. 1 .AND. IFLAG .EQ. 0) THEN
WRITE(3,62) F,M,N,PX
62 FORMAT(/2X,'FREQUENCY='1X,F7.2,'MHZ',5X,'TM',I1,I1,I1,2X,'E FIELD'
1 )
ELSE IF(MFLAG .EQ. 1 .AND. IFLAG .EQ. 1) THEN
WRITE(3,63) F,M,N,PX
63 FORMAT(/2X,'FREQUENCY='1X,F7.2,'MHZ',5X,'TM',I1,I1,I1,2X,'H FIELD'
1 )
END IF
CALL SIMLEXD(Y,P,MP,NP,FTOL,CZ,BX,DY,FX,FY,M,N,PX,IFLAG,MFLAG)
53 CONTINUE
52 CONTINUE
51 CONTINUE
101 CONTINUE
100 CONTINUE
STOP
END

```

Subroutine 1

```

SUBROUTINE AMOEB(A,P,Y,MP,NP,NDIM,FTOL,FUNK,ITER,CZ,BX,DY,FX,FY,M,
1 N,PX,IFLAG,MFLAG)

C FUNK(X)=FUNCTION
C X=NDIM-DIMENSIONAL VECTOR(OUR CASE NDIM=3 I.E X,Y,Z)
C P= THE MATRIX WHOSE NDIM+1 ROWS ARE NDIM-DIMENSIONAL VECTORS
C WHICH ARE VERTICES OF THE STARTING SIMPLEX AND NDIM COLUMNS.
C I.E P(NDIM+1,NDIM) MATRIX. PHYSICAL DIMENSION OF THE P(MP,NP)
C WHICH IS INPUT MATRIX
C Y =THE VECTOR OF LENGTH NDIM+1 WHICH IS A INPUT VECTOR.
C WHOSE COMPONENTS ARE PRE-INITIALIZED TO THE VALUE OF THE
C FUNCTION EVALUATED AT THE NDIM+1 VERTICES(ROW) OF P
C FTOL=CONVERGENCE TOLARENCE
C ITER=NO OF ITERATIONS

PARAMETER(NMAX=20,ALPHA=1.0,BETA=0.5,GAMMA=2.0,ITMAX=1000)

C ALPHA,BETA,GAMMA DEFINE THE AXPANSION AND CONTRACTION

DIMENSION P(MP,NP),Y(NP),PR(NMAX),PRR(NMAX),PBAR(NMAX),XX(ITMAX,4
1 ),YY(ITMAX,4),ZZ(ITMAX,4)
COMMON /DATA/A,B,D
INTEGER PX

```

```

MPTS=NDIM+1
ITER=0
DO 400 I=1,MP
  XX(ITER,I)=P(I,1)
  YY(ITER,I)=P(I,2)
  ZZ(ITER,I)=P(I,3)
400 CONTINUE
1 ILO=1

C FIRST DETERMINE THE POINT WHICH IS HIGHEST(WORST),NEXT HIGHEST AND LOWEST (BEST)

IF(Y(1) .GT. Y(2)) THEN
  IHI=1
  INHI=2
ELSE
  IHI=2
  INHI=1
END IF
DO 11 I=1,MPTS
  IF(Y(I) .LT. Y(ILO)) ILO=I
  IF(Y(I) .GT. Y(IHI)) THEN
    INHI=IHI
    IHI=I
  ELSE IF(Y(I) .GT. Y(INHI)) THEN
    IF(I .NE. IHI) INHI=I
  END IF
11 CONTINUE

C COMPUTE THE FRACTIONAL RANGE FROM HIGHEST TO LOWEST AND RETURN IF SATISFACTORY

IF((ABS(Y(IHI))+ABS(Y(ILO))) .EQ. 0) RETURN
RTOL=2.*ABS(Y(IHI)-Y(ILO))/(ABS(Y(IHI))+ABS(Y(ILO)))
IF(RTOL.LT.FTOL) RETURN
IF(ITER .EQ. ITMAX) GO TO 40
ITER=ITER+1

C BEGINING OF NEW ITERATION. COMPUTE THE VECTOR AVERAGE OF ALL POINTS EXCEPT THE HIGHEST

DO 12 J=1,NDIM
  PBAR(J)=0.0
12 CONTINUE
DO 14 I=1,MPTS
  IF(I .NE. IHI) THEN
    DO 13 J=1,NDIM
      PBAR(J)=PBAR(J)+P(I,J)
13 CONTINUE
    END IF
14 CONTINUE

C EXTRAPOLATE BY A FACTOR ALPHA THROUGH THE FACE I.E REFLECT THE SIMPLEX FROM THE HIGH POINT

DO 15 J=1,NDIM
  PBAR(J)=PBAR(J)/NDIM
  PR(J)=(1.0+ALPHA)*PBAR(J)-ALPHA*P(IHI,J)
15 CONTINUE

C EVALUTATE THE FUNCTION AT THE REFLECTED POINT

YPR=FUNK(PR,M,N,PX,MFLAG,IFLAG,CZ,BX,DY,FX,FY)
IF(YPR .LE. Y(ILO)) THEN

C GIVES A RESULT BETTER THAN THE BEST POINT, SO TRY AN ADDITIONAL EXTRAPOLATION BY A FACTOR GAMMA

DO 16 J=1,NDIM
  PRR(J)=GAMMA*PR(J)+(1.-GAMMA)*PBAR(J)
16 CONTINUE

C CHECK OUT THE FUNCTION THERE.

YPRR=FUNK(PRR,M,N,PX,MFLAG,IFLAG,CZ,BX,DY,FX,FY)
IF(YPRR .LT. Y(ILO)) THEN

C THE ADDITIONAL EXTRAPOLATION SUCCEDED AND REPLACES THE HIGH POINT.

DO 17 J=1,NDIM
  P(IHI,J)=PRR(J)
17 CONTINUE
  Y(IHI)=YPRR
ELSE

```

```

C      THE EXTRAPOLATION FAILED ,BUT WE CAN STILL USE THE REFLECTED POINT.
      DO 18 J=1,NDIM
      P(IH,J)= PR(J)
18     CONTINUE
      Y(IH)=YPR
      END IF
      ELSE IF (YPR .GE. Y(IH)) THEN

C      THE REFLECTED POINT IS WORSE THAN THE SECOND-HIGHEST. IF IT IS BETTER
C      THAN THE HIGHEST, THEN REPLACE THE HIGHEST.

      IF (YPR .LT. Y(IH)) THEN
      DO 19 J=1,NDIM
      P(IH,J)=PR(J)
19     CONTINUE
      Y(IH)=YPR
      END IF

C      LOOK FOR AN INTERMEDIATE LOWER POINT.

      DO 21 J=1,NDIM
      PRR(J)=BETA*P(IH,J)+(1.-BETA)*PBAR(J)
21     CONTINUE
      YPRR=FUNK(PRR,M,N,PX,MFLAG,IFLAG,CZ,BX,DY,FX,FY)

C      CONTRACTION GIVES AN IMPROVEMENT SO ACCEPT IT

      IF (YPRR .LT. Y(IH)) THEN
      DO 22 J=1,NDIM
      P(IH,J)=PRR(J)
22     CONTINUE
      Y(IH)=YPRR
      ELSE

C      TO GET RID OF THAT HIGH POINT. BETTER CONTRACT AROUND THE LOWEST (BEST) POINT

      DO 24 I=1,MPTS
      IF (.NE. IL0) THEN
      DO 23 J=1,NDIM
      PR(J)=0.5*(P(I,J)+P(LO,J))
      P(I,J)=PR(J)
23     CONTINUE
      Y(I)=FUNK(PR,M,N,PX,MFLAG,IFLAG,CZ,BX,DY,FX,FY)
      END IF
24     CONTINUE
      END IF
      ELSE

C      IF THE ORIGINAL REFLECTION GIVES A MIDDLING POINT. REPLACE THE OLD HIGH POINT AND CONTINUE

      DO 25 J=1,NDIM
      P(IH,J)=PR(J)
25     CONTINUE
      Y(IH)=YPR
      END IF
      ITX=ITER-1
      DO 200 I=1,MP
      IF(P(I,1) .GT. 2.35 .OR. P(I,1) .LT. 0.0) P(I,1)=XX(ITX,I)
      IF(P(I,2) .GT. 2.25 .OR. P(I,2) .LT. 0.0) P(I,2)=YY(ITX,I)
      IF(P(I,3) .GT. 2.35 .OR. P(I,3) .LT. 0.0) P(I,3)=ZZ(ITX,I)
      XX(ITER,I)=P(I,1)
      YY(ITER,I)=P(I,2)
      ZZ(ITER,I)=P(I,3)
200    CONTINUE
      GO TO 1
40     PRINT *,'AMOEBA EXCEEDING MAXIMUM ITERATIONS'
      RETURN
      END

```

Subroutine 2

```

1     SUBROUTINE SIMLEXD(Y,P,MP,NP,FTOL,CZ,BX,DY,FX,FY,M,N,PX,IFLAG,
      MFLAG)
      EXTERNAL FUNK
      DIMENSION P(MP,NP), Y(MP)
      INTEGER PX

```

```

COMMON /DATA/A,B,D
NDIM=NP
DO 100 KL=1,MP
I=KL
WRITE(*,*) (P(I,J), J=1, NP)
100 CONTINUE
CALL AMOEBA(P,Y,MP,NP,NDIM,FTOL,FUNK,ITER,CZ,BX,DY,FX,FY,M,N,PX,
1 IFLAG,MFLAG)
WRITE(3,32) ITER
32 FORMAT(/1X,NO OF ITERATIONS=I4)
WRITE(3,33)
33 FORMAT(/4X,I, 8X,'X(I)',8X,'Y(I)',8X,'Z(I)',8X,'FIELDMAX')
DO 34 I=1,MP
YY=Y(I)*(-1)
WRITE(3,35) I,(P(I,J),J=1, NP),YY
35 FORMAT(/2X,I3,4X,3F12.6,2X,F12.6)
34 CONTINUE
WRITE(3,37) (P(4,J), J=1,3)
37 FORMAT(/2X,THE MAXIMUM FIELD POINT(,1X,F10.5,1X,',',F10.5,1X,',',
1 F10.5,')
RETURN
END

```

Subroutine 3

```

FUNCTION FUNK(X,M,N,PX,MFLAG,IFLAG,CZ,BX,DY,FX,FY)
DIMENSION X(3)
INTEGER PX
COMMON /DATA/A,B,D
PI=3.14159
IF (MFLAG.EQ.0 .AND. IFLAG.EQ.0) THEN

FUNK=(-1)*SQRT((FX*COS(M*X(1)*PI/A)*SIN(N*X(2)*PI/B)*SIN(PX
1 *X(3)*PI/D))**2+(FY*SIN(M*X(1)*PI/A)*COS(N*X(2)*PI/B)*SIN(
2 PX*X(3)*PI/D))**2)

ELSE IF (MFLAG.EQ.0 .AND. IFLAG.EQ.1) THEN

FUNK=(-1)*SQRT((CZ*COS(M*X(1)*PI/A)*COS(N*X(2)*PI/B)*SIN(PX*X(3)*
1 PI/D))**2+(BX*SIN(M*X(1)*PI/A)*COS(N*X(2)*PI/B)*SIN(PX*X(3)*
2 PI/D))**2+(DY*COS(M*X(1)*PI/A)*SIN(N*X(2)*PI/B)*COS(PX*X(3)*
3 PI/D))**2)

ELSE IF (MFLAG.EQ.1 .AND. IFLAG.EQ.0) THEN

FUNK=(-1)*SQRT((CZ*SIN(M*X(1)*PI/A)*SIN(N*X(2)*PI/B)*COS(PX*X(3)*
1 PI/D))**2+(BX*COS(M*X(1)*PI/A)*SIN(N*X(2)*PI/B)*SIN(PX*X(3)*
2 PI/D))**2+(DY*SIN(M*X(1)*PI/A)*COS(N*X(2)*PI/B)*SIN(PX*X(3)*
3 PI/D))**2)

ELSE IF (MFLAG.EQ.1 .AND. IFLAG.EQ.1) THEN

FUNK=(-1)*SQRT((FX*SIN(M*X(1)*PI/A)*COS(N*X(2)*PI/B)*COS(PX*X(3)*
1 PI/D))**2+(FY*COS(M*X(1)*PI/A)*SIN(N*X(2)*PI/B)*COS(PX*X(3)*
2 PI/D))**2)
END IF
RETURN
END

```

Subroutine 4

```

SUBROUTINE CONS(M,N,PX,OMEGA,C,DD,CZ,BX,DY,FX,FY,MFLAG)
INTEGER PX
REAL KC,KCC,MU,OMEGA
COMMON /DATA/A,B,D
PI=3.14159
MU=4*PI*1.0E-7
EPR=8.854*1.0E-12
KC=SQRT((M*PI/A)**2+(N*PI/B)**2)
KCC=KC**2
IF (MFLAG.EQ.0) THEN
1 C=SQRT((8/(A*B*D*MU))*((M/A)**2+(N/B)**2)/((M/A)**2+(N/B)**2+
(PX/D)**2))
CZ=C
IF (KCC.EQ.0) GO TO 301
BX=(-1)*C*(PX*PI/D)*(M*PI/A)/KCC
DY=(-1)*C*(PX*PI/D)*(N*PI/B)/KCC
FX=(OMEGA*MU*C*(N*PI/B))/KCC

```

```

301  FY=(OMEGA*MU*C*(M*PI/A))/KCC
      WRITE(*,*) KCC
      ELSE IF(MFLAG .EQ. 1) THEN
1    DD=SQRT((8/(A*B*D*EPR))*((M/A)**2+(N/B)**2)/((M/A)**2+(N/B)**2+
      (PX/D)**2))
      CZ=DD
      IF (KCC .EQ. 0) GO TO 300
      BX=(-1)*DD*(PX*PI/D)*(M*PI/A)/KCC
      DY=(-1)*DD*(PX*PI/D)*(N*PI/B)/KCC
      FX=(OMEGA*EPR*DD*(N*PI/B))/KCC
      FY=(OMEGA*EPR*DD*(M*PI/A))/KCC
300  END IF
      WRITE(4,*)M,N,PX, KCC,CZ,BX,DY,FX,FY
      RETURN
      END

```

F8: PERFORMANCE OF THE ECCOSORB AN 79

The performance of an absorber can be found from its reflectivity level or its absorption characteristics. A good quality absorber should have a low reflectivity level. The reflectivity profile of the ECCOSORB® AN-79 is shown in Fig. F8-1.

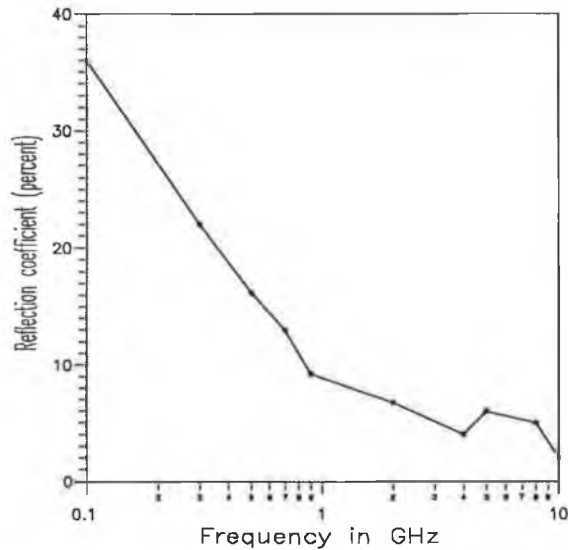


Fig. F8-1 Reflection coefficient in % of the ECCOSORB AN 79 good quality flexible foam sheet commercial absorbers. Expressed in % from the reflectivity profile (in dB) supplied by Emerson and Cuming (UK) (supplier of the absorbing foam).

F9: ABSORPTION CHARACTERISTICS OF FERRITE TILE (BE 15)

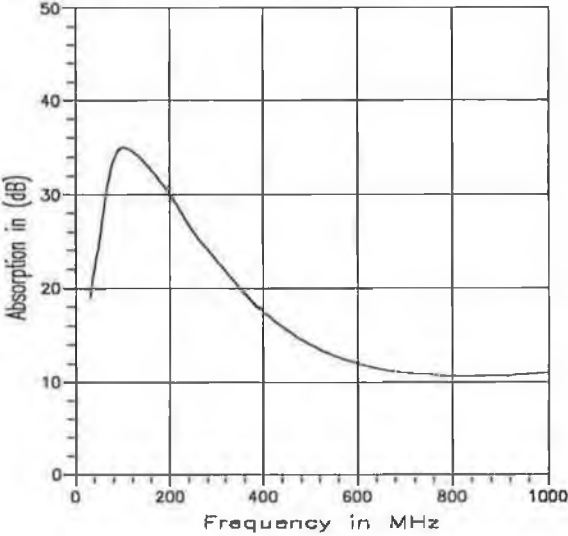


Fig. F9-1 Absorption characteristic of the ferrite absorber BE 15 supplied by the Pacific West electronics (USA) (supplier of the absorber).

G1: SIZE OF A PCB**Table TG1:** Maximum number of tracks and components in a PCB.

Tracks, pads, vias and components	Maximum number
Track	100
Placed pad	50
Placed via	50
IC	10
Resistor	20
Inductor	20
Capacitor	20
Transistor	10
Diode	10
Signal source	4

G2. LIST OF PUBLICATIONS FROM THIS RESEARCH

- [1] P. K. Saha and Jim Dowling, "A combined CAD package to predict and minimise EM radiation from a PCB at design stage," *EMC' 94 ROMA International Symposium on Electromagnetic Compatibility*, Rome, Italy, September 13-16, 1994, Symposium proceedings, Vol. 2, pp. 631-637.
- [2] P. K. Saha and Jim Dowling, "Prediction of PCB radiation using NEC software combined with commercial CAD packages," *19th ARMMS Conference Digest*, pp. 5/1-7, Leeds, September 27-28, 1993.
- [3] H. Rahman, P. K. Saha, Jim Dowling and T. Curran, "Shielding effectiveness measurement techniques for various materials used for EMI shielding," *IEE colloquium Digest on Screening of Connectors, Cables and Enclosures*, no. 1992/012, pp. 9/1-6, London, January 1992.
- [4] P. K. Saha and Jim Dowling, "Prediction of EM radiation from a PCB using extended transmission line modelling," accepted for oral presentation in the *IEEE international conference on EMC, ICEMC'95 KUL* and for publication in the conference proceeding, *ICEMC'95*, April 11-13, 1995, Kuala Lumpur, Malaysia.

REFERENCES

- [1] Keith Armstrong, "Profit from EMC," *Electronic Engineering Magazine, EMC supplement*, July 1994, pp. S-24- S-25.
- [2] J. Ruiters, "Electromagnetic compatibility (1)," *Elektor Electronics*, May 1993, pp. 24-26.
- [3] Bernard Cooperstein, "Radiation from printed wiring boards," *IEEE international symposium on EMC*.
- [4] Henry W.Ott, "Controlling EMI by proper printed wiring board layout," *IEEE international symposium on EMC*, Mar. 1985, Switzerland, pp. 127-132.
- [5] C.R. Paul and D.R. Bush, "Radiated Emissions from Common mode currents," *IEEE international symposium on EMC*, August 1987, pp. 197-203.
- [6] C.R. Paul, "A comparison of the contributions of common mode and differential-mode currents in radiated emissions," *IEEE Transactions on EMC*, Vol. 31, no. 2 pp. 189-193, May 1989.
- [7] D.R. Bush, "Radiated emissions of printed circuit board clock circuits," *IEEE international symposium on EMC*, 5-7 March, 1985, Switzerland, pp. 121-126.
- [8] J.D. Osburn and D.R.J White, "Methodology for developing expected values of radiated emissions from cables," *IEEE international symposium on EMC*, October 1979, pp. 39-45.
- [9] Lewis JR. and Luban D.G, "Graphical Rapid pulse spectrum analysis using the Lewis Locus," *IEEE international symposium on EMC 1983*, pp. 386-390.
- [10] A.T.Parker, Instruments, components and Accessories for the RFI/EMI Engineer, *Solar Electronics company*, 1979.
- [11] R.M. Keith, "Shielding: How to achieve the optimum level," *ITEM*, 1988, pp. 186, 188, 190, 364, and 366.
- [12] L.W. Beard, "Laboratory substantiation of interference prediction techniques," *Sprague technical paper*, October 1962.
- [13] Stutzman W.L. and Thiele G.A., "Antenna theory and design," John wiley, 1981.
- [14] Costa M. T.K. Sarker, B.J. Strait and S. Bennettet, "On radiation from printed circuit boards," *IEEE international symposium on EMC 1981*, Boulder, Co, USA, pp. 246-249..
- [15] Keenan, R.K., "Digital design for interference specifications," The keenan corporation, 1983, p.3.6-1.
- [16] R. Raut "On the computation of electromagnetic field components from a practical printed circuit board," *IEEE international symposium on EMC*, 1986, San Diego, CA. pp. 161-163.

- [17] R. Raut, Willem J. Steenaart and George I. Costache, "A note on the optimum layout of electronic Circuits to minimise the radiated electromagnetic field strength," *IEEE Transactions on EMC*, vol. 30, no. 1, Feb. 1988.
- [18] A. J. Sistino, "Radiation from a printed circuit board: theory and application," *The 8th international Zurich symposium on electromagnetic compatibility*, Mar. 1989, pp. 57-62.
- [19] J.P. Simpson , R.R. Goulette and G.I. Costache, "Radiation from microstrip transmission lines," *IEEE international symposium on EMC*, 1988, pp. 340-343.
- [20] V. Costa , S. Caniggia and L. Catello, "On the computation of electromagnetic field components from a transmission line: theory and application," *IEEE international symposium on EMC*, 1990, pp. 651-656.
- [21] Mardiguian, M. "*Interference control in computers and microprocessor-based equipment*," Don White consultants , inc., Gainesville, Virginia 22065, USA, 1984, Ch. 2.
- [22] S.A.Schelkunoff, "*Electromagnetic waves*," 1956 D.Van Nostrand Company Inc.
- [23] S. Daijavad, J. Janak, H. Heeb, A. Ruehil and D. McBride "A fast method for computing radiation from printed Circuit boards," *IEEE international symposium on EMC*, 1990, pp. 300-304.
- [24] A. E. Ruehli, "Equivalent circuit models for three- dimensional multiconductor systems," *IEEE Transaction on Microwave theory and techniques*, vol. MTT-22, pp. 216-221, March 1974.
- [25] Raouf Lawrence Khan and G. I. Costache, "Finite element method applied to modelling crosstalk problems on printed Circuit boards," *IEEE Transaction on electromagnetic compatibility*, vol. 31, no. 1, February 1989, pp. 5-15.
- [26] C.R.Paul, "Applications of multiconductor transmission line theory to the prediction of cable coupling, vol. 1, multiconductor transmission line theory," *Technical report, RADC-TR-76-101*, Rome Air Development Centre, Griffiss, AFB, NY. April 1976.
- [27] C.J Railton, K M Richardson, J P McGeehan and K F Elder "The prediction of radiation levels from printed circuit boards by means of the finite difference time domain method," *IEE international conference on electromagnetic compatibility*, November 1991, London, UK., pp. 339-343.
- [28] Xialoei Zhang and Kenneth K. Mei, "Time-Domain Finite Difference approach to the calculation of the frequency-dependent characteristics of microstrip discontinuities," *IEEE Transactions on MTT*, vol. 36, no. 12, December 1988, pp. 1775-1787.

- [29] Luc B. Gravelle and Perry F. Wilson, "EMI/EMC in Printed Circuit Boards - A literature review," *IEEE Transactions on EMC*, vol. 34, no. 2, May 1992, pp. 109-116.
- [30] Y. Kami and R. Sato, "Analysis of radiation characteristic of a finite length transmission line using a circuit concept approach," *IEEE Transaction on EMC*, vol. 30, no. 2, May 1988, pp. 114-121.
- [31] Y. Kami and R. Sato, "Circuit-Concept Approach to Externally Excited Transmission Lines," *IEEE Transactions on EMC*, vol. 27, no. 4, November 1985, pp. 177-182.
- [32] Y. Kami and R. Sato, "Radiation from a transmission line carrying current of an arbitrary waveform," *The Proc. of IEEE international symposium on EMC*, Aug. 1988, pp. 124-129.
- [33] Y. Kami and R. Sato, "Radiation model of finite length transmission line," *The Proc. of IEEE international symposium on EMC*, 1986, San Diego, CA. USA. pp. 206-212.
- [34] N. Marcuvitz, "Waveguide handbook," New York, Dover 1965, Ch. 4 pp. 168-216.
- [35] T. Nakamura, N. Okochi, S. Yokokawa and R. Sato, "Radiation from a bend of transmission line," *IEICE Japan*, vol. J79-B, no. 2, pp. 261-268, Feb. 1987.
- [36] Fred Gardiol, "Radiation from high frequency printed circuits," *The 9th international Zurich symposium on EMC*, March 1991, pp. 625-630.
- [37] B.J.Rubin and S.Daijavad, "Radiation and scattering from structures involving finite-size dielectric regions," *IEEE AP-S international symposium*, 1990.
- [38] V. Ungvichian and R. Perez-Rodriquez, "Prediction of electromagnetic radiation of a multilayer board," *Electronics letters*, 2nd July 1987, vol. 23, no. 14, pp. 721-722.
- [39] Springfield, W. K., "Multilayer printed circuitry in computer applications," *presented at fall meeting of printed circuits*, Chicago, IL, Oct. 1964.
- [40] Krishna Naishadham and John B. Berry, "A rigorous model to compute the radiation from printed circuit boards," *IEEE international symposium on EMC*, Denver, Co., 1989, pp. 127-130.
- [41] Krishna Naishadham, John B. Berry and Hassan A. N. Hejase, "Full wave analysis of radiated emission from arbitrarily shaped printed circuit traces," *IEEE Transactions on EMC*, vol. 35, no. 3, August 1993, pp. 366-367.
- [42] J. R. Mosig and F. E. Gardiol, "A dynamical radiation model for microstrip structures," *Advances in Electronics and Electron Physics*, vol. 59, pp. 139-237, 1982.

- [43] Richmond J. H., "Radiation and scattering by thin wire structure in the complex frequency domain," *Ohio State University Electro-Science Laboratory, Dept. of Electrical Engineering, Columbus, OH 43212, Rep. 2902-10, 7/73.*
- [44] Hismatsu Nakano et al. "The moment method solution for printed wire antennas of arbitrary configuration," *IEEE Transaction on antenna and propagation*, vol. 36, no. 12, December 1988, pp. 1667-1673.
- [45] Shahrokh Daijavad and Barry J Rubin, "Modelling common-mode radiation of 3D structures," *IEEE Transactions on EMC*, vol. 34, no. 1, February 1992, pp. 57-61.
- [46] G.Cerri, R. De Leo and V. Mariani Primiani, "A rigorous model for radiated emission prediction in PCB circuits," *IEEE transactions on EMC*, vol. 35, no. 1 , February 1993, pp. 102-109.
- [47] G.Cerri, "The microstrip spiral antenna," *European transaction on telecom. related tech.*, vol. 1 no. 5, pp. 549-555, Sept.-Oct. 1990, pp. 102-109.
- [48] R.W.P. King, "*Antennas and waves: a modern approach*," chap.14, The MIT press, 1969.
- [49] T.H. Hubing and J.F. Kaufman, "Modelling of electromagnetic radiation from a electrically small table-top product," *IEEE Transaction on EMC*, vol. 31, no. 1, February 1989, pp. 74-84.
- [50] H.A.N Hejase, A.T.Adams and R.F. Harrington, " A quasi static technique for evaluation of pigtail connection," *IEEE Transactions on EMC*, vol. 31, no. 2, May 1989, pp. 180-183.
- [51] H.H.Chao and B.J.Strait, "Computer programs for radiation and scattering by arbitrary configurations of bent wires," *AFCRL-70-0374, Science Report 7*, September 15, 1970.
- [52] D.C.Kuo and B.J. Strait, "Improved program for analysis of radiation and scattering by configurations of arbitrarily bent thin wires," *AFCRL-72-0051, Science Report 15*, January 15, 1972 .
- [53] M.D. Tew, "Correction to WIRES program," *IEEE Transaction on Antenna and Propagation*, vol. AP-33, pp. 450-451, May 1975.
- [54] B.E. Keiser, "*Principles of Electromagnetic Compatibility*," Dedham, MA, Artech House 1989.
- [55] R.J. Perez, "First year graduate level course in electromagnetic compatibility," *The seventh international conference on electromagnetic compatibility*, 28-31 August 1990, York, UK, pp. 232-239.

- [56] John W, Rockway, James C. Logan, Daniel W.S. Tam and Shing Ted Li, "*The MININEC System: Microcomputer Analysis for Wire Antennas*," Denver, MA, Arctech House.
- [57] Ernest E Donaldson, William R. Free, Douglas W. Robertson and Jimmy A. Woody, "Field measurement made in an enclosure," *The proceedings of IEEE*, vol. 66, no. 4, April 1978, pp. 464-472.
- [58] Violette, J.L.N., White, D.R.J and Violette, M.F., "*Electromagnetic compatibility Handbook*," Van Nostrand Reinhold, New York, 1987.
- [59] Linda Dawson, "RFI Measurement in screened room," *Ph .D thesis*, The University of York, UK.
- [60] "FCC method of measurement of radio emission from computing devices," *FCC Rules, pt. 15, Subpt. J, Appendix A (July, 1981) and FCC 83-352 order on general docket 80-284, Appendix B*, July 1983.
- [61] R.G.Fitzgerrell, "Site attenuation," *IEEE Transaction on electromagnetic compatibility*, vol. 28, Feb. 1986, pp. 63-66.
- [62] W.R. Free, "Radiated EMI measurement in shielded enclosure," *IEEE international symposium on EMC*, Washington DC, USA, 1967, pp. 43-53.
- [63] R.A. Magnuson, "An experiment in reducing reflections in a shielded room," *IEEE international symposium on EMC*, Santa Clara, 1982, pp. 237-243.
- [64] Horacio A Mendez, "A new approach to electromagnetic field-strength measurements in shielded enclosures," *WESCON technical papers session 19*, USA, 1968.
- [65] L. Steele and A.C. Marvin, "New screened room techniques for the measurement of RFI," *The 5th international conference on EMC*, York, UK, 1-3 October 1986, pp. 175-180.
- [66] P. Corona, G. Latmiral, E. Paolini and L. Piccioli, "Use of a reverberating enclosure for measurement of radiated power in the microwave range," *IEEE Transactions on EMC*, vol. 18, no. 2, May 1976, pp. 54-59.
- [67] P. Corona, G. Latmiral and E. Paolini, "Performance and analysis of reverberating enclosure with variable geometry," *IEEE Transaction on EMC*, vol. 22, no 1, February 1980, pp. 2-5.
- [68] I. Sreenivasiah, D. C. Chang and Mark T. Ma, "Emission characteristics of electrically small radiating sources from tests inside a TEM Cell," *IEEE Transaction on EMC*, vol. EMC-23, no. 3 August 1981, pp.113-121.

- [69] Mark T Ma, M Kanda, M L. Crawford and Ezra B. Larsen, "A review of Electromagnetic Compatibility/Interference measurement methodologies," *The proceedings of the IEEE*, vol. 73, no. 3, March 1985, pp. 388-411.
- [70] M. L. Crawford and C. L. Thomas, "Converting a rectangular shielded enclosure into a TEM transmission cell for EMI measurements," *presented at the IEEE international symposium on EMC*, Seattle, WA, 1977.
- [71] R. Morrison, "Grounding," *The proceeding of EMC expo.*, San Deigo ,CA, T23, May 1987.
- [72] J.D.M. Osburn and D.R.J. White, "Grounding, a recommendation for the future," *The proceeding of IEEE international symposium on EMC*, Atlanta, GA, Aug. 1987, pp. 155-160.
- [73] P.C.T Vander Laan, M.A. Van Houten and A.P.J. Van Deursen, "Grounding philosophy," *The proceeding of IEEE international symposium on EMC*, Zurich, Switzerland, Mar. 1987, pp. 567-572.
- [74] R.F German, "Use of ground grid to reduce printed circuit board radiation," *The proceeding of the 6th international symposium on EMC*, Zurich, Switzerland, March 1985, pp. 133-138.
- [75] C.R. Paul, "Modelling and prediction of ground shift on printed circuit boards," *The proceeding of IEE symposium on EMC*, York, 1986, pp. 37-45.
- [76] B.A. Bowles and C.R. Paul, "Modelling interference properties of SMPS DC power distribution busses," *The proceeding of IEEE national symposium on EMC*, Denver, Co, May 1989, pp. 119-126.
- [77] M.J. Nave, "The effect of duty cycle on SMPS common mode emissions: Theory and experiments," *The proceeding of IEEE national symposium on EMC*, Denver, Co, May 1989, pp. 211-216.
- [78] M.J. Nave, "Switched mode power supply noise: Common mode emissions," *The proceeding of EMC EXPO*, 1986, Washington, DC, June 1986, T11.
- [79] M.J. Nave, "Prediction of conducted emissions in switched power supplies," *The proceeding of IEEE international symposium on EMC*, 1986, San Diego, CA. Aug. 1986, pp. 167-173.
- [80] H.A.N. Hejase, A.T. Adams, R.F. Harrington and T.K. Sarker, "Shielding effectiveness of "pigtail" connections," *IEEE Transaction on EMC*, vol. 31, no. 1, pp. 63-68, Feb. 1989.
- [81] C.R. Paul, "Effect of pigtails on crosstalk to braided-shield cables," *IEEE Transaction on EMC*, vol. EMC-22, no. 3, pp. 161-172, Aug. 1980.

- [82] J.R. Moser, "Peripheral cable-shield termination: The system EMC kernel," *IEEE Transaction on EMC*, vol. EMC-28, no. 1, pp. 40-45, Feb. 1986.
- [83] D.E. Thomas, L.O. Hoeft, J.S. Hofstra and J.D. Tricarico, "Measurements and calculations of the cross-talk due to capacitive coupling between connector pins," *The proceeding of international symposium on EMC*, Arlington, VA, Aug. 1983, pp. 567-572.
- [84] V. G. Puglielli, "Current status of RFI predictions in electronic systems containing semiconductor devices," *The proceeding of the 3rd international symposium on EMC*, Rotterdam, Netherlands, May 1979, pp. 275-279.
- [85] C. E. Larson and J. M. Roe, "A modified ebers-moll transistor model for RF interference analysis," *IEEE Transaction on EMC*, vol. 21, no. 4, pp. 283-290, Nov. 1979.
- [86] J. J. Whalen, J.G. front, C.E. Larson and J.M. Roe, "Computer aided analysis of RFI effects in digital integrated circuits," *IEEE Transaction on EMC*, vol. 21, no. 4, pp. 291-297, Nov. 1979.
- [87] T.F. Fang, J.J whalen and G.K.C. Chen, "Using NCAP to predict RFI effects in linear bipolar integrated circuits," *IEEE Transaction on EMC*, vol. 22, no. 4, pp. 256-262, Nov. 1980.
- [88] J.G. Tront, J.J. Whalen, C.E. Larson and J.M. Roe, "Computer aided analysis of RFI effects in operational amplifiers," *IEEE Transaction on EMC*, vol. EMC-21, no. 4, pp. 297-306, Nov. 1979.
- [89] C.R. Paul, "Application of multiconductor transmission line theory to the prediction of cable coupling," *The technical report, RADC-TR-76101-Vol. (I-VIII)*, Rome Air Development Center, Griffis AFB, NY, Apr. 1976.
- [90] C. Wei, R.F. Harrington, J.R. Mautz and T.K. Sarker, "Multiconductor transmission line in multilayered dielectric media," *IEEE Transaction on MTT*, vol. MTT-32, no. 4, pp. 439-450, Apr. 1984.
- [91] N. Ari and W. Blumer, "Analytical formulation of the response of a two-wire transmission line excited by a plane wave," *IEEE Transaction on EMC*, vol. 30, no. 4, pp. 437-448, Nov. 1988.
- [92] C.R. Paul, " Frequency response of multiconductor transmission line illuminated by an electromagnetic field," *IEEE Transaction on EMC*, vol. 18, no. 4, pp. 183-190, Nov. 1976.
- [93] G.E.J. Bridges and L. Shafai, "Plane wave coupling to multiple conductor transmission line above a lossy earth," *IEEE Transaction on EMC*, vol. 31, no. 1, pp. 21-33, Feb. 1989.

- [94] H. Garbe and D. Hansen, "EMI response of cable systems to transients considering complex transfer impedance," *The proceeding of international symposium on EMC*, Seattle, WA, 1988, pp. 24-29.
- [95] S Ramo, J.R.Whinnery, T.Van Duzer, "*Fields and Waves in Communication Electronics*," 1965, John Wiley and Sons, Inc.
- [96] Edward C. Jordan and Keith G. Balmain, "*Electromagnetic waves and radiating systems*," Prentice Hall, inc. Englewood Cliffs, New Jersey, 1968.
- [97] C.R. Paul, "*Introduction to Electromagnetic compatibility*," John Wiley and sons Ltd, New York, 1992.
- [98] C.A. Balanis, "*Antenna theory analysis and design*," Harper and Row, 1982
- [99] Samuel Y. Liao, "*Microwave device and circuits*," Prentice Hall, Inc., Englewood Cliffs, New Jersey, 1980.
- [100] IEEE editorial policy statement (1987), *IEEE Transactions on electromagnetic compatibility*, EMC-29, pp. 202-206.
- [101] H.A. Wheeler, "Transmission line properties of parallel strips separated by a dielectric sheet," *IEEE Transactions on MTT*, MTT-13, pp. 172-185, 1965.
- [102] H. Rahman, "Development of EMC antennas and their application in on-line SE measurement of conductive composite plastic materials," *Ph. D. thesis*, The School of Electronic Engineering, DCU, March 1994.
- [103] G. Jackson, "An EMC progress report," *Electronic engineering magazine*, March 1994, pp. 27.
- [104] "Preselector enhance EMI measurements," *Electronic engineering magazine*, January 1993, pp. 21.
- [105] Bob Buxton, "Automated EMC measurement," *Electronic engineering magazine*, November 1990, pp. 85-92.
- [106] Akio Matsumoto, "*Microwave filters and circuits*," Ch. V, Academic Press, New York, 1970.
- [107] P.A. Chatterton and M.A. Houldon, "*EMC, electromagnetic theory and design*," John Wiley & Sons, 1992.
- [108] "*Boardmaker™ user's manual*," Tsien UK. Ltd.
- [109] "*ORCAD™ user's manual*", ORCAD corporation, Oregon, USA.
- [110] Jian Peng, Constantine A. Balanis and George C. Barber, "NEC and ESP codes : Guidelines, limitations, and EMC applications," *IEEE Transactions on EMC*, vol. 35, no. 2., May 1993, pp. 124-133.

- [111] J. Burke and A. J. Poggio, "Numerical electromagnetic code (NEC)- method of moments part 1, 2 and 3," *Naval Ocean Systems Center, San Diego, CA, in report NOOSC TD 116*, Jan. 1980.
- [112] R. F. Harrington, "*Field computation by moment methods*," New York, MacMillan, 1968.
- [113] William H. Press et al., "*Numerical Recipes*," Cambridge University press, Cambridge, New York 1986.
- [114] *RADC-TR-83-217*, Rome Air Development Center, Air Force System Command, Sept. 1983, "GEMACS", RADC, Rome, NY, USA.
- [115] C.W. Harrison and C.D. Taylor, "Response of a terminated transmission line excited by a plane wave field for arbitrary angle of incidence," *IEEE Transactions on EMC*, vol. 15, no. 3 August 1973.
- [116] John D. Kraus, "*Antennas*," McCraw-Hill, Inc, Singapore, 1988.
- [117] Santokh S. Basi, "*Semiconductor Pulse and Switching Circuits*," John Wiley & Sons Ltd.
- [118] Walter Banzhaf, "*Computer aided circuit analysis using SPICE*," Prentice Hall, Englewood Cliffs, New Jersey, 1989.
- [119] R. B. Schulz, C. Plantz and R. Brush, "Shielding theory and Practice," *IEEE Transaction on EMC*, vol. 30, no. 3, pp. 187-201, August 1988.
- [120] T.C. Edwards, "*Foundation of Microstrip Engineering*," John Wiley, New York, 1981.
- [121] *MATHCAD*, Mathsoft Inc., 201 Broadway, Cambridge, Massachusetts, 02139, USA.
- [122] Technical brochure, *EMI Test Receiver model no. ESVS 30*, Rohde and Schwarz, Germany.
- [123] K.C. Gupta, R. Garg and I.J. Bahl, "*Microstrip lines and Slotlines*," Arctech House, Dedham, MA 1979.
- [124] The chase guide to EMC emission measurement, *Poster published by Chase ADVANTEST*, 1992.
- [125] -----, "*Crystal product data Book*," International Quartz Devices (IQD) Ltd. UK, 1993.
- [126] -----, "*Radionics catalogue*," Radionic Ltd. UK, 1993.
- [127] W.T. Weeks, "Calculation of coefficients of capacitance of multiconductor transmission lines in the presence of a dielectric interface," *IEEE Transaction on MTT*, vol. 18, pp. 35-43, 1970.

- [128] E. K. Miller, "A selective survey of computational Electromagnetic," *IEEE Transaction on AP*, vol. 36, no. 9, September 1988, pp. 1281-1305.
- [129] Nelly Recrosio, Georges Fine and Marc Helier, "Analysis of radiation characteristic of distribution line carriers with the NEC code," *IEEE Transaction on EMC*, vol. 35, no. 1, February 1993.
- [130] A. Vladimirescu, A. Vladimirescu, Kaihe Zhang, A.R. Newton, D.O. Pederson and A.Sangiovanni-Vincentelli, "*SPICE Version 2G User's guide*," Department of Electrical Engineering and computer Sciences, University of California, Berkeley, Ca. 94720, pp. 1-38, 1981.
- [131] T. J. F. Carr-Brion and S. J. Porter, "Prediction of PCB radiation in the presence of scattering bodies," *Seventh international conference on EMC*, 28-31 August 1990, The University of York, York, UK, pp. 137-139.
- [132] Miles E.G. Upton and A.C. Marvin, "The fields due to a small loaded loop in free space," *IEEE Transaction on EMC*, vol. 36, no. 1, Feb. 1994, pp. 7-13.
- [133] R. F. Harrington, "*Time-Harmonics Electromagnetic Fields*," ch. 8, Mcgraw-Hill book company, NY, 1961.
- [134] A. C. Marvin, J.M. Tealby, T.J.F. Carr-Brion, S.J. Porter and S.M. Mann,, "Computer aided design for radio-frequency interference reduction," *Seventh international conference on EMC*, 28-31 August 1990, The University of York, York, UK, pp. 140-143.
- [135] Kenneth D. Marx and Rex I. Eastin, "A configuration-oriented SPICE model for multiconductor transmission lines with homogeneous dielectrics," *IEEE Transactions on MTT*, vol. 38, no. 8, Aug. 1990, pp. 1123-1129
- [136] DRM Green, "PCBs: Designing to minimise EMI problems," *CIE*, November 1991, pp. 3-5.
- [137] P. K.Saha and Jim Dowling, "A combined CAD package to predict and minimise EM radiation from a PCB at design stage," *International Symposium on Electromagnetic Compatibility*, Rome, Italy, September 13-16, 1994, pp. 631-637.
- [138] C. R. Paul, "Modelling electromagnetic interference properties of printed circuit boards," *IBM Journal of research and development*, vol. 33, no. 1, January 1989, pp. 33-49.
- [139] Henry W. Ott, "*Noise reduction techniques in electronic systems*," John Wiley & Sons, 1976.
- [140] Curtis B White, "A comparison of simplified methods for predicting radiated emission," *IEEE international symposium on electromagnetic compatibility*, 1990.

- [141] Panayiotis A. Tirkas, Constantine A. Balanis, Michael P. Purchine and George C. Barber, "Finite-Difference Time-Domain method for electromagnetic radiation, interference, and interaction with complex structures," *IEEE transactions on EMC*, vol. 35, no. 2, May 1993, pp. 192-203.
- [142] Preben Lond, "*Generation of Precision Artwork for Printed Circuit Boards*," John Wiley & Sons Ltd. New York, 1978.
- [143] J.A. Scarlett, "*Printed Circuit Boards for Microelectronics*," 2nd edition, Electrochemical publications Ltd. 1980.
- [144] Robert S. Elliott, "*Antenna theory and design*," Prentice-Hall, Inc., Englewood Cliffs, New Jersey, 1981, pp. 325.
- [145] R. B Cowdell, "Simple equations to compute radiated emissions," *IEEE international symposium on EMC*, August 1983, pp. 203-206.
- [146] H. Rahman, P. K. Saha, Jim Dowling and T. Curran, "Shielding effectiveness measurement techniques for various materials used for EMI shielding," *IEE colloquium Digest on Screening of Connectors, Cables and Enclosures*, no. 1992/012, pp. 9/1-6, London, January 1992.
- [147] P. K. Saha and Jim Dowling, "Prediction of PCB radiation using NEC software combined with commercial CAD packages," *19th ARMMS Conference Digest*, pp. 5/1-7, Leeds, September 1993.
- [148] Theodore S. Saad, Robert C. Hansen and Gershon J. Wheeler, "*Microwave Engineer's Handbook*," vol. 1, pp. 119, Artech House Inc. Dedham, 1971.
- [149] B. Audone, E.R. Totto and M.D. Barba, "The computer- aided approach to emission testing," *IEEE Transaction on EMC*, vol. 26, no. 1, February 1984, pp. 43-49.
- [150] R. Mittra, "*Computer techniques for electromagnetics*," Pergamon Press, 1973.
- [151] R.F.German et al., "Effect of image plane on printed circuit board layout," *IEEE international symposium on EMC*, Washington DC, August 1990.
- [152] "*User's manual*," HP 8657B Synthesised Signal Generator, Hewlett-Packard Limited 1989, USA.
- [153] Ramesh Garg and I. J. Bahl, "Characteristics of coupled microstriplines," *IEEE Transactions on MTT*, vol. 27, no. 7, July 1979, pp. 700-705.
- [154] Kai Chang, "*Microwave solid state circuits and applications*," John Wiley and Sons Ltd. New York, 1994, pp. 50-59.
- [155] F. Garidol, "*Microstrip Circuit*," John Wiley and Sons Ltd. New York, 1994, pp. 34-45.

- [156] W. Boxleitner, "How to defeat electrostatic discharge," *IEEE Spectrum*, pp. 36-40, August 1989.
- [157] J. F. Dawson, J. Ahmadi and A. C. Marvin, "Reduction of radiated emissions from apertures in resonant enclosures by the use of lossy materials," *IEE colloquium Digest on Screening of Connectors, Cables and Enclosures*, no. 1992/012, pp. 9/1-6, London, January 1992.
- [158] James P. Keener, "*Principles of applied mathematics: Transformation and Approximation*," Addison-Wesley publishing company, USA, 1988.
- [159] Tai T. Wu and Ronald W.P. King, "The tapered antenna and its application to the junction problems for thin wires," *IEEE Transactions on Antenna and Propagation*, vol. 24, no. 1, Jan. 1976, pp. 42-45.
- [160] G. J. Burke, "Recent advances to NEC: Application and validation," *Lawrence Livermore National Laboratory*, preprint number UCRL-100651, Mar. 1989.